National Library of Canada
Acquisitions and Bibliographic Services Branch
395 Wellington Street
Ottawa, Ontario
K1A 0N4

Bibliothèque nationale du Canada
Direction des acquisitions et des services bibliographiques
395, rue Wellington
Ottawa (Ontario)
K1A 0N4

Your file Votre référence

Our file Notre référence

NOTICE

The quality of this microform is heavily dependent upon the quality of the original thesis submitted for microfilming. Every effort has been made to ensure the highest quality of reproduction possible.

If pages are missing, contact the university which granted the degree.

Some pages may have indistinct print especially if the original pages were typed with a poor typewriter ribbon or if the university sent us an inferior photocopy.

Reproduction in full or in part of this microform is governed by the Canadian Copyright Act, R.S.C. 1970, c. C-30, and subsequent amendments.

AVIS

La qualité de cette microforme dépend grandement de la qualité de la thèse soumise au microfilmage. Nous avons tout fait pour assurer une qualité supérieure de reproduction.

S'il manque des pages, veuillez communiquer avec l'université qui a conféré le grade.

La qualité d'impression de certaines pages peut laisser à désirer, surtout si les pages originales ont été dactylographiées à l'aide d'un ruban usé ou si l'université nous a fait parvenir une photocopie de qualité inférieure.

La reproduction, même partielle, de cette microforme est soumise à la Loi canadienne sur le droit d'auteur, SRC 1970, c. C-30, et ses amendements subséquents.

Canada

FORMATION OF IRON-BEARING INTERMETALLICS IN ALUMINUM-SILICON CASTING ALLOYS

SAEED G. SHABESTARI

Department of Mining and Metallurgical Engineering
McGill University
Montreal, Canada

A thesis submitted to the Faculty of Graduate Studies and Research
in partial fulfilment of the requirements for the degree of
Doctor of Philosophy

December, 1994

National Library
of Canada

Acquisitions and
Bibliographic Services Branch

395 Wellington Street
Ottawa, Ontario
K1A 0N4

Bibliothèque nationale
du Canada

Direction des acquisitions et
des services bibliographiques

395, rue Wellington
Ottawa (Ontario)
K1A 0N4

ISBN 0-612-05793-3

To the memory of

***Dr. MOSTAFA CHAMRAN**, scientist and philanthropist,*

who sacrificed his life to enlighten society.

Abstract

The formation of iron-bearing intermetallics in the 413 type of aluminum alloys was investigated comprehensively. Both synthetic and commercial 413 alloys were studied with iron concentrations in the range of 0.4 - 1.2 wt.% and manganese up to 0.5 wt.%. The effects of cooling rate during solidification and of melt chemistry on the morphology of iron intermetallic phases were determined. Image analysis was used to quantify the intermetallic size, volume fraction, and number, as a function of both melt chemistry and cooling rate. The total volume fraction of intermetallic compounds in these alloys was related to cooling rate by an exponential equation.

The kinetics of both dissolution of intermetallics on melting, and of re-formation on cooling of the liquid were investigated by means of quenching experiments. Superheating the melt to temperatures of 800-850°C for up to 1.5 hours is necessary to completely dissolve all pre-existing intermetallics. Once dissolved, they will not reform until a certain temperature is reached. This temperature depends on the alloy chemistry, particularly the iron concentration. The relationship between iron content and the formation temperature can be expressed by a power equation. The kinetics of formation, considering the roles of holding temperature, holding time, and iron content, were studied. Quantitative evaluation of intermetallic size and number revealed that the change in volume fraction of intermetallics in the liquid state is controlled by nucleation. Thus, the average size does not change appreciably with holding time in the liquid, but the number of intermetallics is a strong function of holding time because the nucleation kinetics are slow.

The effect of settling time and the rate of gravity segregation of intermetallic compounds in a stagnant liquid metal were investigated. The rate of settling varies with location in the mold due to depletion of intermetallics at the top and accumulation at the bottom. It was found that, in the absence of convection, settling obeys Stokes' law with the terminal velocity reached at very short times and very close to the melt surface.

Strontium was used to modify or eliminate the iron-intermetallics. It completely eliminates all intermetallic compounds in commercial alloys in the permanent mold cast condition, and causes the fragmentation of needles (β-phases) in the sand cast condition. Strontium is also an effective element in changing the β-phase to the α-phase morphology in these alloys.

Résumé

La formation d'intermétalliques contenant du fer dans les alliages du type 413 a été examinée. Des alliages 413, synthétiques et commerciaux, avec des teneurs en fer entre 0.4 et 1.2% en poids et des teneurs en manganèse jusqu'à 0.5% en poids, ont été étudiés. Les effets de la vitesse de refroidissement pendant la solidification ainsi que les effets de la composition chimique de la coulée sur la morphologie des phases intermétalliques au fer ont été déterminés. Un analyseur d'images a été utilisé pour quantifier la taille, la fraction volumique et le nombre d'intermétalliques en fonction de la composition chimique de la coulée et de la vitesse de refroidissement. La fraction volumique totale des composés intermétalliques dans ces alliages est reliée à la vitesse de refroidissement par une équation exponentielle.

Les cinétiques de dissolution des intermétalliques lors de la fusion, ainsi que leur reformation lors du refroidissement du liquide, ont été examinées au moyen d'expériences de trempe. Le surchauffage de la coulée à des températures de l'ordre de 800-850°C pendant au moins une heure et demie est nécessaire pour dissoudre complétement tous les intermétalliques pré-existants. Une fois dissous, ils ne se reformeront pas tant qu'une certaine température ne sera pas atteinte. Cette température dépend de la composition de l'alliage, plus particulièrement de la teneur en fer. La relation entre la teneur en fer et la température de formation peut être exprimée par une équation en puissance. L'influence de la température de maintien, du temps d'attente et de la teneur en fer sur les cinétiques de formation a été étudiée. L'évaluation quantitative de la taille et du nombre d'intermétalliques a révélé que le changement de la fraction volumique des intermétalliques dans l'état liquide est contrôllé par la germination. Ainsi, la taille moyenne ne change pas d'une façon significative avec le temps d'attente dans le liquide, mais le nombre d'intermétalliques est très dépendent du temps d'attente car les cinétiques de germination sont lentes.

L'effet du temps de sédimentation et du taux de ségrégation gravitationnelle des composés intermétalliques dans un liquide stagnant, a été analysé. Le taux de sédimentation varie avec la position dans le moule à cause de la déplétion en intermétalliques dans le haut et leur accumulation dans le bas. Il a été trouvé qu'en l'absence de convection, la sédimentation obéit à la loi de Stokes avec la vélocité terminale atteinte très rapidement et très proche de la surface de la coulée.

Du strontium a été utilisé pour modifier ou éliminer les intermétalliques contenant du fer. Il élimine complétement tous les composés intermétalliques dans les alliages coulés en coquille et provoque la fragmentation des aiguilles (phases ß) dans les alliages coulés dans le sable. Dans ces alliages, le strontium est aussi un élément efficace pour changer la phase ß en la morphologie de la phase α.

Acknowledgements

I would like to express my sincere gratitude to my supervisor, Prof. J.E. Gruzleski, for his guidance, helpful suggestions and constant encouragements during the course of this research.

I would like to thank and to express my deep gratitude to my parents for their love and encouragement. I am particularly indebted to my wife for her continuous emotional support and patience during the years of my postgraduate studies. Without her devotion, this work could not have been accomplished.

Thanks are also due to my colleagues and friends in the Department of Mining and Metallurgical Engineering particularly the members of Aluminum Group for providing a stimulating environment; they have been helpful in many ways. Special thanks are due to Dr. Florence Paray for translation of the abstract into French.

I express my appreciation to the technical personnel of the department, in particular Ms. Helen Campbell, Mr. Robert Paquette, Mr. Martin Knoepfel, and Mr. François Dallaire. I also acknowledge Mr. Glenn Poirier (Department of Geological Sciences) for his help with the electron probe microanalyzer, and personnel of the Physical Sciences and Engineering library, particularly Mr. Henry Lim Soo.

Finally, I would like to extend my deep appreciation to the Iranian Ministry of Culture and Higher Education as well as Iran University of Science and Technology for making my postgraduate studies possible. I would also like to thank the Natural Sciences and Engineering Research Council of Canada (NSERC) for the financial support of this research.

TABLE OF CONTENTS

Chapter 3 : Effect of Melt Chemistry and Temperature on the Formation of Intermetallic Compounds

Chapter 4 : Kinetics of the Formation of Intermetallic Compounds

Chapter 5 : Effect of Solidification Conditions on the Formation and Morphology of Intermetallic Compounds

Chapter 6 : Gravity Segregation of Intermetallic Compounds

Chapter 7 : Modification of Intermetallic Compounds

Chapter 8 : Conclusions and Future Work

List of Figures

Chapter 1 : **Introduction**

Chapter 2 : **Literature Survey**

Chapter 3 : Effect of Melt Chemistry and Temperature on the Formation of Intermetallic Compounds

Chapter 4 : Kinetics of the Formation of Intermetallic Compounds

Chapter 5 : Effect of Solidification Conditions on the Formation and Morphology of Intermetallic Compounds

Chapter 6 : Gravity Segregation of Intermetallic Compounds

Chapter 7 : Modification of Intermetallic Compounds

List of Tables

Chapter 1 : Introduction

Chapter 2 : Literature Survey

Chapter 3 : Effect of Melt Chemistry and Temperature on the Formation of Intermetallic Compounds

Chapter 4 : Kinetics of the Formation of Intermetallic Compounds

Chapter 5 : Effect of Solidification Conditions on the Formation and Morphology of Intermetallic Compounds

Chapter 6 : Gravity Segregation of Intermetallic Compounds

Chapter 7 : Modification of Intermetallic Compounds

Chapter 1

Introduction

1.1. Aluminum Casting Alloys

Aluminum casting alloys are used extensively in various applications requiring a high strength-to-weight ratio, such as automotive, aerospace, and other structural components. These alloys are characterized by their low specific gravity which can vary slightly above and below the specific gravity of pure aluminum depending on the major alloying elements. In addition to their light weight, other advantages of aluminum casting alloys include relatively low melting temperatures, negligible gas solubility with the exception of hydrogen, excellent castability especially near the eutectic composition of 12.6%, good machinability and surface finishing, good corrosion resistance, and good electrical and thermal conductivity. A volumetric shrinkage of between 3.5% and 8.5% occurring during solidification constitutes the major drawback of aluminum casting alloys. The shrinkage coefficient is taken into account during mold design in order to obtain dimensional accuracy and to avoid hot tearing and shrinkage porosity. While the mechanical properties are usually inferior to those of wrought products, the heat treatment of some alloys considerably improves their mechanical properties.

The soundness and mechanical behaviour of these structure-sensitive alloys are greatly affected by the impurity containing phases and compounds. The composition, morphology, size, amount, and distribution of the impurity containing structures have a strong influence on the mechanical properties of the aluminum castings. An increasing volume of aluminum castings is produced by utilizing recycled aluminum in which impurities have a tendency to accumulate. The economical use of recycled (secondary) aluminum is possible, if the effects of impurities on the solidification and mechanical properties of aluminum castings are recognized. The presence of impurities may not be ignored either, during the use of electrolytically refined (primary) aluminum alloys.

1.2 Constitution of Aluminum Alloys

The composition of aluminum alloys is based on the solubilities of elements in aluminum, the economical considerations, as well as the desired properties of the castings. The elements present in aluminum alloys can be categorized as the principal alloying elements, the additional alloying elements, and the impurities. Commercial purity aluminum as well as aluminum alloys frequently contain impurities which affect molten metal treatment, castability, and properties. The impurities and alloying elements, in general, partly go into solid solution in the matrix and partly form intermetallic particles during the solidification process.

1.2.1 Alloying Elements

Alloying elements are usually added to aluminum to increase its strength, although improvements in other properties are very important. The two most commonly used methods of increasing the strength of aluminum alloys are to :

- Disperse alloying elements or elements in solid solution and cold work the alloy (work-hardening alloys).

- Dissolve the alloying elements into solid solution and precipitate them as coherent submicroscopic particles (precipitation-hardening alloys).

The solubilities of elements in aluminum are reviewed in the literature[1]. None of the elements is reported to have complete miscibility with aluminum in the solid state. Zinc, magnesium, copper, manganese, and silicon form the basis for the principal commercial aluminum alloys. Altenpohl[2] has summarized the most important aluminum alloys in Figure 1.1. The most widely used aluminum alloys are based on the aluminum-silicon system, in which magnesium and copper may also be used as alloying elements.

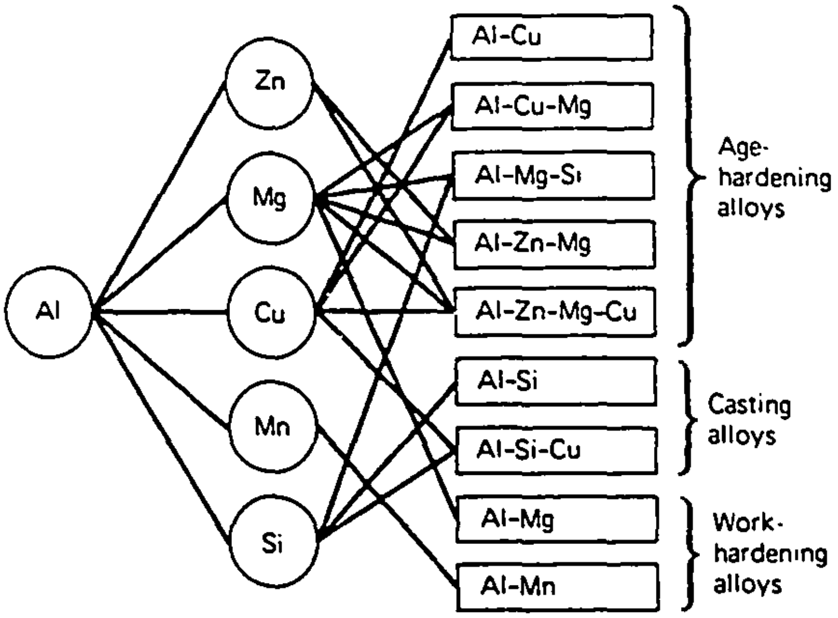

Figure 1.1 : Principal aluminum alloys. [2]

Most casting alloys have silicon as the major alloying addition because aluminum-silicon alloys are able to fill the mold completely and are not sensitive to hot cracking. The silicon in shape casting produces a modest increase in strength because of the large volume fraction of hard silicon particles or fibers formed during solidification.[1]

Altenpohl[2] lists the aluminum alloys as age hardenable alloys, cast alloys, and work hardenable alloys (Figure 1.1) on the basis of whether the alloys are heat treatable or not. The Al-Si and Al-Si-Cu alloys are included into the group of cast alloys, most probably on the basis of the fact that these alloys do not show any age hardening during the heat treatment, and therefore are not heat treated.

1.2.2 Additional Alloying Elements

The additional alloying elements are considered to be the elements, the presence of which in aluminum alloys is beneficial, in addition to the principal alloying elements. The additional alloying elements may be the refining inoculants (Ti,B), modifying inoculants (Sr, Na, Sb, Ce, Nb, Be) as well as the transition metals (Mn, Cr, Zr) and metals having low melting points (Pb, Bi, Sn).

Transition metals with moderate solid solubilities, such as manganese, chromium, and zirconium are added to aluminum alloys because they can be precipitated as a dispersion of fine intermetallic particles, less than 1 μm in diameter, which do not dissolve during hot working or annealing. This fine, stable dispersion of particles can be used to pin grain or subgrain boundaries and improve strength, toughness, and resistance to stress-corrosion cracking.[1]

1.2.3 Impurities

The elements and compounds which have a negative effect on the castability, mechanical properties, and/or heat treatment of cast aluminum alloys, or whose effects on these concepts are unknown, are regarded as impurities.[3] In other words, anything which is not added on purpose, or all elements which are not categorized as the alloying or additional alloying elements are impurities. The impurities originate from four main sources :

1. Mixed alloys due to poor scrap segregation, recovery of metal from furnace dross, remelting of multialloy products such as used beverage cans and clad sheet,
2. Contamination of the scrap by extraneous materials such as banding iron, sand, painted sheet, and coatings on cans,
3. Incorporation of nonmetallic inclusions, such as oxide films and aluminum-magnesium spinel, into the metal during melting and casting,

4. Contamination from furnace tools, refractories, and hydrogen from furnace atmospheres.

Depending on the impurity contents, different impurity containing phases and compounds may exist in the microstructure of cast aluminum alloys. The impurity rich structures impairing the mechanical properties of aluminum alloys frequently lie within the intergranular/interdendritic regions.

1.3 Primary and Secondary Aluminum Alloys

Attention is paid to the definition of primary and secondary aluminum alloys as well as to the impurities accumulating in secondary alloys. The primary aluminum alloys are based on electrolytically refined aluminum. The electrolytically refined aluminum is alloyed according to the specifications by adding virtually pure alloying elements into the melt. Since the alloying elements (Si, Mg, Cu, Zn, and Mn) of aluminum can be separately refined before adding them into electrolytically refined aluminum, and since the purity of the electrolytic aluminum is high, the impurity contents of primary aluminum alloys are low.

The production of secondary aluminum alloys, on the other hand, is based on the remelting of aluminum scrap. The desired specification analyses are achieved by the careful selection of scrap material as well as by molten metal treatments. The impurity contents of secondary alloys are relatively high, duc to the nature of the production method.

1.4 Inclusions in Aluminum Melts

Inclusions present in an aluminum melt can be either non-metallic or intermetallic. The commonly encountered inclusions are oxides, e.g., Al_2O_3, Al_2O_3-MgO, aluminum carbides (Al_4C_3), titanium boride (TiB_2), etc. These particles, apart from being a porosity inducer during solidification, can also be detrimental to the mechanical properties of a casting.

1.4.1 Non-metallic Inclusions

The wearing process (erosion and impact) of the refractory linings of melting furnaces is difficult to avoid in practice. Groteke[4] as well as Kaye[5] have shown that the refractory materials of the melting crucibles and tools may find their way into the aluminum melt as solid particles. The fluxes used during the melting of aluminum alloys can also produce inclusions in the melt. The chemical composition of the fluxes indicates that the nature of these inclusions is non-metallic.[3]

A hard non-metallic inclusion will act as a stress intensifier while the part is in service. This could lead to an initiation of cracking in the intensified stress field around the inclusion, thus impairing the fatigue properties of the part.

The oxidation of the aluminum melt results in the formation of solid Al_2O_3 films on and in the melt. The Al_2O_3 films are often trapped in the microstructure of aluminum alloys during solidification. Although solid aluminum has a thin film of oxide which is protective, the molten metal forms oxide at a rate which increases with temperature, and this is a major cause of hard spots. Any disruption of this film on the surface of the metal from turbulence during pouring or excessive disturbance when ladling will lead to a continuous build-up of further oxide formation. The density of aluminum oxide is not significantly different from that of the molten alloy and consequently the oxide particles remain suspended in the melt and are transferred to the casting. Sometimes oxide skin sticking to the pouring ladle after the casting operation is inadvertantly returned to the melt. Oxides may act as nucleation centres so that primary crystals of high melting point compounds may be observed on this kind of inclusion.[6]

1.4.2 Intermetallic Compounds

Groteke[4] and Kaye[5] have shown that solid intermetallic (sludge) is formed during the melting of secondary aluminum alloys if the aluminum scrap contains moderate amounts of iron, chromium, and manganese which causes phases rich in these elements to precipitate from the aluminum melt. Accordingly, sludge consists of solid intermetallics, more precisely of complex intermetallic compounds. Complex intermetallic compounds are brittle; they act as stress raisers and are points of weakness which reduce the strength and ductility of the alloy.

Groteke[7] has observed that the formation of sludge consisting of complex intermetallics is almost impossible to avoid during the melting of commercial die cast aluminum alloys. This is due to the fact that the strength and soldering properties of these alloys require a relatively high iron content. Manganese additions modify the shape of (Fe, Mn, Si) containing precipitates to cause globular instead of needle-like particles.

1.5 Aluminum-Silicon Alloys

The Al-Si binary system[8] shown in Figure 1.2 exhibits a simple phase diagram with a single eutectic point at 577°C and 12.6 wt% Si. It consists of two solid solution phases, Al (FCC) and Si (diamond cubic). The maximum solubility of Si in (Al) is 1.5 ± 0.1 atomic% at the eutectic temperature, and it decreases to 0.05 atomic% at 300°C. The maximum solubility of Al in (Si) is 0.016 ± 0.003 atomic% at 1190°C. Al-Si alloys have not been reported to form metastable intermetallic compounds or glassy alloys.[8]

Aluminum-Silicon alloys can be broadly classified into three categories, based on their silicon content. The alloys which contain 2-9 wt% Si are classified as hypoeutectic alloys, 10-13 wt% Si are classified as eutectic alloys and 14-25 wt% are classified as hypereutectic alloys.

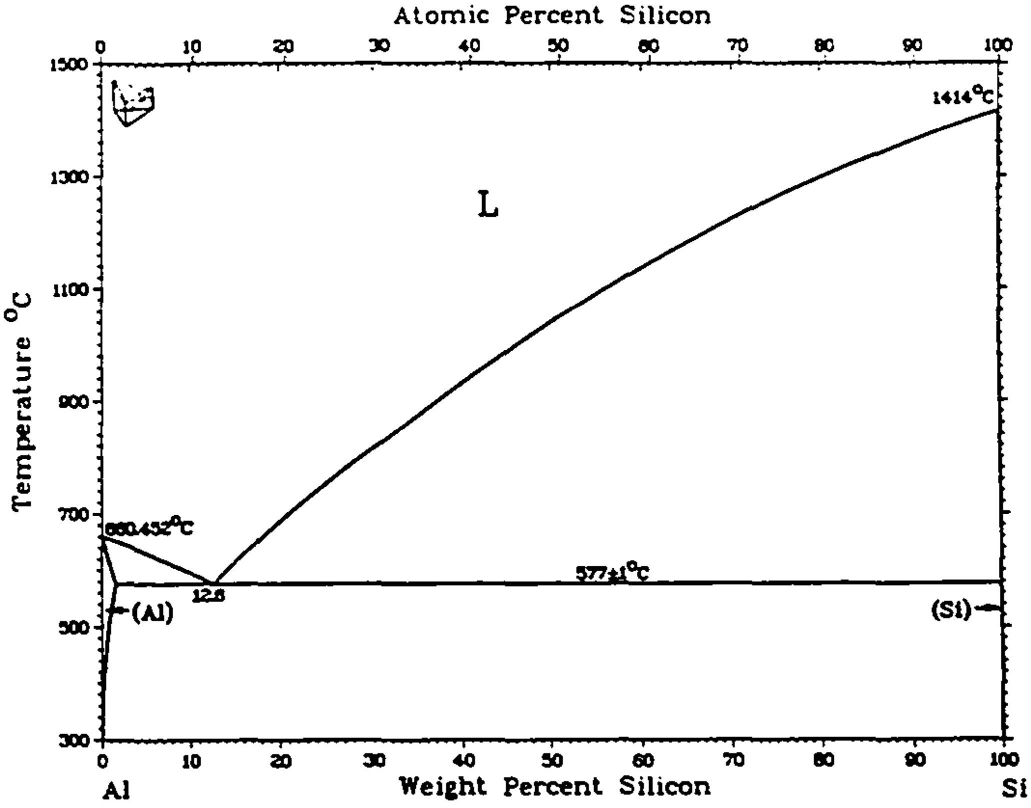

Figure 1.2 : Equilibrium binary Al-Si phase diagram.[8]

Aluminum-silicon castings constitute 85 to 90% of the total aluminum cast parts produced. The most common aluminum casting alloys are listed in Table 1.1. Aluminum alloys containing silicon as the major alloying element offer excellent castability, good corrosion resistance, and can be machined and welded. From the phase diagram in Figure 1.2 it is seen that the 413.0 alloy (approximately 12% Si) contains a predominant eutectic phase, and therefore must be modified with either strontium or sodium to ensure adequate tensile strength and ductility. For high pressure die casting, alloy 413.0 has better castability than alloy 443.0. All casting processes can be used to cast 443.0 parts when ductility, corrosion resistance and pressure tightness are more important than strength.[9]

Table 1.1 : Composition of Common Aluminum-Silicon Alloys(a) [ref.9]

		Elements (wt%)					
Alloy	Method(b)	Si	Cu	Mg	Fe	Zn	Others
319.0	S,P	6.0	3.5	<0.10	<1.0	<1.0	
332.0	P	9.5	3.0	1.0	1.2	1.0	
355.0	S,P	5.0	1.25	0.5	<0.06	<0.35	
A356.0	S,P	7.0	<0.20	0.35	<0.2	<0.1	
A357.0	S,P	7.0	<0.20	0.35	<0.2	<0.1	0.05 Be
380.0	D	8.5	3.5	<0.1	<1.3	<3.0	
383.0	D	10.0	2.5	0.10	1.3	3.0	0.15 Sn
384.0	D	11.0	2.0	<0.3	<1.3	<3.0	0.35 Sn
390.0	D	17.0	4.5	0.55	<1.3	<0.1	<0.1 Mn
413.0	D	12.5	<0.1	<0.10	<2.0	-	
443.0	S,P	5.25	<0.3	<0.05	<0.8	<0.5	

(a) Remainder : Aluminum and other impurities
(b) S, Sand Casting; P, Permanent Mold Casting:
D, High Pressure Die Casting

Strengthening of Al-Si alloys is achieved by adding small amounts of Cu, Mg or Ni. In this family of alloys of hypoeutectic composition, silicon provides good casting properties and copper improves tensile strength, machinability, high temperature properties, and thermal conductivity at the expense of a reduction in ductility and corrosion resistance. Alloy 319.0 is used extensively for sand and permanent mold casting, while the 380.0 alloy has been used for many years as the principal high pressure die casting alloy. Generally 319.0 and 380.0 alloys are supplied in the as-cast temper, but strength and machinability of a 319.0 alloy can be improved by T6 or T5 heat treatments.

1.6 Eutectic Aluminum-Silicon Alloys

Binary aluminum-silicon alloys close to the eutectic composition (12% Si) exhibit, in the unmodified state, an acicular or a lamellar eutectic silicon well dispersed throughout the aluminum matrix (Figure 1.3a). Because of non-equilibrium cooling and slight variations in composition, the presence of polyhedric primary silicon particles is also observed frequently. The addition of 0.02% strontium results in a full modification with a completely fibrous structure (Figure 1.3b). Modification causes the alloy to become slightly hypoeutectic with the result that aluminum dendrites appear more frequently in the microstructure.

(a)

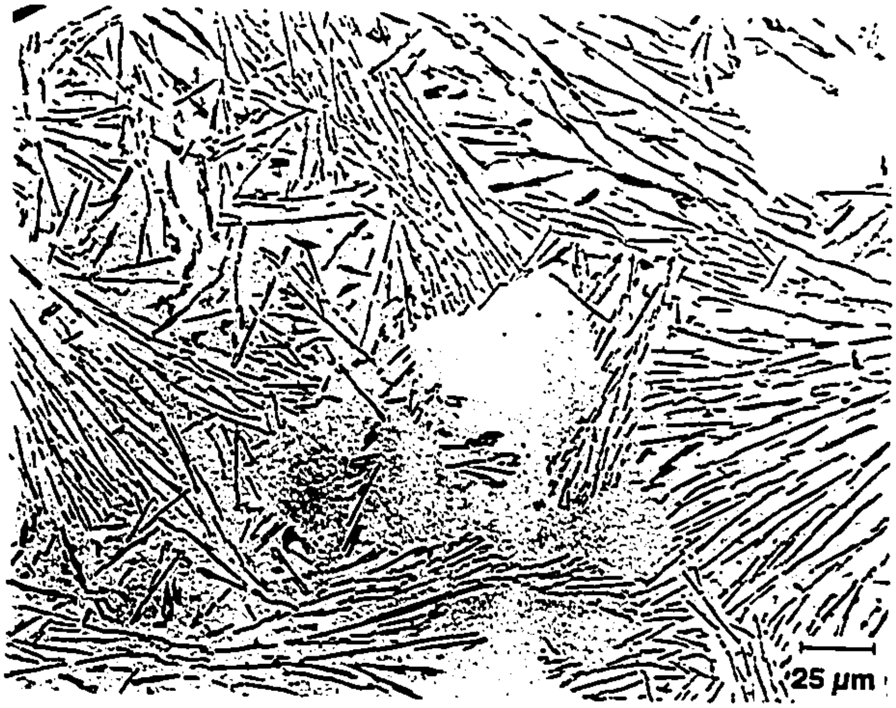

(b)

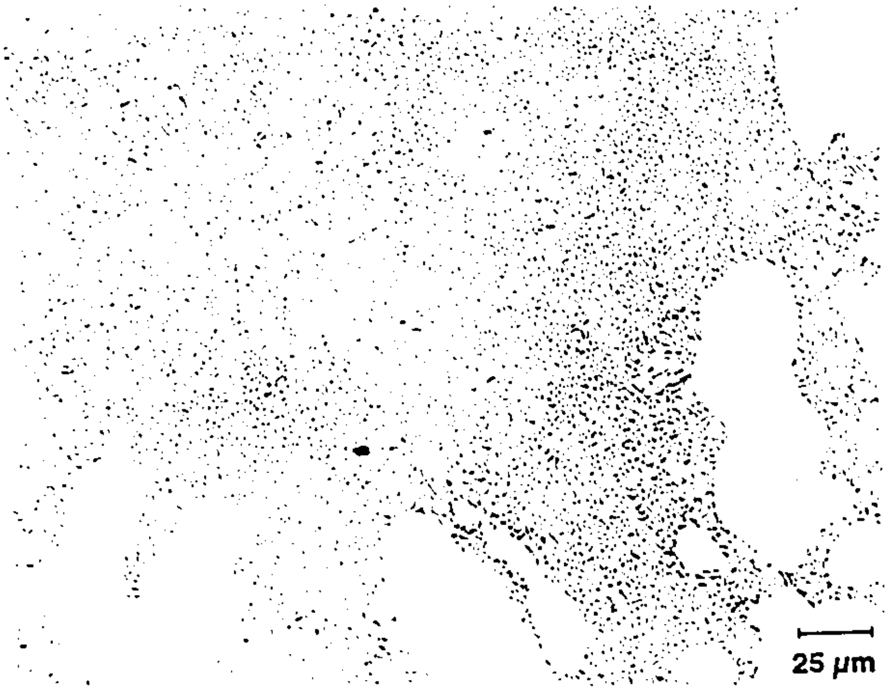

Figure 1.3 : Microstructure of 413 alloy. (a) Unmodified
(b) Fully modified with 0.02% Sr (400X)

1.7 413 Aluminum Alloy

Alloy 413 is a general-purpose alloy with good characteristics for casting large, intricate parts with thin sections. Mechanical properties are good. 413 alloys are used in the die casting and permanent mold processes and have good castability. Since the aim of the present work (which will be discussed in the following sections) is to study the formation and growth of iron-intermetallic compounds in aluminum-silicon alloys, a 413 die-cast alloy was chosen because it contains a high iron concentration (1.2% iron). The chemical composition specification limits for the 413 group of alloys are presented in Table 1.2.

Table 1.2 : Chemical Composition Limits of 413 Group of Alloys [ref.10]

Alloy*	Elements (wt%)						
	Si	Fe	Cu	Mn	Mg	Ni	Zn
413.0	11.0-13.0	2.0	1.0	0.35	0.10	0.50	0.50
A413.0	11.0-13.0	1.3	1.0	0.35	0.10	0.50	0.50

* Both alloys used in : die casting

The physical and mechanical properties of the alloy are listed below [10,11] :

Physical Constants :

Density, kg/m^3	2657
Coefficient of Thermal Expansion, μm/m.K	20.4
Specific Heat, J/kg.K	963
Latent Heat of Fusion, Kj/kg	389
Thermal Conductivity, W/m.K	121
Electrical Conductivity, %IACS	31
Electrical Resistivity, nΩ.m	55.6

Fabrication Characteristics :

Permanent mold casting and die casting.

Melting Temperature	650 to 760°C
Die Casting Temperature	635 to 704°C

Castability :

The fluidity, resistance to hot cracking and pressure tightness of alloys 413.0 and A413.0 are all excellent.

Thermal Treatment :

Stress Relieving

To reduce internal stresses, heat at 177-260°C for 4-6 hr. Cool in still air.

Annealing

To increase ductility, heat at 260-371°C for 4-6 hr. Cool in the furnace or in still air.

Machinability :

Because of the abrasiveness caused by the high silicon content of these alloys, tungsten carbide (or better) tooling is recommended. Otherwise, the alloys have good machinability.

Weldability :

These alloys have good welding characteristics in arc, resistance or gas methods. Brazing is not recommended but is sometimes performed on a limited basis.

Mechanical Properties :

Table 1.3 : Typical Mechanical Properties of 413 Alloy.(as cast)

Alloy	Tensile Strength (MPa)	Yield Strength (MPa)	Elongation % (a)	Shear Strength (MPa)	Fatigue Strength (MPa),(b)
413.0	300	140	2.5	170	130
A413.0	290	130	3.5	170	130

(a) in 50 mm or 2 inches , (b) at 5 × 10^8 cycles

Corrosion Resistance :

Corrosion resistance of alloys 413.0 and A413.0 are very good. Chemical conversion coatings are often used to further increase resistance.

Applications :

These alloys are used for miscellaneous thin-walled and intricately designed castings, and other applications where excellent castability, resistance to corrosion and pressure tightness are required. The alloys are recommended for architectural, marine, food and dairy equipment applications, pressure tight parts, large instrument cases, typewriter frames, dental equipment, engine parts, and pistons.

1.8 Objectives of the Present Work :

Since 1945, the growth of aluminum casting in the U.S. has been mainly due to the expansion of the permanent mold and high pressure die casting industries. Between 1955 and 1986 production of high pressure die castings increased from 178,000 tons to 825,000 tons which corresponds to an average annual growth rate of 11.7%. The rapid expansion of high pressure die casting production can be directly related to the automotive industry especially in a country like Japan where the growth rate over the last 17 years was 13.8% on an average annual basis.

As discussed in earlier sections, impurity elements have a major role in die casting alloys (e.g. 413). One of the sources of impurities is recycled materials. Increased activity in the recycling of spent automobiles, in order to cut down the alloy production cost, has caused the iron level to rise as high as 1.5 to 2.0%. Unlike magnesium and other elements, iron cannot be readily removed from molten aluminum by conventional foundry treatments.

On the other hand, an iron content up to 1.3% is beneficial to die cast parts in terms of improved strength, hardness, and tendency toward hot cracking. The high cooling rate of the die casting process causes iron compounds to be refined. Iron also reduces the tendency of the metal to weld or solder to the die surface, which can cause tearing of the casting surface. However, higher iron contents can cause problems of sludging in holding furnaces or where the melt operating temperature is low. Sludge consists of complex intermetallic compounds which are deleterious to the mechanical properties of cast parts. In order to widen the scope of application of die casting alloys, it is essential to study the influence of various operating parameters on the formation and growth of these intermetallic compounds.

In the present work the 413 type of alloy is chosen for study due to its popularity among aluminum-silicon alloys for its excellent castability and because it contains a high level of iron (1.2 wt%) and high silicon content (12 wt%). The aim of the present work is to carry out a comprehensive investigation on the formation and growth of complex intermetallic compounds in 413 alloys. The main goals of the present study are (i) to understand the influence of important metallurgical parameters such as *melt chemistry, holding temperature, holding time* on the formation of intermetallics in the liquid metal and *the effect of cooling rate during solidification* on the formation of different morphologies of intermetallic compounds; (ii) to discover the *effect of time and the rate of gravity segregation* of intermetallic compounds in a stagnant liquid metal; (iii) to develop *a new technique to modify or eliminate the complex intermetallic compounds* in commercial aluminum alloys to reduce the negative effects of iron-intermetallics.

In order to fulfil the broad objectives of the present work, the study is divided into five different phases as follows :

Phase I : Phase I includes studies on; the effect of melt chemistry on the formation of intermetallic compounds; the influence of iron and manganese concentration on the morphology of complex intermetallics; the relation of volume fraction, number of particles, and size of different morphologies with iron and manganese content.

Phase II : The kinetics of the formation of complex intermetallic compounds is the subject of phase II. This includes an understanding of the relation between the temperature of sludge formation and the iron concentration in Al-Si alloys; the stoichiometry of different morphologies of intermetallic compounds; the influence of temperature, time, and iron concentrations on the volumetric changes of intermetallics.

Phase III : The subject of phase III is the effect of solidification conditions on the formation and morphology of intermetallic compounds including an investigation of the influence of cooling rate on the volume fraction, number, and size of various morphologies.

Phase IV : Gravity segregation of complex intermetallic compounds in liquid aluminum-silicon alloys is investigated in phase IV. This includes the effect of settling time and location in the melt on the volume fraction, number, size of intermetallics, and concentration of elements.

Phase V : Modification of intermetallic compounds by strontium in aluminum-silicon casting alloys is the objective of phase V.

Chapter 2

Literature Survey

2.1. Introduction

Cast aluminum alloys have widespread applications, especially in the aerospace and automotive industries. These foundry alloys possess excellent tensile and fatigue properties and good corrosion resistance. The major alloying element, silicon, imparts good castability and resistance to hot tearing. Also, since silicon increases in volume during solidification, the susceptibility of the castings to shrinkage defects is reduced. Consequently, alloys containing silicon are ideally suited for high-volume production in the aluminum foundry.

In most cast aluminum alloys, solidification begins with the development of a dendritic network of primary (α) aluminum. The secondary dendrite arm spacing (DAS) is essentially determined by alloy composition, cooling rate, local solidification time and temperature gradient. Among the primary alloying elements, silicon has been reported to have an influence on DAS.[12] Increasing the silicon content leads to a decrease in the secondary dendrite spacing. It has been shown that DAS varies with cooling rate in alloy A356.0 according to the relation :[13]

$$\log(dT/dt) = -[\log(DAS) - 1.66]/0.40$$

where dT/dt, the cooling rate, is given in °C/s. and DAS is in micrometers. The secondary dendrite arm spacing controls the size and the distribution of porosity and second phase constituents are dispersed more finely and uniformly as DAS decreases. This refinement of the microstructure leads to a substantial improvement in mechanical properties.[12,14,15]

2.2. Aluminum-Silicon Alloys

Alloys with silicon as a major alloying ingredient are by far the most important commercial casting alloys, primarily because of their superior casting characteristics in comparison to other alloys. A wide range of physical and mechanical properties is afforded by these alloys. Binary aluminum-silicon alloys combine the advantages of high corrosion resistance, good weldability, and low specific gravity, but castings of these alloys are somewhat more difficult to machine than the aluminum-copper or aluminum-magnesium alloys.[1]

Aluminum-silicon alloys which are widely used to produce a large number of components for the automotive industry usually contain some transition metals such as manganese, iron, and chromium. These elements exist in the alloy either as impurities or as intentional additions, and can react in the liquid phase to form complex intermetallic compounds. One of the most harmful impurity elements in aluminum alloys is iron, which together with aluminum and silicon forms several compounds which cause a deleterious effect on the mechanical properties of the alloys being produced.[16,17,18]

2.3. The Effect of Melt Chemistry

The chemical composition of the melt has a significant influence on microstructure and mechanical properties in the cast component. In Al-Si alloys of commercial importance, there are a number of naturally occuring impurities and great care must be exercised in minimizing their concentration to produce premium quality castings. Iron is one of the most important elements to control because it forms brittle intermetallic compounds which seriously impair ductility of the alloy.

2.3.1. The Influence of Iron

As iron can be readily picked up by aluminum from numerous sources, tools, scrap, etc., the limit can be easily exceeded if proper care is not exercised to avoid contamination. With the current accent on recycling of used products there is an increased risk of metal contamination.[19,20]

Bonsack[18] says that iron is probably the most undesirable impurity in binary Al-Si alloys. Iron forms a ternary eutectic with Al and Si that contains 87% Al, 12.5% Si and 0.5% Fe. According to Bonsack[18] any amount of Fe over 0.5% will be present as Al-Fe silicide in large platelets(needles) which, up to about 0.8% Fe, increase strength and hardness but slightly reduce ductility. Above 0.8% Fe, the strength and elongation drop rapidly. Grand[21] states that increasing Fe from 0.50 to 1.2% in Al-13% Si alloy dramatically reduces the mechanical properties, particularly elongation. It is also reported[22] that elongation and Charpy impact strength were decreased by adding iron. The elongation and impact values of Al-5% Si are 13% and 18J at 0.75% Fe and 10% and 10J at 2.05% Fe.

The solubility of iron and other alloying elements in aluminum is very low. As a result of this, during solidification, liquid in the interdendritic regions becomes enriched with alloying materials, and iron forms complex intermetallic compounds with aluminum, silicon, manganese, and chromium. These are insoluble complexes and their volume percentages increase with an increase in iron content. In die-casting alloys, a higher percentage of iron is tolerated. At the high cooling rates prevailing in the die-casting process, iron compounds are refined.[23] In fact, an iron content up to about 1.3% is beneficial because it helps to limit the soldering effect of the die cast metal to the die.[6,23] Iron is attacked by molten aluminum, and although dies are protected by lubrication coatings, areas opposite the gate affected by turbulence of the injected metal become roughened and tend to adhere to the die cast metal. The presence of iron in the alloy reduces this tendency.

It has been reported that the Al-Si-Fe eutectic composition occurs at about 0.8% Fe. When Fe is alloyed to somewhat above this level, the molten metal has little or no tendency to dissolve die steel while the two materials are in intimate contact. Thus, the higher iron content of the alloy reduces the solution potential for the iron components of the casting machine and die, and for this reason, most aluminum pressure die casters desire that their alloys contain between 0.8 and 1.1% iron.[19,22,24,25,26,27] However, the iron content should not be higher than the specified amount otherwise iron creates complex intermetallic compounds with aluminum, silicon, and manganese.[6,28] These compounds act as hard spots and have a detrimental influence on mechanical and physical properties of die-cast parts. It was found that lowering of the iron content resulted in a marked improvement in tool life.[29,17]

Many authors have mentioned the influence of iron on mechanical properties at room temperature; however, Al-Si alloys also have applications at high temperature, as for example in pistons. The present information[30,31,32,33] shows that iron can dramatically increase the tensile strength and yield strength of Al-11.5% Si alloy at 316°C. Some research[32] indicates that a certain amount of iron is of benefit to the creep resistance of an Al-Si alloy.

Increasing iron from 0.50 to 1.20% in an Al-13%Si casting alloy dramatically reduces the mechanical properties, particularly the elongation because of needle or platelet phase formation.[19,34] The platelet phases, which appear as needles in the microstructure, act as stress raisers which contribute to the brittleness of the material. In addition to this effect on mechanical properties, large iron-rich needles which form early in the solidification process tend to prevent the flow of liquid metal through the feeding channels and may cause unsoundness.[19,35] Eklund[3] reported that intermetallic compounds in as cast aluminum alloys may frequently appear in contact with porosity. He showed that compounds of the AlFeSi and AlFeMnSi type favour the formation of shrinkage porosity by blocking the interdendritic feeding channels of hypoeutectic aluminum-silicon alloys.[3] It is therefore important to know how to avoid, or at least control, the precipitation of iron containing intermetallic compounds during alloy solidification.

2.3.2. The Influence of Manganese

Manganese is the most common alloying addition which is used to neutralize the effect of iron and to modify the morphology and type of intermetallic phases.[13,19,36] Mondolfo[30] indicates that chromium can act in a similar manner to manganese, and each element is able to change the morphology of the iron-rich phase from brittle platelets to a more cubic form or to globules. These morphologies improve tensile strength, elongation, and ductility.[22,24,36] Manganese is added to many of the alloys for two purposes : 1) increase of high temperature strength and creep resistance through the formation of high melting compounds; $Cu_2Mn_3Al_{20}$, Mn_3NiAl_{16}, $MnCrAl_{12}$, and also $(FeMn)_3Si_2Al_{15}$, and possibly more complex ones with chromium and nickel; 2) correction of the embrittling effect of iron.

Several authors attribute the beneficial influence of Mn additions in Al-Si alloys to the change of the Fe compounds to less harmful types and shapes.[12,18,21,36,37] Bonsack[18] shows that the presence of 0.5% Mn in an Al-13% Si alloy with as much as 1.5% Fe transforms the harmful AlFeSi-needles into the relatively harmless Chinese script. Colwell and Kissling[22] state that Mn, in the Mn:Fe ratio of 1:2, breaks up the Fe needles and helps both the mechanical properties and castability. An addition of 0.35% Mn to 380 and 413 alloy die castings was investigated as a means of improving machinability and pressure tightness. While machinability was apparently unaffected, pressure tightness was measurably improved.[20] Manganese and chromium additions are also used for the phase modification in silumins (Al-13% Si master alloy) to provide the appearance of $(FeMn)_3Si_2Al_{12}$ and $(FeCr)_4SiAl$ phases, which are crystallized in Chinese script morphology.[38]

Quadt[39] determined the effect of Fe and Mn on the mechanical properties of a sand-cast alloy containing 5% Si-1% Cu-0.5% Mg. The properties were in general reduced when Fe was increased from 0.3 to 0.8% in the absence of Mn. When Mn was added, a distinct improvement in properties was noticed which made them generally equivalent to those of the original alloy with low Fe and low Mn. When 0.37% Mn was present, Fe up to 2.4% only caused a slight deterioration of the properties. Thus, Mn changes the harmful needle-like compound into the less harmful Chinese script. Quadt[39] concludes by saying that Mn should probably be specified in the range 0.3 to 0.7%, and Fe content in castings should be limited to 1%.

The other usage of manganese in aluminum casting alloys has been the enhancement of elevated temperature properties in compositions commonly referred to as heat resistant. Alcoa's research in hypereutectic Al-Si alloys nearly always led to the addition of from 0.7% to 1.0% manganese.[20] The studies on which final compositions were based suggested that the effects of manganese were most pronounced in improved elevated temperature strength and hardness with little or no sacrifice in other properties and characteristics.

Manganese is also used in wrought alloys. The role of manganese in wrought alloys is improved strength as a function of work hardening. In wrought applications, manganese occurs in the microstructure in the form of an extremely stable, essentially insoluble dispersoid. It significantly improves the rate of work hardening for the development of an attractive combination of mechanical properties after hot and cold working.[20] The role of manganese in casting compositions is considerably different because of the absence of work hardening. In the absence of manganese, aluminum-iron-silicon constituent is normally present in platelet or needle morphologies detrimental to fluidity, feeding characteristics, and accordingly their presence increases shrinkage and shrinkage crack tendencies. When manganese is present, the intermetallic phase assumes a more globular form. For this reason, it is common practice to observe a 2:1 iron to manganese ratio in composition control for many alloys.

2.3.3. The Role of Other Alloying Elements

Silicon is usually added for castability, as many of the intricate shapes which are common today could not be cast without it. Unfortunately, silicon adversely affects machinability.[17,40] Increasing silicon content appears to lower the temperature at which iron-rich primary crystals begin to separate. On the other hand, silicon additions lower the liquidus temperature of the base alloy more than they lower the temperature at which iron and manganese separate in the melt. Hence at constant superheat, increasing silicon restricts the permissible iron and manganese content of the alloy.[41]

Glaisher also indicated that an increase of silicon content lowers the "apparent liquidus", giving longer time in the mold before solidification if the same pouring temperature is used. This effect of high silicon content in promoting gravity segregation is likely to be greater in castings of thick section and may be reduced by lowering the pouring temperature.[41]

Small amounts of copper, nickel, magnesium and zinc have been reported to have little effect on the degree of segregation.[41] The normal variations in these elements may therefore be expected to be unimportant in this connection. Colwell and Kissling indicated that a zinc content of about 0.5% helped machinability and had no harmful effects; magnesium in amounts greater than about 0.10% was harmful both to castability and to the mechanical properties obtained.[22]

2.4. Intermetallic Compounds

Complex intermetallic compounds are brittle; they act as stress raisers and are points of weakness which reduce the strength and ductility of the alloy, the reduction depending on the amount present and on the size and type of crystals.[19] Kaye[5] also reported that oxide films readily encourage the nucleation of intermetallic compounds with high hardness, particularly in pressure-die-cast aluminum-silicon-copper alloys containing high levels of iron, manganese or chromium.

It is worth to mention that a feature of aluminum alloy systems is the wide variety of intermetallic phases which occur because aluminum is highly electronegative and trivalent. The complete literature on intermetallic phases has been reviewed by Pearson.[42] Intermetallic phases in aluminum alloy systems have also been discussed as part of a wider review by Mondolfo.[30] The stability of such phases and the narrowness of their compositional range is determined by size and valency factors. In binary systems, some phases can be exactly stoichiometric, for example, AlSb. Other systems can have a very narrow compositional range not containing the composition of their formula, for example $CuAl_2$, thus containing lattice defects. Others such as Ag_2Al show a wider compositional range. Transition metals often exhibit a succession with well defined and sometimes complex stoichiometry. The origin of aluminum-transition metal and silicon-phases is still being investigated. There is some evidence that the valency electrons are absorbed into the d-shell of the transition metals and are replaced by electrons from the aluminum shell.[1] Transition metals also exhibit frequent metastability, in which one phase introduced during fast solidification transforms in the solid state to another, for example, $FeAl_6 \rightarrow FeAl_3$, or a metastable variant such as $MnAl_{12}$ precipitates from supersaturated solid solution.

In ternary alloys, a few intermetallic phases of other binary systems can form a pseudobinary eutectic with primary aluminum solid solution, for example, Mg_2Si or $MgZn_2$. In quaternary systems, intermetallic phases of the respective binary and ternary systems are occasionally isomorphous, forming continuous series of solid solutions in equilibrium with aluminum solid solution. An important example is in the aluminum-iron-manganese-silicon quaternary system; here the stable phase $(FeMn)_3Si_2Al_{15}$ (body-centered cubic) can vary from $Mn_3Si_2Al_{15}$, $a = 12.652$ Å to $(Fe_{0.9}Mn_{0.1})_3Si_2Al_{15}$, a=12.548 Å. The stable phase of the closest composition in aluminum-iron-silicon is Fe_2SiAl_8 (hexagonal); the hexagonal → cubic transition is also accomplished by small additions of vanadium, chromium, molybdenum, and tungsten, and larger additions of copper.[43] Such chemical stabilization effects, coupled with the metastability introduced by casting, frequently cause a complex alloy structure.

2.5. Aluminum-Iron-Silicon System

2.5.1. AlFeSi Phases

A wide range of AlFeSi particle types is reported in the literature. [13,25,30,43,44,45,46,47,48,49] These can generally be divided into three different morphologies :

1. polyhedral crystals (and star-like), (Figure 2.1a)
2. Chinese script (Figure 2.1b)
3. needle-like (thin platelets), (Figure 2.1c)

(a)

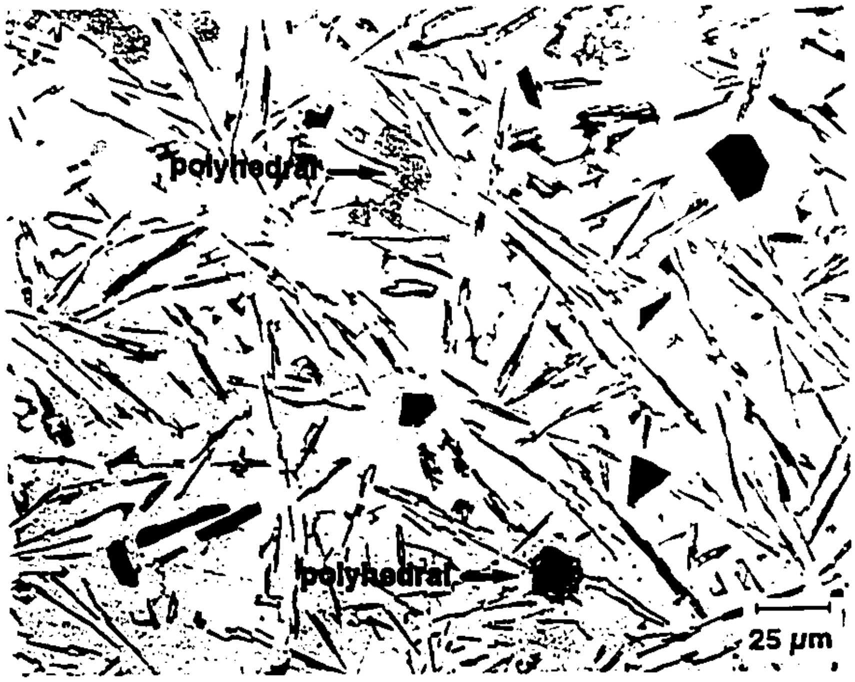

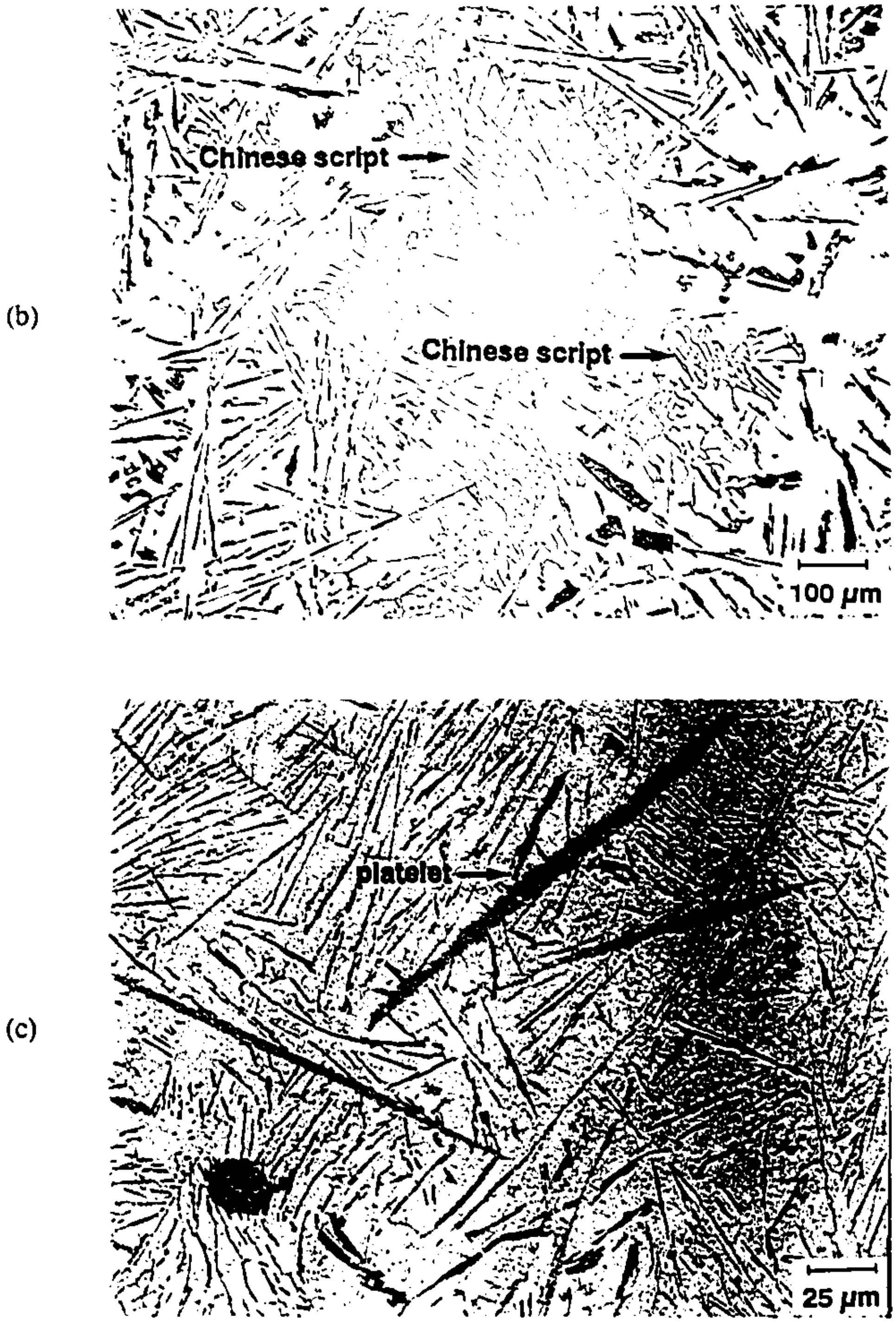

Figure 2.1 : Intermetallics in 413 alloys a) Polyhedral particles (400X)
b) Chinese script (100X) , c) Platelet (needle-like); (400X)

Although investigation of the AlFeSi system began in 1921 [50], because of its complexity the entire system is still unclear.[51] Construction of the phase diagram is made more difficult by the fact that the prevailing peritectic reactions do not take place completely. Solidification is of a non-equilibrium character in almost every case, and while carrying out heat treatment, the equilibrium state is approached very slowly.

In this system, the range of 0 to 35% Si and 0 to 30% Fe has been investigated by Gwyer and Phillips[52] by means of thermal analysis and optical metallography. Within this range the θ-AlFe, α-AlFeSi, β-AlFeSi and δ-AlFeSi phases have been identified and their primary crystallization range and their transformation temperature have been determined. (The phases are designated according to the system of Phillips and Varley.[53]) The authors emphasized that the peritectically solidifying phases formed a crust-like encasement around each other thus excluding the earlier solidified phases from the system.[52] Therefore, in the cast state, more phases may exist simultaneously than ought to be possible according to the phase rule in equilibrium.

Armand[54] distinguished between three independent phases within the α-AlFeSi field and designated them α_1, α_2 and α_3. Similarly, Munson[43] revised the range of 0 to 16% Si and 0 to 12% Fe. In the ternary alloys within the α-field he found two phases which were earlier described by Armand[54] as α_2 and α_3, but he designated them as hexagonal α-AlFeSi and β-AlFeSi. He established that the cubic α-AlFeSi (that is the α_1 phase of Armand) can form in alloys containing small amounts of transition metals (manganese, chromium).

In another investigation, the equilibrium phases in low-alloyed Al-Fe-Si material are reported to be : Θ-Al_3Fe (monoclinic), α-Al_8Fe_2Si (hexagonal) and β-Al_5FeSi (monoclinic). The α-phase has also been reported to have the composition $Al_{12}Fe_3Si_2$ (30.7% Fe, 10.2% Si).[48] These phases are dominant in slowly cooled castings, whereas the metastable phases Al_6Fe (orthorhombic) and α'-$Al_{20}Fe_5Si_2$ (cubic) only occur in rapidly-quenched material.[13,26,30,43,45,48,55] Since many commercial aluminum alloys contain manganese, or chromium, either as impurities or intentional additions, it is to be expected that the cubic α-AlFeSi phase will be found in these alloys rather than the hexagonal α-AlFeSi phase.[43,51]

Mondolfo[30] reported two other phases, $Al_4FeSi_2(\delta)$, in high silicon alloys, and $Al_3FeSi(\gamma)$ in high-iron and high-silicon alloys.[30,51] Phragmen[49] has indicated that α-AlFeSi has 31.9% Fe and 5.57% Si ; β-AlFeSi has 27% Fe and 13.5% Si. Awano et al.[56] also showed that the AlFeSi compounds in a Chinese script form had the composition of $Al_{5.9\text{-}6.4}Fe_{1.3\text{-}1.5}Si$ with higher iron content and lower silicon contents. The crystals of β-AlFeSi appear in needle-like form [44,47,57]. Other investigators have reported widely different formulae for these compounds with the result that no reliance can be placed on these formulae.

The fields of existence of the ternary phases in the solid state are mostly outside their range of primary crystallization, and completion of peritectic reactions is necessary for equilibrium to be established. For this reason most commercial alloys are not in equilibrium and it is common to find alloys in which Al_6Fe, Al_3Fe, Al_8Fe_2Si, Al_5FeSi and Al_4FeSi_2 may coexist with one another and with silicon. Often in heat treated alloys equilibrium may be reached by diffusion in the solid state, and Al_5FeSi may be found in the Chinese script shape characteristics of Al_8Fe_2Si. Thus, identification of the phases from the shape alone may be misleading.[30]

A.L.Dons has studied the crystal structure of AlFeSi compounds in two DC cast and six strip cast alloys. He has compared them with structures reported by other investigators.[47] A number of intermediate non-equilibrium phases which can form in Al-Si-Fe alloys have been also reported elsewhere.[16,26,55] Moreover, three new intermetallic phases have been identified by Liu et al.[55] in dilute Al-Fe-Si alloys. These are termed Al_pFe, q_1-AlFeSi, and q_2-AlFeSi. As a summary, a list of the crystal structures of the intermetallic phases is given in Table 2.1. Several iron-rich intermetallics have also been extracted and analyzed.[58,59,60,61] In most cases, these particles were extracted by dissolution of aluminum matrix in acids [60] or in alcohol (Butanol).[58,59]

Table 2.1 : The Crystal Structures of the Intermetallic Phases

Name	Structure	a (Å)	b (Å)	c (Å)	β (°)	Reference
Al_3Fe	monoclinic	15.49	8.08	12.47	107.5	[42,48]
Al_mFe	bct	8.84	-	21.6	-	[62]
Al_xFe	monoclinic	21.6	9.3	9.05	94	[63]
Al_6Fe	C-centred	6.49	7.44	8.79	-	[64]
α	bcc	12.58	-	-	-	[16,42], as c-AlFeSi [49]
α'	hexagonal	12.3	-	26.2	-	[42], as α-AlFeSi [48]
α''	hexagonal	12.6	-	37.0	-	[16]
α_V	monoclinic	8.47	6.35	6.10	93.4	[65]
α_T	monoclinic	28.1	30.8	20.8	97.74	[66]
β	monoclinic	6.12	6.12	41.5	91	[42,48]
β'	monoclinic	8.9	4.9	41.6	92	[16]
q_1-AlFeSi	C-centred	1.27	3.62	1.27	-	[55]
q_2-AlFeSi	monoclinic	1.25	1.23	1.93	109	[55]

2.5.2. Alpha and Beta Intermetallics

Of the many AlFeSi intermetallics, the most important are generally thought to be the α and β phases. Al_8Fe_2Si (31.6% Fe, 7.8% Si), often reported as $Al_{12}Fe_3Si_2$ (30.7% Fe, 10.2% Si), with a probable range of existence of 30-33% Fe, 6-12% Si, is hexagonal; parameters $a=12.3 \times 10^{-10}$m , $c=26.3 \times 10^{-10}$m; density 3.58 g/cm^3. This is the phase that appears as 'Chinese script' and is commonly referred to as α-AlFeSi (Figure 2.2b). Al_5FeSi (25.6% Fe, 12.8% Si), with a range 25-30% Fe, 12-15% Si, is monoclinic; lattice parameters $a=b=6.12 \times 10^{-10}$m, $c=41.5 \times 10^{-10}$m, $\alpha=91°$; density 3.30-3.35 g/cm^3.[30,67,68,69,70,71] This needle-like phase is the β-AlFeSi (Figure 2.2c).

The cubic α-phase, which is often observed in commercial Al-alloys, forms both as eutectic colonies on grain boundaries and in the interdendritic spacings, as well as in the interior of the dendrites. In the latter case the particles were more or less spherical with a distinct internal subgrain/grain boundary network, giving the particles the appearance of a polygonized structure.[16,65]

Conflicting data have been reported about α-AlFeSi.[43] The phase was designated α(FeSi) by Phillips[72] and c-AlFeSi by Phragmen.[49] The latter found that c-AlFeSi had a cubic unit cell a=12.58 Å and was isomorphous with the ternary c-AlMnSi, described by Phillips as α(MnSi). Pratt and Raynor[48] found that α-AlFeSi had a hexagonal unit cell with lattice parameters $a=12.3 \pm 0.1$ Å, $c=26.2 \pm 0.2$ Å. Munson[43] confirmed that pure α-AlFeSi had a hexagonal unit cell; crystals with a cubic unit cell were formed only when certain other transition metals were present at more than a critical concentration.

According to Munson[43] and Mondolfo[30], the hexagonal α_H-AlFeSi crystallizes in high purity alloys with compositions near to the Al-corner of the AlFeSi system, and the cubic α_C-AlFeSi phase forms only if other alloying elements or impurities are also present.[73] It has been reported that the thermodynamically stable α-AlFeSi which is hexagonal becomes unstable with very small amounts of Mn. The cubic structure has been confirmed as the stable phase up to an Fe:Mn ratio of 4:1, but its unit cell volume is so small as to suggest four vacancies per unit cell.[74]

The β-AlFeSi crystal phase shows lateral or faceted crystal growth. These crystals are bounded by slowly growing planes of low indices. These surfaces are relatively "smooth" on the atomic scale, any further atoms from the liquid find only few possibilities to join the interface and so their growth is restricted and therefore slow.[73] α_C-AlFeSi phase grows in irregular, curved crystal form conforming to the complicated shape of the interdendritic spaces during solidification. The form of the crystals is controlled by temperature gradient and by the diffusion of atoms in the liquid. During crystallization, atoms can add on to the solidified part when they arrive at the interface. In this case there is a "rough" interface between the solid and liquid.[73]

The effect of cooling rate on the aspect ratio of β-phase has been explained[25] by referring to the growth mechanism of this phase i.e. the phase is non-metallic and thus solidifies with a faceted interface, which is comparable to silicon growth in aluminum alloys. However, despite the ability of silicon to branch and to keep up with the more kinetically mobile aluminum phase, the thin platelet intermetallic compound does not show any branching capability and thus is expected to be overgrown by the aluminum phase.

A reduction in ductility, fracture toughness and fatigue properties has been attributed to the precipitation of thin, coarse platelets of $FeSiAl_5$. The size and amount of platelets depends strongly on iron content and solidification rate.[75,76] Yeneva et.al.[46] have studied the appearance of iron intermetallic phases in Al-Si cast alloys at different iron concentrations. They showed that for a given concentration of manganese, the percentage of needle-like phase increases rapidly with increasing iron concentration as shown in Figure 2.2. At 0.9 wt% Fe nearly all iron containing precipitates are needle-like causing a decrease in the fatigue strength. Figure 2.3 shows the decreasing percentage of needle-like compound in Al-Si alloys with lower Si-content.

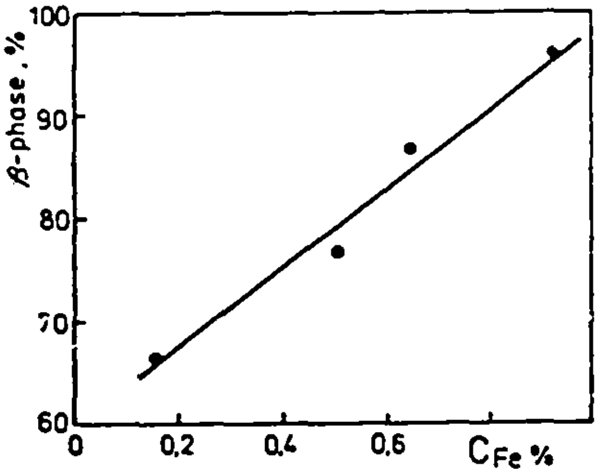

Figure 2.2 : Dependence of the percentage of β-phase vs. iron content [46]

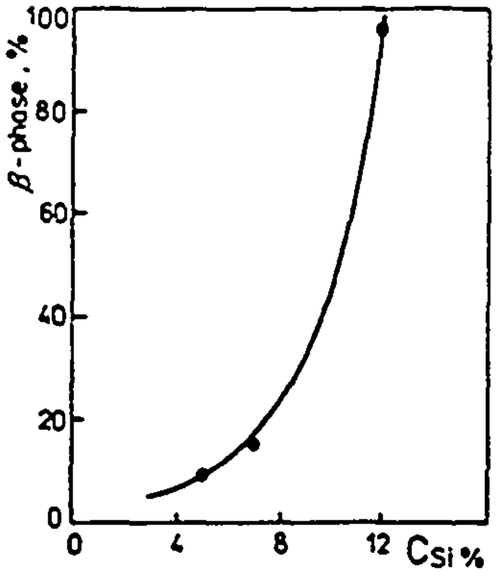

Figure 2.3 : Dependence of the percentage of β-phase vs. silicon content [46]

2.6. Aluminum-Iron-Manganese-Silicon System

2.6.1. AlFeMnSi Phases

In sand casting and permanent mold alloys, AlFeMnSi phases usually assume the shape of a snowflake, known as Chinese script (Figure 2.1b), because these alloys are usually cast above 677°C, preferably 788°C or even higher. When poured from these temperatures into a cold sand mold or a fast chilling permanent mold, the intermetallics become the snowflake like, desirable, strengthening, easy-to-machine crystals. However, die castings are most often cast at temperatures of 682°C or less. At these temperatures, iron complex compounds grow into hardspots.[17,77]

Iron forms $Al_{15}(FeMn)_3Si_2$ with manganese, often in the shape of Chinese script, thus removing the embrittling effect of Al_5FeSi.[30,41,66,78] Mondolfo[30] showed that if the total manganese plus iron content is above 0.8%, the $Al_{15}(FeMn)_3Si_2$ crystals are primary, and they appear as hexagonal globules (although the compound is cubic). These globules do not embrittle the alloy, but reduce appreciably the machinability; therefore, manganese content is often controlled for only partial correction of iron to prevent the formation of primary crystals.[30,79]

The range manganese 0 - 4%, silicon 0 - 4%, iron 0 - 4% has been studied in detail by Phillips and Varley.[53] Several additional alloys, in the neighbourhood of the ternary eutectic points, have also been investigated.[53] According to the literature, the following intermetallic phases can be found in cast Al-Si alloys which contain Fe and Mn: [29,43,44,46,49,53,80]

m-Al(Fe,Mn)Si, a needle-like phase (known as β-phase), which causes deterioration of the mechanical properties of the casting;

α-Al(Fe,Mn)Si phase appears in fine "Chinese script" form. It has a less significant influence on the tensile properties;

c-Al(Fe,Mn)Si particles in polyhedral crystal form (and star-like) are usually observed when the iron content is higher than 0.8 wt.% and Mn-content is moderate (0.2 to 0.3 wt.%).

Composition, shape, and dimension of these intermetallic phases depend on the crystallization conditions.[46]

Table 2.2 presents the electron microprobe analysis of the large, equiaxed particles which were believed to be c-AlFeMnSi in the microstructure of a commercial 380 alloy.[27,29] The shape of c-Al(FeMn)Si intermetallic compounds is shown in Figure 2.1. [40]

Table 2.2 : Composition (wt.%) of c-AlFeMnSi

Al	Fe	Mn	Si	Cr	Cu
62%	20%	6%	10%	1%	1%

This c-phase analysis agrees well with previous determinations of the composition of the c-phase by Phragmen [49] and by Pratt and Raynor [48]. It has also been reported that the star-like (polyhedral) intermetallic phase in alloy 339 has a composition corresponding to $Al_{12}(Fe\ Mn\ Cr)_3Si_2$. [81]

The two iron phases (m-and α-) were investigated[46], and their compositions are shown in Table 2.3. They indicate that even at low Fe and Mn concentrations (<0.15 wt%), quaternary phases are observed.

Table 2.3 : Composition (wt.%) of the Observed Iron Phases.

needle-like phase (m)				chinese script (α)			
Al	Si	Fe	Mn	Al	Si	Fe	Mn
58.25	15.85	21.2	4.01	61.1	7.4	21.27	10.23

The composition of the needle-like m-phase corresponds to the formula $Al_9(Fe,Mn)_2Si_2$, while α-phase's composition corresponds to $Al_{12}(Fe,Mn)_3Si$. However, other investigators state that the composition of α-phase corresponds to $Al_{15}(Mn,Fe)_3Si_2$.[30,36,82] The percentage of m-Al(Fe,Mn)Si depends on the crystallization rate, Si-concentration and the presence of modifying agents. It was found that decreasing solidification rate results in an increase of α-phase (Chinese script) content.[46]

Munson[43] showed that in quaternary aluminum-iron-M-silicon alloys (where M is another transition metal), the crystal symmetry of the primary "α" phase depends on the nature and amount of the quaternary addition. Vanadium, chromium, manganese, copper, molybdenum, and tungesten all cause the formation of a B.C.C. phase with a lattice parameter between 12.5 and 12.7 Å. That this phase has a body-centred unit cell was confirmed by electron diffraction.[43]

2.6.2. Solidification Process in Al-Fe-Mn-Si System

Backerud et al.[82] studied the conditions of formation of $Al_{15}(Fe,Mn)_3Si_2$ phase in the Al-Fe-Mn-Si quaternary system. In Figure 2.4 the composition of alloy 356.0 is indicated; it falls well within the standard specifications (shaded area (A)). The solidification process starts by formation of aluminum dendrites and the interdendritic liquid becomes successively enriched in iron and silicon according to path (1). The segregation line penetrates the $Al_{15}(Mn,Fe)_3Si_2$ surface and starts the second reaction, by which this latter phase is precipitated, path (2a). Some Mn is consumed, and we soon reach the valley between the two iron-bearing phases, $Al_{15}(Mn,Fe)_3Si_2$ and Al_5FeSi, and during the following reaction these two phases precipitate together along path (2b) until the eutectic composition (3) is reached. From there on, Al, Si and Al_5FeSi will precipitate together in the main eutectic reaction. In a similar way the first solidification events can be followed in the various alloys.[82]

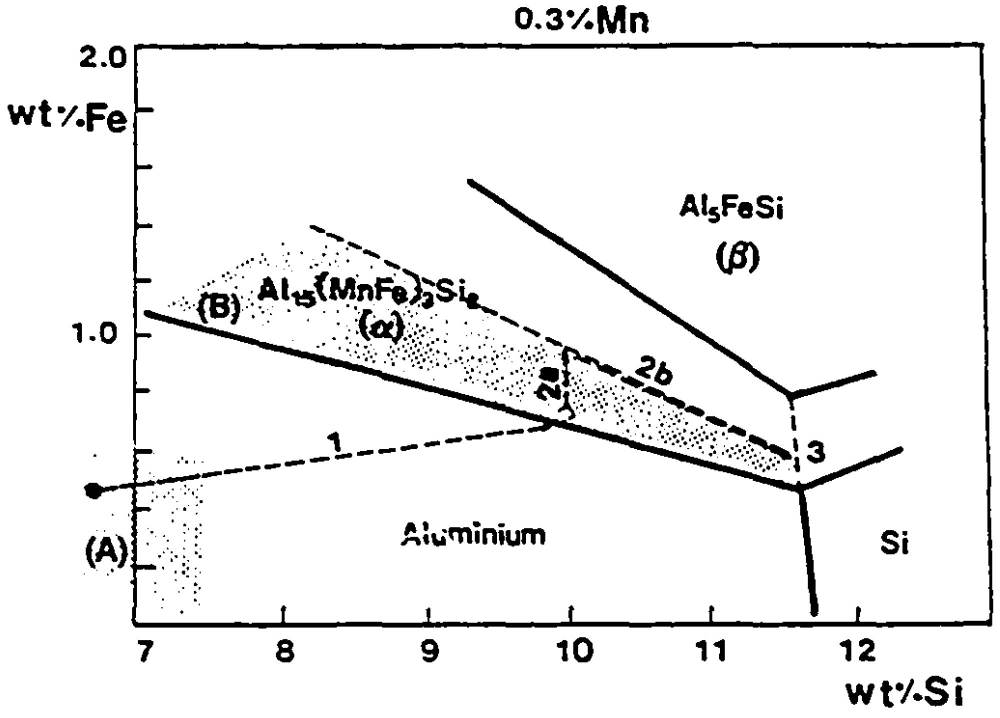

Figure 2.4 : Simplified phase diagram showing original composition of actual sample (representing alloy 356.0) and the segregation line followed by dendritic growth and precipitation of intermetallic phases.

The solidification of alloys in the Al-Fe-Mn-Si system may be divided into four different main events: ***pre-dendritic, dendritic, pre-eutectic*** and ***main eutectic***. The primary precipitation of phases other than aluminum dendrites, is called pre-dendritic. Tamminen[83] has explained the pre-dendritic precipitation of intermetallics for alloy 380. The chemical composition of the alloy is presented in Table 2.4. It is seen from Figure 2.4 that the composition of this alloy is in the region which may cause pre-dendritic precipitation of $Al_{15}Mn_3Si_2$ or even Al_5FeSi, during holding of the melt for extended periods of time before casting. A critical situation appears when holding the melt at low temperature, just above the melting point. At this temperature, crystals of the primary particles may start to grow, and as their density is higher than that of liquid aluminum, they sediment to the bottom of the holding furnace.

The pre-eutectic period takes place after the dendritic growth of aluminum dendrites. The reaction paths for these intermetallics will be different, depending on cooling rate.

Table 2.4 : Chemical Composition of Alloy 380

Alloy	Si	Fe	Cu	Mn	Mg	Ni	Zn	Sn
380.0	7.5-9.5	2.0	3.0-4.0	0.50	0.10	0.50	3.0	0.35
A380.0	7.5-9.5	1.3	3.0-4.0	0.50	0.10	0.50	3.0	0.35

Pre-eutectic and main Eutectic Reactions at low Cooling Rate

If the cooling rate is low enough, large Al_5FeSi intermetallics may start to form from liquid together with a further growth of aluminum and $Al_{15}Mn_3Si_2$.(see Figure 2.4) During the main eutectic reaction Al_5FeSi and silicon will form, partly directly from liquid phase, but also due to a reaction between liquid and $Al_{15}Mn_3Si_2$.

Pre-eutectic and main Eutectic Reactions at high Cooling Rate

At higher cooling rates, closer to die casting conditions, the precipitation of aluminum and $Al_{15}Mn_3Si_2$ continues until the main eutectic, without any formation of Al_5FeSi. In the main eutectic, aluminum and $Al_{15}Mn_3Si_2$ precipitate together with silicon. No formation of Al_5FeSi occurs, neither by precipitation nor by transformation of $Al_{15}Mn_3Si_2$.

Mascre[84] studied the Al-13% Si alloy with 0.55 to 1.20% Fe and up to 1.3% Mn using test bars cast in sand and in permanent molds. His metallographic examination revealed four phases in these alloys :

1) the alpha phase, which is a solid solution of aluminum containing small quantities of iron, silicon and manganese;
2) the silicon-rich phase, which, in fine lamellae, forms a eutectic with the alpha phase, or, in improperly modified alloys, exists as regular silicon crystals;
3) the "m" phase[49], which is the Al_5FeSi compound (β-phase) and exists in the form of long needles or platelets and is very brittle and detrimental to the properties;[30,36] and,
4) the "c" compound[49], whose crystals are compact and therefore less detrimental to the properties than the "m" compound.

He also studied the fields of primary solidification of phases alpha, "m" and "c". Figure 2.5 shows that the boundary positions depend on cooling rate and the Fe and Mn contents of the casting.[84] The diagram illustrates the compensating effect of Mn. For example, a sand-cast test bar with 1% Fe but no Mn will contain much brittle "m" compound and this will markedly reduce the tensile strength and particularly the elongation. If the same casting, again with 1% Fe, contained 0.6% Mn, the "m" compound would be replaced by the less damaging "c" compound and the properties would be improved. Mascre presents contour diagrams and, from these, he arrived at the following general "neutralization" formula for sand and permanent-mold castings :

$$\text{Mn}\ \% = 2(\text{Fe}\ \% - 0.5)$$

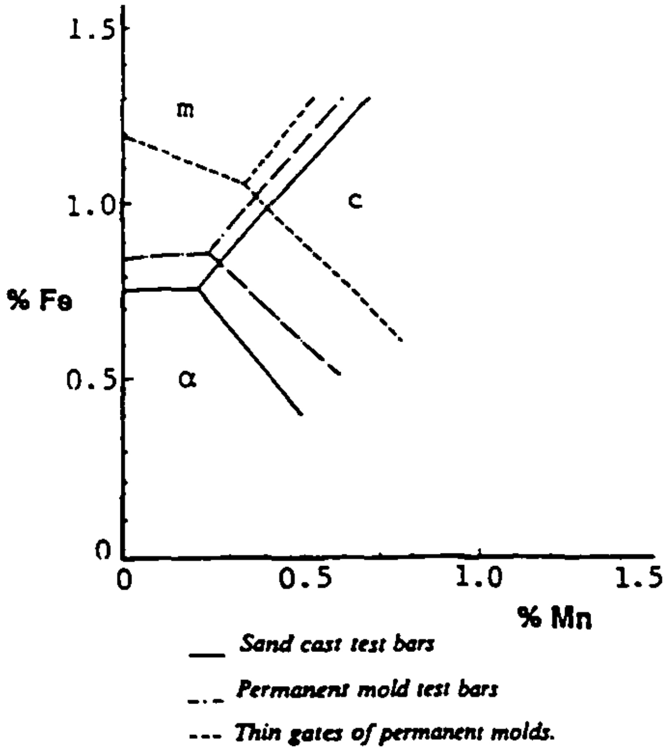

Figure 2.5 : Fields of primary solidification in Al-13% Si alloy containing Fe and Mn.[84]

Similarly, Mascre[84] explained the embrittling phenomenon of the alloy Al-13% Si having 0.55 to 1.20% Fe and up to 1.3% Mn, as follows : When sufficient Fe is present, constituent "m"- Al_5FeSi (known as β-phase)- exists in the primary form, i.e. it crystallizes before the Al-rich alpha phase. As shown in Figure 2.5, the Fe level at which Al_5FeSi appears depends on the cooling rate and the Mn level. In the absence of Mn, Al_5FeSi appears with about 0.75% Fe in sand cast test bars, and probably at somewhat lower Fe contents in large sand castings. However, in thin chilled sections, which cool rapidly, as much as 1.2% Fe may be present without causing the formation of the platelet phase.[84]

So far, the solidification sequence and especially the segregation phenomena have been described in relation to equilibrium phase diagrams. In real casting processes, however, kinetics factors are of importance, since they influence nucleation as well as growth of the various phases precipitated.[82] It is reported that the metallic phase, α-aluminum, grows more easily in its non-faceted manner than silicon crystals and most intermetallic phases, which grow by stepwise nucleation on specific crystallographic planes. But there are also differences in growth rate between intermetallic crystals. The cubic $Al_{15}(Mn,Fe)_3Si_2$ phase grows more easily than the monoclinic Al_5FeSi phase, and therefore dominates at high cooling rates, provided the chemical composition of the alloy permits formation of the former phase.[82]

Barlock and Mondolfo[45] showed that in the non equilibrium conditions, which result from commercial solidification rates, $FeAl_3$, Fe_2SiAl_8 and $FeSiAl_5$ can appear even if the Mn is higher than Fe but no other phases appear. Rapid cooling up to 10°C/s and superheating do not change substantially the structure. Interdenditic spacing and size of intermetallics decrease with increasing cooling rate and increased superheating.

2.6.3. Reactions in Al-Fe-Mn-Si System

When iron is present in aluminum-silicon alloys, it is usually as the $FeSiAl_5$ compound. This compound is brittle and has a relatively low bond strength with the matrix. The addition of manganese reduces this embrittling. In most manganese compounds that form in aluminum alloys, iron can replace large amounts of manganese without change of crystal type. The most common manganese compounds are $(FeMn)Al_6$ and $(FeMn)_3Si_2Al_{15}$ in copper-free alloys; $(CuFeMn)Al_6$, $(CuFeMn)_3Si_2Al_{15}$ and $Cu_2Mn_3Al_{20}$ in copper-bearing alloys. All of these phases form more or less equiaxed crystals and tend to solidify in the form of dendrites, with Chinese script type, thus eliminating most or all of the iron embrittling effect.[36]

The replacement of $FeSiAl_5$ by manganese compounds also increases the corrosion resistance at least in the copper-free alloys because the difference of potential between the iron-bearing compounds and the matrix is greatly reduced. Together with the improvement of ductility produced by the neutralization of the iron, manganese also produces a limited increase in strength and fatigue resistance.[36] If the iron content exceeds 0.45 wt%, it is reported that the manganese content should not be less than half of the iron.[19]

Binary and ternary phase diagrams have limited application when attempting to understand phase formation in commercial alloys of aluminum since these always contain appreciable amounts of other elements which substantially affect the structure. In Figure 2.6 are shown the liquidus and the solid state distributions of phases in the quaternary aluminum-iron-manganese-silicon system. None of the phases that appears is truly quaternary : the $(FeMn)_3Si_2Al_{15}$ is the ternary $Mn_3Si_2Al_{15}$ in which iron replaces up to 90% of the manganese so that its field extends far toward the Fe-Si side.[36] The stoichiometry of these phases is $(FeMn)_3Si_2Al_{15}$, with a composition range of 0-31% Fe, 2-29% Mn, 8-13% Si. $Mn_3Si_2Al_{15}$ is cubic with a lattice parameter which changes from $a=12.65 \times 10^{-10}$ m at 0% Fe to 12.5×10^{-10} m at 31% Fe. There is no work in the literature to identify the crystal structure of $(FeMn)_3Si_2Al_{15}$ precisely.

According to Mondolfo[36], $(FeMn)Al_6$ is the first phase in the Al-Fe-Mn-Si system to form over a good part of the system where many of the commercial alloys are located. In many alloys, $(FeMn)Al_6$ then reacts peritectically with the liquid to form $(FeMn)_3Si_2Al_{15}$. There are many other invariant reactions in the system (see Table 2.5), the only one of some interest for aluminum-base alloys is :

$$\text{Liq.} + FeSiAl_5 \rightarrow Al + Si + (FeMn)_3Si_2Al_{15}$$

By this reaction the $FeSiAl_5$ platelets that badly embrittle high silicon alloys are transformed into the $(FeMn)_3Si_2Al_{15}$ phase that does not appreciably reduce the ductility of the alloys in which it is present.

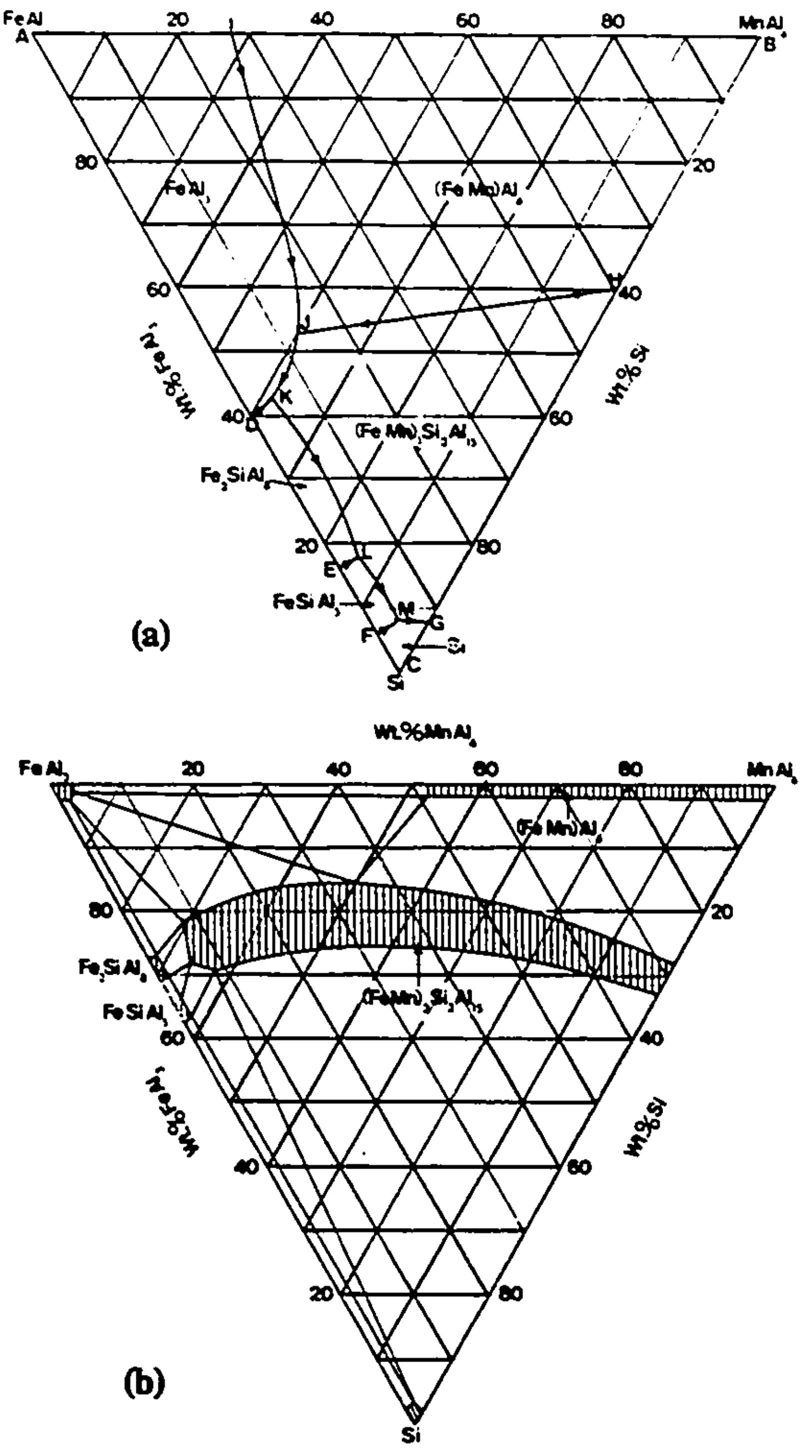

Figure 2.6 : Projection of the aluminum corner of the aluminum-iron-manganese-silicon diagram : (a) Liquidus ; (b) Phase distribution in the solid (after Mondolfo [30,36])

Table 2.5 : Invariant reactions in the aluminum-iron-manganese-silicon system. The letters locate the reactions in Figure 2.6.[ref.30]

Reaction	*Composition*			*Temperature*
	%Fe	%Mn	%Si	(°K)
Binary				
A. $\text{liq.} \rightarrow Al + FeAl_3$	1.9	—	—	928
B. $\text{liq.} \rightarrow Al + MnAl_6$	—	1.9	—	931
C. $\text{liq.} \rightarrow Al + Si$	—	—	12.5	850
$\text{liq.} + MnAl_4 \rightarrow MnAl_6$	—	4.1	—	983
Ternary				
D. $\text{liq.} + FeAl_3 \rightarrow Fe_2SiAl_8 + Al$	2.5	—	4.0	923
E. $\text{liq.} + Fe_2SiAl_8 \rightarrow Al + FeSiAl_5$	1.7	—	7.5	885
F. $\text{liq.} \rightarrow Al + FeSiAl_5 + Si$	0.7	—	12.0	848
G. $\text{liq.} \rightarrow Al + Si + Mn_3Si_2Al_{15}$	—	0.75	11.75	846
H. $\text{liq.} + MnAl_6 \rightarrow Al + Mn_3Si_2Al_{15}$	—	2.0	1.3	922
I. $\text{liq.} \rightarrow Al + (FeMn)Al_6 + FeAl_3$	1.7	0.7	—	927
$\text{liq.} + MnAl_4 \rightarrow MnAl_6 + Mn_3SiAl_{10}$	—	4.5	0.5	963
$\text{liq.} + Mn_3SiAl_{10} \rightarrow MnAl_6 + Mn_3Si_2Al_{15}$	—	2.65	1.6	928
Quaternary				
J. $\text{liq.} + FeAl_3 + (FeMn)Al_6 \rightarrow Al + (FeMn)_3Si_2Al_{15}$	2.0	0.35	1.75	921
K. $\text{liq.} + FeAl_3 \rightarrow Al + (FeMn)_3Si_2Al_{15} + Fe_2SiAl_8$	2–2.5	<0.2	3–5	900–905
L. $\text{liq.} + Fe_2SiAl_8 \rightarrow Al + FeSiAl_5 + (FeMn)_3Si_2Al_{15}$	1–2	0.1–0.5	5–10	870–880
M. $\text{liq.} + FeSiAl_5 \rightarrow Al + Si + (FeMn)_3Si_2Al_{15}$	0.6	0.2	11.7	848
liq., $MnAl_4$, Mn_3SiAl_{10}, $(FeMn)Al_6$, $FeAl_3$	2.35	3.9	0.35	1 002
liq., Mn_3SiAl_{10}, $(FeMn)Al_6$, $FeAl_3$, Fe_2SiAl_8	2.35	2.6	1.35	968

Only the reactions with a letter are shown in the projections, because the others under equilibrium conditions cannot take place in aluminum-rich alloys. They are listed, however, because in commercial alloys some of the phases involved may be present, although not in equilibrium.

Practically no commercial alloys fall within the fields in which $FeAl_3$, Fe_2SiAl_8 or $FeSiAl_5$ are the phases that crystallize after the primary aluminum phase. If manganese is added to correct for the iron, its amount is made sufficient not only to avoid those fields, but also to prevent the formation of $FeAl_3$ or FeSi even at the later stages of solidification. If there are other elements (cobalt, chromium, nickel, etc.) which also combine with iron, less manganese is needed. In high silicon alloys, $(FeMn)_3Si_2Al_{15}$ may be primary, and since its crystals tend to be limited by the (111) faces, it appears as more or less well formed hexagons.[36]

In the alloys in which $(FeMn)Al_6$ is the first to form, but that are close to the peritectic line $(FeMn)Al_6 \rightarrow (FeMn)_3Si_2Al_{15}$, fast cooling, as can be obtained in die casting suppresses the nucleation of the $(FeMn)Al_6$ phase and $(FeMn)_3Si_2Al_{15}$ may become the first manganese-bearing phase to crystallize. This results in a change of phase appearance : instead of having the sharp cornered structure of $(FeMn)Al_6$, the Chinese script is more rounded and smaller. Superheating of the melt, which also tends to suppress nucleation of $(FeMn)Al_6$ has the same effect.[85] In the high silicon alloys fast cooling has no special effect. It reduces the size of the phases and may result in the silicon assuming a more or less modified appearance, but no new phases are formed nor do equilibrium ones disappear.

2.7. Sludge Formation

The primary phases or complex intermetallic compounds formed with aluminum, silicon, iron, manganese, and chromium are called "sludge". These compounds have high melting points and high specific gravities, two properties which cause them to settle to the floor of the melt. They occur in melts having sufficiently large amounts of iron, manganese, and chromium in relation to the furnace-operating temperature. [24,40,44,57,86] (Figure 2.7)

Intermetallic phase separation from the melt occurs most often in the die casting industry where low melt holding and casting temperatures are typical. The problem is encountered in Al-Si casting alloys, and the phase that precipitates and accumulates in the bottom of the furnace is an Al(Fe Mn Cr)Si-type intermetallic. This is a hard phase that is extremely detrimental to the mechanical properties and surface machining characteristics of cast products if it is drawn into the casting during melt transfer. [5,24,28,87] Sludge can be a serious problem to die casters when it forms in the alloy or when gross particles become entrapped in the casting. The former causes tool wear during machining and the latter can cause tool breakage. Sludge shows up in a machined casting surface as a raised, shiny spot.

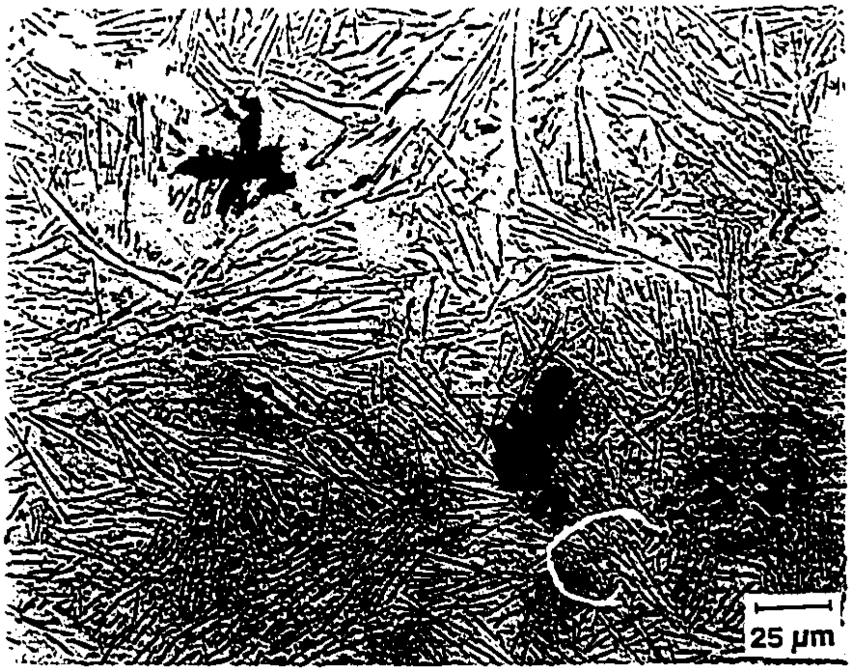

Figure 2.7 : Sludge particles in 413 alloys. (400X)

In sludge formation, temperature is more important than time.[43] Gobrecht reported the limiting temperature of segregation as a function of the content of the segregating elements in some Al-Si alloys.[44,86] Miller[88] has shown that the formation of sludge is dependent on the temperature. It was noticed that more polyhedral particles segregated at lower pouring temperatures, but no suggestion has been put forward to explain this observation. Granger reported that holding a melt of alloy 339 for a short time at 760°C, and pouring from a temperature of 704°C, ensured that the intermetallic phase went into solution.[81]

The iron content of sludge typically is about 4%, but it can range up to 20%. The formation of sludge consumes the iron in the melt sometimes to a level high enough to cause the alloy to tend to solder to the casting die.[24] The sludge can not be diluted and re-alloyed effectively at die casting temperatures because it contains a large amount of iron, manganese, and chromium.[27] Nevertheless, if it is present, it is best to have sludge as spheroidized and dispersed as possible.[17,29]

2.7.1. The Sources of Sludge Formation

It is reported[89] that high silicon alloys are susceptible to precipitation of the alloying elements, thus forming sludge. The rate of sludge formation increases as the temperature of the molten bath decreases and the concentration of impurities increases. Local high concentrations of Fe, Mn and Cr or a combination of each or all, result in an insoluble sludge compound. Titanium-boron, strontium-silicon and beryllium based hardener alloys as well as iron pickup from foundry tools are some of the sources of Fe, Mn and Cr which may form harmful sludges in the melting furnace. In addition, charging of cold ingots to the molten bath may cause sludge precipitation as a result of the temperature drop.

It is reported that the source of sludge is usually the holding furnace.[34] When metal is melted in a holding furnace, localized chilling of the bath can cause sludge to form.[27] The formation of sludge indicates that the aluminum melt has been held for extensive time periods at too low temperatures, or that the melting furnace has been operated above its melting capacity. The sludge obviously forms even above the sludge formation temperature when rejected castings are added into the aluminum melt, since the melt temporarily cools locally below this critical temperature.[3] Accordingly, sludge is also formed near the cold refractory linings of the melting furnace. Groteke[7] has observed that the dissolution of sludge requires an extensive holding time above the sludge formation temperature.

Unfortunately, with the demands for increased production and throughput from the primary melting furnaces, and the normal agitation associated with charging and tapping the melt, most die casting alloys contain a percentage of sludge crystals that is directly related to the quality of the melt practice and the chemical composition. The question often becomes a matter of size of the inclusions, rather than their presence or absence.

2.7.2. Segregation Factor

Gobrecht[44,57,86] and Jorstad[24] have defined a segregation factor (sludge factor; SF) in Al-Si-Cu alloys which is a useful first step to determine how much Fe, Mn, and Cr can cause sludge to form. The segregation factor can be used to predict the occurrence of sludge in the bottom of crucibles or furnaces as a function of temperature and initial chemical composition.[90] This factor is calculated from the formula :[24,44,57,86]

$$\text{Segregation Factor} = (1 \times \text{wt\% Fe}) + (2 \times \text{wt\% Mn}) + (3 \times \text{wt\% Cr})$$

The above formula is useful for predicting susceptibility to sludge formation. However, metal temperature and, to some extent, agitation of the molten metal also influence susceptibility to sludge formation. At higher holding temperatures, or with an agitated bath (as in induction furnaces), a segregation factor higher than 1.9 can be tolerated.[34]

Dunn[27] reported on the chemical composition of sludges in the alloy A.380. The material removed from the bottom of a melt gave an analysis which included 6.5% Fe, 3.03% Mn and 1.44% Cr. The actual crystals of the compound in the sludge were analyzed by microprobe, giving a composition which included 20% Fe, 10% Si, 6% Mn, 1% Cr and 1% Cu. Another analysis was made of large crystals of sludge which had accumulated over a long period in a reverberatory furnace melting A.380 alloy. This sludge had a melting point of over 800°C and contained 9.4% Si, 11.4% Fe, 6.07% Mn, 2.16% Cu, 1.77% Cr and 0.4% Zn. The results of Dunn in alloy A380 verify that the factors 1, 2, 3, for Fe, Mn, Cr, respectively, in the sludge formula are reasonably correct and can be used as a melting control.[27]

Gobrecht[86] also showed the relationship between holding temperature and segregation factor (SF) for several important aluminum-silicon alloys. His work revealed that segregation occurs at a critical holding temperature for different alloys when SF > 1. Therefore, no segregation occurs if the melt is kept at higher temperatures. It has been reported[23] that increasing iron beyond that of a specified SF of 1.8 to 2.1 did not result in the formation of sludge, but merely resulted in increasing the amount of platelet phase. However, increasing manganese to maintain a specified 2:1 (iron : manganese) ratio, resulted in the precipitation of sludge in the microstructure. This shows that manganese plays a more important role in the formation of the sludge than iron, and it requires a more critical control in die-casting alloys.

2.8. Sedimentation of Intermetallic Compounds

2.8.1. Gravity Segregation

The temperature at which primary compounds begin to separate depends on the combined content of sludge forming elements, and when these are sufficiently high, separation of iron-rich compounds may occur even above the pouring temperature. Slow cooling of the metal in the mould also favours gravity segregation, since these crystals grow larger and have more time to sink than when cooling is more rapid.[41]

Kaye et al.[6] reported that when melting and metal treatment conditions are not controlled efficiently, the intermetallic compounds are formed around solidification centres provided by aluminum oxide nuclei present in the molten metal. Being heavier than the aluminum, the solidified intermetallics settle to the bottom of the melt, causing a sludge to form. The rate of precipitation is temperature dependent. Maintaining too low a temperature (generally in holding furnaces) encourages their precipitation and when the metal is retained longer in the crucible more segregation occurs.

Groteke[7] and Kaye[5] have shown that the density of the intermetallic compounds connected with the formation of sludge is relatively high compared with that of the aluminum melt, and therefore the sludge has a tendency to settle to the bottom of the melt. The commercial melting and casting processes are, however, relatively fast processes, thus causing agitation of the melt which in turn hinders the settlement of sludge on the bottom of the melt. Therefore, it is better to consider the size of the intermetallic particles rather than simply the existence or absence of them.

It has been reported that lower Cu-containing alloys show less tendency to segregation.[81] The results of Glaisher[41] on a series of Al-5%Si alloys show that a manganese content over 0.6% causes segregation whether the iron content is 0.8 or 2.3%. Manganese is more powerful than iron in causing gravity segregation, and the combined effect of the two may be expressed approximately by the formula Fe% + 1.5 Mn%. In the absence of manganese, no segregation occurred, even with 2.3% iron.

In alloy A380 the thin platelet and $CuAl_2$ intermetallics are mainly segregated within the eutectic regions, while the polyhedral and a few Chinese Script particles are reported to be uniformly dispersed throughout the bulk specimen.[25] Segregation is more likely to occur in large sand castings and slowly cooled ingots than in small sand castings or die castings.[41] Gravity segregation was not experienced in melts which were thoroughly stirred after heating to at least 720°C and which maintained the melt temperature above 670°C. [40,41] Therefore, gravity segregation of intermetallic compounds can be prevented by proper temperature control during holding and by thorough stirring of the molten bath.

2.8.2. Iron Removal by Segregation Method

The use of aluminum scrap in the secondary aluminum industry, has increased markedly over the past ten years.[91] The use of aluminum scrap involves several technical drawbacks because it is generally associated with other metals or materials which cause chemical contamination. One of the most harmful impurities in aluminum alloys is iron. It is reported that iron removal from aluminum scrap can be done by the use of a segregation process that allows the production of a liquid alloy with an iron content below 0.3 wt.%, with an efficiency in the liquid close to 90%.[90,91,92] Iron removal occurs through the formation, growth and sedimentation of the $Al_{15}(Fe,Mn)_3Si_2$ phase containing about 30 wt.% iron.[82] This phase is solid in the range of temperature in which the alloy is liquid and further purification is obtained by filtration.[91,92]

2.8.3. Agglomeration

Sludge particles sometimes agglomerate in some sections of castings. Agglomeration usually arises from interaction between particles, as a result of which they adhere to one another to form clusters. The main mechanisms giving rise to agglomeration are:[93]

1) ***Mechanical interlocking.*** This can occur particularly if the particles are long and thin in shape, in which case large masses may become completely interlocked.
2) ***Surface attraction.*** Surface forces, including van der Waals' forces, may give rise to substantial bonds between particles, particularly where particles are very fine (<10 μm), with the result that their surface area per unit volume is high. In general, a freshly formed surface, such as that resulting from particle fracture, gives rise to high surface forces.
3) ***Plastic welding.*** When irregular particles are in contact, the forces between the particles will be borne on extremely small surfaces and the very high pressures developed may give rise to plastic welding.

4) *Electrostatic attraction*. Particles may become charged as they are fed into equipment and significant electrostatic charges may be built up, particularly on fine solids.

5) *Temperature fluctuations* give rise to changes in particle structure and to greater cohesiveness.

2.9. Effect of Casting Variables

2.9.1. The Influence of Cooling Rate

Different statements, which are often contradictory, have been made[13,17,25,46,56] about the effect of cooling rate on the morphology of intermetallic compounds. Yaneva et al.[46] reported that even at low-iron content (< 0.15%) intermetallic phases appear, especially in zones where solidification is slow (i.e. the thick sections of the castings). It is reported that casting into cold ingot molds results in Chinese script compounds, but as the molds heat and the alloy cools more slowly, the intermetallics grow into a fatter polyhedral shape.[17] Ghomashchi[25] reported that the polyhedral and Chinese script morphologies are independent of the cooling rate, and the thin platelet morphology is dependent upon cooling rate. The thin-platelet intermetallic morphology is sensitive to cooling rate in which both the volume fraction and aspect-ratio of this phase decrease with increasing cooling rate. Finer and longer particles form at longer times, (i.e. at lower cooling rates). The volume fraction of thin platelets also reduces at shorter times. In fact, these are beneficial results for castings prepared at higher cooling rates, (e.g. die-casting), since thin platelets are reported to be detrimental to mechanical properties of the component and act as two dimensional defects. The reduction in volume fraction of the thin-platelet phases at higher cooling rates may be due to the aluminum's ability to dissolve more impurity elements.[25] Gustafsson et al.[13] worked on A356 alloy with two different levels of iron and found that all types of intermetallic phases which appear in the alloys were independent of cooling rate in the range investigated (0.2 to 16°C per second).

It has also been reported that the Chinese script intermetallic forms when the solidification rate is high.[56] Gobrecht[44] showed that the shape of primary crystals depends on solidification conditions. During cooling of the melt, when the temperature of the melt falls below the liquidus, compact crystals form which cause rapid segregation and which can be transferred into the casting during pouring of the melt. Generally, a high cooling rate favours a fine particle dispersion.[16] It has been shown that the size and amount of iron-containing phases is strongly influenced by solidification rate.[13,16,49] Grand[21] mentions that slow cooling increases the size of the Al-Si-Fe particles if enough Fe is present.

Mascre[84] showed that increasing the rate of cooling increases the level of Fe at which the brittle "m" constituent (β-phase) first appears (see Figure 2.5). For instance, with no Mn, that point is at :

0.75% Fe when the cooling rate is 1°C/s

0.9% Fe when the cooling rate is 5°C/s, and

1.0% Fe when the cooling rate is 10°C/s.

These results are plotted in Figure 2.8. Thus, the effect of Fe on properties is less marked in rapidly cooled castings than in slowly cooled ones.

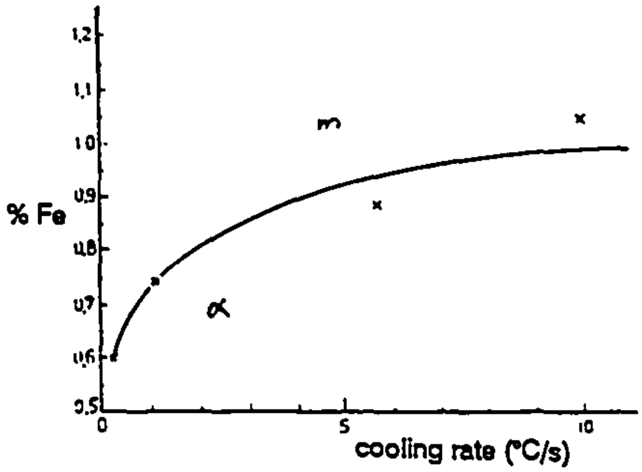

Figure 2.8 : Influence of Fe content and cooling rate on the structure of Mn-free Al-13% Si alloy. [84]

It has also been reported that at low cooling rates, $FeSiAl_5$ needles are coarse and concentrated at grain boundaries, where they promote a brittle fracture. At higher cooling rates, $FeSiAl_5$ particles are quite small and interspersed more uniformly. Consequently, Fe levels tolerable in permanent mold casting alloys are greater than in sand casting alloys.[12,75]

2.9.2. Melt Superheat

Awano and Shimizu[56] reported that the morphology of an AlFeSi compound was found to change from a needle-like to a Chinese script form by superheating the melt. The AlFeSi compound in a Chinese script form crystallized in the Fe-enriched residual liquid through non-equilibrium solidification at a later period than the crystallization of the compound in a needle-like form. The AlFeSi compound crystallized in a Chinese script form even when the melt was superheated to lower temperatures as long as the solidification rate became faster. They showed that if the melt is once superheated to the temperature at which the iron compound crystallizes in a Chinese script form, the change in the shape of the iron compound is not affected by the thermal history of the melt.[56]

Awano and Shimizu[56] also studied the relationship between melt superheating temperature and shape of the iron compound upon crystallization, as well as the effects of iron, silicon and magnesium content and solidification time. The influence of these parameters on microstructure is plotted in Figures 2.9 - 2.11. Their results highlight the importance of low iron, silicon and magnesium content as well as high cooling rate in order to achieve complete crystallization of iron compounds in α-AlFeSi form.

Yaneva et al.[46] carried out some experiments to check an assumption, that the appearance of intermetallics results from the incomplete dissolution in the melt of the iron phases carried over from the bulk material. Test bars obtained by slow solidification were remelted and held at 750°C for different times. According to [86] this temperature is high enough for dissolution of iron phases even when SF=1.8 while in their case SF=0.44. A uniform distribution of α-Al(FeMn)Si particles with nearly equal size was observed in the microstructure. The m-phase was not discovered though it had been present as at least 55 vol.% in the initial ingot material.

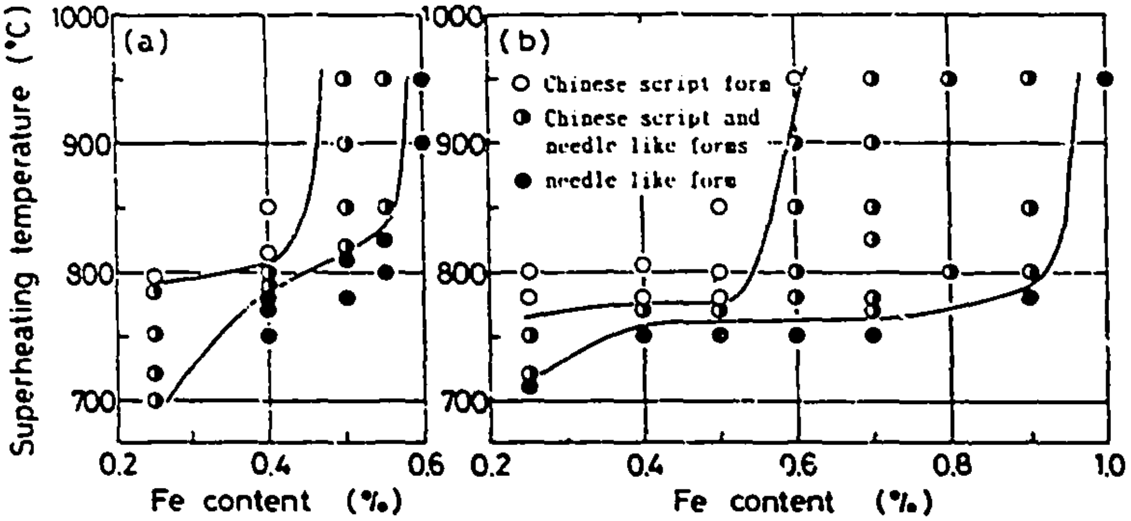

Figure 2.9 : Effects of superheating temperature and iron content on crystallized structure of iron compounds in (a) Al-6%Si-Fe alloy and (b) Al-11%Si-Fe alloy. [56]

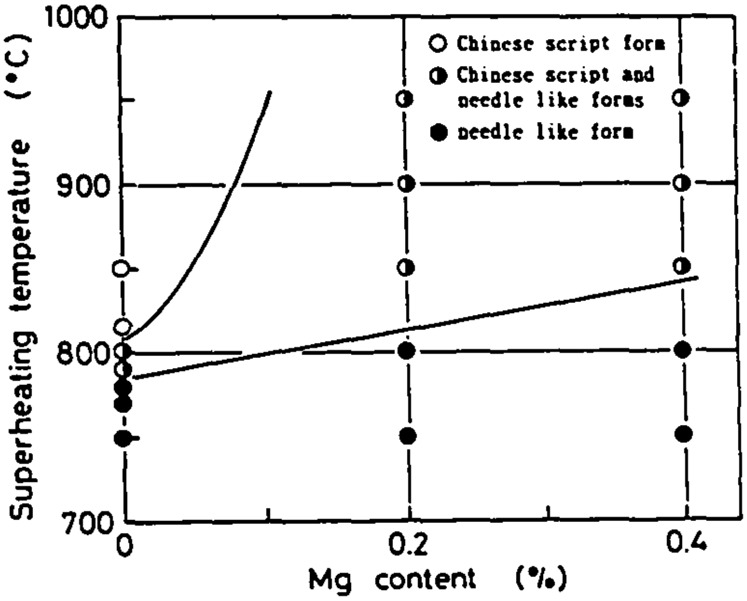

Figure 2.10 : Effect of magnesium content on crystallized structure of iron compounds in Al-6%Si-Mg-0.4%Fe alloy castings. [56]

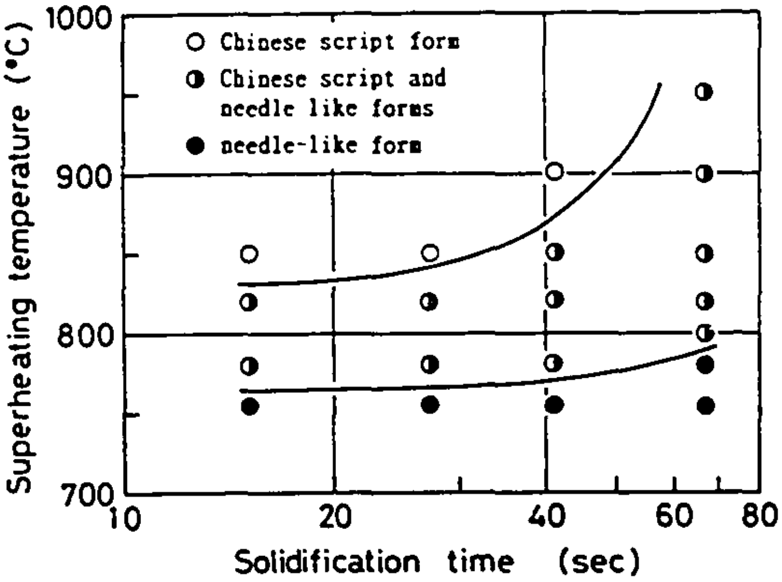

Figure 2.11 : Effect of solidification time on crystallized structure of AlFeSi compounds in Al-7%Si-0.3%Mg-0.4%Fe alloy. [56]

It is reported that in any aluminum-silicon alloy where the iron content is between 0.8 to 1.8%, the morphology of the iron compounds changes from a long needle form, to rosettes, and thence to a spheroidal shape as the melt-temperature changes from low to high.[33] For example, when an allov containing 1.2% Fe is heated to a temperature below 840°C, the morphology of the iron compound present in the sample poured at that temperature is needle-like. An increase in the pouring temperature to above 920°C causes the form to become spheroidal. When poured in the range 840°C-920°C it will be seen that most of the iron compounds appear as rosettes, with only a small proportion appearing as needles or spheroids.

Where the needle-form compounds in an Al-Si alloy have been transformed into spheroids, the room-temperature tensile strength of an alloy containing 1.8% Fe is increased by 83% and the elongation by 115%. The high-temperature(300°C) tensile strength and elongation for the same material increase respectively by 32% and 80%.[33]

Mondolfo and Barlock[85] reported that the higher the superheat, the faster the solidification rate. With increase in solidification rate, interdendritic spacing, size of intermetallic compounds and grain size decrease. It appears that the effect of superheating is due to a reduction in the size and possibly number of nucleant particles, which forces the early growth of the nuclei at increased undercoolings, so that the interdendritic spacing starts much smaller, and, in spite of the extra coarsening due to increased freezing time, remains smaller.[45,85,94]

A remelting test has shown that the spheroidal form of iron compounds still exists after remelting and recasting.[33] If the superheat temperature is well above the precipitation temperature, then the iron compounds in the melt will go into solution. At high cooling rates the iron compounds solidify as spheroidal solids. As a result, high temperature treatment and a high rate of cooling are the two important factors which guarantee the formation of spheroidal-form iron compounds.

2.10. Modification of Iron-Rich Intermetallics

Khudokormov[37] reported that the addition of more than 1% Mn to Al-12% Si-2% Fe alloy led to the intermetallics solidifying in the form of polygons in a matrix of lamellar silicon eutectic.

An alloy with the more complex Fe-rich phase (12% Si, 2% Fe, 1.5% Mn) was then modified with 0.05-0.5% of Na, K, Li, P, Sb, Bi, S, Se and Te. The strongest effects on the form of the Fe-rich phase were produced by S, Se and Te. The particles became much finer and were also reduced to a more equi-axed form. The effects of these additives on the crystallization of the silicon eutectic are independent of the presence of transition elements.

The most powerful compensators for iron in silumins were found to be Cr and

Mo. They refined and globularized the iron-rich phase particles at relatively low concentrations of about 0.5%. When silumin (Al-13% Si master alloy) was subsequently modified with a group VI element, the intermetallic particles became very fine and uniformly distributed.[37]

It has recently been reported about the use of strontium in modification of intermetallics in wrought aluminum alloys. There is now considerable evidence that strontium modifies and refines many of the detrimental intermetallic compounds in wrought alloys. A 1975 Alcan patent[95] indicates that at 0.05% Sr, substantially all of the AlFeSi intermetallics in 6063 alloy billet are in the α form. In a 1987 patent by ALCOA [96], it is reported that the addition of 0.01% to 0.10% strontium (nominally 0.05% Sr) to Al-Cu-Mg-Zn wrought alloys refines the intermetallic phases including Mg_2Si, Al-Cu-Fe and Al-Cu-Mg particles. As a result of the refinement of the intermetallics, the strontium-treated alloy has enhanced toughness, shorter homogenizing time and finer grain size than a non-strontium containing alloy. A 1987 Japanese patent[97] also indicates that the addition of 0.005% to 0.10% strontium, in combination with similar quantities of zinc, effectively reduces the formation of deleterious $(Mn,Fe)Al_6$ intermetallics in Al-Mg-Mn alloy sheet for can end stock. In these alloys, microadditions of strontium reduce both the number and size of detrimental intermetallics. It has also been reported that Sr addition of 0.06% alters the needle-like β-phase to the Chinese script α-phase in synthetic 1XXX and 6061 alloys, and in DC cast commercial 6061 alloys. The volume percent of α-phase is shown to be dependent on cooling rate, Fe/Si ratio, and Sr levels of the alloy.[98]

Chapter 3

Effect of Melt Chemistry and Temperature on the Formation of Intermetallic Compounds

3.1. Introduction

The amounts of iron and manganese play important roles in establishing the mechanical properties of aluminum-silicon casting alloys. It is therefore of special interest to study the precipitation of iron and manganese containing phases in these alloys. Iron, as one of the main impurities in aluminum, is always present in alloys made from commercially pure base material. The solid solubility of iron in aluminum is very low with the result that most iron present forms intermetallic compounds, the nature of which depends strongly on other impurities or alloying elements present. Except in pressure die-casting alloys, it is well known that iron is a harmful element and in high concentration is responsible for inferior mechanical properties of aluminum-silicon alloys. Melting temperature is the other important parameter in the formation of intermetallic compounds. Therefore, it is also of particular interest to investigate the role of temperature in the formation of intermetallics.

As recycling of aluminum alloys becomes more common, sludge will be a problem of increasing importance due to the concentration of Fe, Mn, Cr and Si in the scrap cycle. Control of complex intermetallics in cast structures will require increased knowledge of and control of temperature and melt chemistry. The increasing importance of complex intermetallics in Al-Si alloy metallurgy and the relatively small amount of knowledge pertaining to them make this subject an important one for further research. In the present chapter the effect of melt chemistry, particularly Fe and Mn concentration, on the formation of intermetallic compounds has been studied in an Al-12.7% Si alloy containing 0.1% Cr with three levels of iron (0.4, 0.8, 1.2%), and five different levels of manganese ranging from 0.0 to 0.5%. Temperature of intermetallic formation has also been investigated in commercial and synthetic aluminum-silicon alloys by means of quenching experiments and thermal analysis.

3.2. Experimental Procedure

3.2.1. Effect of Melt Chemistry on the Formation of Intermetallic Compounds

The chemical composition of the alloys prepared for the present investigation is shown in Tables 3.1, 3.2, and 3.3. These alloys were prepared by making appropriate additions to an Al-12.7% Si alloy manufactured from commercial purity aluminum and silicon in an induction furnace. Fe, Cr and Mn additions were made to this alloy by means of commercial master alloys of composition : Al-24.7% Fe, Al-20.1% Cr and Al-25.2% Mn. Their complete chemical analysis is given in Table 3.4. 18 alloys were prepared with 0.1% chromium, three levels of iron (0.4, 0.8, 1.2%), and five levels of manganese ranging from 0.0 to 0.5%. 120 g of each alloy composition was remelted in an induction furnace and two samples were cast from 670°C into the copper molds. The time interval between remelting and casting was 5 minutes. One sample was used for emission spectrometry to verify the chemical analysis of the alloy. The other was subsequently examined metallographically in order to determine the effect of variations in chemistry on the intermetallic morphology.

Table 3.1 : Chemical Composition of Alloys in Batch 1, wt%

alloy	Si	Fe	Cu	Mn	Mg	Cr	Ni
A1	13.10	0.41	0.003	<0.008	0.011	<0.001	<0.001
A2	12.73	0.37	0.003	<0.008	0.10	0.10	<0.001
A3	12.74	0.38	0.003	0.14	0.011	0.11	<0.001
A4	12.75	0.39	0.003	0.22	0.011	0.11	<0.001
A5	12.85	0.37	0.003	0.33	0.012	0.10	<0.001
A6	12.94	0.36	0.003	0.50	0.013	0.10	<0.001

Table 3.2 : Chemical Composition of Alloys in Batch 2, wt%

alloy	Si	Fe	Cu	Mn	Mg	Cr	Ni
B1	12.87	0.78	0.003	<0.008	0.010	<0.001	0.006
B2	12.53	0.75	0.003	<0.008	0.010	0.10	0.005
B3	12.88	0.77	0.003	0.12	0.010	0.11	0.007
B4	12.79	0.80	0.003	0.23	0.010	0.11	0.007
B5	12.28	0.77	0.003	0.31	0.010	0.10	0.007
B6	12.51	0.75	0.003	0.53	0.011	0.10	0.007

Table 3.3 : Chemical Composition of Alloys in Batch 3, wt%

alloy	Si	Fe	Cu	Mn	Mg	Cr	Ni
C1	12.71	1.20	0.003	<0.008	0.010	<0.001	0.006
C2	12.10	1.17	0.003	<0.008	0.010	0.10	0.006
C3	12.51	1.17	0.003	0.10	0.010	0.10	0.006
C4	12.49	1.16	0.003	0.21	0.010	0.10	0.006
C5	11.86	1.15	0.003	0.31	0.010	0.10	0.006
C6	12.18	1.16	0.003	0.51	0.011	0.10	0.006

Table 3.4 : Chemical Analysis of the Master Alloys, wt%

Master Alloy	Fe	Cr	Mn	Si	Zn	V	Ni
Al-24.7% Fe	24.7	<0.01	0.15	0.05	0.01	0.01	0.01
Al-20.1% Cr	0.14	20.1	0.01	0.15	0.01	0.02	<0.01
Al-25.2% Mn	0.14	<0.01	25.2	0.06	<0.01	0.01	<0.01

3.2.2. Temperature of Sludge Formation

Temperature of sludge formation has been investigated on one commercial alloy and three synthetic aluminum alloys.

3.2.2.1. Commercial 413P alloy

413P is a die-casting alloy which is used in piston manufacturing. The alloy used in this work is produced by Roth Brothers Smelting Company. Sludge has been observed in the alloy and from this view point, it is a good material on which to investigate sludge formation. The chemical analysis of alloy 413P is given in Table 3.5 and the microstructure of the ingot showing sludge particles is presented in Figure 3.1.

Table 3.5 : Chemical Composition of Alloy 413P, wt.%

Al	Si	Fe	Mn	Cr	Ni	Cu	Mg	Zn	Ti
rem.	12.9	0.68	<0.5	0.07	1.23	0.87	1.16	0.24	0.03

Figure 3.1 : Sludge particles in 413P ingot (400X)

To investigate the temperature of sludge formation, a system was designed to carry out a rapid quenching of molten droplets directly in water. The system consists of a bottom pour graphite crucible with a conic graphite stopper which controls the exit of molten metal. Small pieces of alloy were charged into the crucible and melting was carried out in an induction furnace. The temperature was controlled continuously by a K-type thermocouple. Molten droplets of alloy 413P were quenched directly in the cold water at different temperatures in the range of 660°C-720°C. The system of rapid quenching is shown in Figure 3.2.

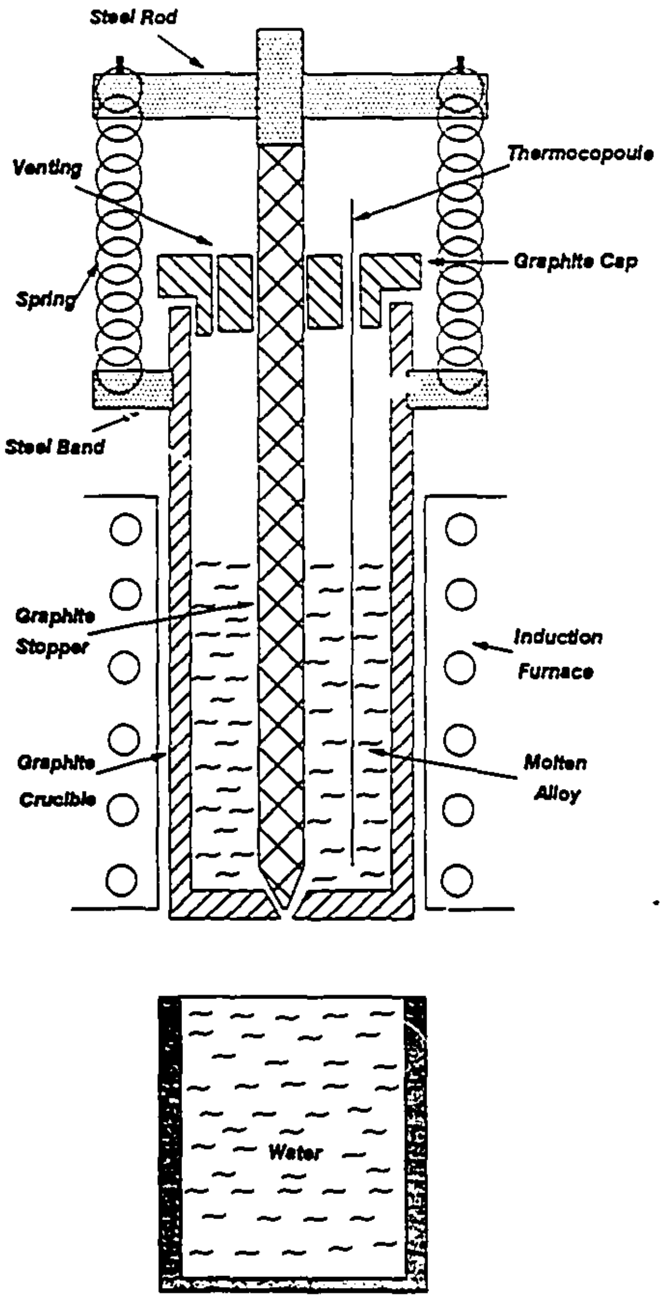

Figure 3.2: Experimental set-up for rapid quenching of molten metal

Thermal analysis was also performed on this alloy to investigate at which temperature sludge forms and to compare the results with those obtained in the previous experiment. In thermal analysis a very slow cooling rate of 0.1°C/s was achieved through use of a fire clay cup pre-heated to 300°C and encased in a fiber-frax insulation box. The geometry of the sample cup is shown in Figure 3.3. After melting the alloy in an induction furnace, the thermal analysis sample was poured at 720°C, and the temperature was read by chromel-alumel thermocouples located at two positions near the cup wall and at the cup center, both at mid-height. Data was logged on a computer via a commercial interface (Data Acquisition System). Thermocouples were protected in a 1 mm inside diameter stainless steel sheath so that they could be removed from the solidified sample. One sample was cut from the section at which the tip of the thermocouples was located. It was mounted, polished and prepared for metallographic study.

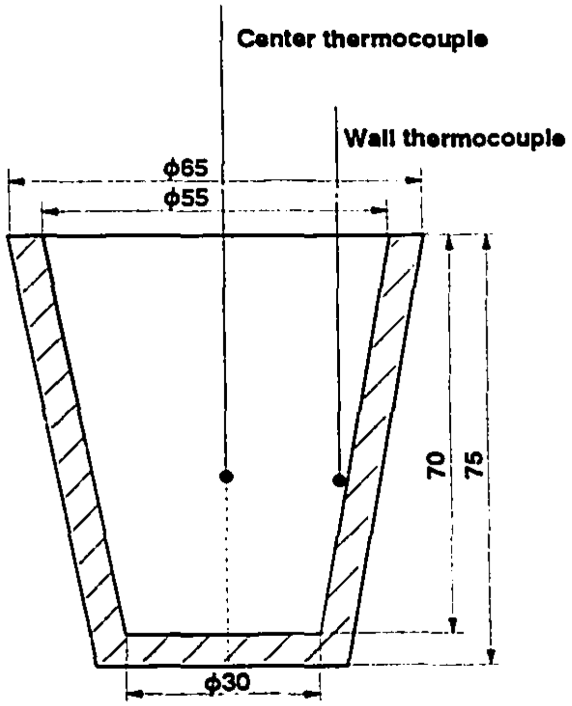

Figure 3.3 : Sample cup used in thermal analysis (dimensions in mm)

3.2.2.2. Synthetic Alloys

Three alloys with nominal iron levels of 0.4, 0.8, or 1.2% and constant manganese and chromium were prepared in an induction furnace to investigate the effect of iron content on the temperature of sludge formation. Their initial chemical composition is shown in Table 3.6. To study the temperature of sludge formation precisely one must assure the dissolution of the intermetallics contained in the starting material. 200 g of each alloy was therefore melted in a fire clay crucible in an induction furnace, and the melt was maintained at 850°C for a long time (1.5 - 2.0 hours) to cause complete dissolution of the intermetallics. After dissolution of the compounds, the alloys were maintained at different temperatures in the range 850°C - 630°C for 20 minutes at each temperature. A molten droplet of each alloy was then quenched rapidly from each temperature by using a thin quartz tube. Rapid quenching was performed in three different media: water, a mixture of dry ice and ethanol, and liquid nitrogen. The solidified droplets were mounted and prepared for metallographic study to determine if they contained sludge particles.

Table 3.6 : Chemical Composition of Alloys (wt.%) Used to Study the Temperature of Sludge Formation

Alloy	Si	Fe	Cu	Mn	Mg	Cr	Ni	Zn
1	12.88	0.42	<0.002	0.31	<0.009	0.11	<0.001	<0.008
2	12.74	0.80	<0.002	0.30	<0.009	0.11	<0.001	<0.008
3	12.46	1.21	<0.002	0.29	<0.009	0.10	<0.001	<0.008

3.2.3. Microstructural Study and Phase Analysis

All samples of the alloys listed in Tables 3.1, 3.2, and 3.3 were prepared for metallographic study and image analysis. Various microstructural parameters were investigated and measured using image analysis, such as the particle area (μm^2), average size (μm), number of particles per unit area (mm^{-2}), and particle area percentage (%). The data was automatically processed in Leco 2005 image analysis software using statistical programs and the mean values are reported in this chapter. The phases were investigated by scanning electron microscope (SEM) and the element distribution in the phases was determined by X-Ray mapping. The chemical composition of all complex intermetallic compounds observed in this work was also determined by electron probe microanalyzer (EPMA).

Sludge particles in the experiment on temperature of sludge formation were analyzed through SEM-EDS (Energy Dispersive Spectrometry) and EPMA. All samples of 413P alloy and synthetic alloys were also studied through metallography.

3.3. Results and Discussion

3.3.1. Effect of Melt Chemistry on the Formation of Intermetallic Compounds

Metallographic study of the alloys revealed that the intermetallic compounds do not form when the level of iron, manganese, and chromium is low. In the alloys of batch 1 which contained 0.4% Fe and 0.1% Cr, iron platelets (β-phase) and star-like intermetallics did not form if the manganese concentration was less than 0.3%. In the alloys of batch 2 which contained 0.8% Fe and 0.1% Cr, the star-like compounds were formed in the range from 0.1 to 0.3% Mn and the amount of these phases increased as the content of manganese increased. Large iron containing platelets formed in the high iron-bearing alloys with 1.2% Fe (batch 3). These phases shown in Figure 3.4 decreased in amount when 0.1% Cr was added, and some of them changed to the star-like compounds also seen in Figure 3.4. The decrease in the amount of platelets continued by adding 0.1% Mn (alloy C3). All platelets were changed to the star-like compounds if the manganese content exceeded 0.2%. The microstructures of the alloys studied in the present work are shown in Figures 3.5 - 3.7.

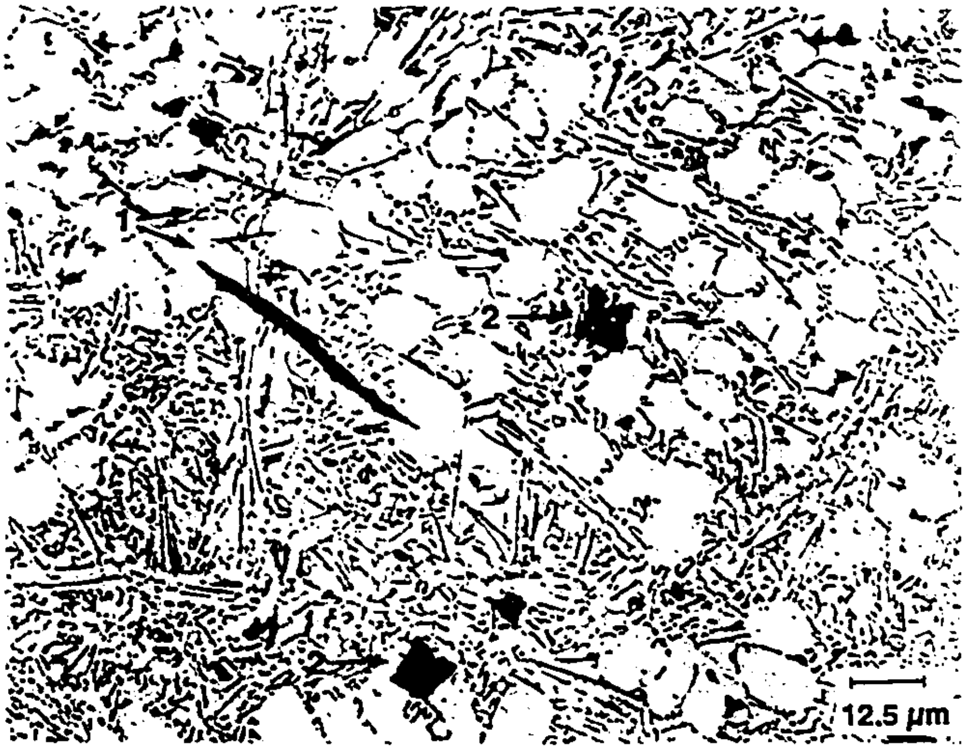

Figure 3.4 : Needle or platelet phase (1) and star-like (2) intermetallics in alloy C3.

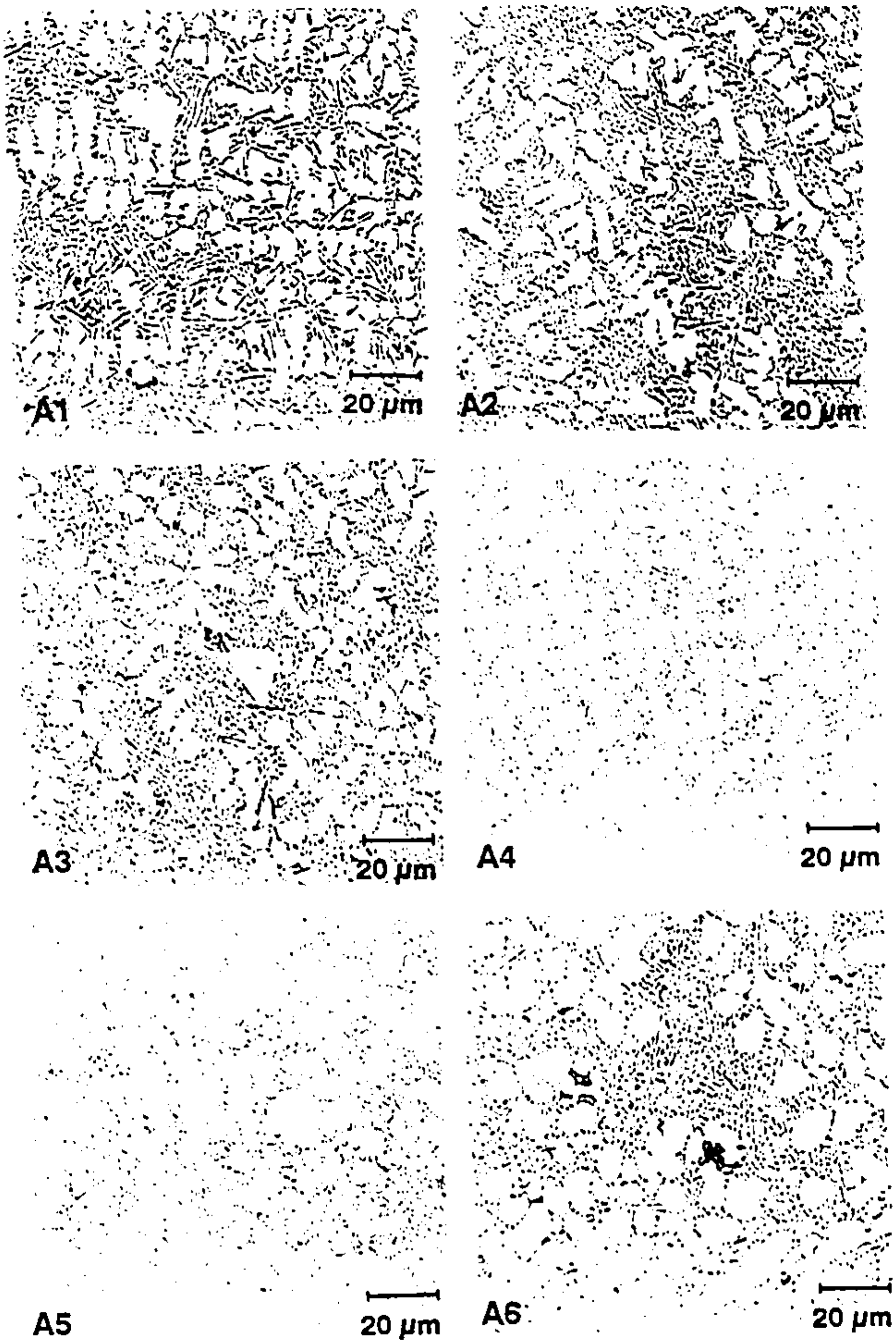

Figure 3.5 : Microstructures of the alloys containing 0.4% Fe. (Table 3.1)

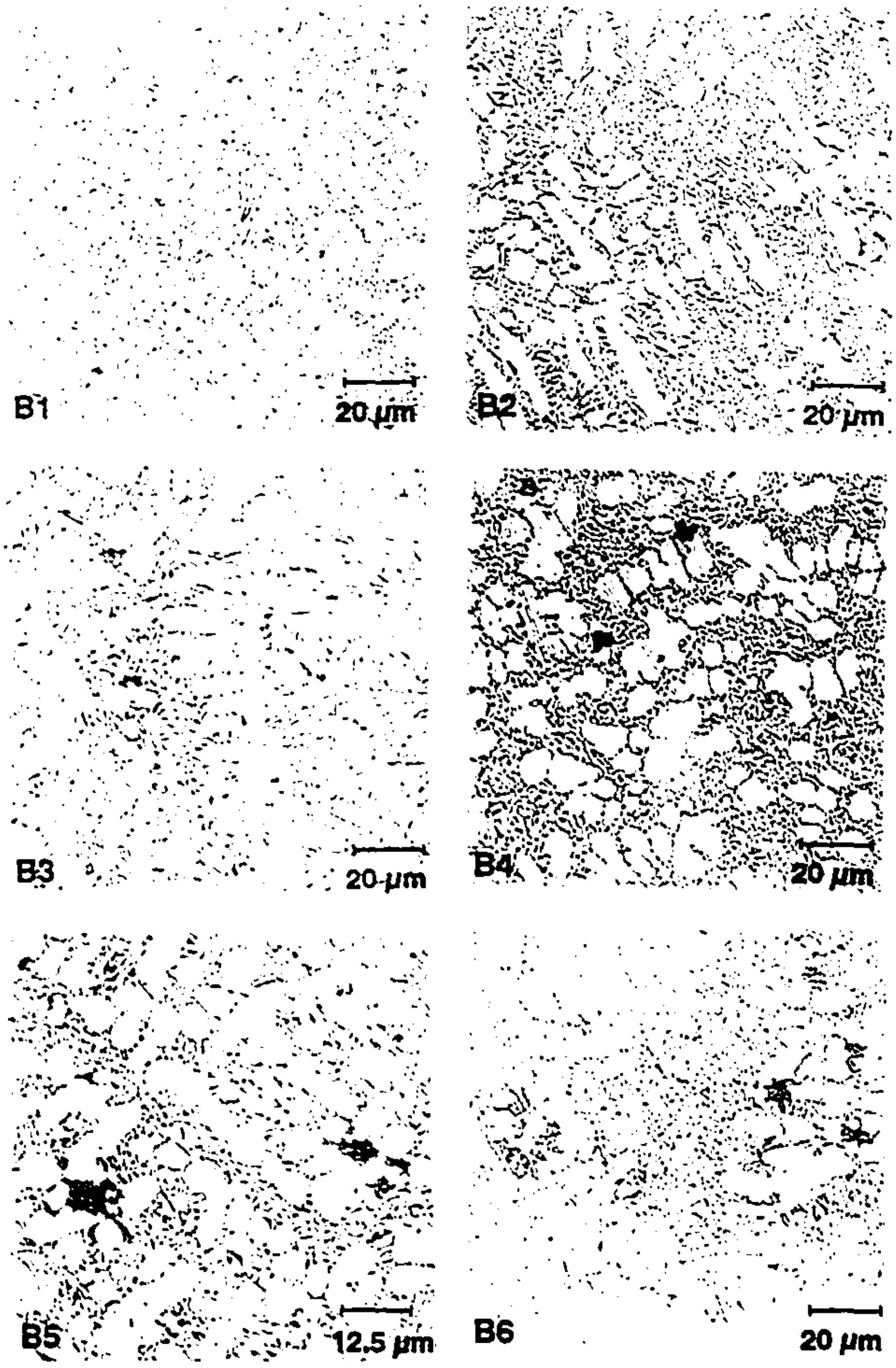

Figure 3.6 : Microstructures of the alloys containing 0.8% Fe. (Table 3.2)

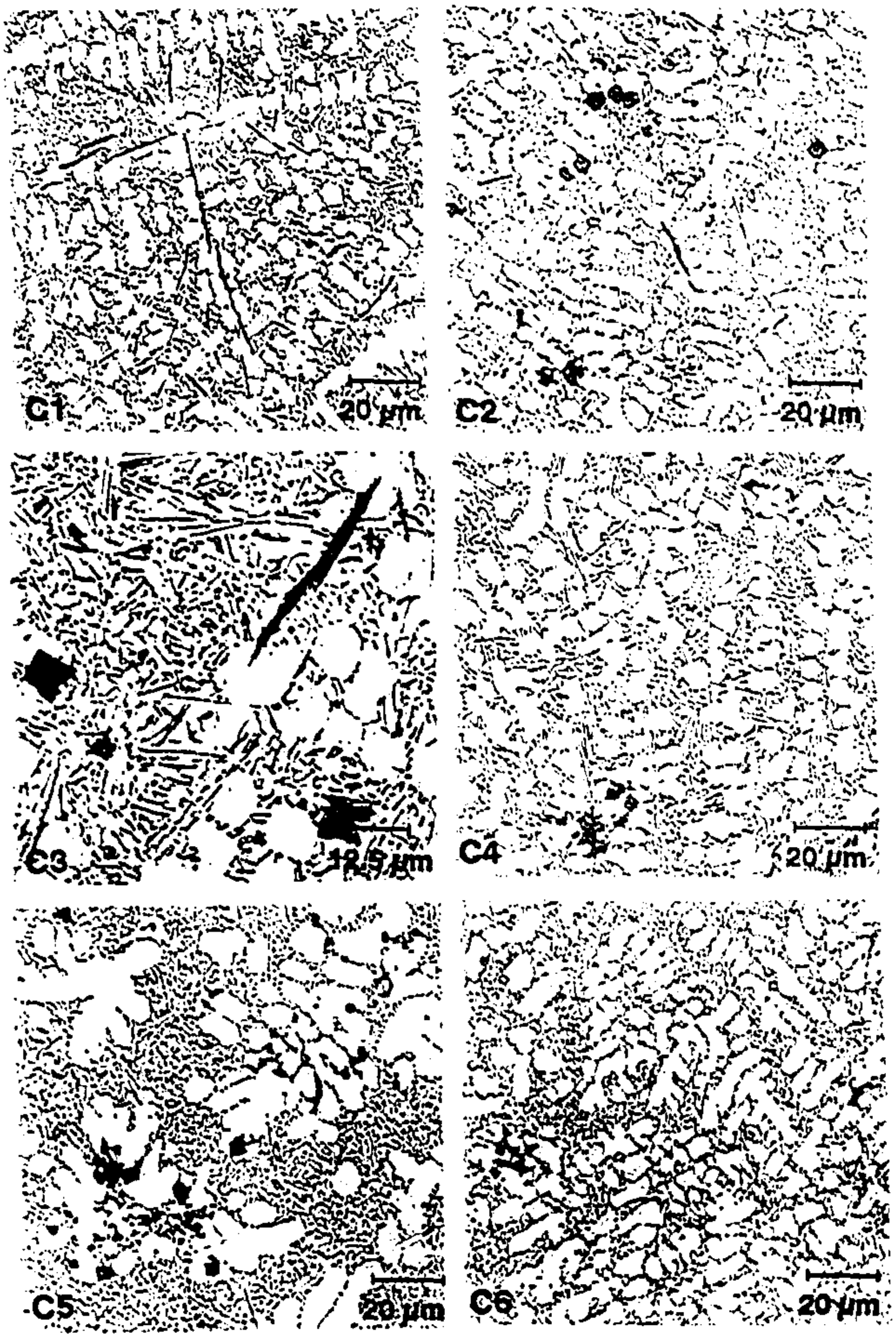

Figure 3.7 : Microstructures of the alloys containing 1.2% Fe. (Table 3.3)

The segregation factor (SF) was calculated for each alloy based on the formula given in Chapter 2 (section 2.7.2). To relate the effect of chemical composition to the microstructure and the phases which form in the alloys, the segregation factor was plotted versus manganese concentration. Figure 3.8 shows the effect of manganese content at each level of iron on the formation of intermetallic compounds. Star-like compounds form at higher manganese concentrations (Mn > 0.3%) in alloys which have 0.4% Fe and in which the segregation factor is greater than 1.30. However, in alloys which have 0.8% Fe, star-like intermetallics form at lower manganese concentrations (0.1% Mn) with the same segregation factor (SF > 1.30). To convert all platelet phases to small star-like intermetallics, in alloys which have 1.2% Fe, more than 0.2% manganese and 0.1% chromium are needed and the segregation factor is about 1.85.

The influence of iron concentration at each level of manganese on the formation of intermetallics is shown in Figure 3.9. It is seen that when the iron content increases from 0.4 to 1.2%, star-like compounds form at low levels of manganese and chromium, and if the manganese content is high enough all intermetallics are star-like. The combined effect of manganese and iron on the formation of intermetallics is shown in Figure 3.10. Two regions are apparent : one in which no intermetallics form and one in which they do. The onset of sludge formation in this 0.1% Cr alloy can then be represented by the equation:

$$\% \text{ Fe} + 1.7 \% \text{ Mn} = 0.97$$

This relation is indicated by the straight line shown in Figure 3.10. The results shown in this figure and the equation are in a reasonable agreement with the segregation factor (SF) equation used by Gobrecht[57,86] and Jorstad[24] in which the coefficients of iron, manganese, and chromium are 1, 2, and 3, respectively.

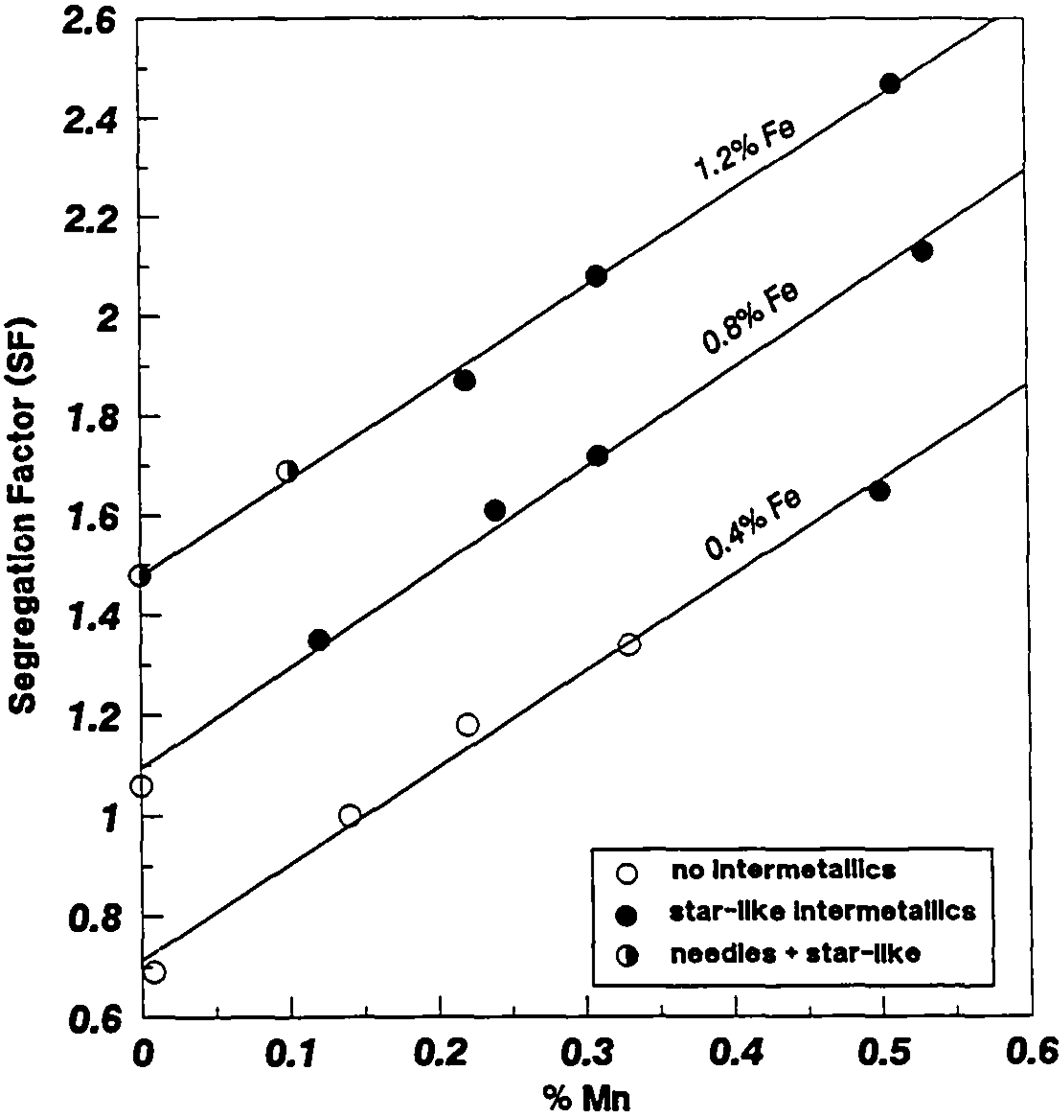

Figure 3.8: Effect of manganese at each level of iron in Al-12.7%Si-0.1%Cr alloy

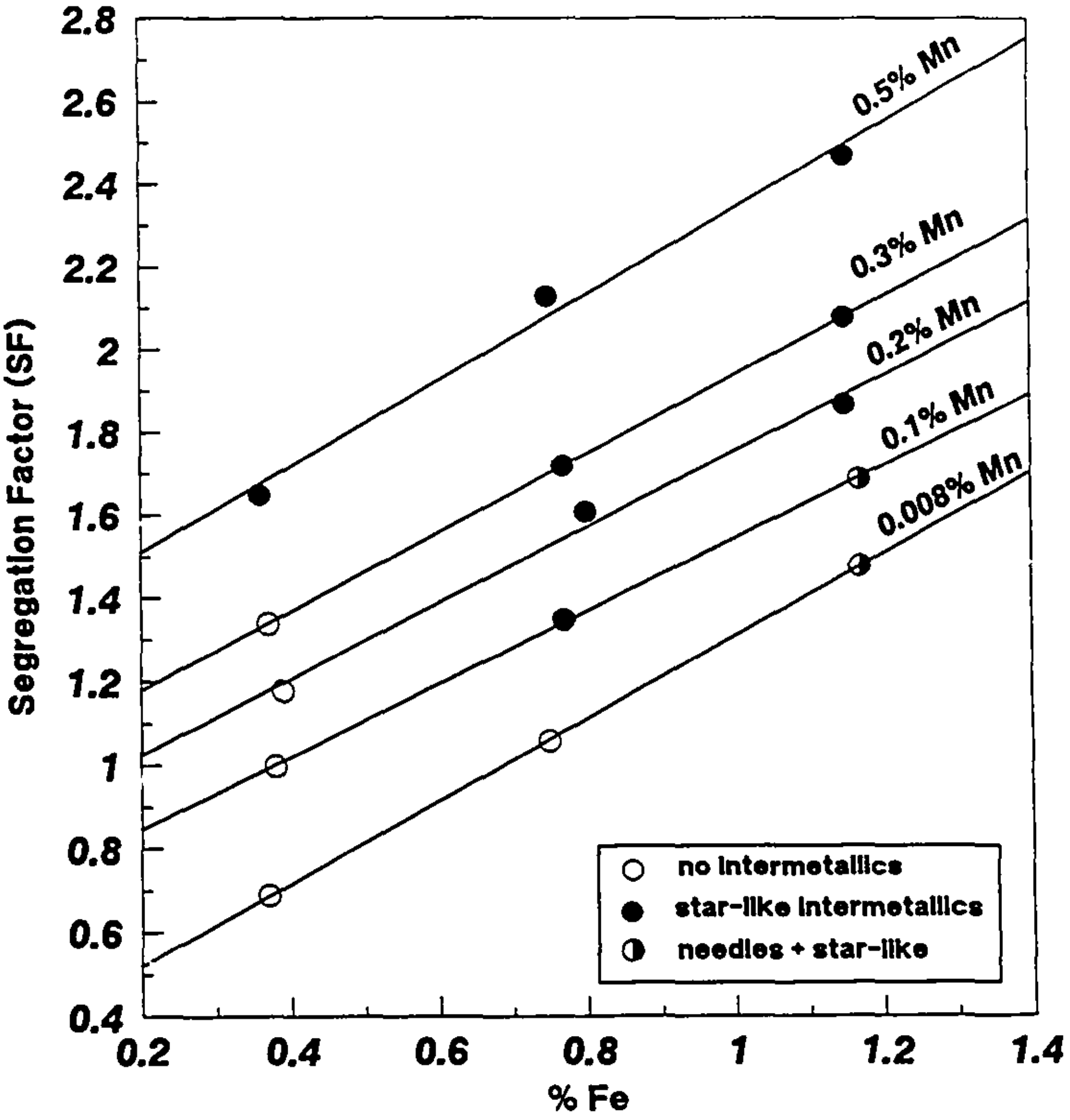

Figure 3.9: Effect of iron at each level of manganese in Al-12.7%Si-0.1%Cr alloy

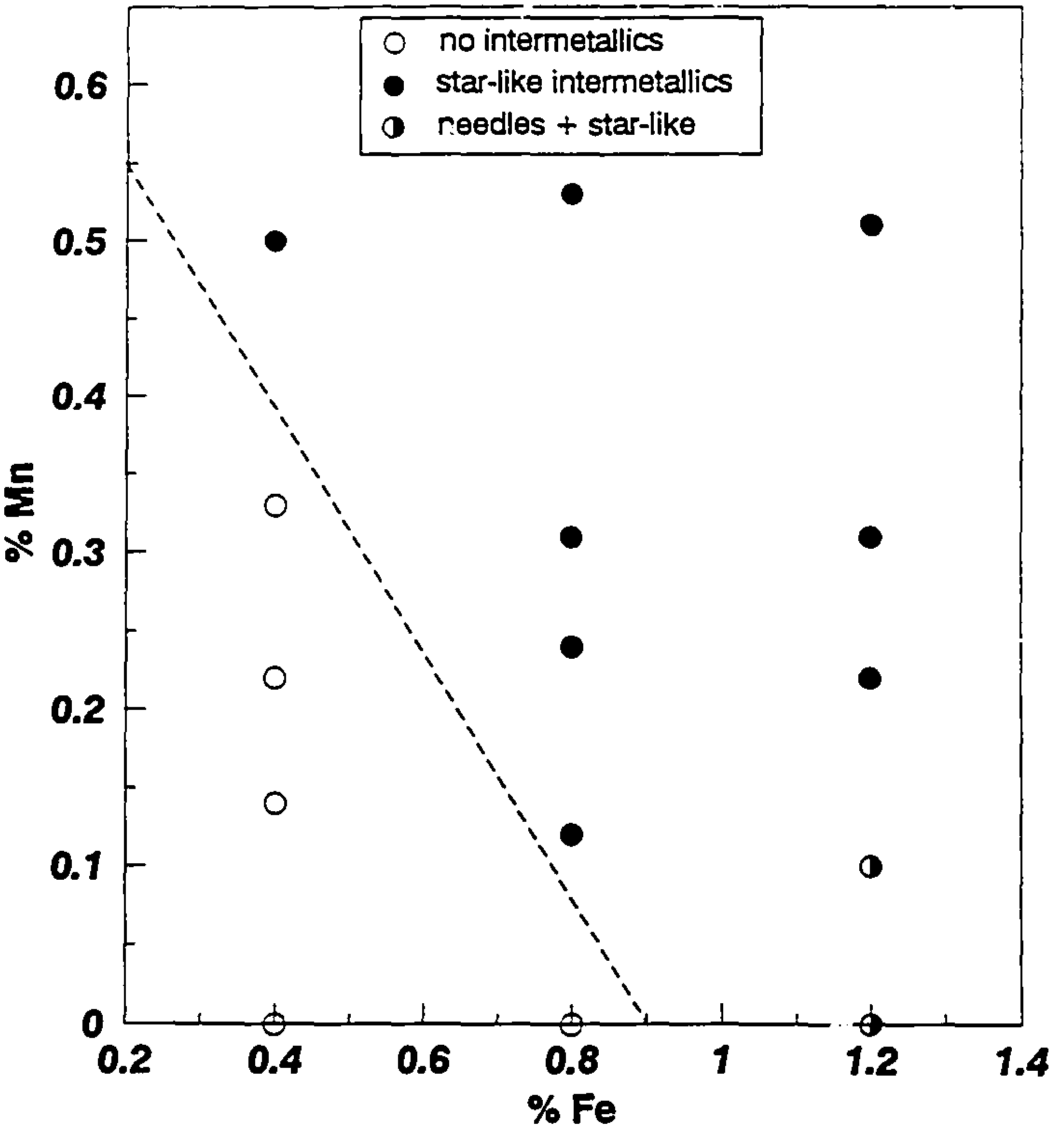

Figure 3.10: Effect of manganese and iron on the formation of intermetallic compounds in Al-12.7% Si-0.1% Cr alloy

The results of image analysis of the samples are shown in Figures 3.11, 3.12, and 3.13. In Figure 3.11, the volume percent of intermetallics is plotted as a function of iron concentration at various levels of manganese content. As the iron content increases in each alloy, more intermetallic compounds form and consequently the volume percentage of these compounds increases. The iron effect is more significant in the alloys which have higher levels of manganese. Any increase in volume percentage of intermetallics in all alloys is related to the size and the number of particles formed in a unit area. The results of the average size and the number of particles measured by image analysis are given in Table 3.7. This table indicates that the size of intermetallics as well as the number of particles increases with manganese, and/or iron content in the alloys. However, the contribution of the number of particles in increasing the volume percent of intermetallics is more significant than that of particle size.

The effect of manganese content at each level of iron on the volume percent of intermetallics is shown in Figure 3.12. This figure shows that no intermetallic forms at low iron and manganese concentration. The amount of intermetallics increases with manganese content in high iron concentration alloys.(eg. 0.8 and 1.2% Fe)

The volume percentage of intermetallics formed in each alloy as a function of segregation factor (SF) is plotted in Figure 3.13. This figure indicates that the volume percent of intermetallics increases linearly with segregation factor (SF) according to :

$$\text{Volume \%} = 1.33\,\text{SF} - 1.53$$

Use of this equation allows an estimation of the volume percent of intermetallics from the segregation factor (SF). It is seen from this equation that no intermetallics form in alloys with a segregation factor (SF) less than about 1.20. It is important to note that this equation applies only to the short holding time of 5 minutes at 670°C. In a comprehensive investigation reported in chapter 4, it is shown that the amount of intermetallics increases with holding time and decreases with holding temperature.

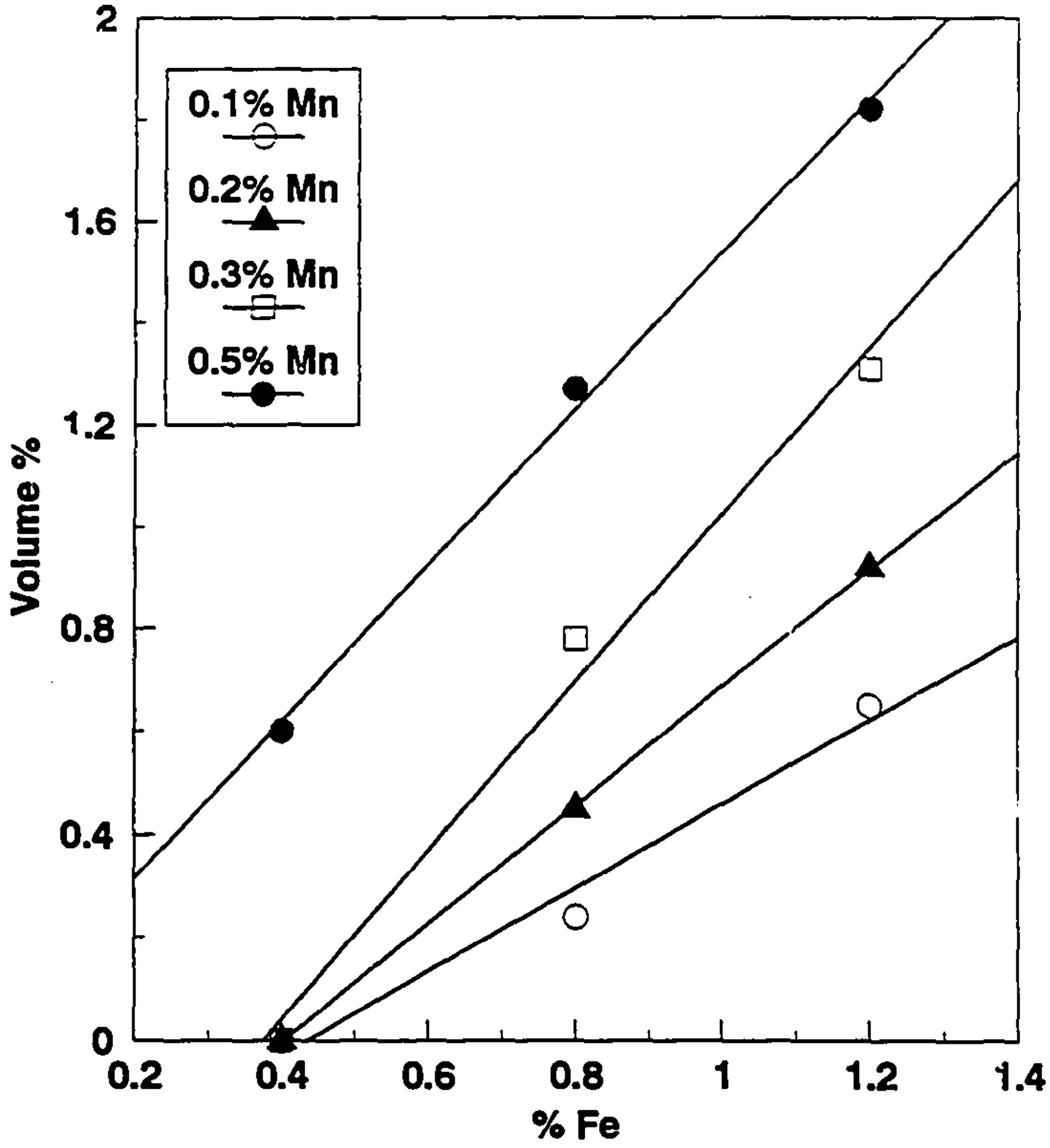

Figure 3.11: Volume percent of intermetallics as a function of iron concentration at various levels of manganese

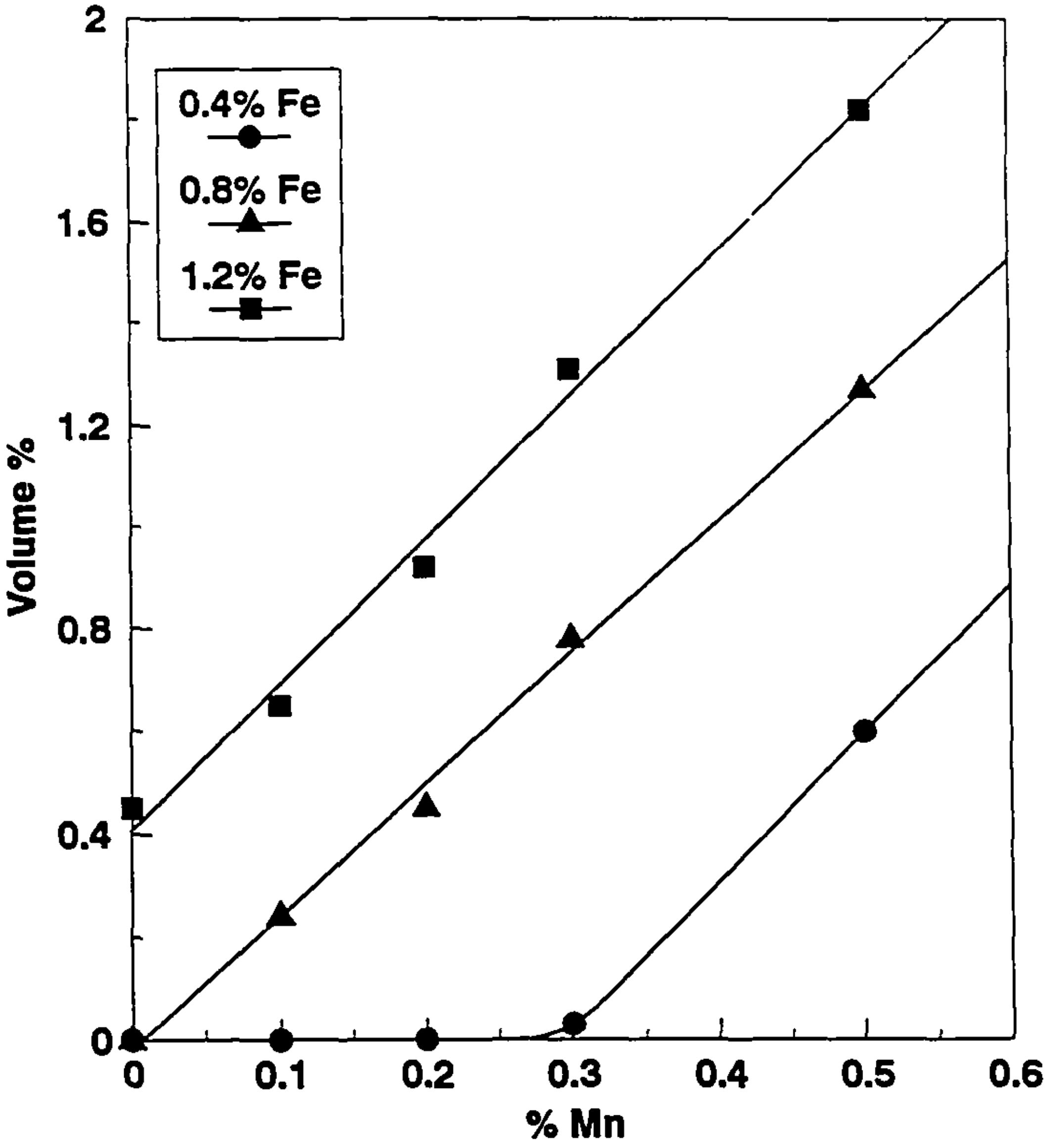

Figure 3.12: Volume percent of intermetallics versus manganese content at each level of iron

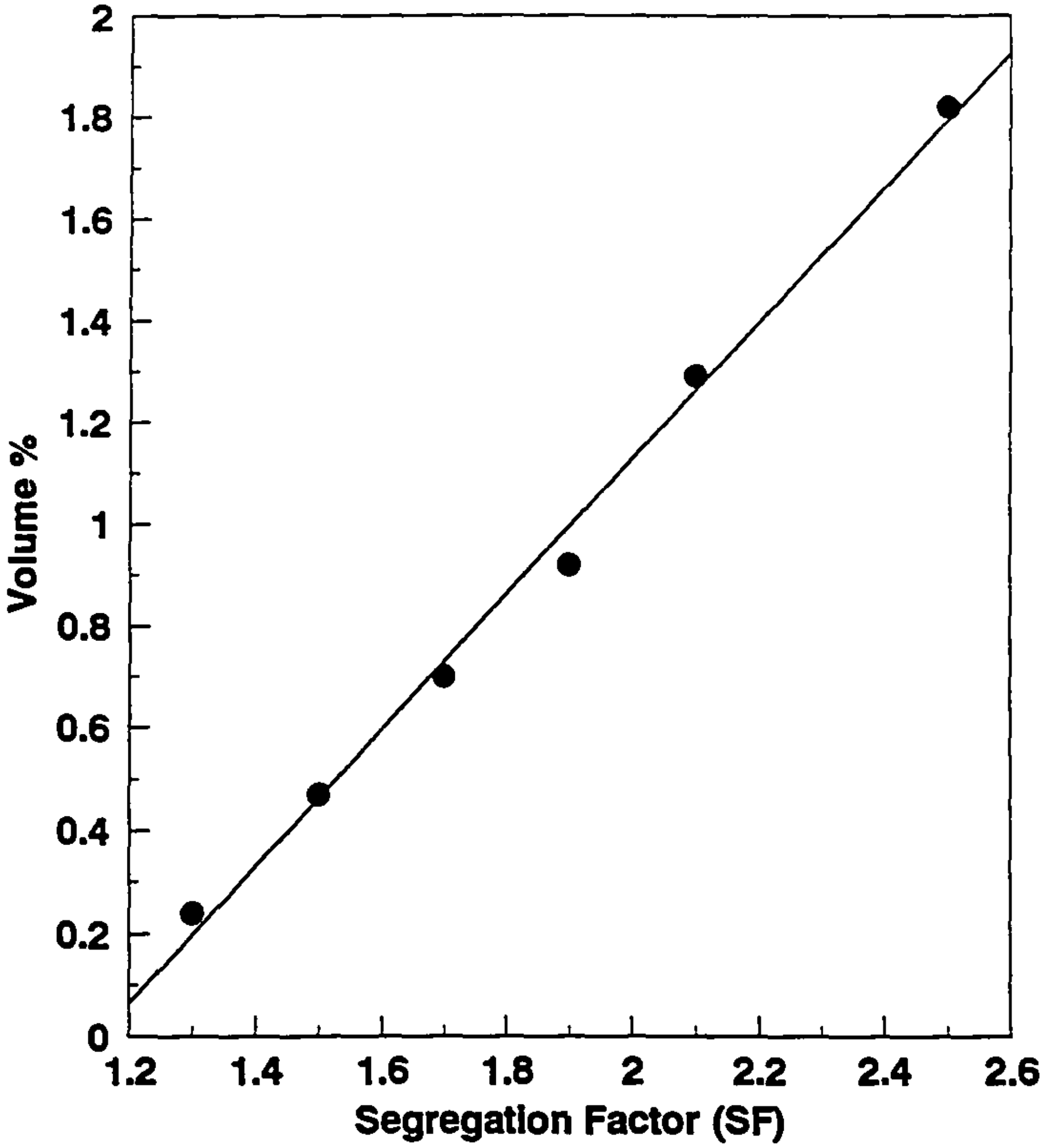

Figure 3.13: Volume percentage of intermetallics as a function of segregation factor (SF)

Table 3.7 : The Average Size and the Number of Intermetallics per unit Area

alloy	size(μm)	particle/mm^2
A6	8.81 ± 7.0	211 ± 97.2
B3	6.10 ± 4.1	75 ± 46.8
B4	6.25 ± 5.1	173 ± 101.8
B5	6.37 ± 3.4	458 ± 162.0
B6	8.84 ± 5.6	505 ± 67.8
C2	6.61 ± 3.0	286 ± 83.3
C3	7.40 ± 4.0	317 ± 115.7
C4	8.70 ± 5.8	339 ± 92.6
C5	9.20 ± 6.1	429 ± 88.8
C6	9.87 ± 6.8	556 ± 106.9

3.3.2. Temperature of Sludge Formation

3.3.2.1. 413P Alloy

The results of metallographic observations are given in Table 3.8. Sludge was not observed in samples quenched at temperatures above 690°C. Their microstructures consist of some primary silicon and very fine eutectic silicon in an aluminum matrix. In Figure 3.14(a) is shown the microstructure of alloy 413P quenched at 710°C. Star-like sludge plus primary silicon and eutectic silicon were found in a fine microstructure of alloy 413P quenched at temperatures below 690°C. Figure 3.14(b) shows the microstructure of the alloy quenched at 680°C. The results showed that the temperature of sludge formation in this alloy was 690°C.

Table 3.8 : Sludge Formation in Alloy 413P

temperature(°C)	660	670	680	690	700	710	720
sludge	yes	yes	yes	yes	no	no	no

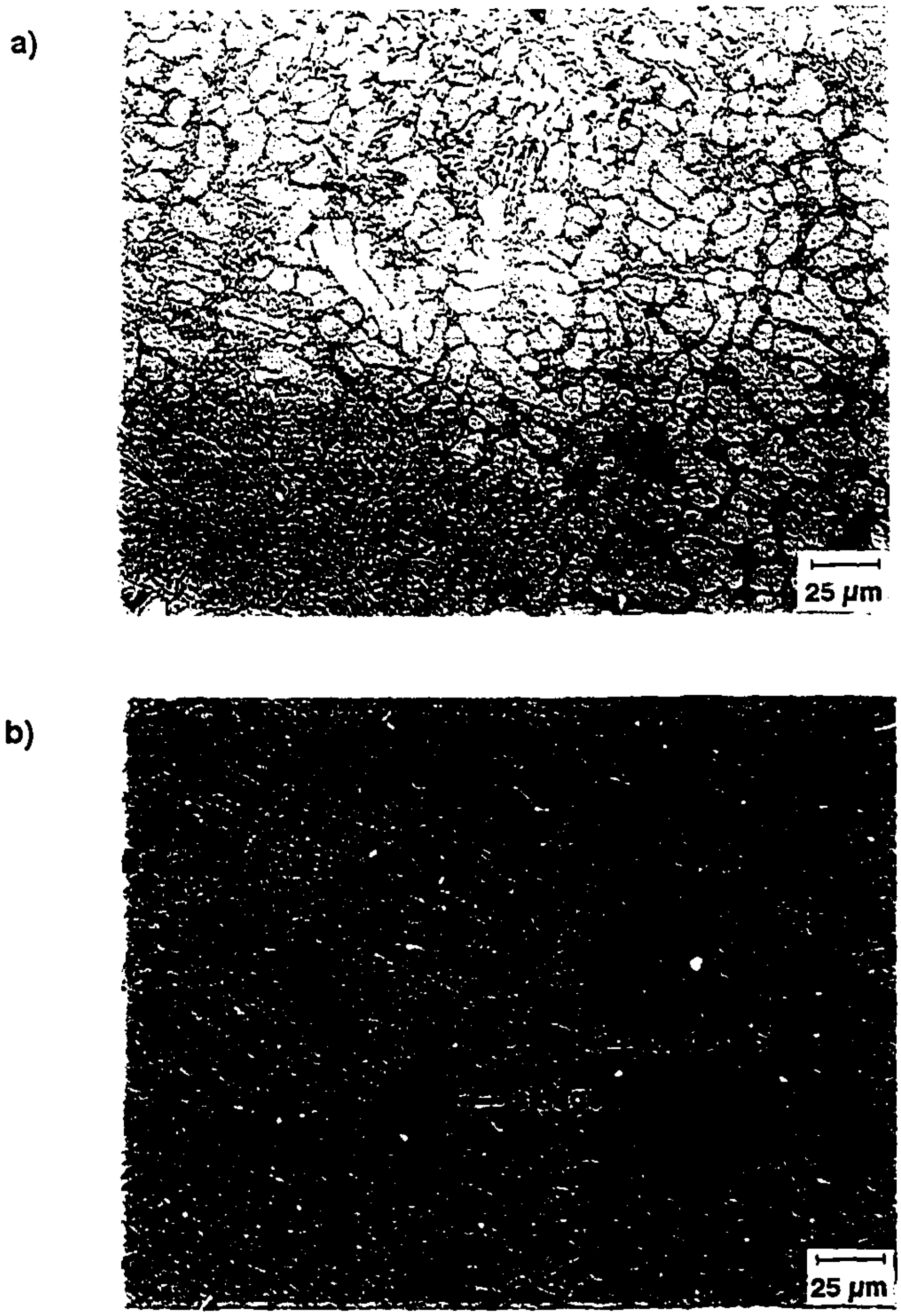

Figure 3.14 : Alloy 413P quenched at (a) 710°C , (b) 680°C

Thermal analysis curves are shown in Figures 3.15 - 3.18. The first derivative curve was calculated and plotted, and regions of interest on the curve were expanded to allow measurements to be made on both the temperature-time curve and the derivative curve. The results of thermal analysis showed that the eutectic temperature in the alloy was 567°C. In order to study the temperature of sludge formation by thermal analysis, the cooling curve was expanded in temperatures between 670-705°C (Figure 3.16) and the first derivative curve was calculated and plotted in this region. The curves revealed that sludge started to form at time, 22 seconds and formation was complete at 45 seconds after pouring.(Figure 3.18) This means that the intermetallic compounds form in 23 seconds within the temperature range 687-693°C. The results of thermal analysis and the microstructures verified the quenching experiments in which sludge formed in a short time at a temperature of 690°C.

These two series of experiments also revealed that star-like intermetallics form when the cooling rate is high, as in the quenching experiments. The Chinese script morphology is observed when the cooling rate is slow, as in the thermal analysis experiment. The Chinese script intermetallics are more numerous than the star-like compounds. In Figure 3.19 is shown the Chinese script and star-like compounds in the thermal analysis sample of alloy 413P. This result is in a good agreement to what was reported by Yaneva et al.[46] and is contradictory to the results of Ghomashchi[25] which showed that the polyhedral and Chinese script morphologies were independent of the cooling rate. This observation has been investigated comprehensively and will be discussed in detail in Chapter 5.

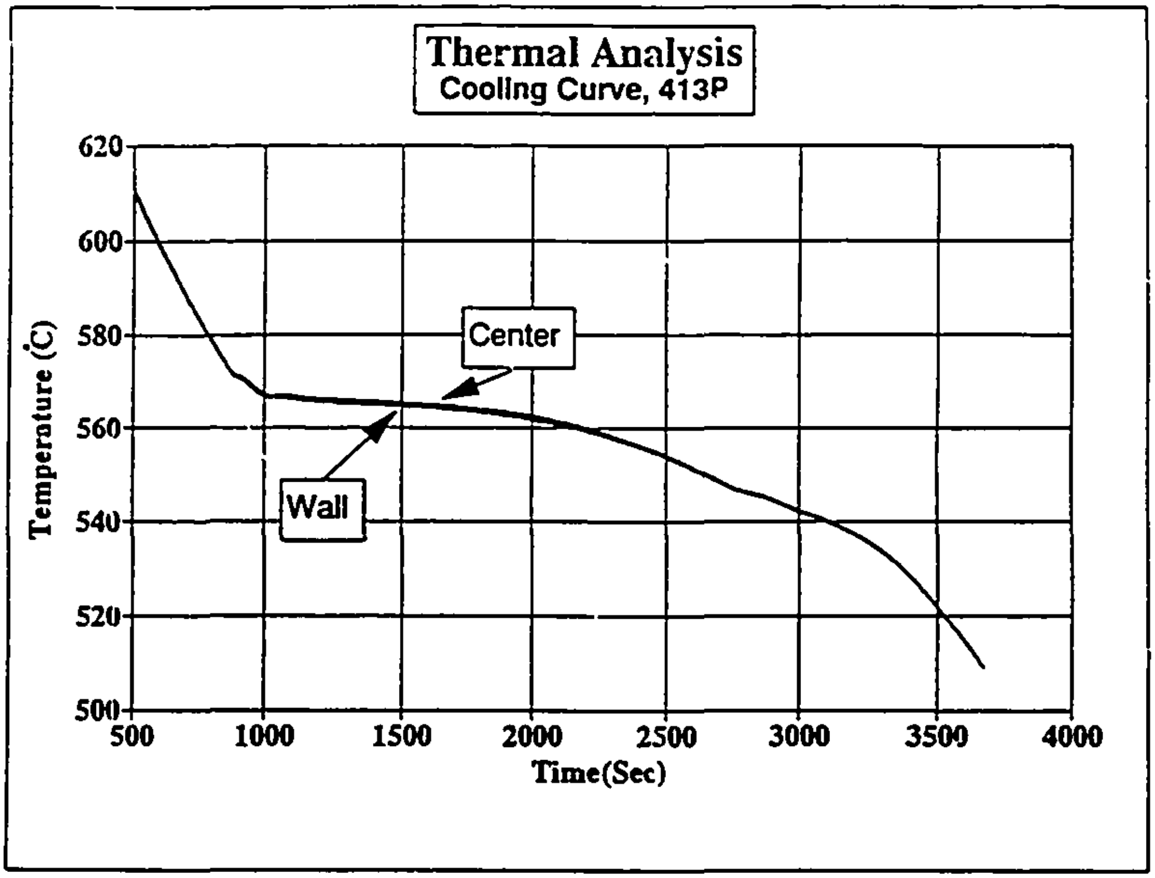

Figure 3.15: Cooling curve of alloy 413P in the range of 500-620°C

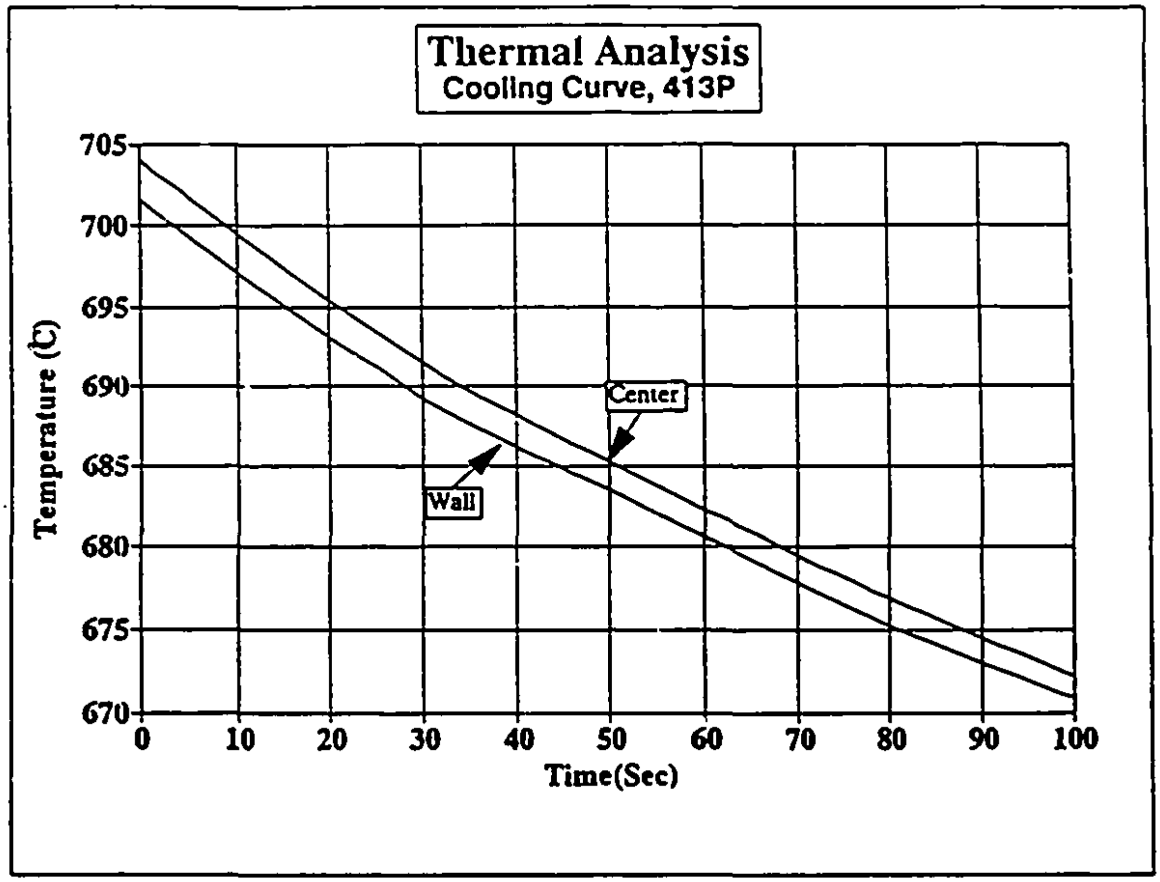

Figure 3.16: Cooling curve of alloy 413P in the range of 670-705°C

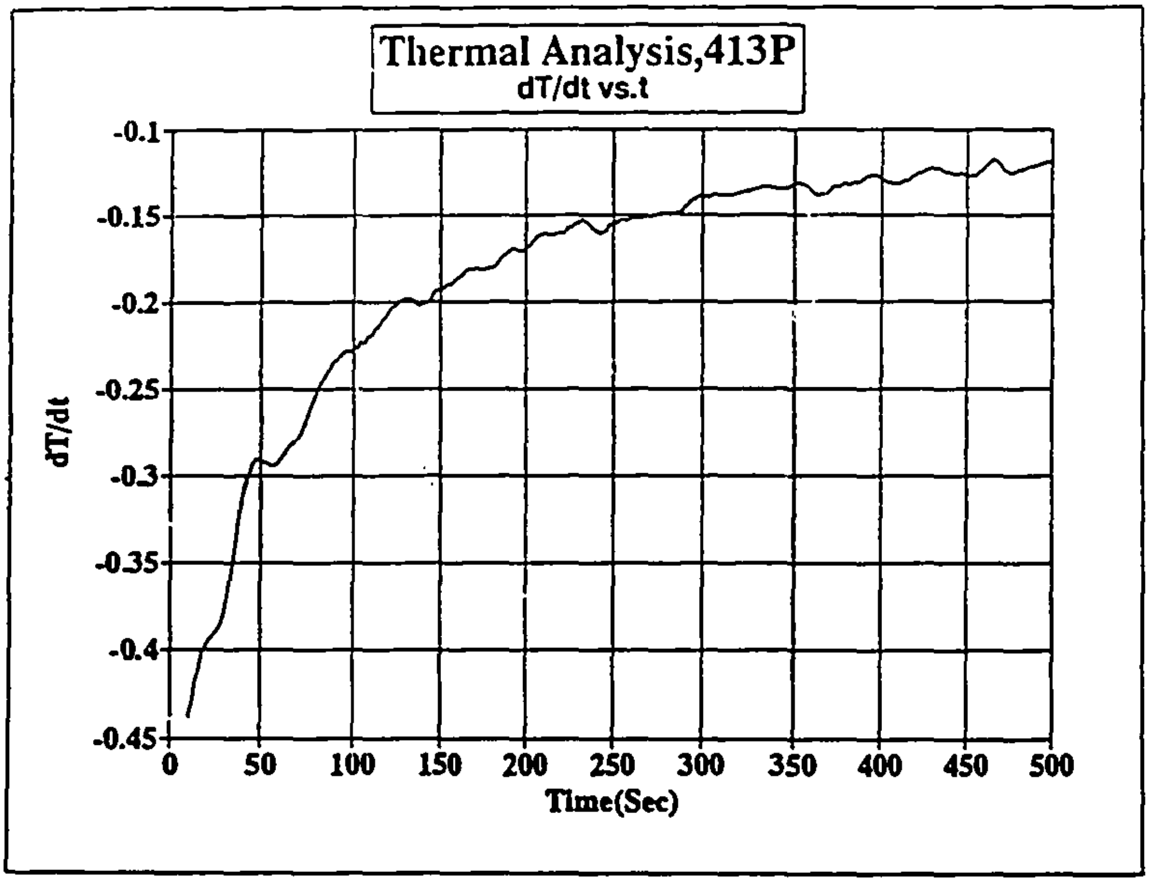

Figure 3.17: Derivative cooling curve of alloy 413P in the range of 610-705°C

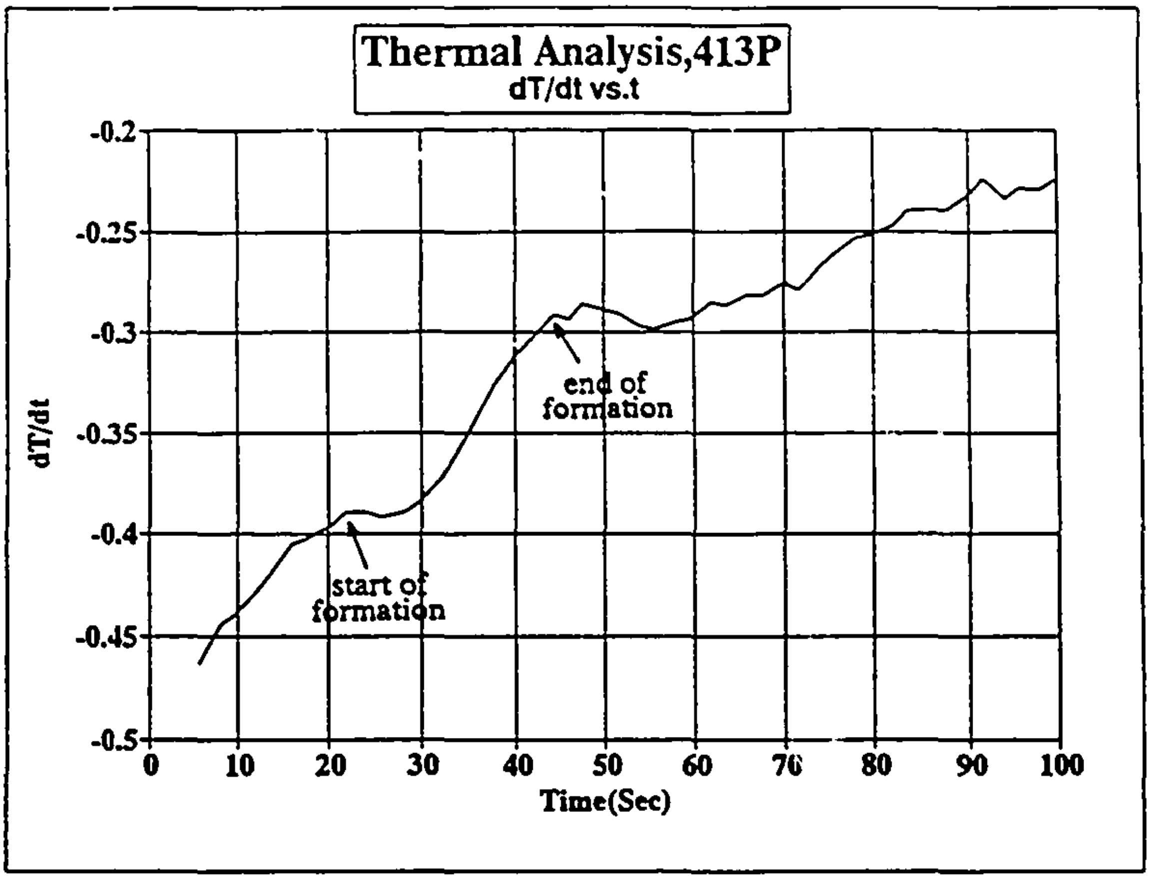

Figure 3.18: Derivative cooling curve of alloy 413P in the range of 670-705°C

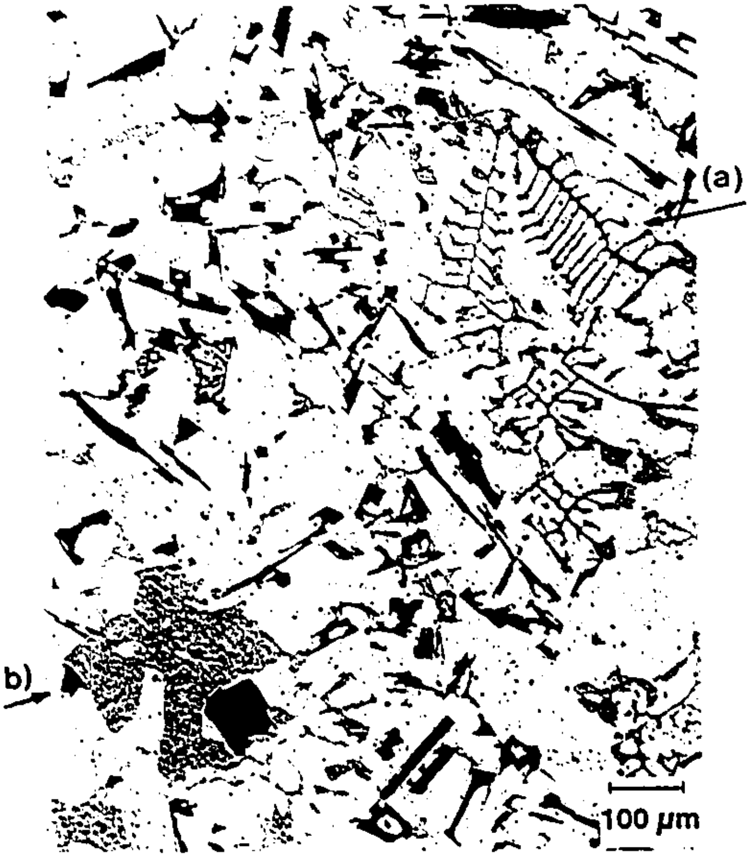

Figure 3.19 : Chinese script(a) and star-like(b) compounds in thermal analysis sample of alloy 413P (100X)

3.3.2.2. Synthetic Alloys

It was found from metallographic observations that holding the melt at temperatures of 800 - 850°C for 1.5 hours was sufficient to dissolve the intermetallics completely. The variation of the temperature of sludge formation with iron content is shown in Figure 3.20. When sludge was dissolved at 850°C, it did not reform until a certain characteristic temperature in each alloy. Sludge is thermodynamically unstable at temperatures above this value, which as seen from Figure 3.20 increases when the content of iron in the alloy is increased. The variation of temperature of sludge formation with iron content is given by a power equation as :

$$\text{Temperature}(^\circ\text{C}) = 645.7 + 34.2 \times (\%\ \text{Fe})^2$$

Figure 3.21 shows the microstructure of alloy 1 (Table 3.6) which contains 0.4% Fe. The microstructure of the alloy quenched at 700°C in liquid nitrogen is shown in Figure 3.21(a). Sludge is not formed at this temperature. Figure 3.21(b) shows sludge particles formed in the same alloy quenched at 640°C in liquid nitrogen.

3.3.3. Microstructural Study and Phase Analysis

The intermetallic compounds which were observed in most alloys studied in the present work were star-like in shape. Figures 3.22(a) and (b) show the SEM micrographs of these star-like intermetallic compounds in the eutectic aluminum-silicon alloys of B5 (0.8% Fe) and C5 (1.2% Fe), respectively. The distribution of iron, manganese, chromium, silicon, and aluminum in these phases is shown in Figure 3.23. This figure shows that the concentration of iron, manganese, and chromium is high in the star-like compounds.

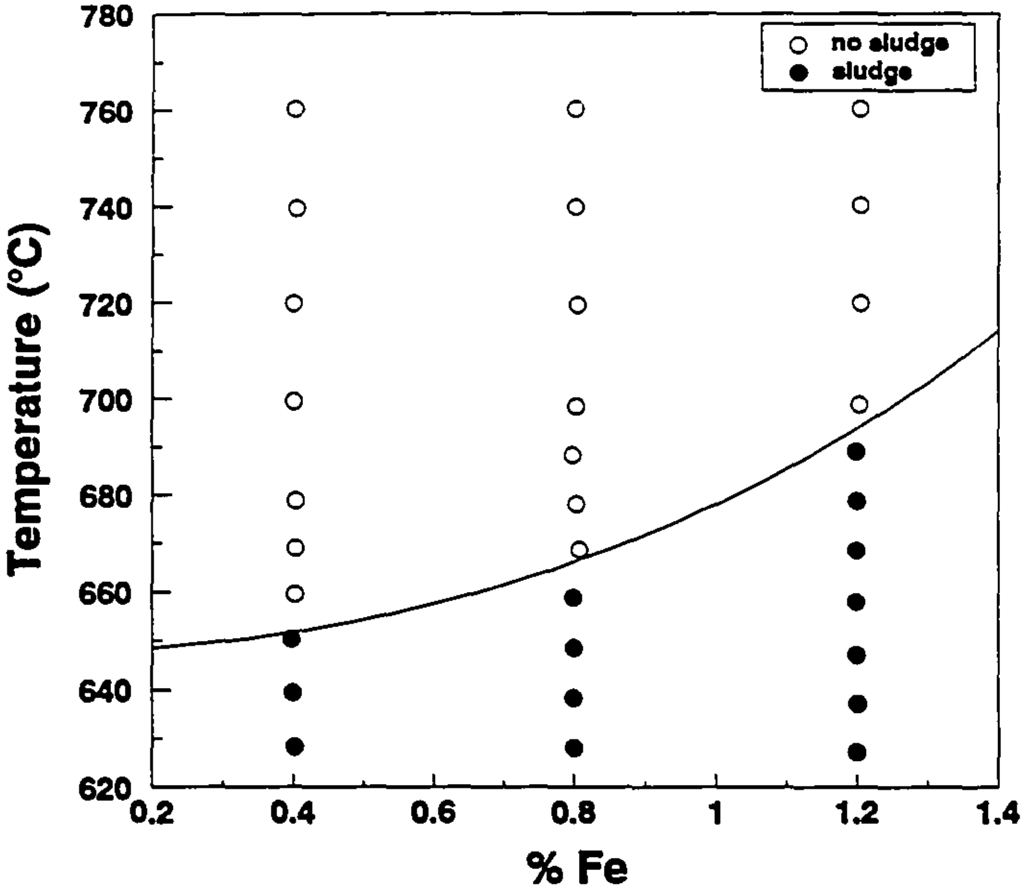

Figure 3.20: Temperature of sludge formation in alloys 1, 2, and 3.

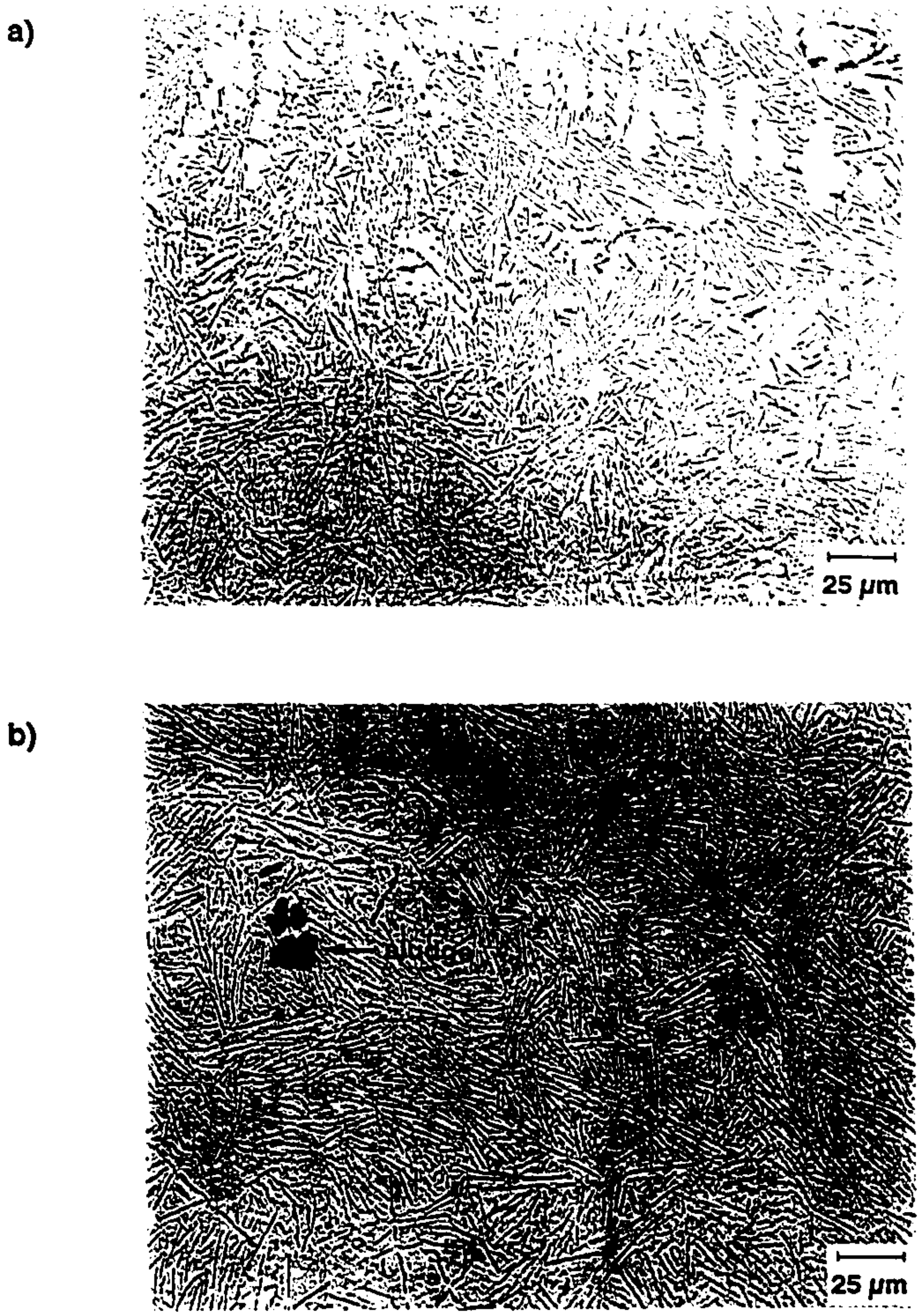

Figure 3.21 : Alloy 1 (0.4% Fe) quenched in liquid N_2 at (a) 700°C , (b) 640°C

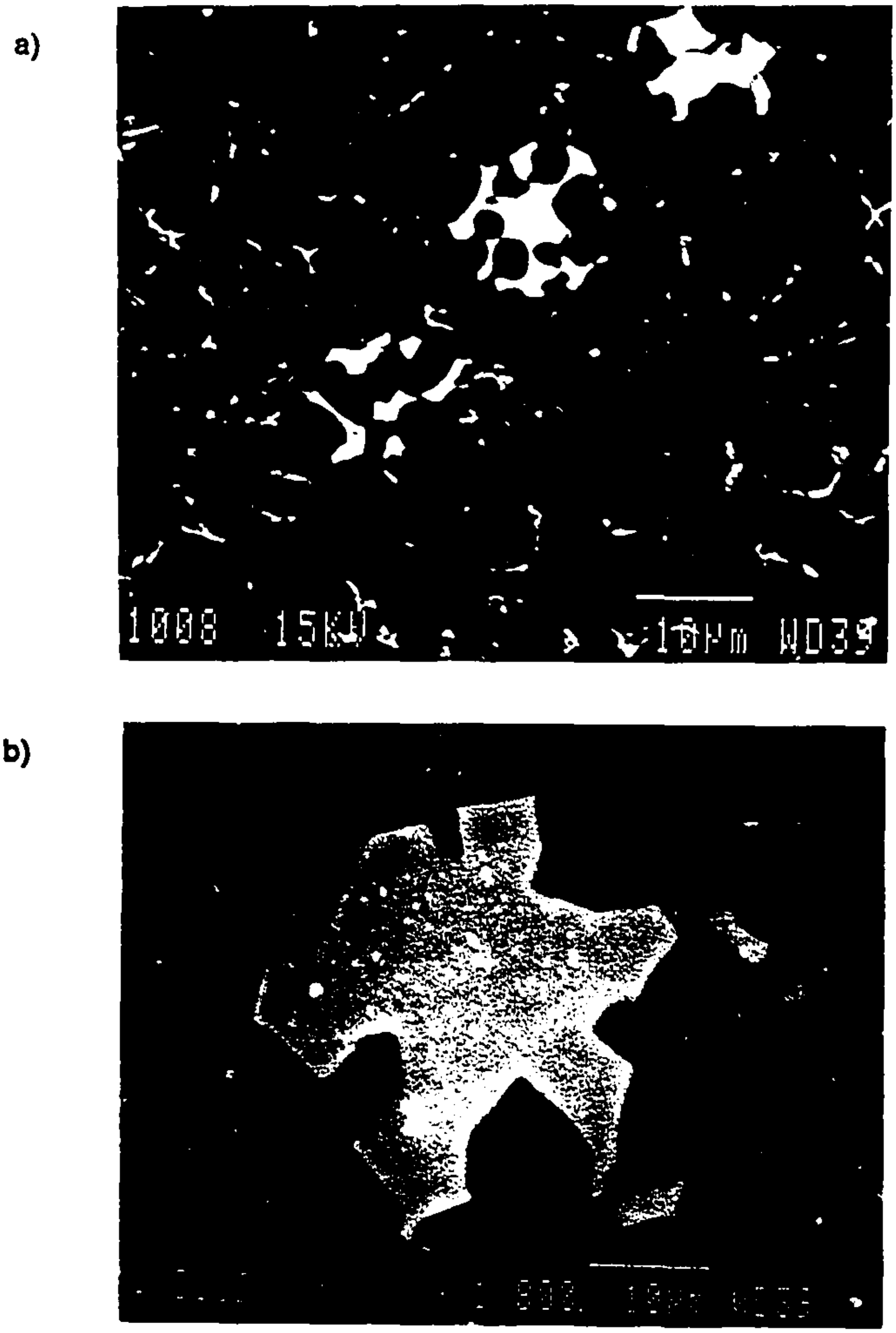

Figure 3.22 : SEM micrograph of star-like intermetallics in
(a) alloy B5 (0.8% Fe) , (b) alloy C5 (1.2% Fe)

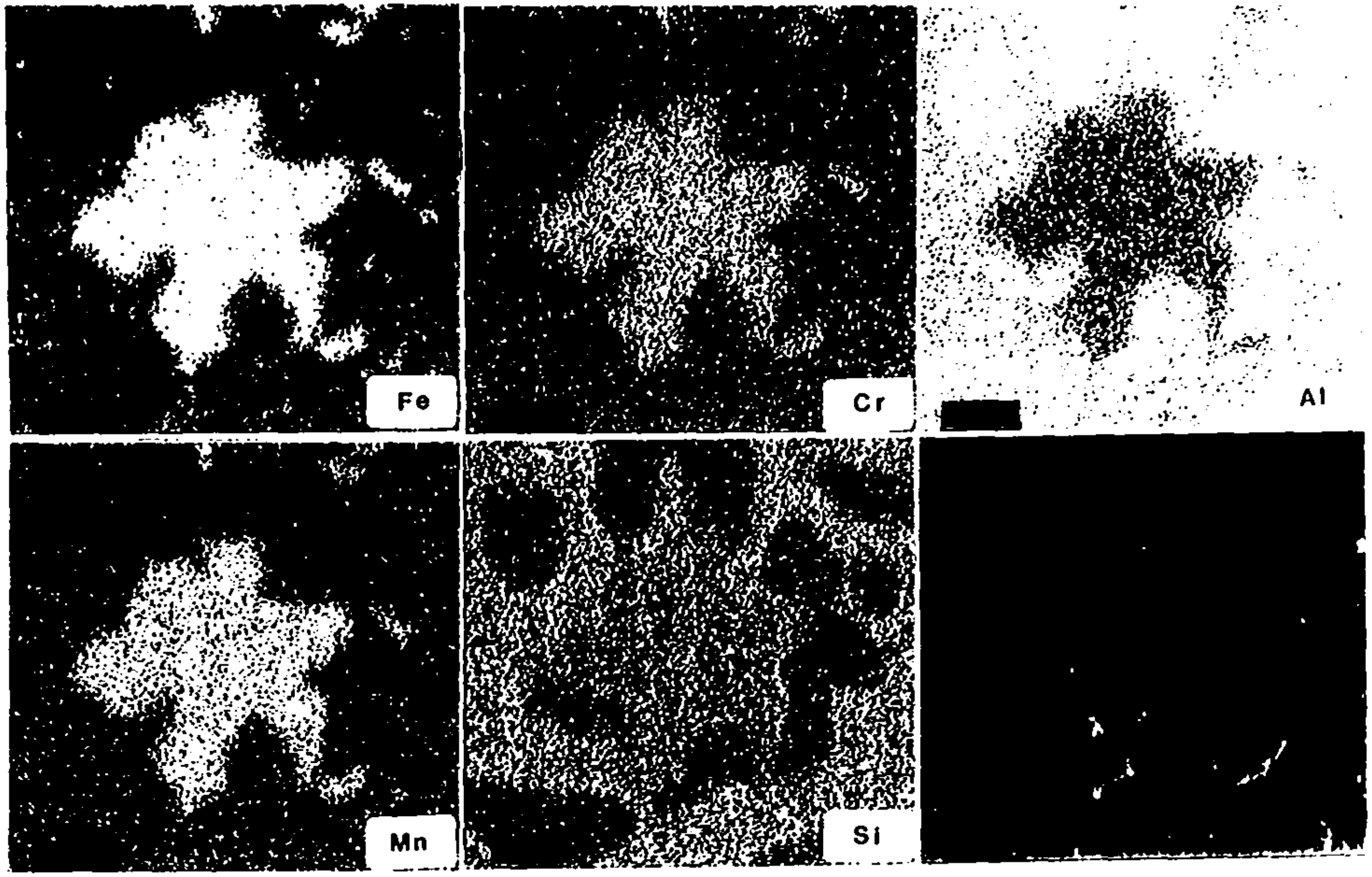

Figure 3.23 : X-Ray mapping of elements in the star-like compound shown in Figure 3.22(b)

The EDS spectrum of elements in sludge of alloy 413P is illustrated in Figure 3.24. This Figure gives a qualitative analysis which shows the existence of different elements in the sludge. The quantitative analysis has been performed by means of electron probe microanalyzer (EPMA). The chemical composition of sludge in alloy 413P analyzed by EPMA is given in Table 3.9.

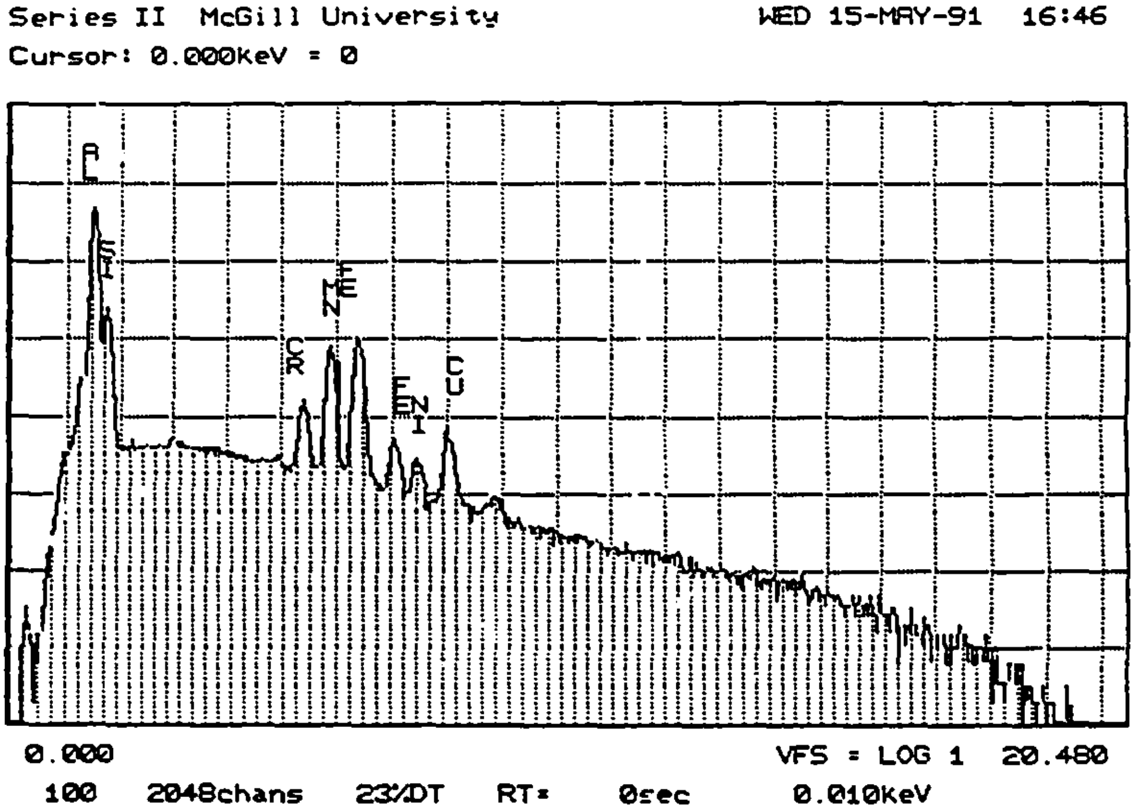

Figure 3.24 : EDS spectrum of the relative intensities of K_α lines of elements in sludge of 413P alloy

The shape of sludge formed in the experiment on temperature of sludge formation was mostly star-like or exploded (Figure 3.25), and the intermetallics were often found within primary aluminum dendrites. The intermetallics which form at high temperature consume some of the silicon present in the alloy and shift the local chemical composition of the melt to the aluminum side of the phase diagram, with the result that primary aluminum dendrites form around the intermetallics.

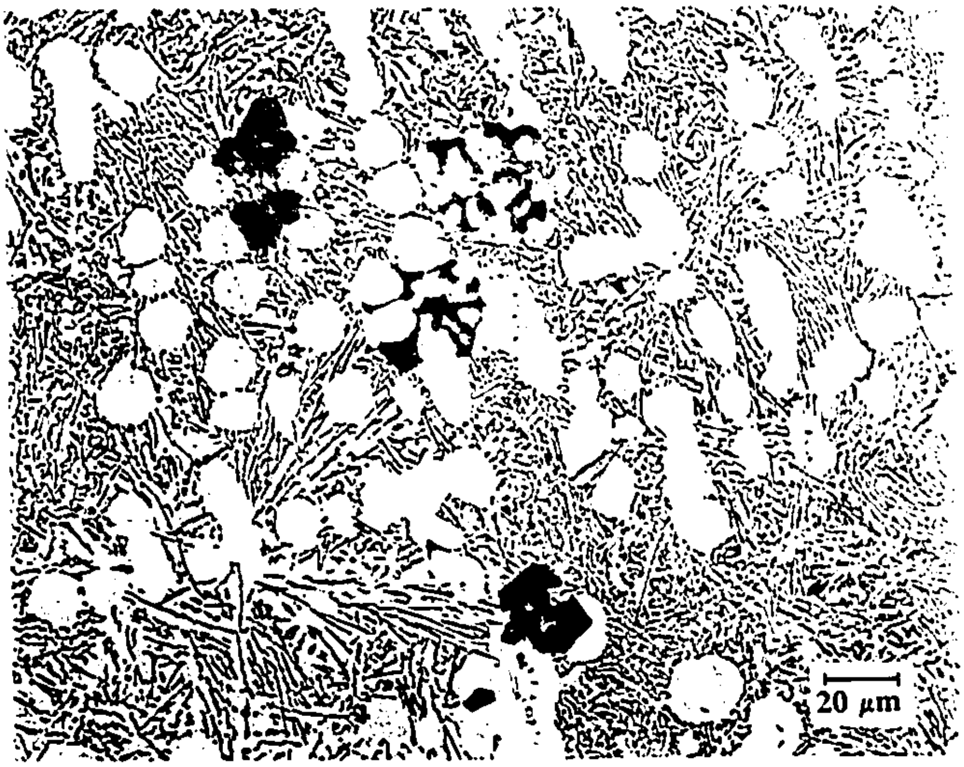

Figure 3.25 : Exploded intermetallic compounds in the quenched samples of alloy 2 (Table 3.6)

Table 3.9 : Chemical Composition of the Intermetallic Compounds (atomic %)

study on:	phase	Al	Si	Fe	Mn	Cr	Ni	Cu
melt chemistry	platelet	66.28	18.24	13.86	1.52	0.10	-	-
	star-like	71.54	11.46	9.47	5.18	2.34	-	-
synthetic alloys	star-like	71.41	11.72	7.88	5.36	3.64	-	-
(1, 2, 3)	exploded	71.75	11.35	9.81	4.61	2.49	-	-
413P alloy	star-like	71.85	11.54	8.48	5.97	1.57	0.61	-
thermal analysis	Chinese script	69.05	11.51	10.72	6.48	1.30	0.58	0.40

Table 3.9 gives the electron probe microanalysis (EPMA) of all of the complex intermetallic types studied in the present work. The chemical analysis given in this table is the average of at least five measurements. The star-like and exploded intermetallic compounds found in the experiments to determine temperature of sludge formation had the same chemical composition in all three alloys and their stoichiometry corresponds to $Al_{12}(Fe,Mn,Cr)_3Si_2$. Iron, manganese, and chromium, as transition elements, can substitute for each other in the same crystal structure which is body centred cubic and similar to the primary $Al_{15}(Fe,Mn,Cr)_3Si_2$ phase observed by Mondolfo.[36] The stoichiometry of the platelet morphology is $Al_5(Fe,Mn,Cr)Si$ which is similar to the β-Al_5FeSi.

The composition of the star-like and Chinese script intermetallic compounds in alloy 413P also corresponds to the formula $Al_{12}(Fe,Mn,Cr)_3Si_2$. This formula is in good agreement with the phase $Al_{12}(Fe,Mn,Cr)_3Si_2$ observed by Granger[81] and the phase $Al_{15}(Fe,Mn,Cr)_3Si_2$ reported by Tamminen[83] and Mondolfo[30]. Chemical analysis of the star-like intermetallic compounds given in Table 3.9 is very close to the results of Dunn[27], and Queener and Mitchell [29] reported for commercial 380 alloy. These results are in comparatively good agreement with determinations of the composition of the C-phase by Phragmen[49], and by Pratt and Raynor[48].

3.4. Summary

The effect of iron and manganese concentration on the formation of complex intermetallics has been studied by means of image analysis and metallography in an Al-12.7% Si alloy containing 0.1% Cr with three levels of iron (0.4, 0.8, 1.2%), and five different levels of manganese ranging from 0.0 to 0.5%. Temperature of sludge formation was investigated on commercial and synthetic alloys through quenching experiments and thermal analysis. The results obtained and conclusions drawn may be summarized as follows :

(I) Sludge forms at a high content of iron eg. 1.2% Fe, or at high concentrations of manganese and chromium with low contents of iron eg. 0.4% Fe. More than 0.2% Mn and 0.1% Cr are needed to convert all iron platelet phases to star-like intermetallics.

(II) The combined effect of manganese and iron on the formation of intermetallics is represented by the equation: %Fe + 1.7 %Mn = 0.97. Intermetallics form at any values higher than this line. This equation is in a reasonable agreement with the segregation factor (SF) equation.

(III) The volume percentage of intermetallic compounds increases as the iron or manganese content increases in any alloy. This increase has been found to be as a result of both size and number of star-like compounds.

(IV) The amount of intermetallic compounds can be estimated from a segregation factor by a linear relationship at short holding time.

(V) The stoichiometry of star-like and exploded intermetallic compounds corresponds to $Al_{12}(Fe,Mn,Cr)_3Si_2$ while needle or platelet compounds have the stoichiometry $Al_5(Fe,Mn,Cr)Si$. Iron, manganese, and chromium, as transition elements in $Al_{12}(Fe,Mn,Cr)_3Si_2$, can substitute for each other in the B.C.C crystal structure. The distribution of elements in these phases revealed that the concentration of iron, manganese, and chromium is high in the intermetallics.

(VI) Superheating the melt to temperatures of 800-850°C and holding for 1.5 hours dissolves the intermetallics completely. When sludge is dissolved, it will not reform until a certain temperature in each alloy.

(VII) Quenching experiments and thermal analysis revealed that sludge forms in a short period of time. The temperature of sludge formation in 413P alloy is 690°C. In general, temperature of sludge formation depends on the alloy composition and particularly, iron concentration. This temperature increases when the content of iron in the alloy is increased. A power equation describes the relation between sludge formation temperature and iron content.

Chapter 4

Kinetics of the Formation of Intermetallic Compounds

4.1. Introduction

The chemical composition of the melt, particularly iron content, has a significant influence on the formation of intermetallic compounds. Holding temperature and holding time are the other important parameters which should be considered in the formation of intermetallic compounds in aluminum melts. There is very little information available in the literature in this regard.

In the present chapter, the kinetics of the formation of intermetallics considering the roles of holding temperature, holding time, and initial chemical composition have been studied on three aluminum alloys containing 12.7% Si, 0.3% Mn, and 0.1% Cr with different levels of iron. All alloys at any given temperature and time were investigated quantitatively by means of image analysis and metallography.

4.2. Experimental Procedure

4.2.1. Materials

Three alloys with nominal iron levels of 0.4, 0.8, or 1.2% and constant manganese and chromium were prepared in an induction furnace. Melting was performed at 750°C and the liquid alloy was degassed for 15 minutes with nitrogen. 20 kg of each alloy was prepared and cast at 720°C into ingot molds. Commercial purity aluminum and silicon were used in manufacturing these alloys and the appropriate Fe, Cr, and Mn additions were made to the alloys by means of commercial master alloys of composition: Al-24.7% Fe, Al-20.1% Cr and Al-25.2% Mn. The complete chemical analysis of the master alloys was given in Table 3.4 (chapter 3) and the initial chemical composition of the alloys is given in Table 4.1.

Table 4.1: The Initial Chemical Composition of the Alloys (wt%)

Alloy	Si	Fe	Cu	Mn	Mg	Cr	Ni	Zn
1	12.88	0.42	<0.002	0.31	<0.009	0.11	<0.001	<0.008
2	12.74	0.80	<0.002	0.30	<0.009	0.11	<0.001	<0.008
3	12.46	1.21	<0.002	0.29	<0.009	0.10	<0.001	<0.008

4.2.2. Effect of Holding Temperature, Time, and Initial Chemical Composition

To study the kinetics of the formation of intermetallic compounds, it is important to consider the roles of temperature, time, and initial chemical composition. To study the effect of holding temperature on the formation and growth of the intermetallics, each alloy was maintained at a constant temperature of 600, 630, 660, or 690°C in an alumina crucible held in an electric resistance furnace. To investigate the effect of holding time, each melt was held for 0, 30, 60, 120, or 180 minutes at each constant holding temperature for each alloy. The influence of the chemical composition on the formation and growth of the intermetallics was determined by using the three different alloys listed in Table 4.1. Each batch of melt contained 1.5 kg of alloy and was stirred for 90 seconds at a constant temperature before sampling. Two samples were taken each time; one poured into a permanent metallic mold and the other into a graphite mold preheated to 500°C (2.5 cm in diameter and 5.0 cm in height). The operational cycle at a holding temperature of 600°C is shown in Figure 4.1.

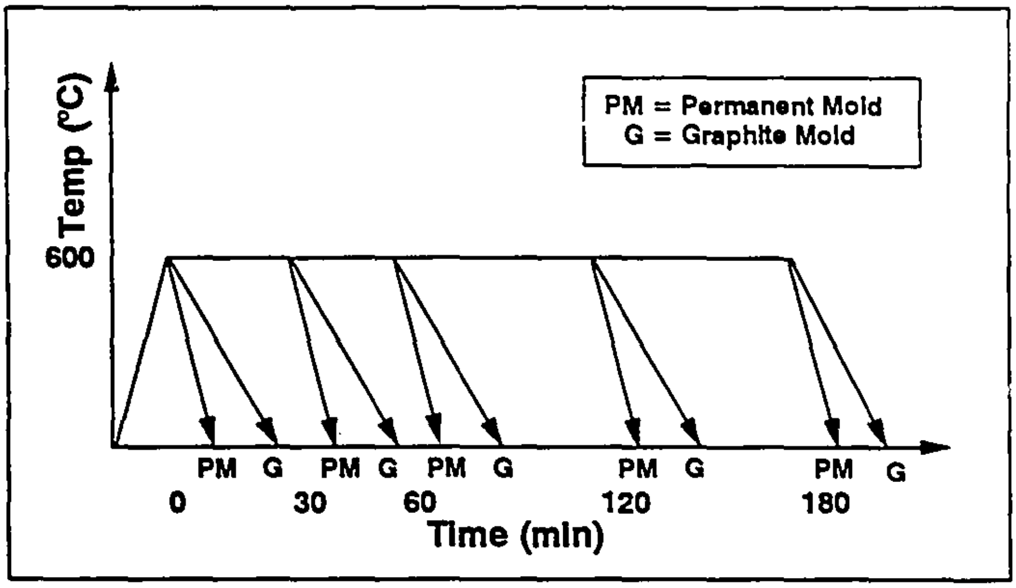

Figure 4.1: Operational cycle at 600°C

4.2.3. Microstructural Study and Image Analysis

Metallographic analysis was carried out on all alloys in all cases studied. The samples were polished up to 0.03 μm alumina powder then continued with colloidal silica and observed by the optical NEOPHOT 21 microscope and scanning microscope (SEM), JOEL 840. In order to develop a more consistent and less subjective evaluation of the microstructure, quantitative metallography was employed using a LECO image analyzer interfaced with an optical microscope through the 2005 image analysis program. Various microstructural parameters were investigated and measured, such as the particle area (μm^2), average size (μm), number of particles per unit area (mm^2), particle area percentage (%), roundness, and aspect ratio.

A total of 12 fields at 100X magnification was evaluated on each sample giving an analyzed area of about 8.4 mm x 5.0 mm per sample. The data was processed automatically using statistical programs, and the mean values reported for each sample. Figure 4.2 shows a photograph of a typical sample with the phases highlighted by the image analyzer.

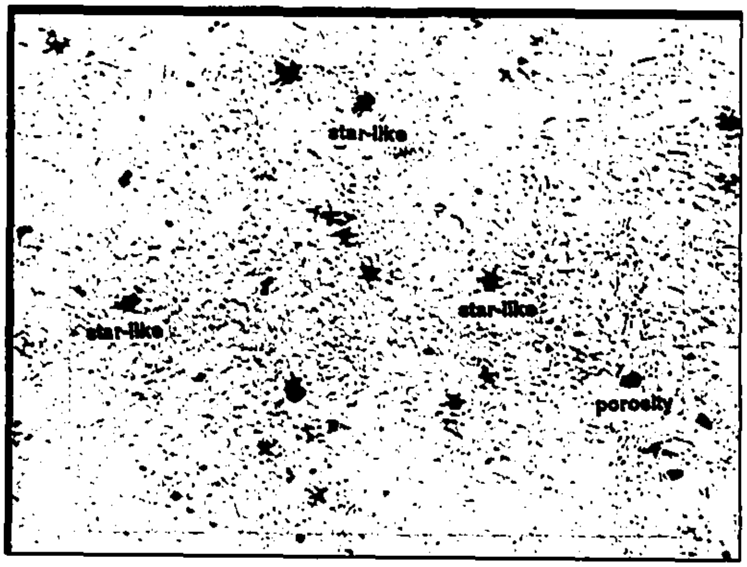

Figure 4.2: Photograph of a typical sample using an image analyzer (100X)

The stoichiometry of the phases was also determined by electron probe microanalyzer. EPMA was used at a voltage level of 15KV for chemical analysis of the phases, and the average of five readings was calculated for each phase. For the element analysis, ZAF correction was made with reference to the standard pure element. The entire experimental procedure is summarized in Figure 4.3.

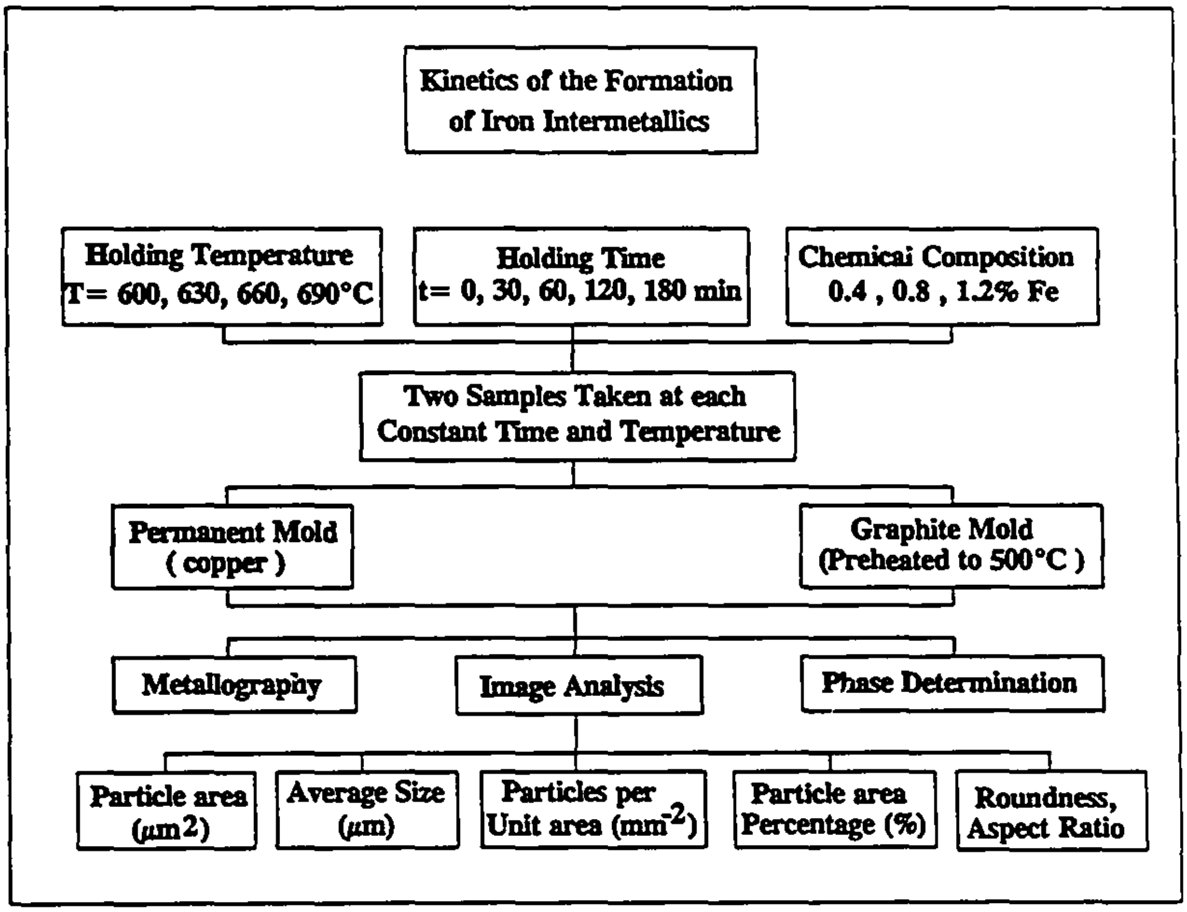

Figure 4.3: Experimental procedure used to study the kinetics of the formation of iron intermetallics

4.3. Results

4.3.1. Metallography and Phase Analysis

Metallographic observations of the samples revealed that the microstructure of the alloys consisted of primary aluminum, eutectic silicon, and intermetallic compounds. The compounds had star-like shapes and in alloy 3 (1.2% Fe), needle-like (platelet) intermetallics were also observed. The microstructure of the alloy 1 (0.4% Fe) and alloy 3 (1.2% Fe) are shown in Figure 4.4 (a,b).

Table 4.2 gives the EPMA analysis of the intermetallic compounds. According to EPMA, the star-like intermetallics had the same chemical composition in all three alloys with their stoichiometry corresponding to $Al_{12}(Fe,Mn,Cr)_3Si_2$ while the needle-like (platelet) phase had the stoichiometry of $Al_5(Fe,Mn,Cr)Si$. The compositions of the phases are similar to those analyzed in chapter 3 (Table 3.9).

Table 4.2: Chemical Composition of the Intermetallic Compounds (atomic %)

Alloy	Phase	Al	Si	Fe	Mn	Cr
1 (0.4% Fe)	star-like	71.4	11.7	8.0	5.4	3.6
2 (0.8% Fe)	star-like	72.3	11.3	9.4	4.6	2.4
3 (1.2% Fe)	star-like	71.6	11.2	9.6	4.7	2.9
3 (1.2% Fe)	platelet	66.8	18.8	12.1	2.0	0.2

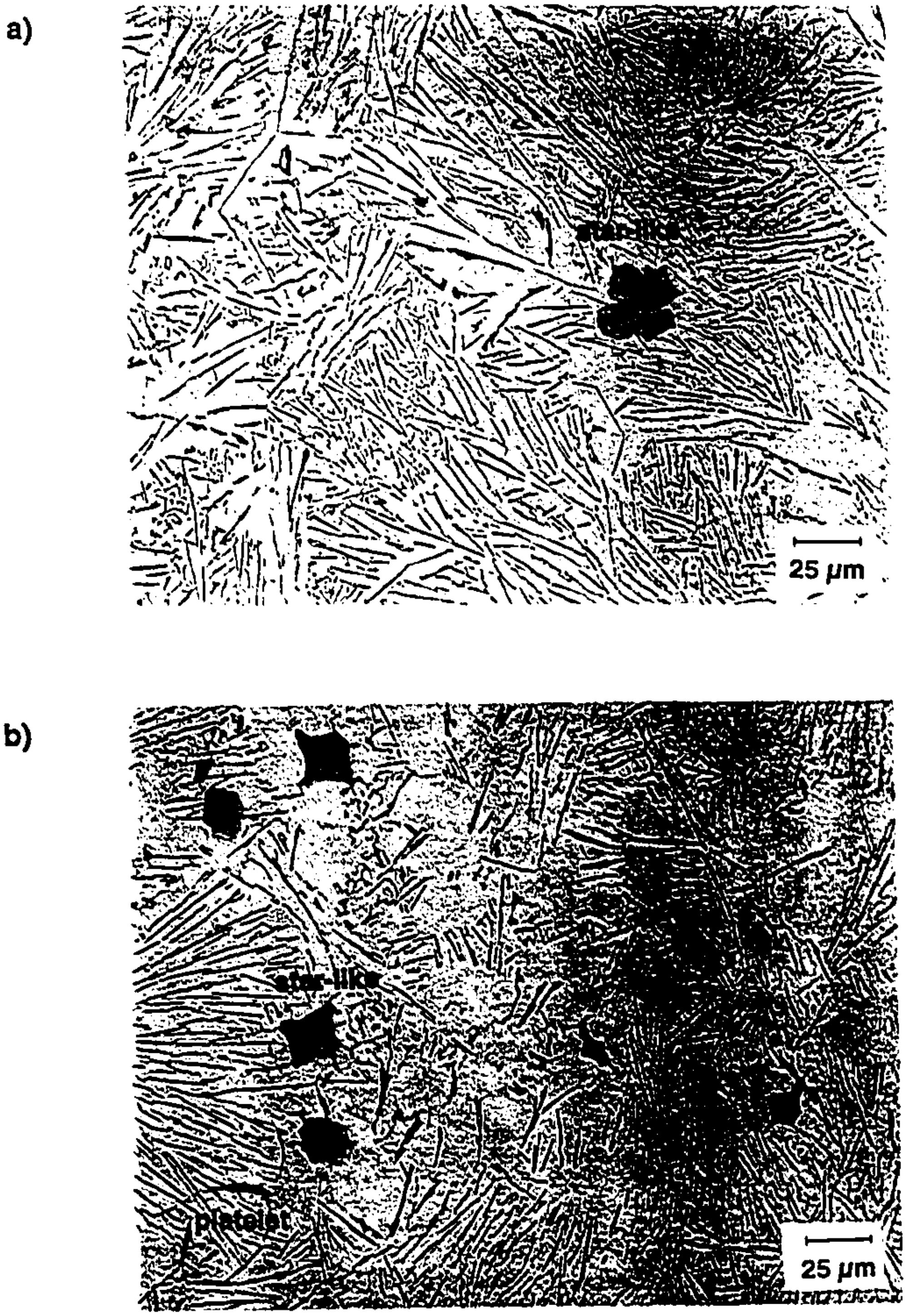

Figure 4.4: Intermetallic compounds in: a) alloy 1(0.4% Fe) b) alloy 3(1.2% Fe)

4.3.2. Effect of Holding Temperature, Time, and Initial Chemical Composition

The process of the formation of complex intermetallic compounds in liquid aluminum-silicon alloys depends on the mechanism of nucleation and growth. Therefore, in the course of the present work, the nucleation process was studied through measurement of the number of particles formed per unit area while growth was investigated by determining the average size of the particles.

The total effect of nucleation and growth of the intermetallic compounds is measured by the total volume percentage of intermetallics formed during each experiment. The volumetric changes of the intermetallics formed during the process at each constant temperature with respect to initial chemical composition of the alloys are shown in Figure 4.5(a - d).

Figure 4.5(a) shows that the volume percentage of the particles in each alloy increases with holding time at 600°C with more intermetallics formed as the iron content increases from 0.4% to 1.2%. When the melt is maintained for a long time (3.0 hr), a large amount of intermetallic is formed, and this is particularly significant in alloy 3 which has 1.2% Fe (the volume percentage is about 6%).

Figure 4.5(b) indicates the effect of holding time and iron content on the volume percentage of intermetallics formed at a holding temperature of 630°C. The same situation exists as at 600°C. When the iron content increases from 0.4 to 1.2% more intermetallics form and the volume percent increases with holding time.

Figure 4.5(c) shows that at 660°C the volume percent of particles increased in alloy 3 (1.2% Fe), but decreased in alloy 1 (0.4% Fe) and alloy 2 (0.8% Fe). The reduction in volume percent in these two alloys is very significant when the holding time

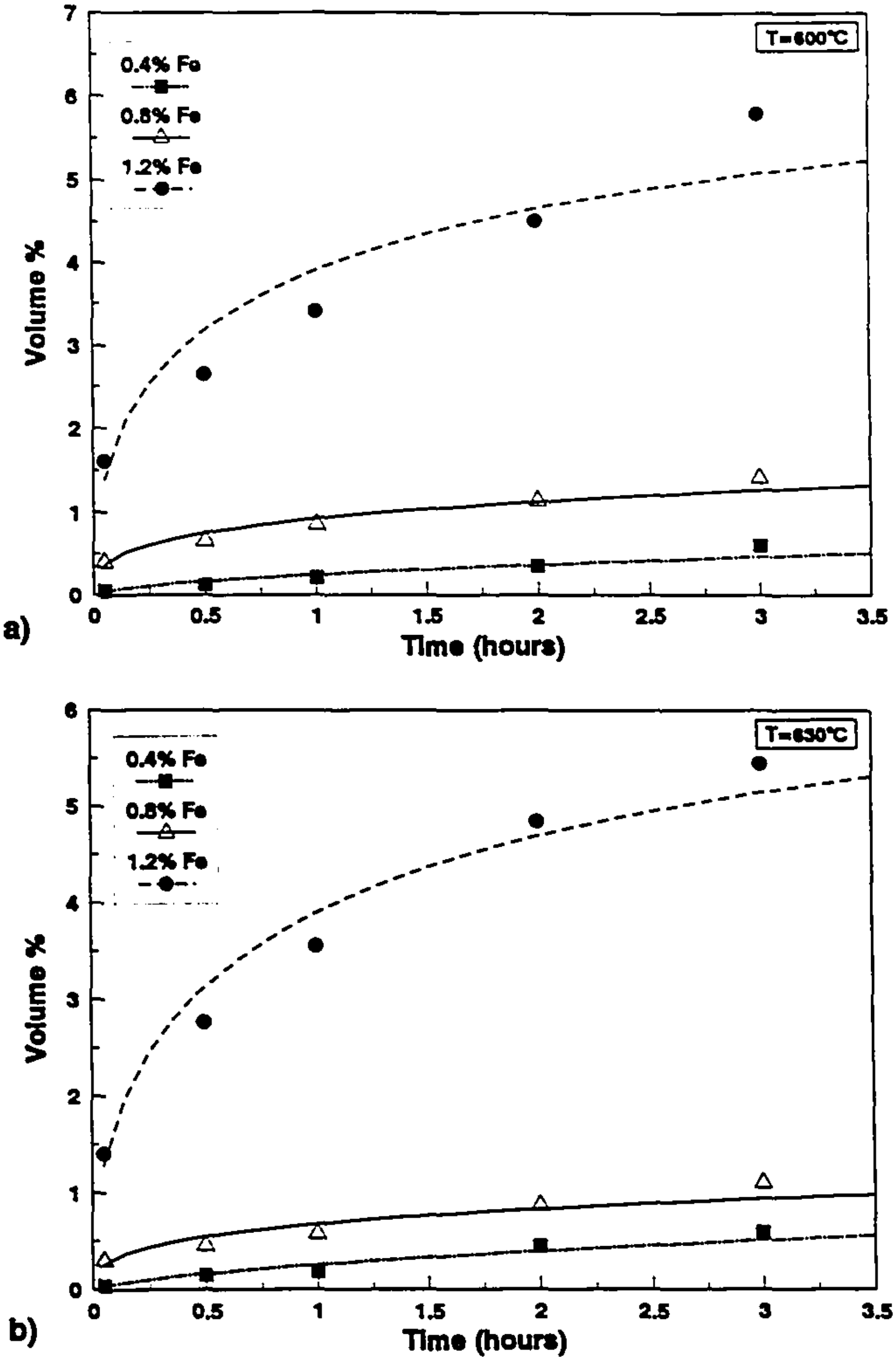

Figure 4.5: The volumetric changes of intermetallics in alloys 1, 2, and 3
a) T=600°C b) T=630°C c) T=660°C d) T=690°C

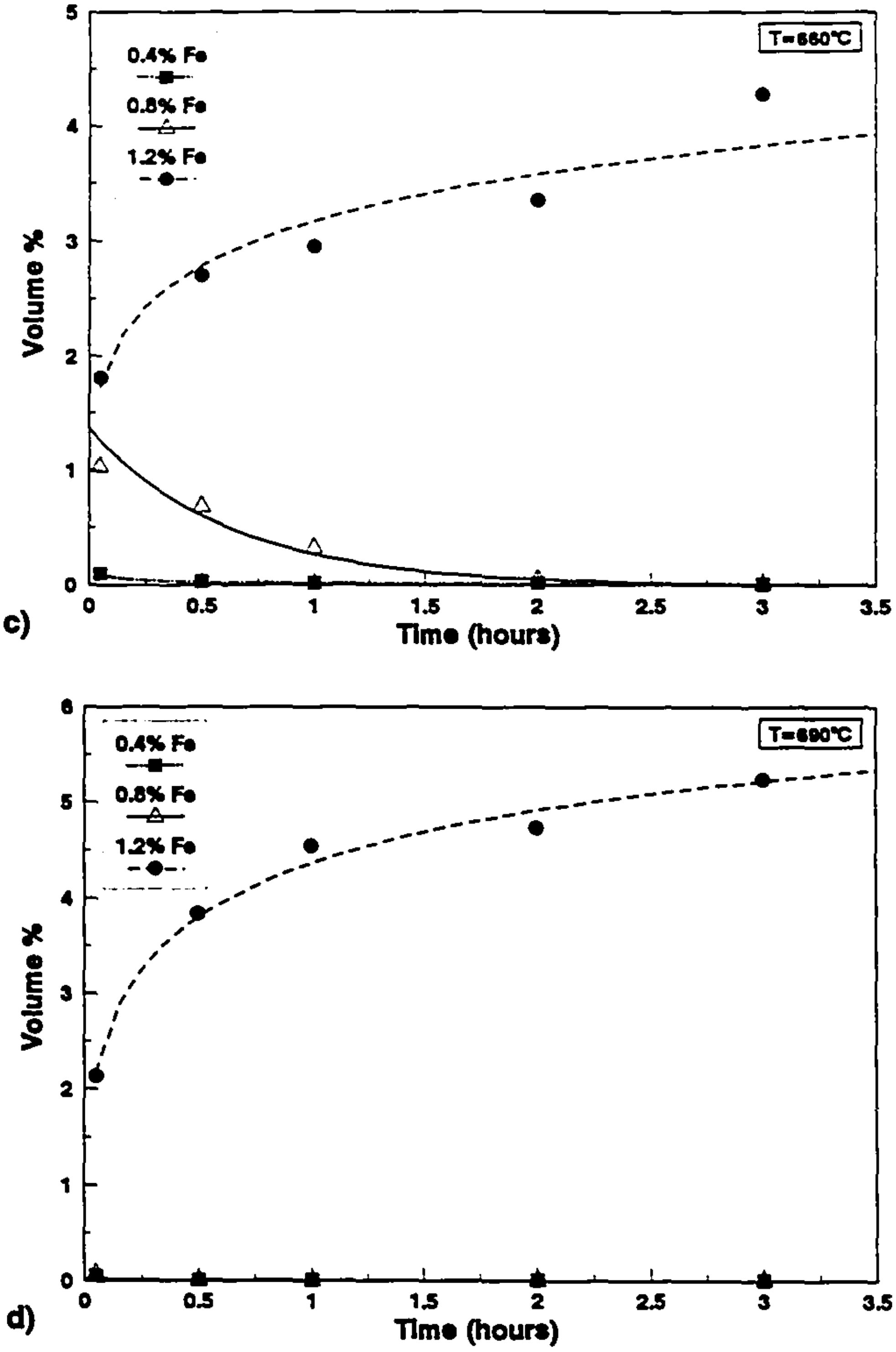

Figure 4.5: continued

is longer than two hours. The reason for this reduction of volume percentage is related to the temperature of sludge formation as shown in Figure 3.20 (chapter 3). The holding temperature of 660°C is higher than the temperature of sludge formation in alloys 1 and 2, and the sludge is unstable and dissolves.

The volumetric changes of intermetallics at 690°C are shown in Figure 4.5(d). When the holding temperature increases from 660°C to 690°C, the volume percentage of intermetallics falls sharply in alloys 1 and 2, but holding the melt at 690°C for 3.0 hours is not sufficient for dissolution in alloy 3. According to Figure 3.20, sludge is stable at 690°C when the iron content is 1.2%, and the true formation temperature must be slightly higher as some increase with time does still occur at 690°C.

The number of intermetallic particles per unit area formed as a function of time at the four test temperatures in all three alloys is shown in Figure 4.6 (a - c). Figures 4.6(a) and (b) indicate that the number of phase particles in alloys 1(0.4% Fe) and 2(0.8% Fe) increased significantly at both 600°C and 630°C, but decreased at 660°C and 690°C. In alloy 3(1.2% Fe), the number of particles increased at all temperatures (Figure 4.6(c)), and because of the formation of some needle phases, the number of particles per square millimetre is significantly higher than in alloys 1 and 2.

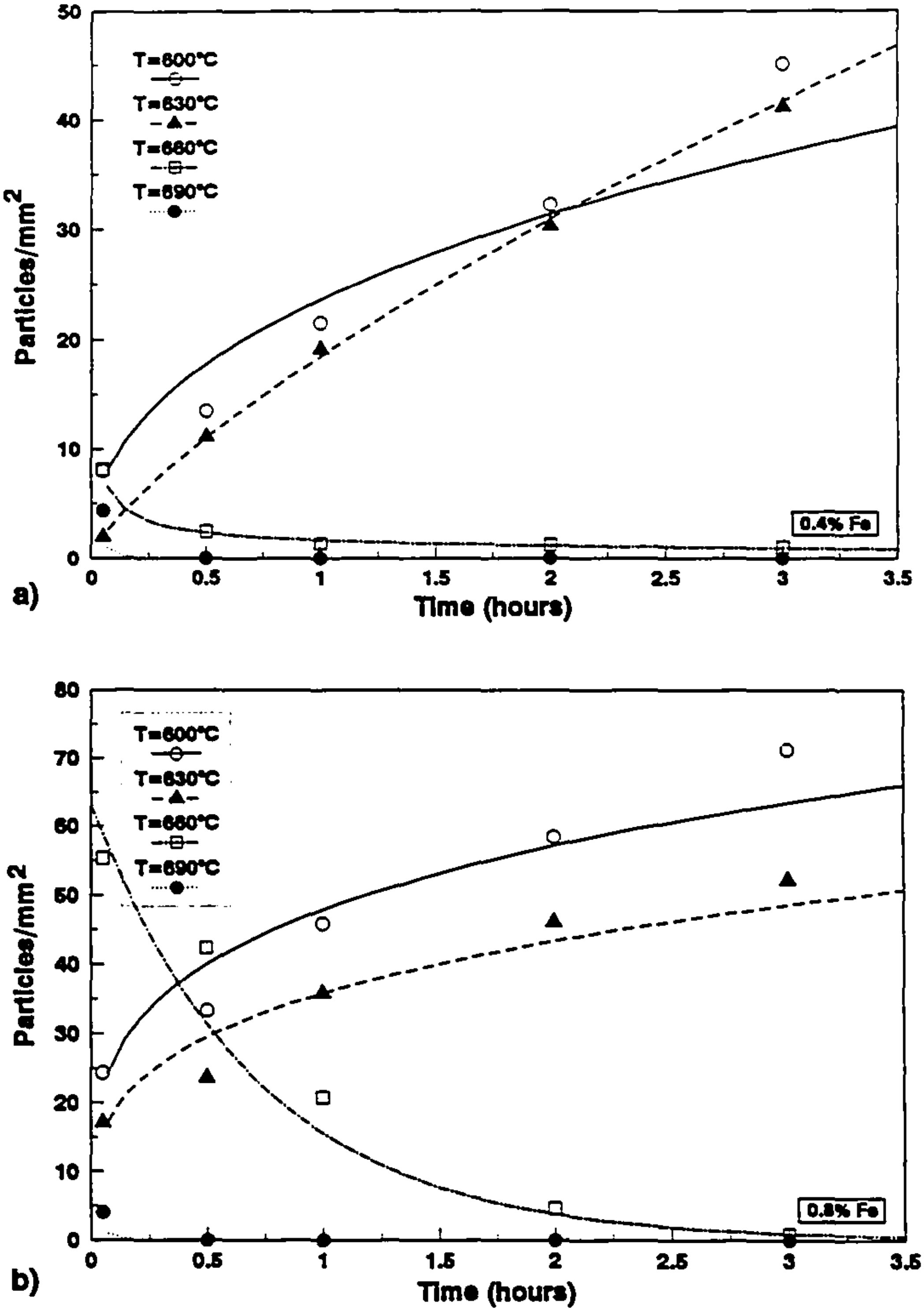

Figure 4.6: The number of particles per unit area as a function of time
a) alloy 1 (0.4% Fe) b) alloy 2 (0.8% Fe) c) alloy 3 (1.2% Fe)

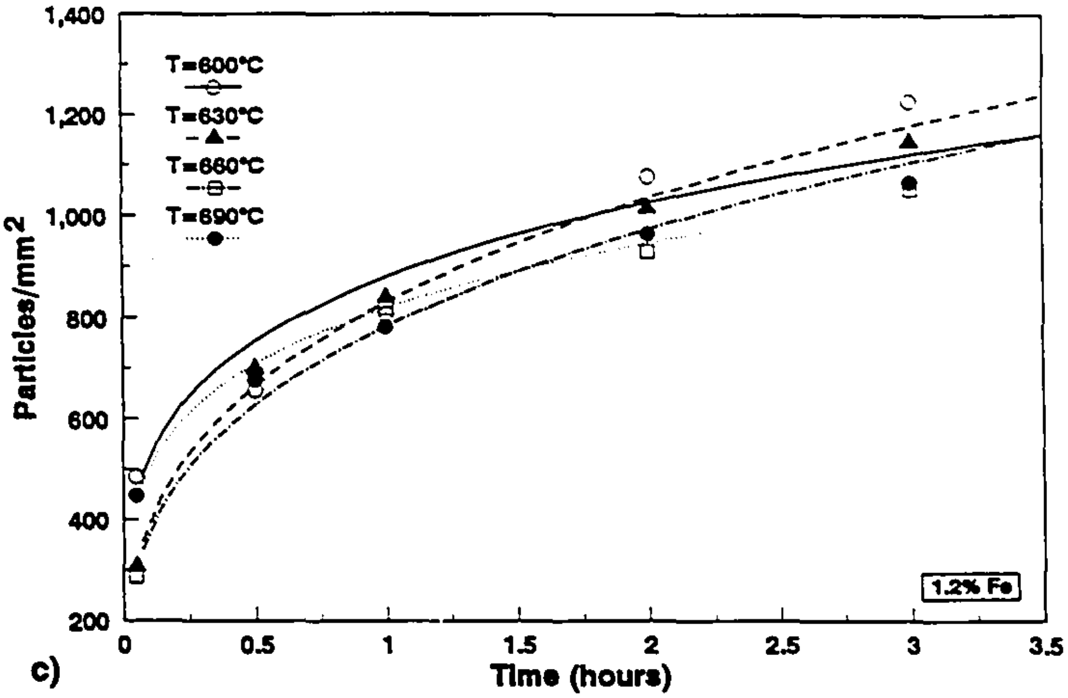

Figure 4.6: continued

The variation of the average size of the intermetallics formed at each temperature is given in Table 4.3. In alloy 1(0.4% Fe) and 2(0.8% Fe), there is no systematic variation in the size of particles with time at each constant temperature in the range from 600°C to 690°C. However in alloy 3(1.2% Fe), there is some size increase at holding times greater than two hours due to coalescence. This coalescence phenomenon in alloy 3(1.2% Fe) is shown metallographically in Figure 4.7(a,b) where it can be seen that the polyhedral intermetallics agglomerate in some areas. The results given in Table 4.3 suggest that intermetallics grow rapidly to some certain size after nucleation with little further growth caused by time or temperature.

Table 4.3: The Variation of the Particle Size (μm)

Alloy	Temperature	Size (μm)				
		Holding time (hours)				
	(°C)	0	0.5	1	2	3
0.4% Fe	600	14.5	12.4	10.6	12.7	14.3
	630	14.3	15.0	11.6	14.4	14.4
	660	19.2	18.4	15.5	19.4	15.4
	690	15.4	Nil	Nil	Nil	Nil
0.8% Fe	600	18.0	15.9	12.3	13.2	16.8
	630	15.7	21.9	15.3	19.5	17.5
	660	17.1	16.1	13.8	15.8	16.6
	690	20.8	Nil	Nil	Nil	Nil
1.2% Fe	600	9.5	8.5	7.9	8.2	11.2
	630	8.4	8.7	9.3	9.7	10.4
	660	9.3	10.2	10.5	10.3	12.4
	690	9.6	8.9	8.7	9.5	13.7

a)

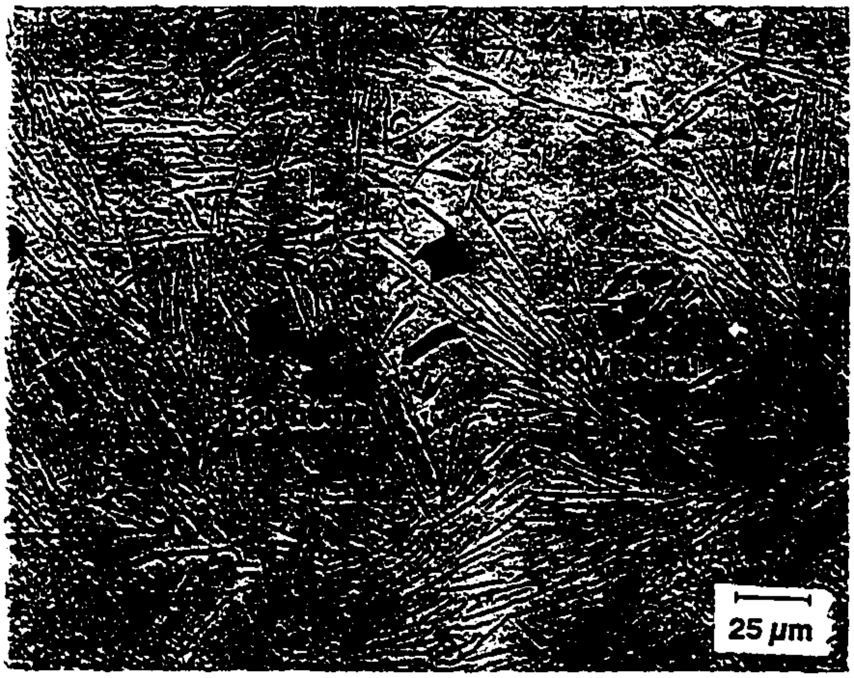

Figure 4.7: The coalescence of the polyhedral intermetallics in alloy 3(1.2% Fe) holding 3 hours at a) 600°C

b)

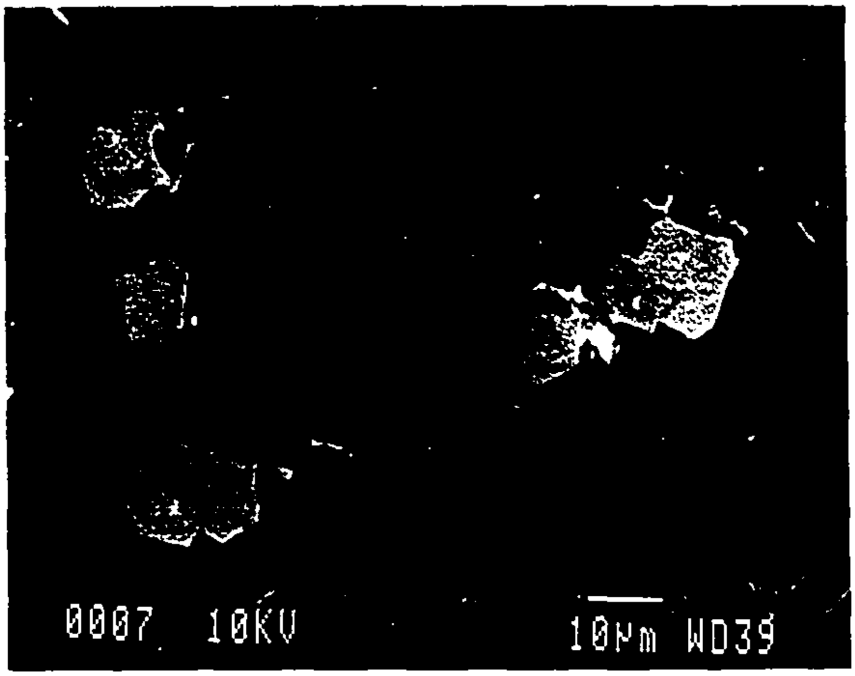

Figure 4.7, continued b) 630°C (SEM)

4.4. Discussion

The results obtained indicate that the volume percentage of intermetallics increased with holding time at 600°C and 630°C in all three alloys studied, and decreased at 660°C and 690°C in alloys 1 and 2. The results of size measurements show that in the absence of coalsence the average size of sludge particles does not change appreciably with holding time and temperature, and that any volumetric changes are related to the number of particles formed in a unit area. From Figures 4.5 and 4.6 it can be seen that the volumetric change of intermetallics is directly related to the number of particles nucleated in a unit area (and hence in a unit volume). The nucleation behaviour of these intermetallics is apparently like that of non-metals (e.g. oxides and organic polymers) which have a slow nucleation rate requiring long times to reach the maximum. This is quite different from the nucleation process in metallic systems in which rapid nucleation occurs and the entire process is accomplished in a short time.[105] Therefore, nucleation plays a major role in the process of volumetric changes of intermetallic compounds.

The formation of intermetallic compounds in liquid aluminum alloys is based on a phase transformation, and therefore, the transformation kinetics can be described by the Avrami equation. This equation has the general form of:

$$X = 1 - \exp(-b \times t^n) \tag{1}$$

where, X is the volume fraction transformed, t is time, b and n are the equation constants.

In order to analyze the effect of time and temperature on the formation of intermetallics this equation was applied to the experimental data. By applying a double natural logarithm to the equation, it can be converted to a linear form of:

$$\ln \ln \left[\frac{1}{(1-X)}\right] = n \times \ln t + \ln b \tag{2}$$

The parameters n and b in the Avrami equation were obtained from a least-squares fit of the experimental data to a plot of $\ln \ln[1/(1-X)]$ vs. $\ln t$ of which an example for alloy 3 (1.2% Fe) at 630°C is shown in Figure 4.8. However, because the total fraction of intermetallics formed at a given temperature was less than 1 and the Avrami equation is based on a total fraction of unity, the experimental data had to be normalized before the least-squares fit was made.[106] Thus, the measured volume fraction of intermetallics formed at each time was divided by the maximum volume fraction of intermetallics formed in each alloy. This quantity is defined as the relative volume fraction. The maximum volume fraction of intermetallics was used to normalize the data points as the amount of intermetallic formation in the equilibrium state was not known due to the limited time scale of the experiments.

The maximum volume fraction of intermetallics was calculated based on the stoichiometry of the compounds, $Al_{12}(Fe,Mn,Cr)_3Si_2$, and the alloy iron content. For example, in the alloy which had 0.4% Fe, 100 g of the alloy contained 0.4 g iron which could produce a maximum 2.86 g of intermetallics which would result in 0.83 cm^3 of intermetallics assuming its density to be 3.46 g/cm^3. This would lead to a volume percent of intermetallics of 2.23%. With the same calculation, the maximum volume percent of intermetallics in the alloys which had 0.8% and 1.2% Fe, were respectively, 4.46% and 6.70%.

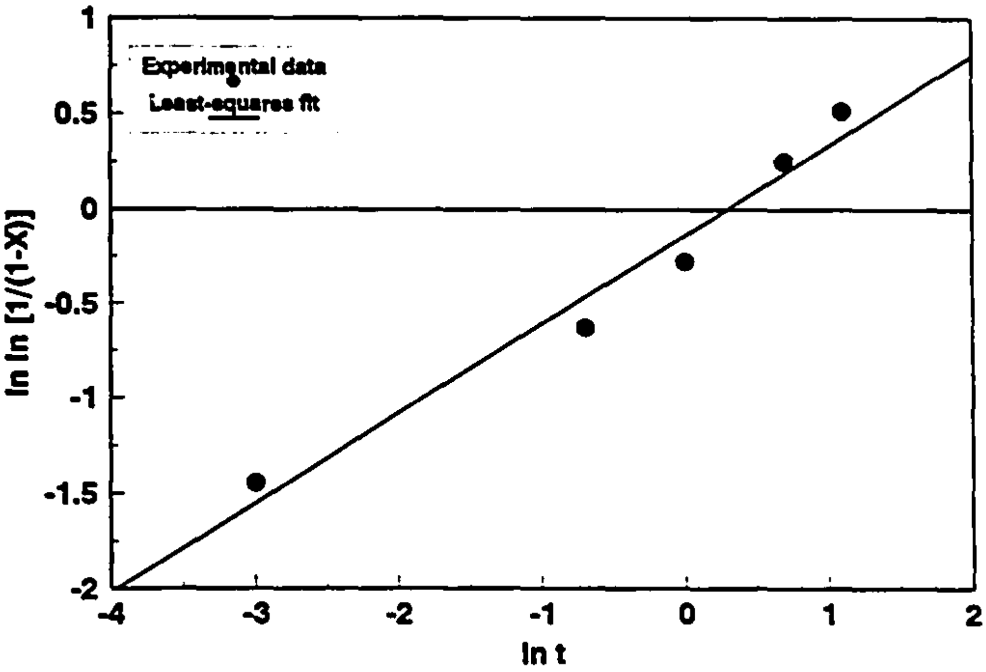

Figure 4.8: Linear Avrami regression in alloy 3 (1.2% Fe) at 630°C

The normalized volume fraction of intermetallics formed at various times from 0 to 3 hours was used in equation (2) to calculate the parameters n and b by a least-squares fit. This calculation was performed on all alloys (0.4, 0.8. 1.2% Fe) at temperatures from 600 to 690°C. The parameters n and b obtained from the least-squares fit were then used in the Avrami equation (1). Various isothermal curves were plotted which indicate the increase in the relative volume fraction of intermetallics. The relative volume fraction was then converted to volume percent of intermetallics formed as a function of time and plotted as the curves in Figure 4.5 (a - d). The points indicated in Figure 4.5 show the experimental data. In general, the curves have the form of the modified Avrami equation as:

$$Volume\ \% = k\,[\,1 - \exp(\,-b \times t^{n}\,)\,] \tag{3}$$

where the parameters k, b, and n are summarized in Table 4.4 for each curve. This equation was not applied to the cases involving the dissolution of intermetallics e.g. alloy 1(0.4% Fe) at 690°C.

Table 4.4: Constants in the Modified Avrami Equation (3)

Alloy	Temperature	k	n	b
1 (0.4% Fe)	600°C	2.23	0.62	0.12
	630°C		0.68	0.12
2 (0.8% Fe)	600°C	4.46	0.32	0.23
	630°C		0.33	0.16
3 (1.2% Fe)	600°C	6.70	0.44	0.87
	630°C		0.47	0.87
	660°C		0.26	0.64
	690°C		0.33	1.05

The trend of the curves in Figure 4.5 (a - d) indicates that the volumetric change of intermetallics follows the Avrami equation and there is a good agreement between the experimental data and the modified Avrami equation with a correlation coefficient of more than 90% in most cases.

4.5. Summary

The kinetics of the formation of intermetallic compounds was investigated by considering the roles of temperature, time, and initial chemical composition of the alloy. Three alloys with different iron contents of 0.4, 0.8, or 1.2% were studied at constant temperatures of 600, 630, 660, or 690°C and holding times ranging from 0 to 180 minutes at each temperature. The microstructures of all samples were studied quantitatively by image analysis and metallography. The conclusions of this study are summarized as follows:

(I) As the iron content increases from 0.4 to 1.2%, more intermetallics form at each holding temperature and holding time, and the volume percent of intermetallics increases.

(II) High holding temperature and low iron content can eliminate intermetallic compounds in aluminum alloys.

(III) Holding the melt for a long time at high temperature can dissolve the intermetallic compounds.

(IV) The average size of intermetallics does not change appreciably with time at each constant temperature. The volumetric changes of intermetallics are dominated by the nucleation process requiring long times to reach the maximum.

(V) A modified Avrami equation can describe the transformation kinetics of the intermetallics adequately.

Chapter 5

Effect of Solidification Conditions on the Formation and Morphology of Intermetallic Compounds

5.1. Introduction

With the wide differences in cooling conditions that prevail in industrial casting processes, ranging from 0.5 to 10 °C/s, the information contained in phase diagrams may not necessarily be applicable to the casting process. Phase diagrams have been constructed from data obtained from experiments in which mixtures of two or three very pure elements have been given time to reach equilibrium at a given temperature. Industrial alloys, which may contain many more elements, are usually cooled to room temperature as fast as economically possible.

A further complication which may arise in industrial alloys is that certain minor alloying/impurity elements may stabilize phases other than those indicated on the phase diagram. This, coupled with rapid cooling favours the formation of metastable phases. In addition, the local cooling rate varies from the surface to the centre of actual castings. Accordingly, different Al(Fe,Mn,Cr)Si phases may form throughout the casting and gradients in the phase distribution may be introduced.

Different statements, which are often contradictory, have been made[13,17,25,46,56] about the effect of cooling rate on the morphology, size, and volume percent of intermetallic compounds. Yaneva et al.[46] have studied the appearance of iron intermetallic phases in Al-Si cast alloys. They reported that even at low-iron content (< 0.15%) intermetallic phases appear, especially in zones where solidification is slow. Ghomashchi[25] reported that the polyhedral and Chinese script morphologies are independent of the cooling rate, and the thin platelet morphology is dependent upon cooling rate. The thin-platelet intermetallic morphology is sensitive to cooling rate in that both the volume fraction and aspect-ratio of this phase decrease with increasing cooling rate. Since thin platelets are reported to be detrimental to mechanical properties of the component and act as two dimensional defects there are advantages to more rapid solidification. The reduction in volume fraction of the thin-platelet phases at higher cooling rates may be due to the ability of aluminum to dissolve more impurity elements.[25]

Gustafsson et al.[13] reported that all types of intermetallic phases which appear in A356 alloy were independent of cooling rate in the range investigated (0.2 to 16°C per second), but the size and the amount of iron-containing phases were strongly influenced by solidification rate. It has also been reported that the Chinese script intermetallic (α-AlFeSi) forms when the solidification rate is high.[56] Gobrecht[44] showed that the shape of primary crystals depends on solidification conditions. During cooling of the melt, when the temperature of the melt falls below the liquidus, compact crystals form which segregate rapidly and which can be transferred into the casting during pouring of the melt.

According to the literature, there are many uncertainties about the effect of cooling rate on the shape, size, and the amount of iron intermetallics, particularly the relationship between the morphology and shape of iron compounds and cooling rate. Therefore, in order to clarify the changes in the formation of iron compounds, the effect of solidification conditions on the morphology, size, and volume percent of iron intermetallic phases was studied on three Al-Si alloys containing various levels of iron.

5.2. Experimental Procedure

5.2.1. Materials

The same alloys prepared in chapter 4 (section 4.2.1) were used and the initial chemical composition of the alloys was given in Table 4.1.

5.2.2. Effect of Cooling Rate

About 270 g of each alloy was melted in an induction furnace, and the melt temperature of 850°C was maintained for 90 minutes to dissolve any intermetallic compounds in the starting material. Thermal analysis was performed on each alloy under three different solidification conditions designed to simulate slow cooling rates (0.1 °C/s), sand casting (0.9 °C/s), and permanent mold casting (10 °C/s). The approximate equilibrium cooling rate (0.1 °C/s) was achieved by using a small fire clay crucible preheated to 750°C in a cylindrical resistance furnace. Thermal analysis samples were poured at 780-800°C into the preheated crucible which remained in the resistance furnace. The furnace was switched off and the temperature read by chromel-alumel thermocouples located at mid-height at the crucible centre. Data was logged on a computer via a commercial interface (Data Acquision System), and the thermocouples were protected in a 0.97 mm internal diameter and 1.27 mm outer diameter stainless steel sheath, so that they could be removed from the solidified sample. A sand casting cooling rate was simulated by pouring the alloy into the same type of crucible maintained at room temperature. The highest cooling rate (10 °C/s) was obtained by using a permanent copper mold.

5.2.3. Microstructural Study and Phase Analysis

Metallographic analysis was carried out on all alloys solidified at different cooling rates. Pieces were cut from each thermal analysis sample, mounted and prepared for metallographic study and image analysis. Quantitative metallography was employed using a LECO image analyzer interfaced with an optical microscope through the 2005 image analysis program. Various microstructural parameters were investigated and measured, such as the intermetallic area (μm^2), average size (μm), number of intermetallics per unit area (mm^2), intermetallic area percentage (%), roundness, and aspect ratio. The size of intermetallics was measured by the FERET AVERAGE function available in the LECO 2005 image analyzer. By this function the average of thirty two straight line measurements made between tangents at various angles (0 to 157.5°) was calculated for each particle. A total of 12 fields at 100X magnification was evaluated on each sample. The data was processed automatically using statistical programs, and the mean values reported for each sample.

The stoichiometry of the phases was also determined by electron probe microanalyzer. EPMA was used at a voltage level of 15KV for chemical analysis of the phases, and the average of five readings was calculated for each phase. For the element analysis, ZAF correction was made with reference to the standard pure element.

5.3. Results and Discussion

5.3.1. Effect of Cooling Rate

Metallographic study and image analysis results revealed that both the volume percent and average size of the iron intermetallics decreased significantly with increasing cooling rates. Very large intermetallics form in a coarse microstructure when the cooling rate is slow. The effect of cooling rate on the morphology and the volume percent of intermetallic compounds in the alloys that contained 0.4, 0.8, 1.2% Fe is shown in Figure 5.1 (a - c). At 0.4% Fe alloy, large amounts of Chinese script (α-phase) intermetallics formed at the slowest cooling rate (0.1 °C/s). The amount and the size of

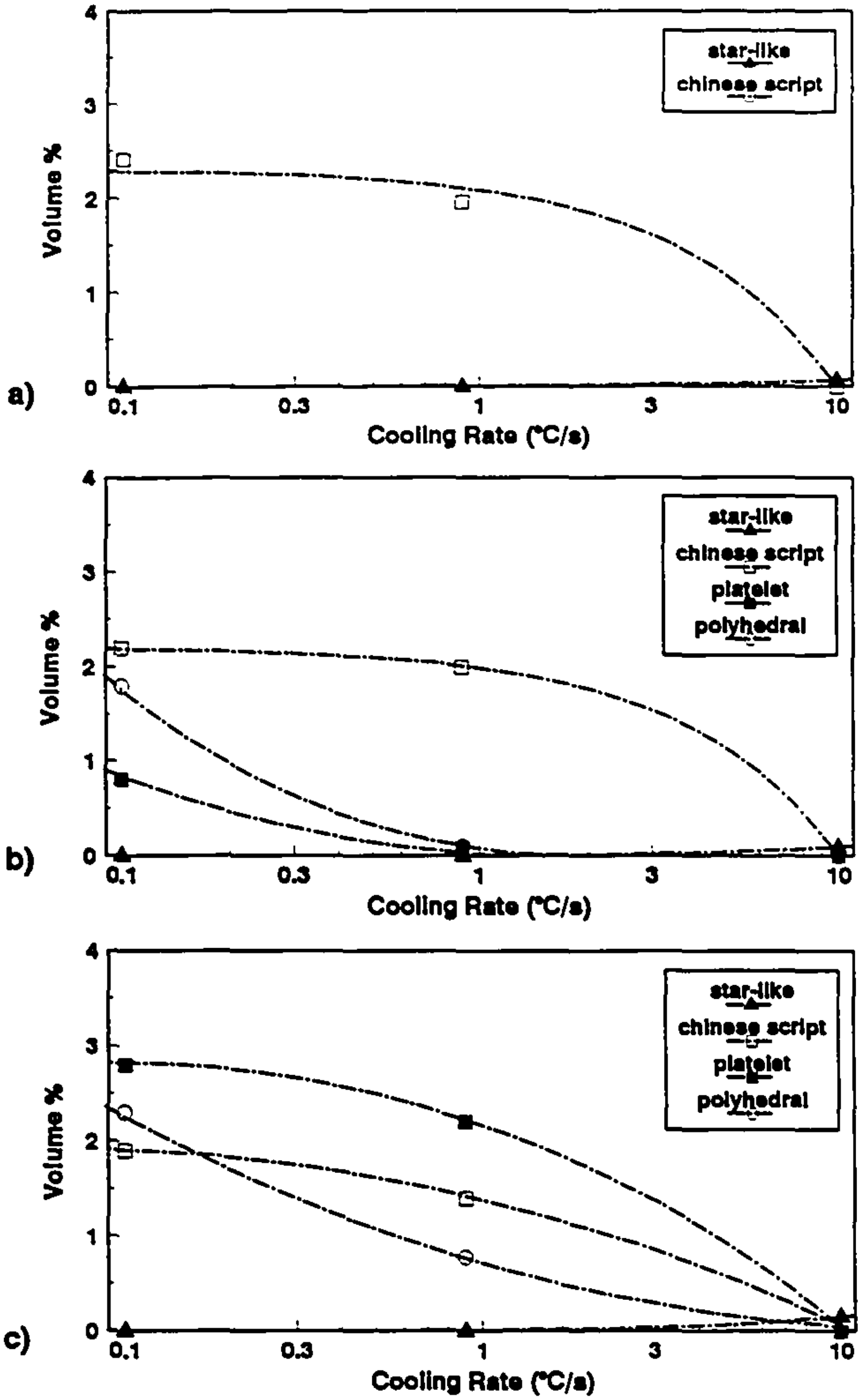

Figure 5.1: The effect of cooling rate on the volume percent of intermetallics
a) 0.4% Fe b) 0.8% Fe c) 1.2% Fe

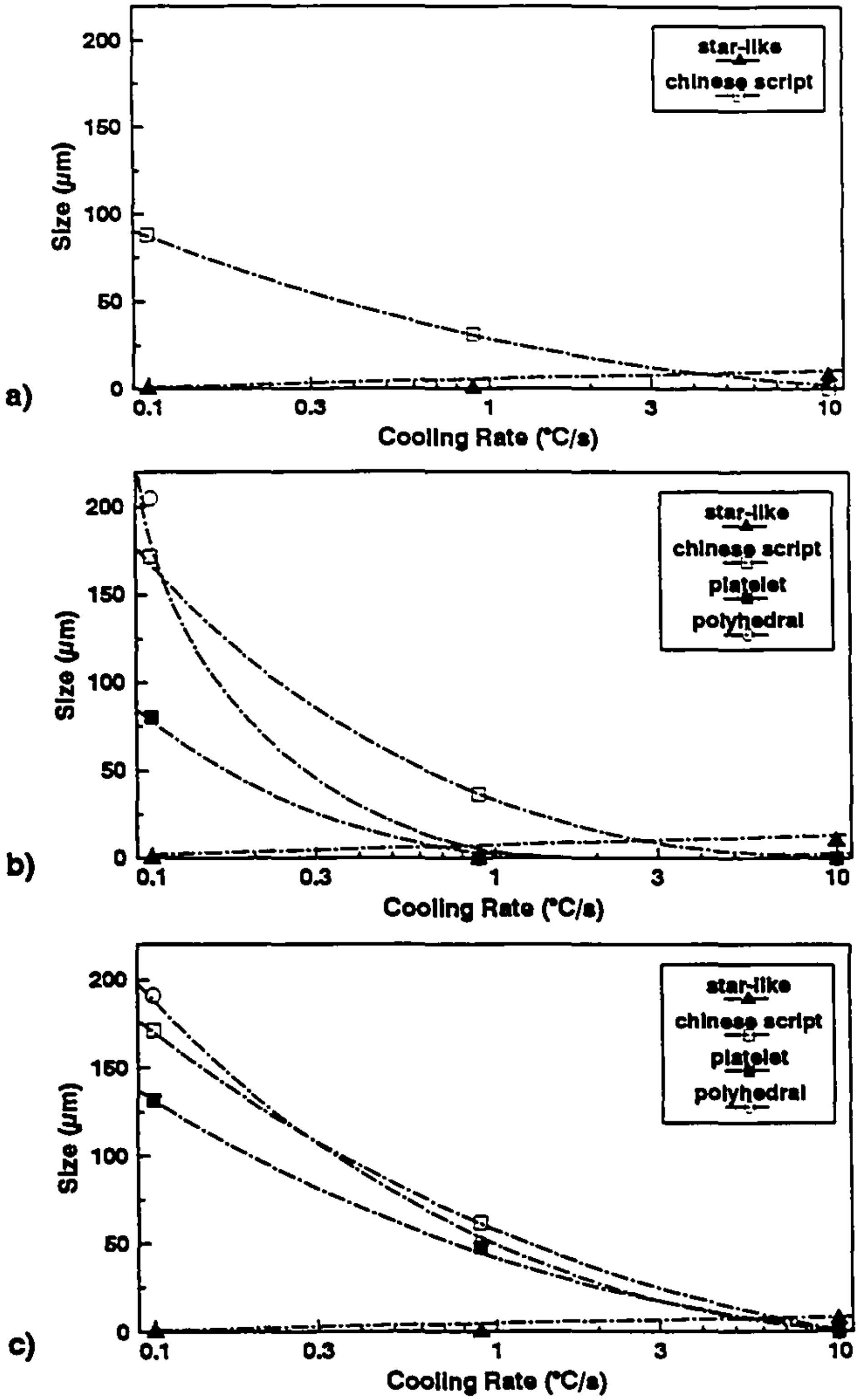

Figure 5.2: The effect of cooling rate on the average size of intermetallics
a) 0.4% Fe b) 0.8% Fe c) 1.2% Fe

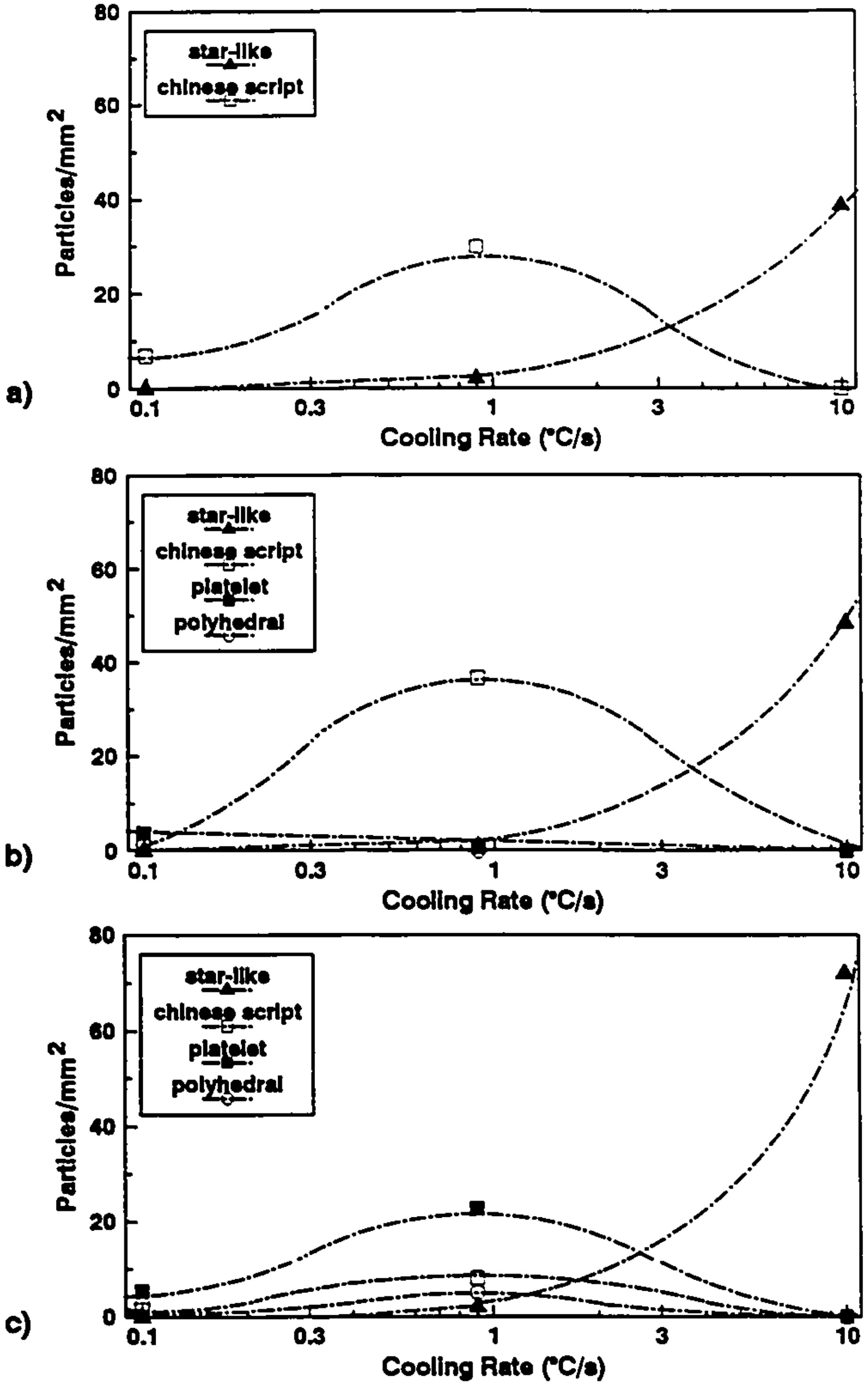

Figure 5.3: The effect of cooling rate on the number of particles formed per unit area
a) 0.4% Fe b) 0.8% Fe c) 1.2% Fe

the Chinese script morphology decreased at the medium cooling rate (0.9 °C/s), and very fine star-like compounds occupying at a maximum 0.1 volume percent formed at the highest cooling rate (Figure 5.1 (a)).

Large platelets (primary β-phase) and polyhedral particles (primary α-phase) form at a very slow cooling rate in the alloy which has 0.8% Fe (Figure 5.1 (b)). These large polyhedral particles (sludge) act as hard spots and with the large platelet phases drastically decrease toughness and strength of the alloy. When the iron level increases to 1.2% (Figure 5.1 (c)) these large platelets and polyhedral compounds form at a medium cooling rate i.e. sand casting conditions (0.9 °C/s) although their amount is less than at 0.1 °C/s. At 0.1 °C/s, the iron compounds crystallized predominately in the platelet (β-phase) form, and to a lesser extent as polyhedral particles and Chinese script (α-phase). At 10 °C/s, all of the iron compounds were absent except for the star-like intermetallics, the volume percent of which was minimal ($<$0.2 %).

The effect of cooling rate on the average size of intermetallics is shown in Figure 5.2 (a - c). The results of size measurements revealed that the size of iron intermetallics is dependent on cooling rate. The size of all morphologies is decreased by an increase in cooling rate. Among all the intermetallic compounds, polyhedral particles are the largest followed by the Chinese script (α-phase) and platelet (β-phase) when the alloy is solidified at 0.1 °C/s. In general, the average size at the same cooling rate is increased when the level of iron is increased from 0.4 to 1.2% Fe.

Figure 5.3 (a - c) shows the effect of cooling rate on the total number of particles per unit area (mm^2). The plot of number of particles/mm^2 versus cooling rate shows a bell-type curve for all the iron intermetallics except for star-like particles. The reason for this type of behaviour can be explained as follows. At low cooling rates of 0.1 °C/s, the intermetallic compounds grow to large sizes and thus particle density (particles/mm^2) is reduced to a minimum. At high cooling rates of 10 °C/s, all types of intermetallics

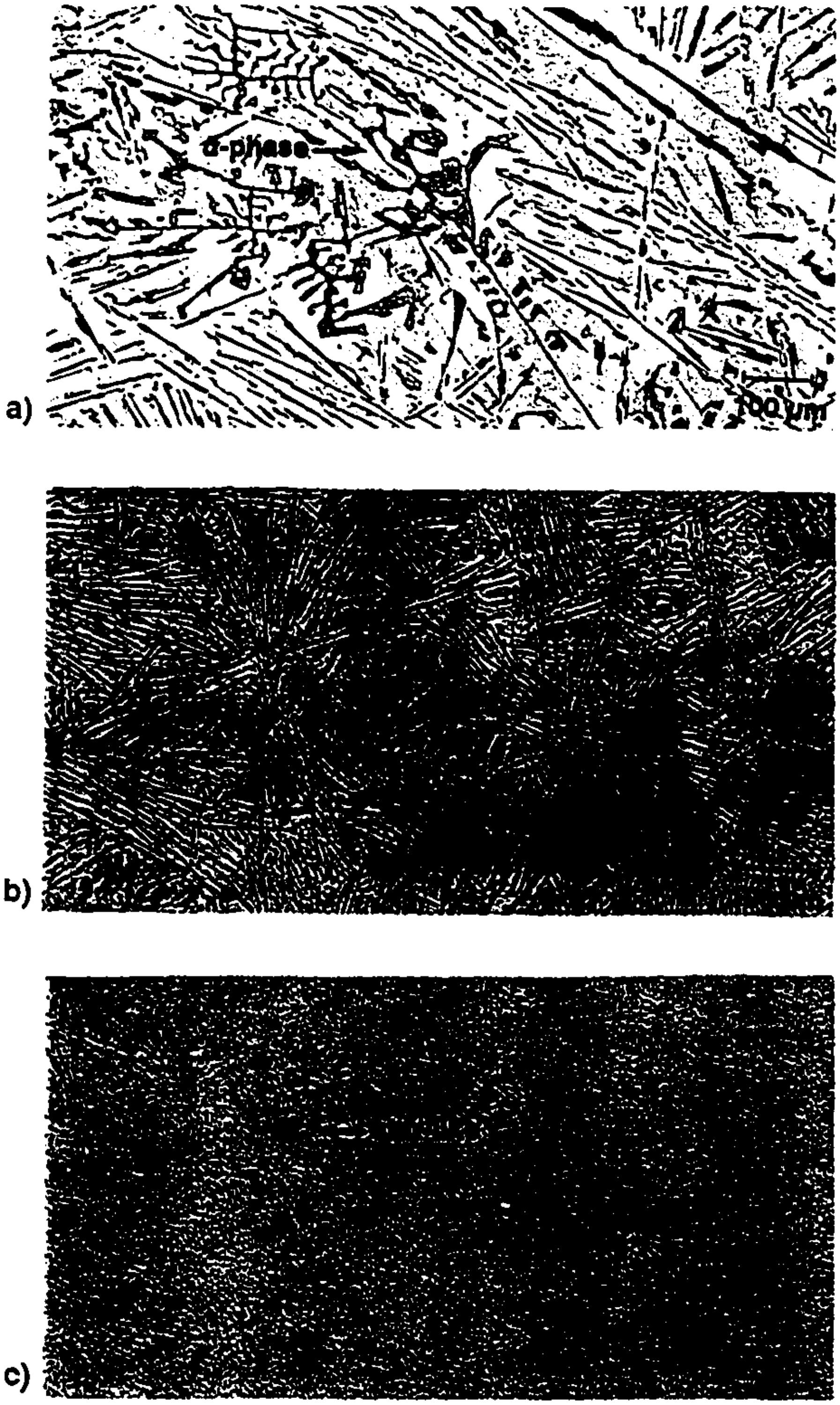

Figure 5.4: Intermetallic compounds in alloy 1 (0.4% Fe)
a) 0.1°C/s b) 0.9°C/s c) 10°C/s

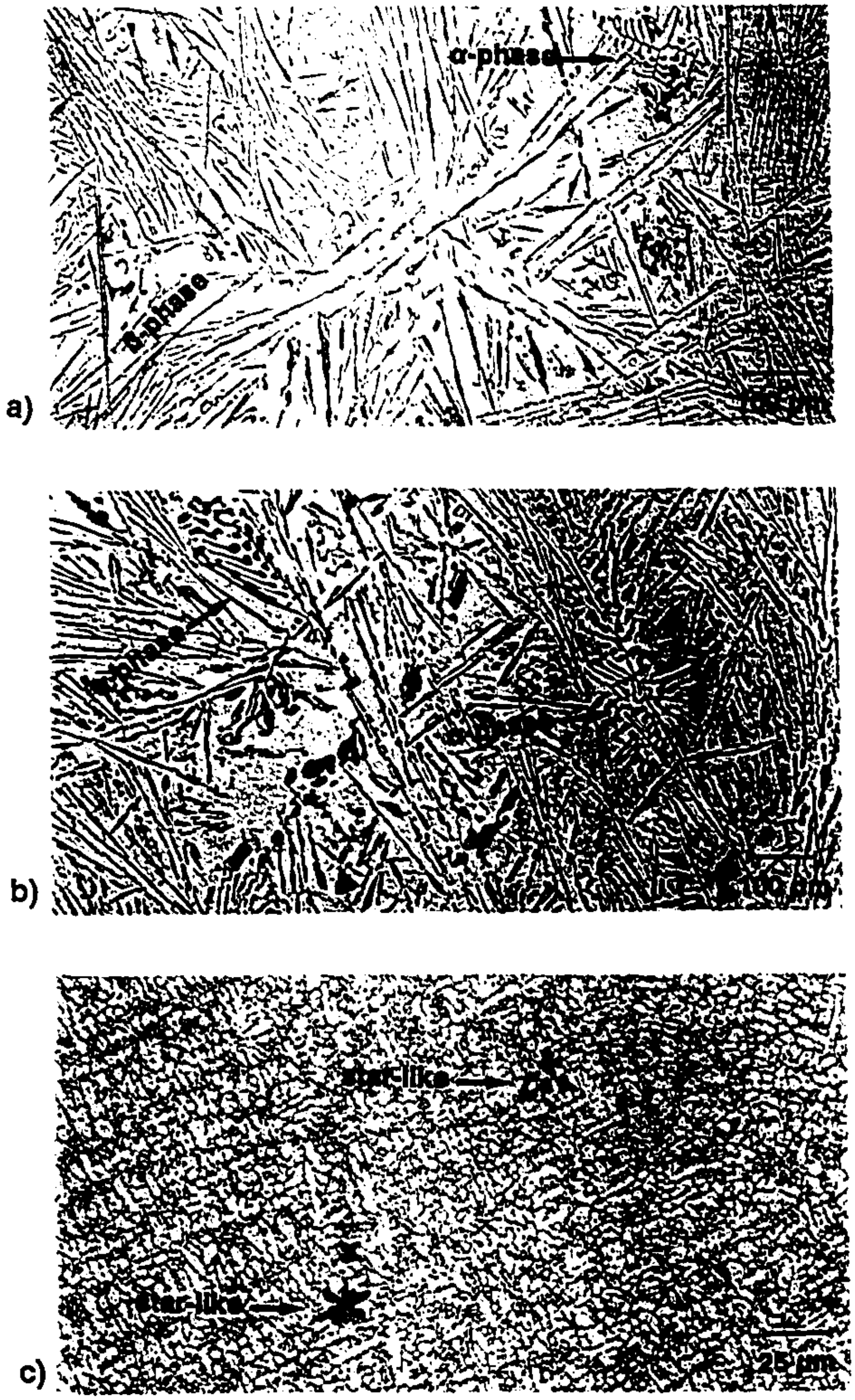

Figure 5.5: Intermetallic compounds in alloy 2 (0.8% Fe)
a) 0.1°C/s b) 0.9°C/s c) 10°C/s

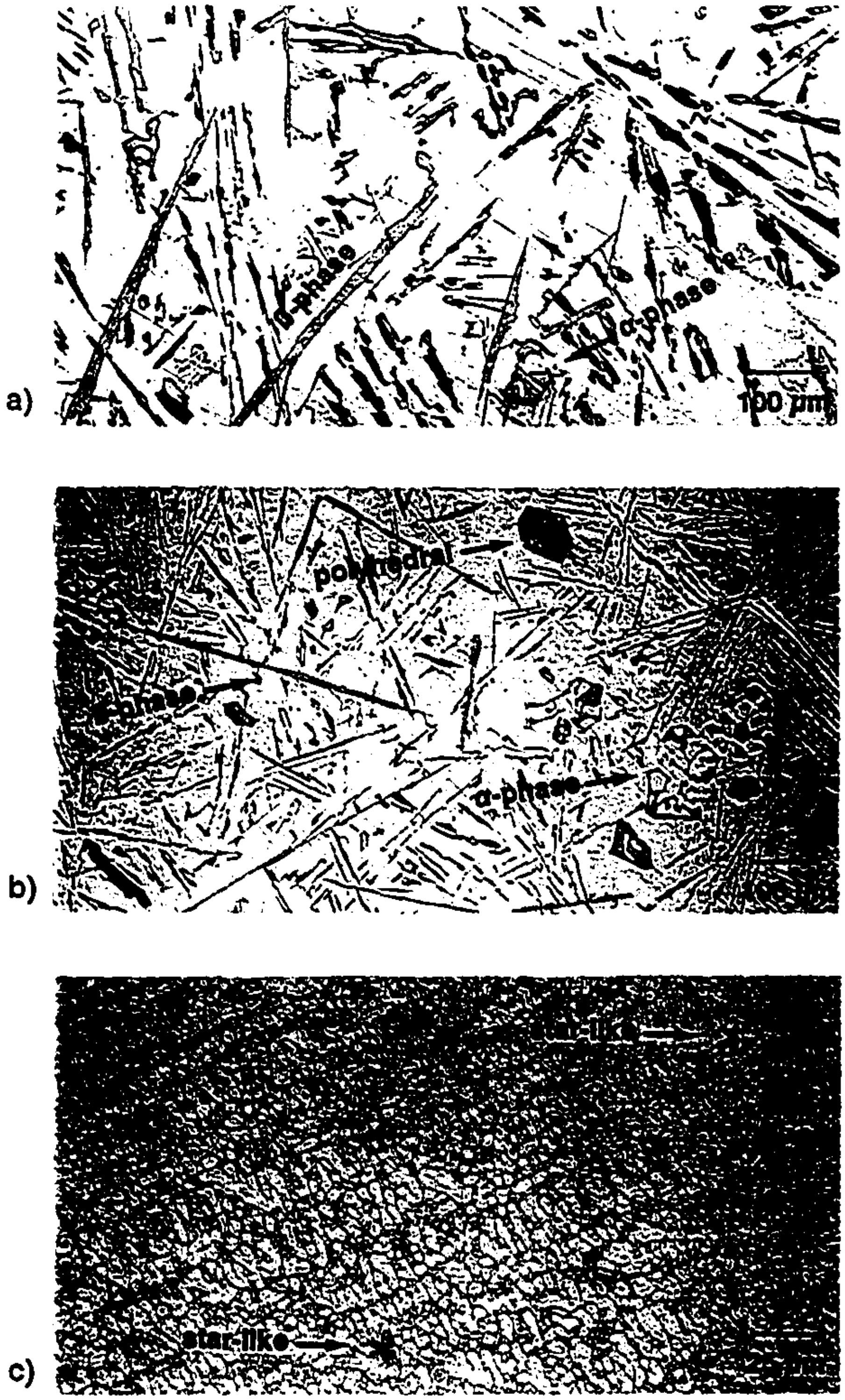

Figure 5.6: Intermetallic compounds in alloy 3 (1.2% Fe)
a) 0.1°C/s b) 0.9°C/s c) 10°C/s

except star-like compounds are absent in microstructure, and thus their particle density is reduced to zero. At these high cooling rates the star-like particles are very fine and their particle density increases to 39, 48, and 72 particles/mm^2 in the alloys which contain 0.4, 0.8, and 1.2% Fe respectively. For all particle types, except the star-like. their growth-nucleation characteristics lend to a maximum particle density at intermediate cooling rates.

Photomicrographs of the alloys solidified at 0.1 °C/s to 10 °C/s are shown in Figures 5.4 - 5.6. In all three alloys when the cooling rate was high i.e. 10 °C/s very fine star-like intermetallics formed in a fine modified eutectic microstructure. The reason for the low volume percent of iron intermetallics at high cooling rates (10 °C/s) may be due to the higher solubility of alloying elements/impurities in the matrix, and/or decreased nucleation and growth of the iron intermetallics.

In general, large Chinese script, platelet, and polyhedral compounds formed in the microstructure at the slowest rate while these phases were not observed at a high cooling rate. The same phases and large polyhedral compounds (sludge) also form at higher iron concentrations and sand casting cooling rates (0.9°C/s) as shown in Figure 5.6 (b). Since the morphology and volume fraction of all types of intermetallic compounds are dependent on cooling rate, these results do not support Ghomashchi[25] who stated that the polyhedral and Chinese script morphologies were independent of cooling rate.

The effect of cooling rate on the total volume percent of intermetallics formed is shown in Figure 5.7. The total amount of intermetallic compounds increases with decreasing cooling rate with the maximum amount occuring at 0.1 °C/s in all three alloys. While the total volume percent of intermetallics increases with decreasing cooling rate, the number of particles of each phase per unit area decreases and the size of each morphology increases. This figure also shows that the maximum amount of intermetallics

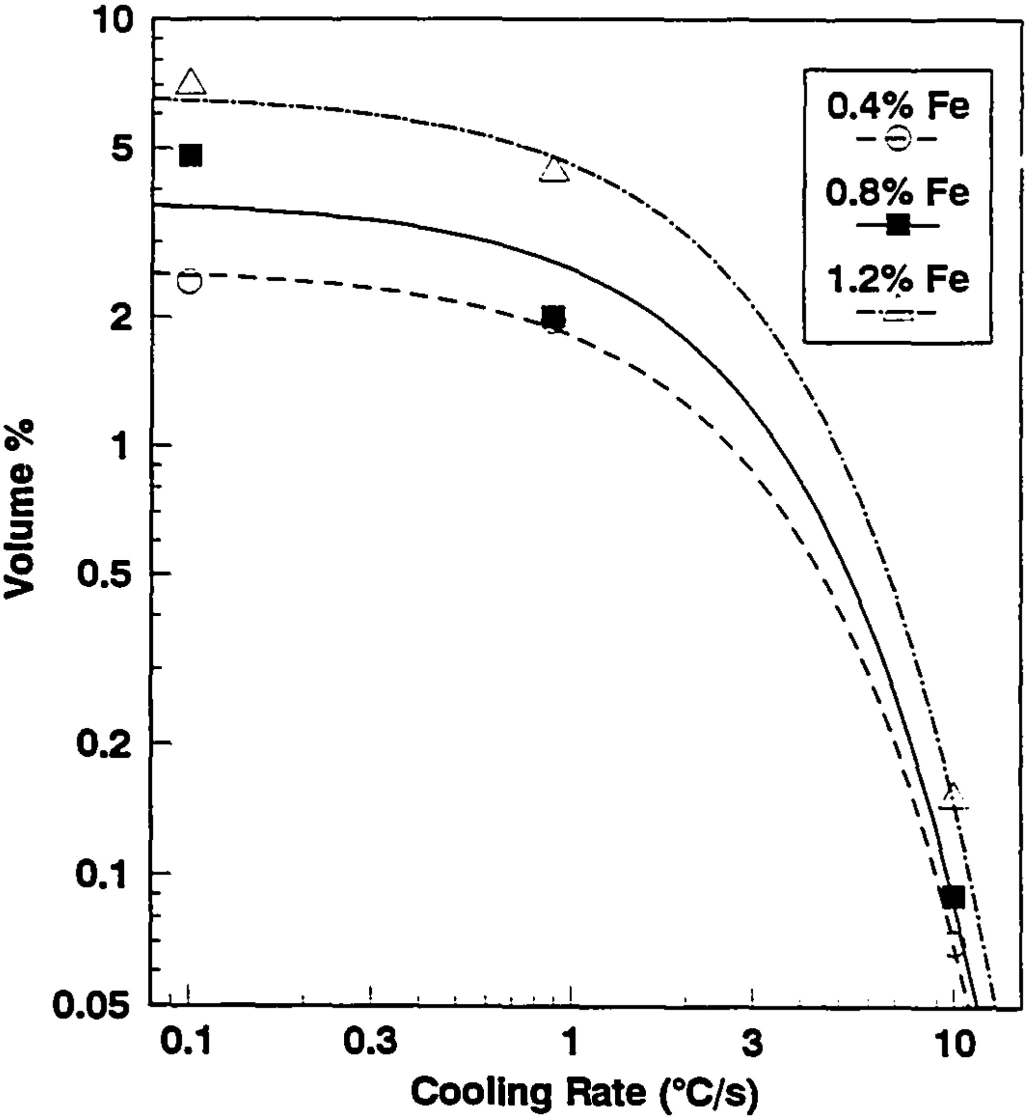

Figure 5.7: Effect of cooling rate on the total volume percent of intermetallic compounds formed in the alloys

forms at high iron content and slow cooling rate. An equation can be fitted to the exponential relationship expressed in Figure 5.7 to allow calculation of the amount of intermetallics as a function of cooling rate. This equation has the form :

$$\text{volume \% of intermetallics} = a \,.\, \exp(b \,.\, \text{cooling rate})$$

where,

cooling rate : °C/s

a and b : constants of the equation

Constants of the equation and the correlation coefficient for all alloys investigated are given in Table 5.1 where it is seen that a correlation of better than 98% with the experimental data is obtained.

Table 5.1: Constant parameters for the exponential equation

alloy	a	b	C.C.*
1 (0.4 % Fe)	2.60	- 0.36	0.999
2 (0.8 % Fe)	3.78	- 0.37	0.981
3 (1.2 % Fe)	6.72	- 0.38	0.998

C.C.* : Correlation Coefficient

According to the results of this investigation, it can be concluded that with decreasing cooling rate both the volume percent and size of the intermetallic compounds increased. Moreover, at 0.1 °C/s, the iron compounds crystallized in all three different forms, i.e., β-phase, α-phase and polyhedral. At 10 °C/s, they crystallized entirely as fine star-like particles, and the volume fraction of the other compounds particularly platelets reduced to zero. In fact, these are beneficial results for castings prepared at high cooling rates, e.g. die-casting, since platelets are detrimental to mechanical properties of the component, and therefore, cooling rates of 10 °C/s or above are suggested as the optimum.

5.3.2. Phase Analysis

Table 5.2 gives the electron probe microanalysis (EPMA) of the complex intermetallic types studied compared with those reported by other authors [46,80,81]. According to EPMA results, the stoichiometry of the star-like and Chinese script morphology (α-phase) corresponds to $Al_{12}(Fe,Mn,Cr)_3Si_2$ which is B.C.C. The stoichiometry of the platelet morphology (β-phase) corresponds to Al_5FeSi where some iron atoms are replaced by a maximum of 3.0 wt% manganese and chromium. These two elements are dissolved in the monoclinic crystal structure of β-phase. The present results show that the composition of the platelet β-phase and the Chinese script(α-phase) are in

Table 5.2: Chemical Composition of the Intermetallic Compounds (atomic %)

	Phase	Al	Si	Fe	Mn	Cr
this work	needle phase	66.87	18.02	13.88	1.19	0.05
	Chinese script	72.58	10.42	11.19	3.59	2.21
	star-like	71.45	11.33	10.01	4.71	2.52
ref.[46]	needle phase	66.55	17.40	11.70	2.26	-
	Chinese script	70.75	8.23	11.89	5.81	-
ref.[80]	needle phase	67.65	15.03	15.07*		-
	Chinese script	70.39	5.86	17.67*		-
ref.[81]	star-like	71.0	11.8	8.9	5.6	2.6

* total (Fe + Mn)

reasonable agreement with values reported by others[46,80]. The stoichiometry of the β-phase is more or less $Al_5(Fe,Mn,Cr)Si$ while α-phase has an approximate composition of $Al_{12}(Fe,Mn,Cr)_3Si_2$. It is evident that these phases can have a somewhat variable stoichiometry as small differences do appear in the values reported by various authors. Despite different opinions on the exact compositions of the iron phases, it is seen here that α-phase has less silicon and more manganese and chromium than β-phase.

5.4. Summary

The influence of solidification conditions and iron concentration on the morphology, size, and volume percent of iron intermetallic phases was investigated on three Al-Si alloys. The alloys with iron contents of 0.4, 0.8, or 1.2% and 0.3% Mn, 0.1% Cr were studied at various cooling rates of 0.1, 0.9, or 10 °C/s. The microstructures of the samples were investigated quantitatively by image analysis and metallography. The conclusions of this study are summarized as follows :

(I) When the cooling rate is slow, very large intermetallics of Chinese script morphology form in a coarse microstructure. Polyhedral (sludge) particles form at a slow cooling rate and high iron concentration. The size and the volume percentage of the compounds increase significantly with decreasing cooling rate.

(II) When the total volume percent of intermetallics increases with decreasing cooling rate, the number of particles of each phase per unit area decreases and the size of each morphology increases.

(III) The morphology and volume fraction of all types of intermetallic compounds are dependent on cooling rate. A fast cooling rate can transform the brittle iron platelet phases which are harmful to mechanical properties of the alloy into very small star-like compounds.

(IV) The volume percentage of intermetallics decreases significantly with increasing cooling rate; a relatively large amount of impurity elements can be dissolved in the microstructure when the cooling rate is high.

(V) The stoichiometry of star-like and Chinese-script (α-phase) intermetallics corresponds to $Al_{12}(Fe,Mn,Cr)_3Si_2$, while platelet (β-phase) compounds have the stoichiometry $Al_5(Fe,Mn,Cr)Si$.

(VI) An exponential equation can express the effect of cooling rate on the total volume percentage of intermetallic compounds with a good correlation between the experimental data and the equation.

Chapter 6

Gravity Segregation of Intermetallic Compounds

6.1. Introduction

Segregation of intermetallics may occur either in the mold during casting, or in the furnace or ladle during melt processing. In the first case, slow cooling of the metal in the mold favours gravity segregation, since primary crystals grow larger and have more time to sink. Segregation is thus more likely to occur in large sand castings and slowly cooled ingots than in permanent mold or die castings. In the previous chapter, the effect of solidification conditions on the formation and morphology of complex intermetallic compounds was studied. It was found that the morphology and volume fraction of all types of intermetallics are dependent on the cooling rate. When the total volume percent of intermetallics increases with decreasing cooling rate, the number of particles of each phase decreases and the size of particles of each morphology increases. A relatively large amount of impurity elements can be dissolved in the microstructure, without sludge formation, when the cooling rate is high.

It has been reported [41] that segregation during melt holding may occur with high manganese levels even when the iron content is very low. Whether gravity segregation occurs or not depends on the content of iron, manganese and silicon and the thermal conditions of the melt. Gravity segregation will not occur in melts with the recommended Fe, Mn, Cr compositions provided they are thoroughly stirred after heating to at least 720°C.[41]

In the present chapter, the kinetics of the segregation of intermetallic compounds in liquid Al-12.5% Si alloy are discussed. Sedimentation has been investigated based upon the chemical composition of the alloy and the holding temperature. Of particular interest was the settling velocity of particles in the melt, and the relationship of settling speed obtained by experiments to that calculated from the classical Stokes' law relationship for the motion of solid particles in a viscous fluid.

6.2. Experimental Procedure

6.2.1. Materials

The chemical composition of the alloy prepared for this investigation is shown in Table 6.1. The alloy was manufactured by making appropriate additions to an Al-12.5% Si alloy prepared from commercial purity aluminum and silicon. Iron, chromium, and manganese additions were made to this alloy by means of commercial master alloys of composition : Al-24.7% Fe, Al-20.1% Cr, and Al-25.2% Mn. The chemical analysis of the alloy was verified by emission spectrometry.

Table 6.1: Chemical Composition of the Alloy (wt%)

Si	Fe	Cu	Mn	Mg	Cr	Ni	Zn
12.46	1.21	<0.002	0.29	<0.009	0.10	<0.001	<0.008

6.2.2. Melting Practice

Aluminum-12.5% silicon alloy was prepared in an induction furnace. The melt was degassed with nitrogen for 15 minutes at 750°C before adding the iron, manganese and chromium master alloys. It was then poured into ingot molds at temperatures in the range 720-750°C. To investigate the settling of intermetallic compounds, the alloy was melted in an induction furnace and held at 850°C for 15 minutes to homogenize the liquid. The temperature was then quickly lowered to the required temperature and transfered to the settling experiment apparatus.

6.2.3. Sedimentation Experiments

In order to investigate the sedimentation process, a holding temperature of 630°C was selected based on the results obtained in chapter 3 (section 3.3.2.2) in which it was found that the temperature of sludge formation for this alloy is 690°C. Therefore, at 630°C a considerable amount of sludge is guaranteed. Settling was investigated by using a vertical electric resistance furnace and boron nitride coated steel molds 3 cm × 3 cm × 22 cm high. These molds were placed in the furnace at 630°C for over one hour before the liquid alloy was added in order to ensure constant thermal conditions in the furnace and to minimize convection in the system.

520 g of the melt prepared in the induction furnace was then transferred into the preheated mold in the resistance furnace. The top of the furnace was completely insulated with fiberfrax insulation, and the temperature of the melt was controlled continuously by a K-type thermocouple located in the mold. Sedimentation was allowed to proceed for three holding times of 30, 90, and 180 minutes at a constant holding temperature of 630°C. At the end of each sedimentation period the steel mold was vertically quenched into cold water. Solidification was complete in approximately three seconds.

Rectangular ingots obtained from quenching were longitudinally sectioned in the middle. Both halves were then sectioned into six divisions as shown in Figure 6.1. One half of the ingot was used for chemical analysis by emission spectrometery at different locations. The other half was prepared for image analysis and metallographic investigation. The volume fraction, size, and the number of intermetallic particles were

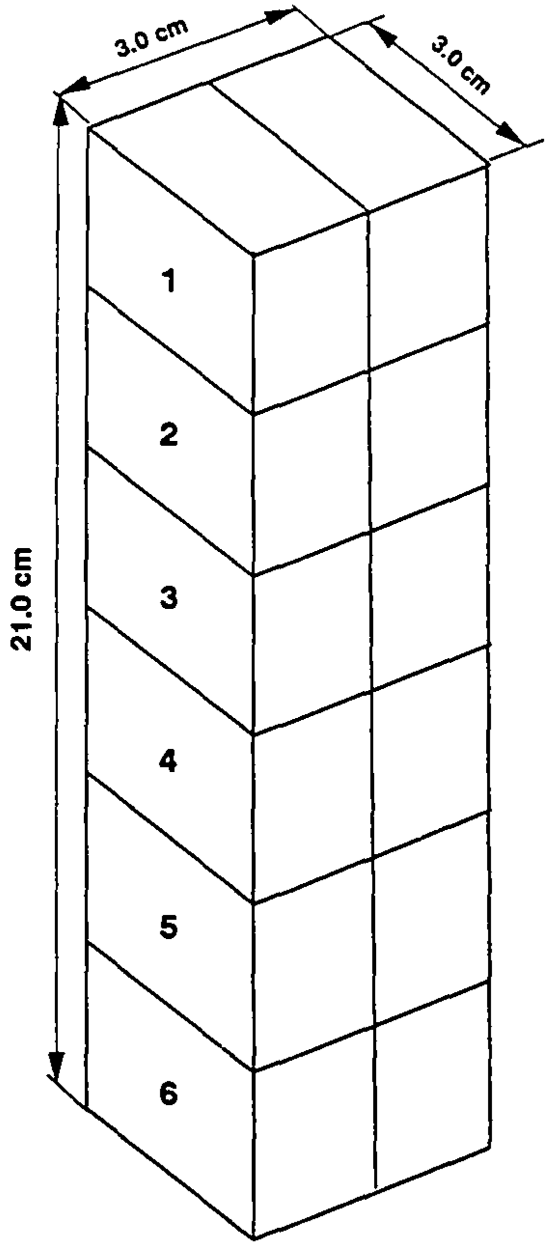

Figure 6.1: Location of samples in quenched ingot

then measured at different locations using the LECO 2005 image analysis system. Image analysis was performed on an area of 3.0 × 3.5 cm of each division shown in Figure 6.1. The values reported are the average of measurements taken over this area. This relatively large area was chosen to eliminate microscopic effects such as particle pushing and local convection during quenching on the results.

6.3. Results

6.3.1. Sedimentation of Intermetallic Compounds

The effect of holding time on the settling of intermetallics from top to bottom of the mold is shown in Figure 6.2. As the distance from the top of the mold increases at each holding time, the volume percent of intermetallics increases, and settling is more significant at longer times, particularly at 180 minutes. A linear relationship exists in all cases between the volume percent of intermetallics and distance from the top of the mold.

Figure 6.3 shows the effect of sedimentation time on the average size of particles. As the distance from the top of the mold increases, the size of intermetallics also increases since the settling speed of large particles is higher than that of small particles, and is more significant at longer times. Large polyhedral particles (about 50 μm) were often observed at the floor of the melt. These polyhedral intermetallics are formed by coalescence of intermetallic compounds and agglomeration which metallographic observations indicated occurred only near the very bottom of the sample.

The variation of the number of particles formed in a unit area at different heights in the mold is shown in Figure 6.4. As distance from the top of the mold increases, the number of particles also increases. Over most of the mold length the lowest number of particles is found at the largest settling time (180 min.) due to the longer time for settling of particles.

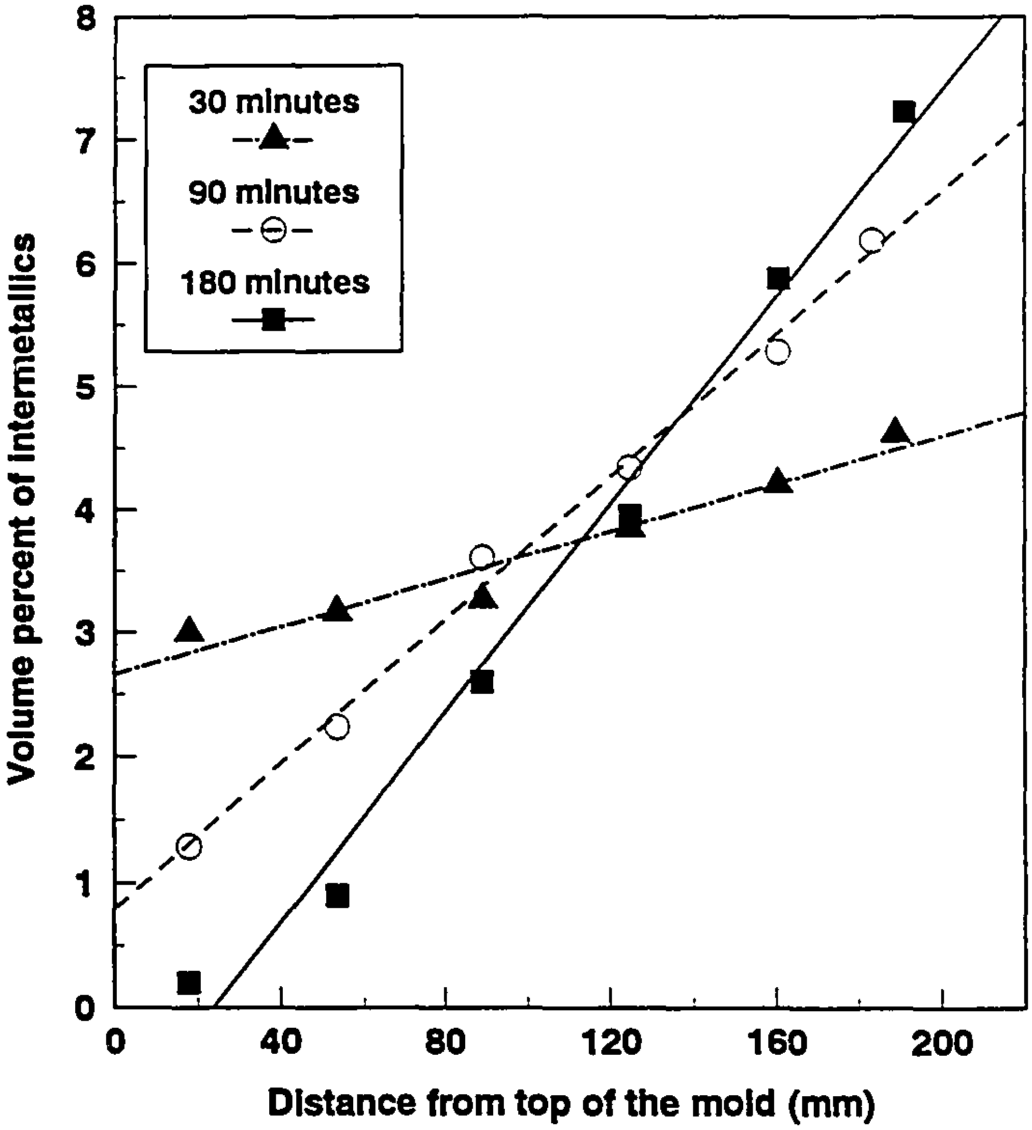

Figure 6.2: Vclume percent of intermetallics segregated at different distances from top of the mold

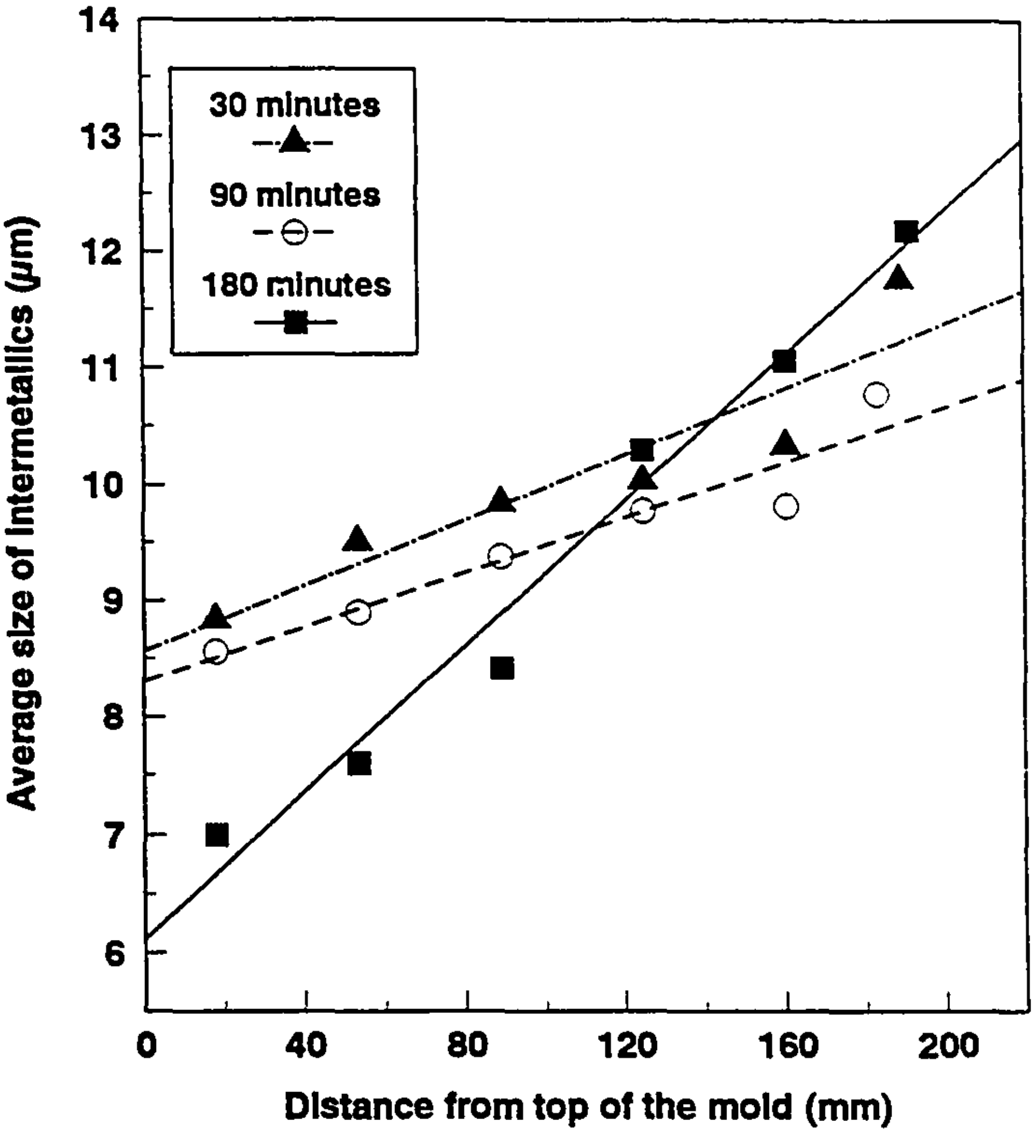

Figure 6.3: Average size of intermetallics versus distance from top of the mold

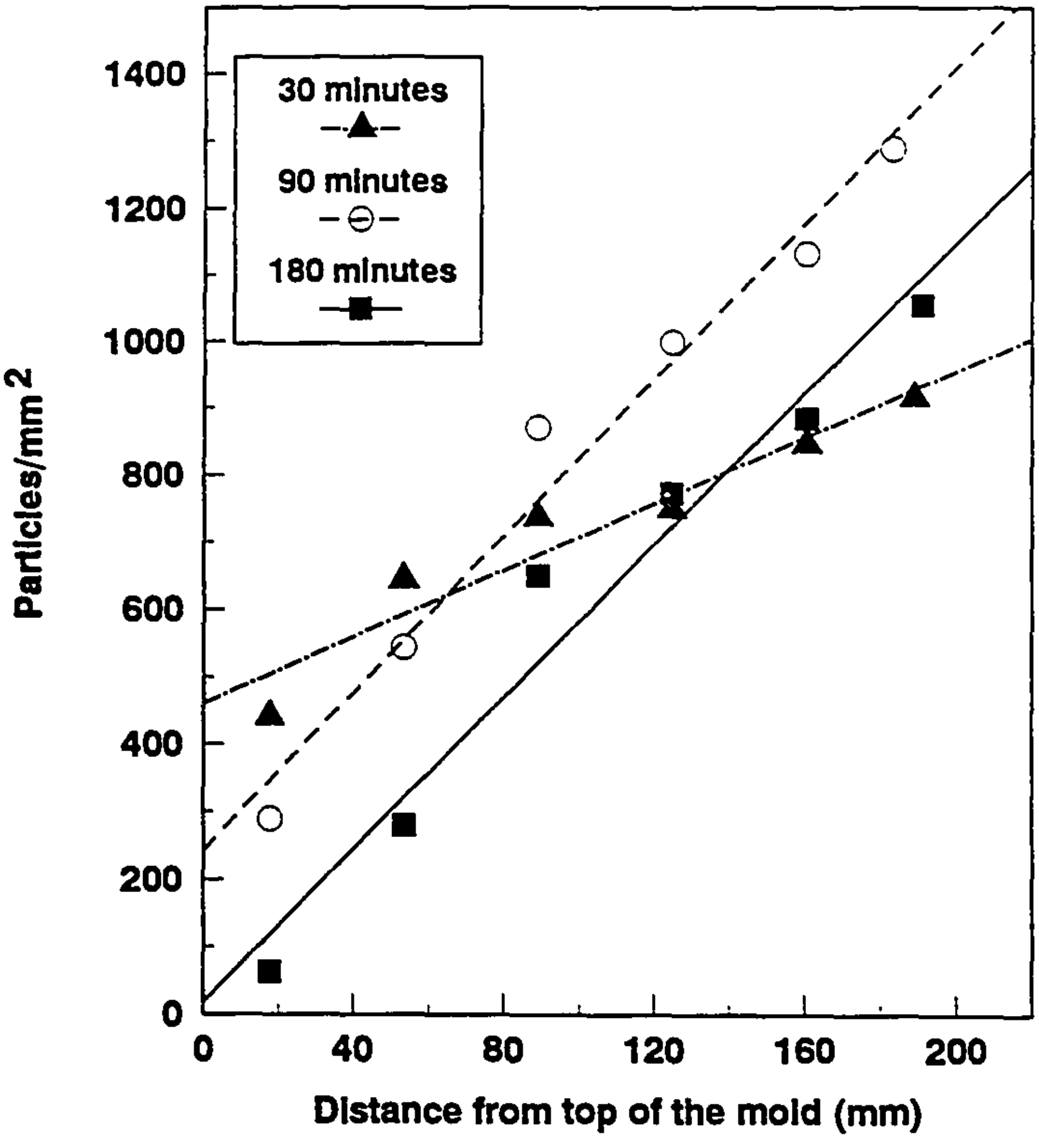

Figure 6.4: The variation of the number of particles formed in a unit area at different locations in the mold

Figure 6.5 shows the effect of settling time on the volume percentage of compounds at six locations in the mold. The amount of intermetallics in the centre of the mold at locations L3 and L4 is approximately constant. Below these positions there is an increase in the amount, while above there is a decrease. The slope of the lines given in Figure 6.5 quantifies the rate of sedimentation at the six positions in the mold. These rates are plotted as a function of position in Figure 6.6 where a negative value indicates depletion and a positive value denotes an accumulation of intermetallics.

6.3.2. Segregation of elements

The intermetallics which segregate are complex compounds of (Al,Si,Cr,Mn,Fe), and therefore, it is expected that the concentration of iron, manganese, and chromium should increase from top to bottom of the ingot. Figures 6.7, 6.8, and 6.9 show the effect of settling time on the variation of iron, manganese, and chromium. As the distance from the top of the mold increases, the content of each element increases due to the gravity segregation of the intermetallic compounds, with greater concentrations at longer times, e.g. 180 minutes. The compositional variations follow a linear relationship with different slopes which are qualitatively in good agreement with the measurements of volume percentage of intermetallics as a function of location.

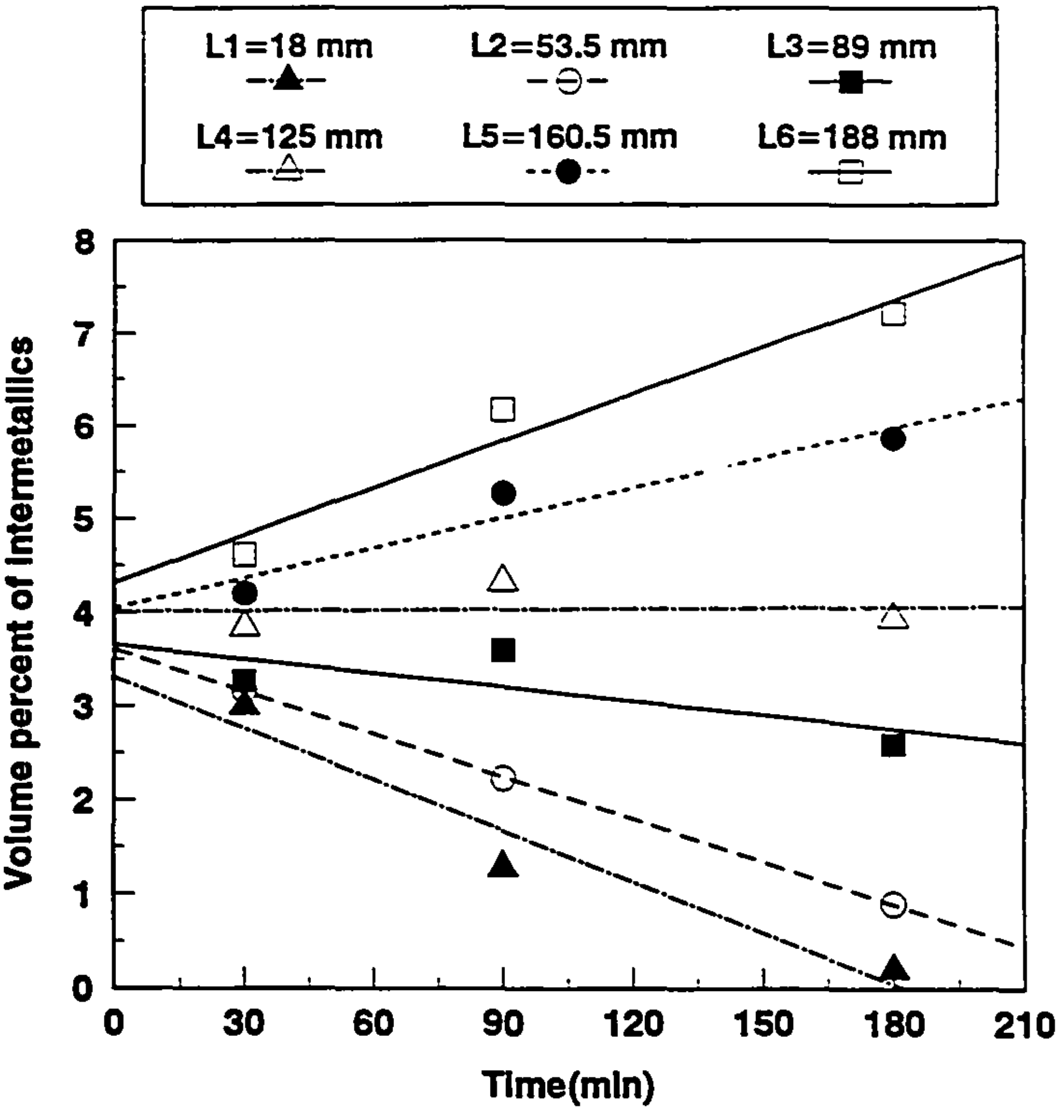

Figure 6.5: The effect of settling time on the volume percent of intermetallics

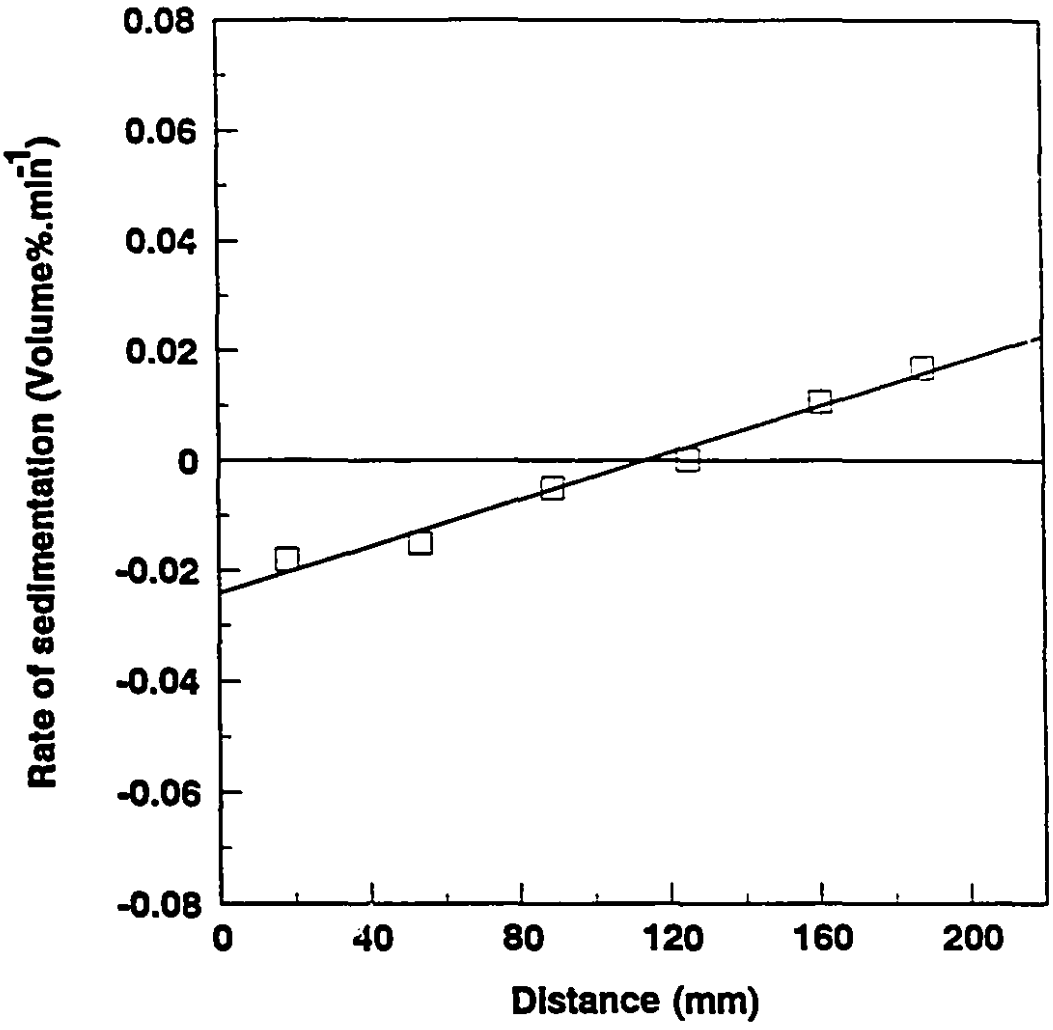

Figure 6.6: The rate of sedimentation at different locations in the mold

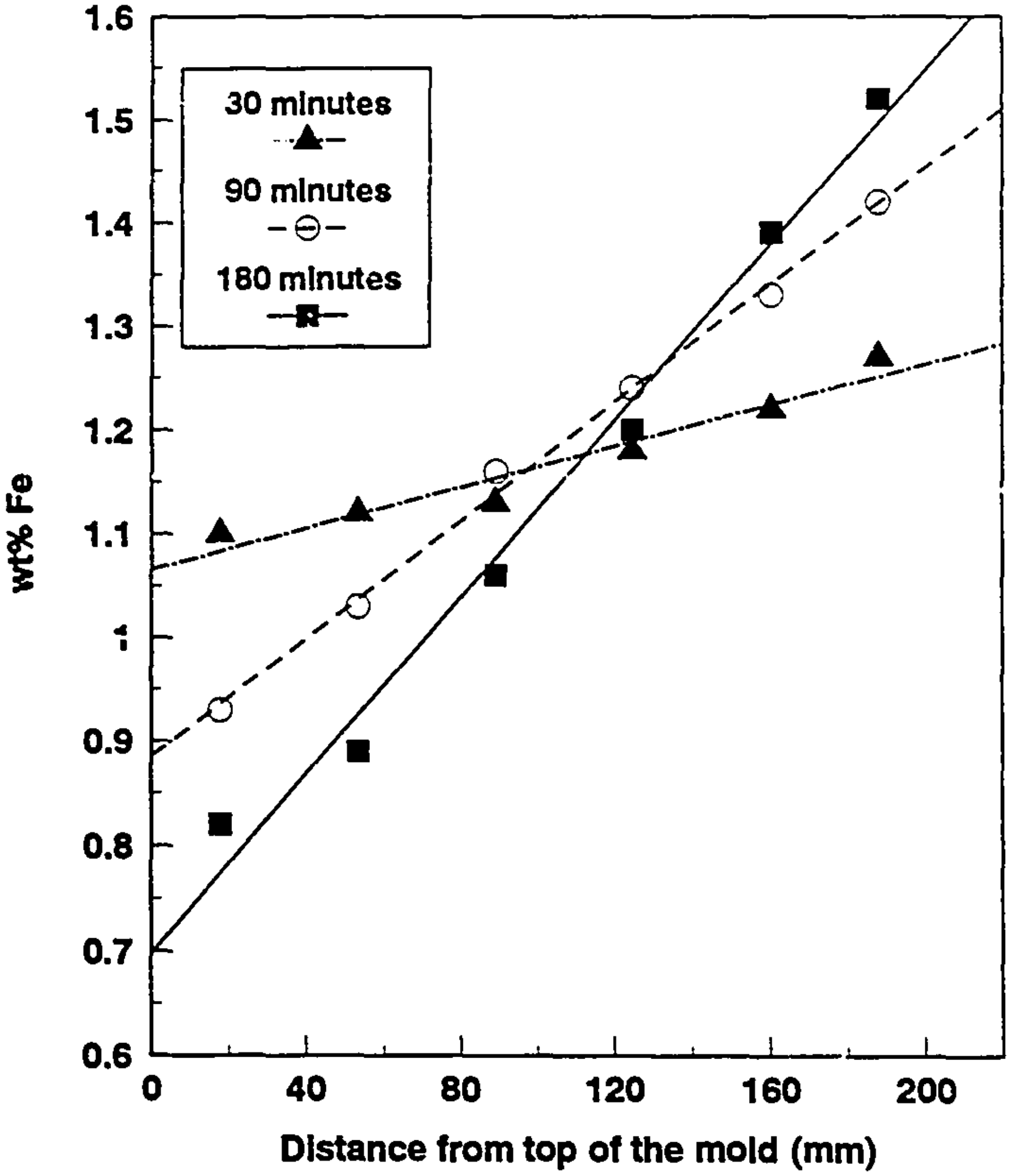

Figure 6.7: The effect of settling time and location in the mold on the iron concentration

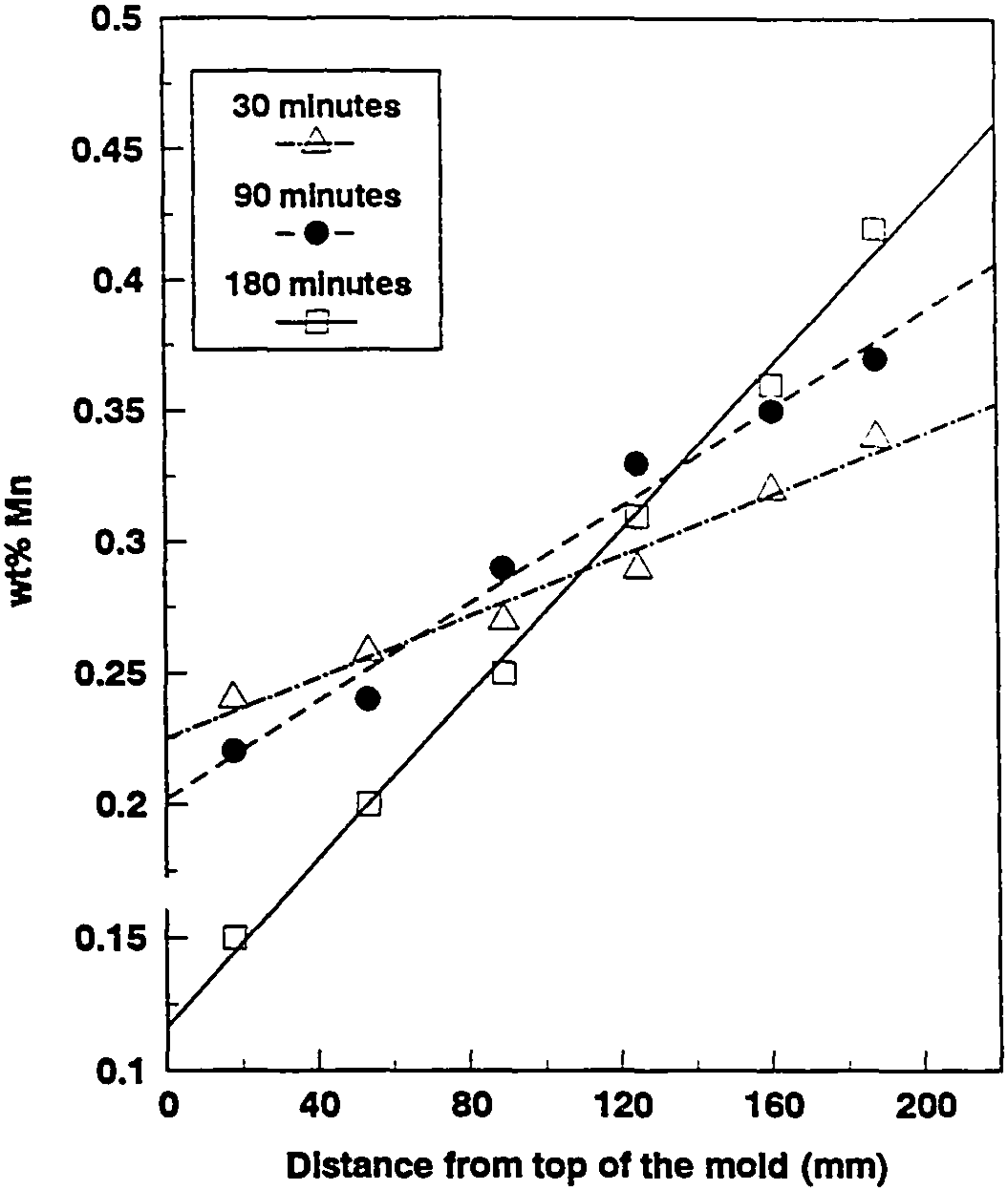

Figure 6.S: The effect of settling time and location in the mold on the manganese concentration

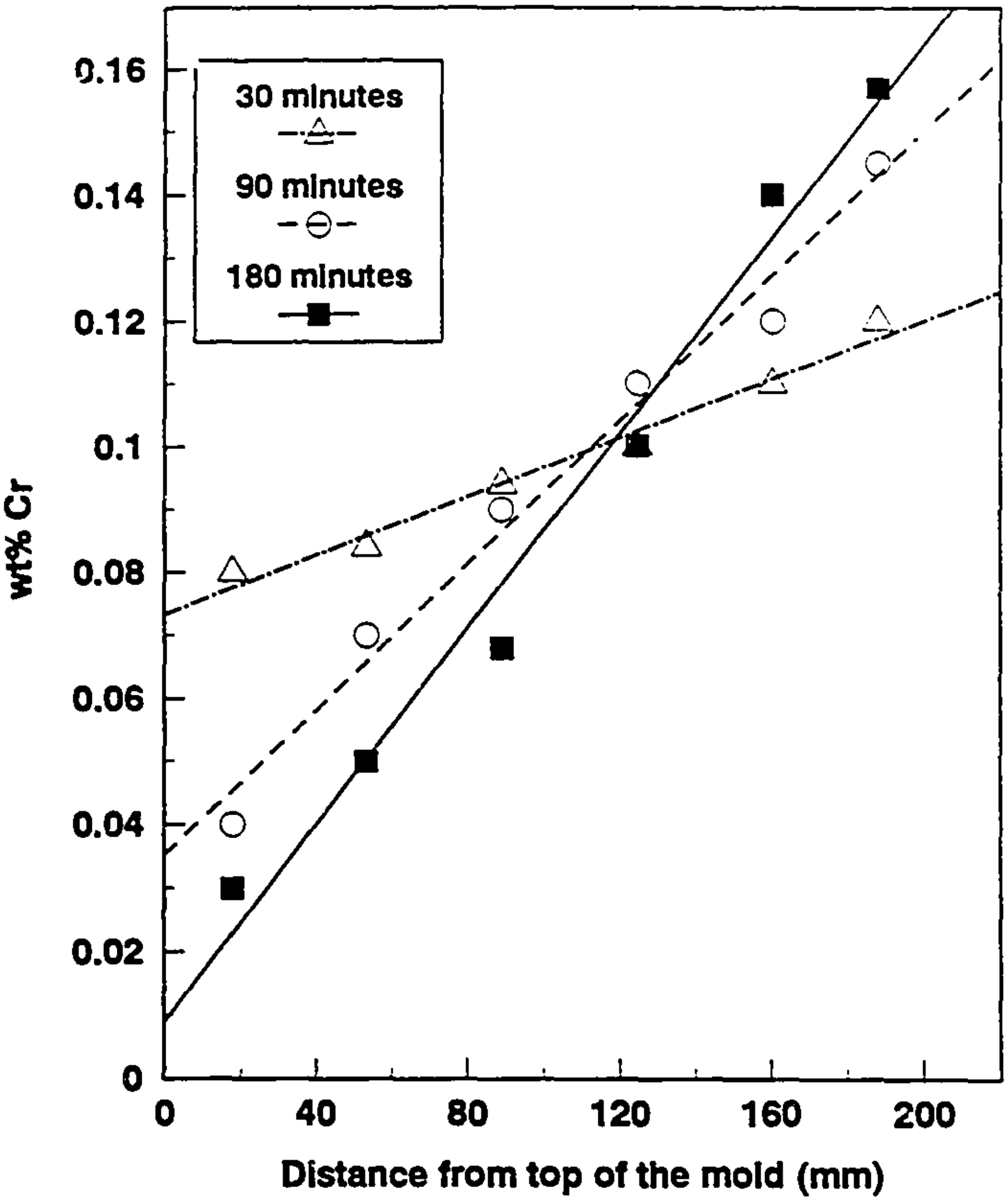

Figure 6.9: The effect of settling time and location in the mold on the chromium concentration

6.3.3. Study of the Segregated Phases

The complex intermetallic compounds observed in this investigation were mostly in platelet (needle in cross-section), star-like, and polyhedral morphology. Polyhedral forms were found at long settling times at the bottom of the mold. Figure 6.10 (a) shows the microstructure of the alloy at location L5 at a settling time of 30 minutes. Both platelets and star-like compounds are observed in the eutectic microstructure of the aluminum-silicon alloy along with some very fine undefined particles (< 1 μm). The polyhedral particles observed at settling times of 180 minutes at the floor of the melt are shown in Figure 6.10 (b) where coalescence is very evident.

The intermetallic compounds observed in Figure 6.10 were analyzed by SEM-EDS. The EDS spectra of elements in the intermetallics are illustrated in Figure 6.11 (a - c). This measurement is a qualitative analysis which shows the existence of different elements in the compounds. Figure 6.11 (a) and (b) shows respectively, the EDS spectra of platelet and star-like intermetallics at location L5 at settling time of 30 minutes, while Figure 6.11 (c) shows the EDS spectrum of polyhedral particles at a settling time of 180 minutes at the floor of the melt.

The platelet and star-like intermetallics shown in Figure 6.10 (a) were analyzed by means of X-Ray mapping. The distribution of iron, manganese, and chromium in these phases is presented in Figure 6.12. This figure shows that the concentration of iron, manganese, and chromium is high in the compounds.

A quantitative analysis was performed on the intermetallics by means of electron probe microanalyzer (EPMA). Table 6.2 gives the EPMA analysis of all types of intermetallics studied in the present work. The chemical analysis given in this table is the average of at least five measurements. According to the EPMA results, the stoichiometry of the platelet morphology, (β-phase), corresponds to $Al_5(Fe,Mn,Cr)Si$ where some iron

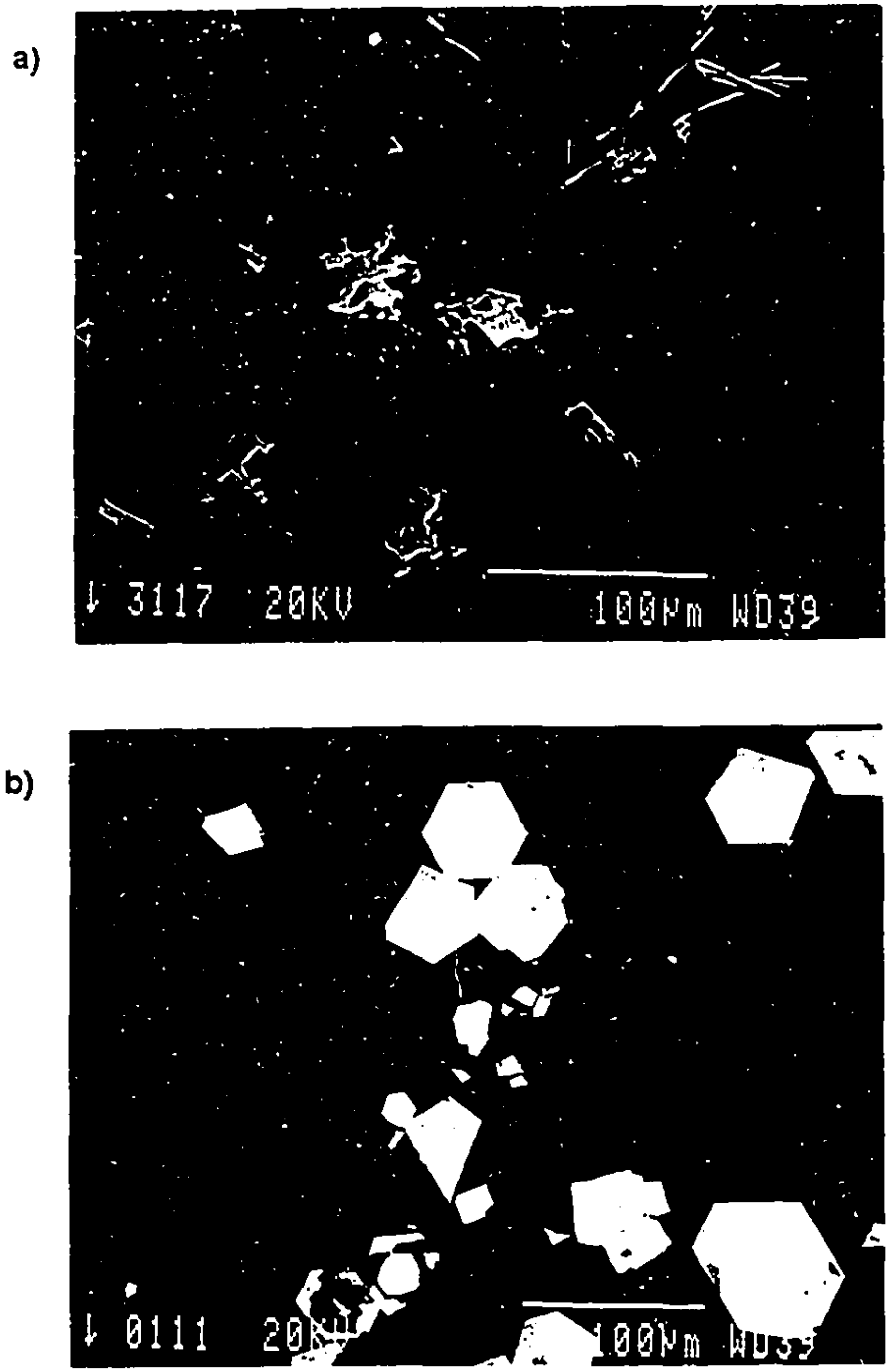

Figure 6.10: SEM photograph of a) star-like and platelet phases at L5 = 160.5 mm from top of the mold (t=30 min) b) polyhedral particles at the floor of the melt (t=180 min)

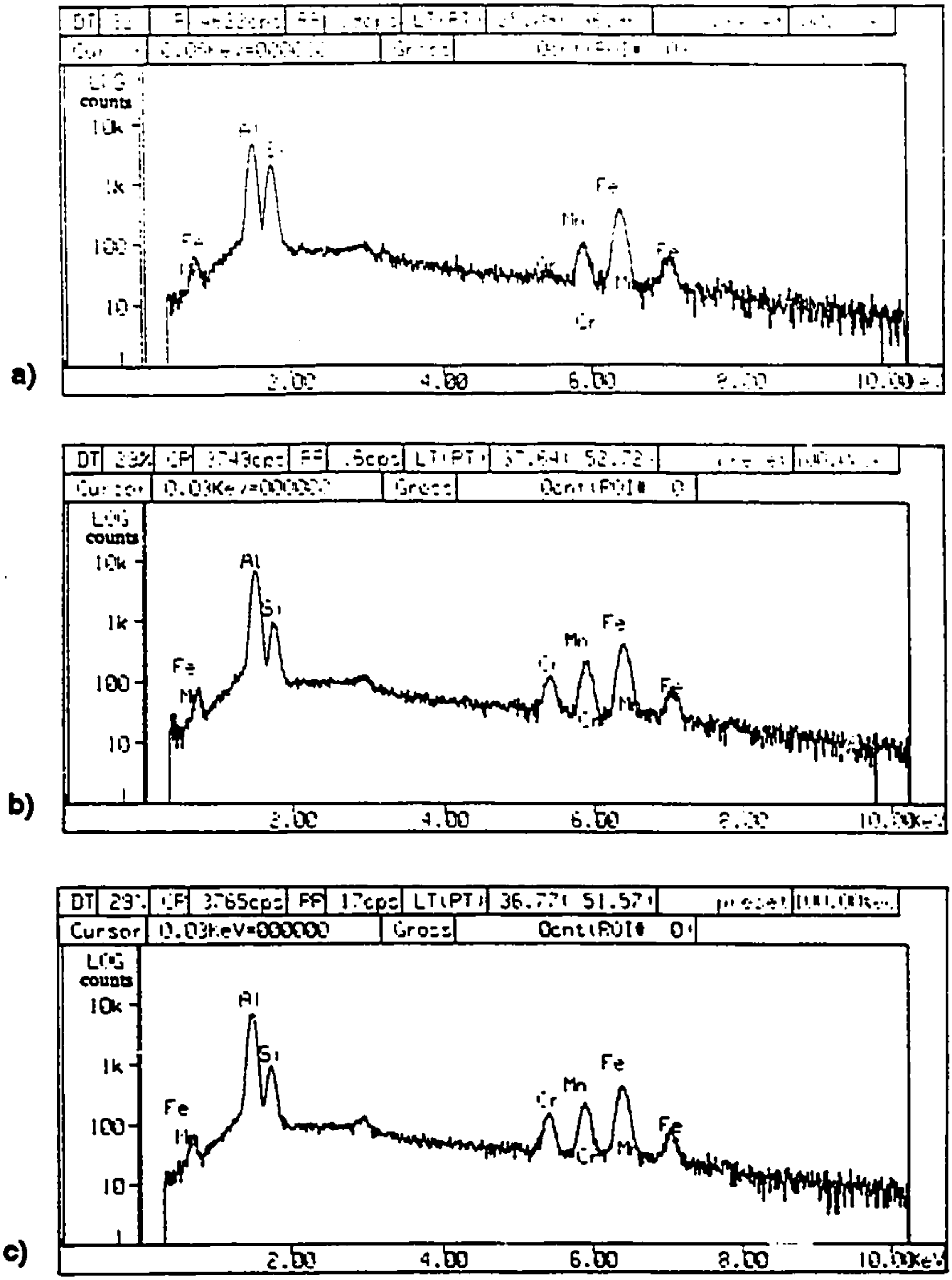

Figure 6.11: EDS spectrum of intermetallics a) platelet b) star-like c) polyhedral

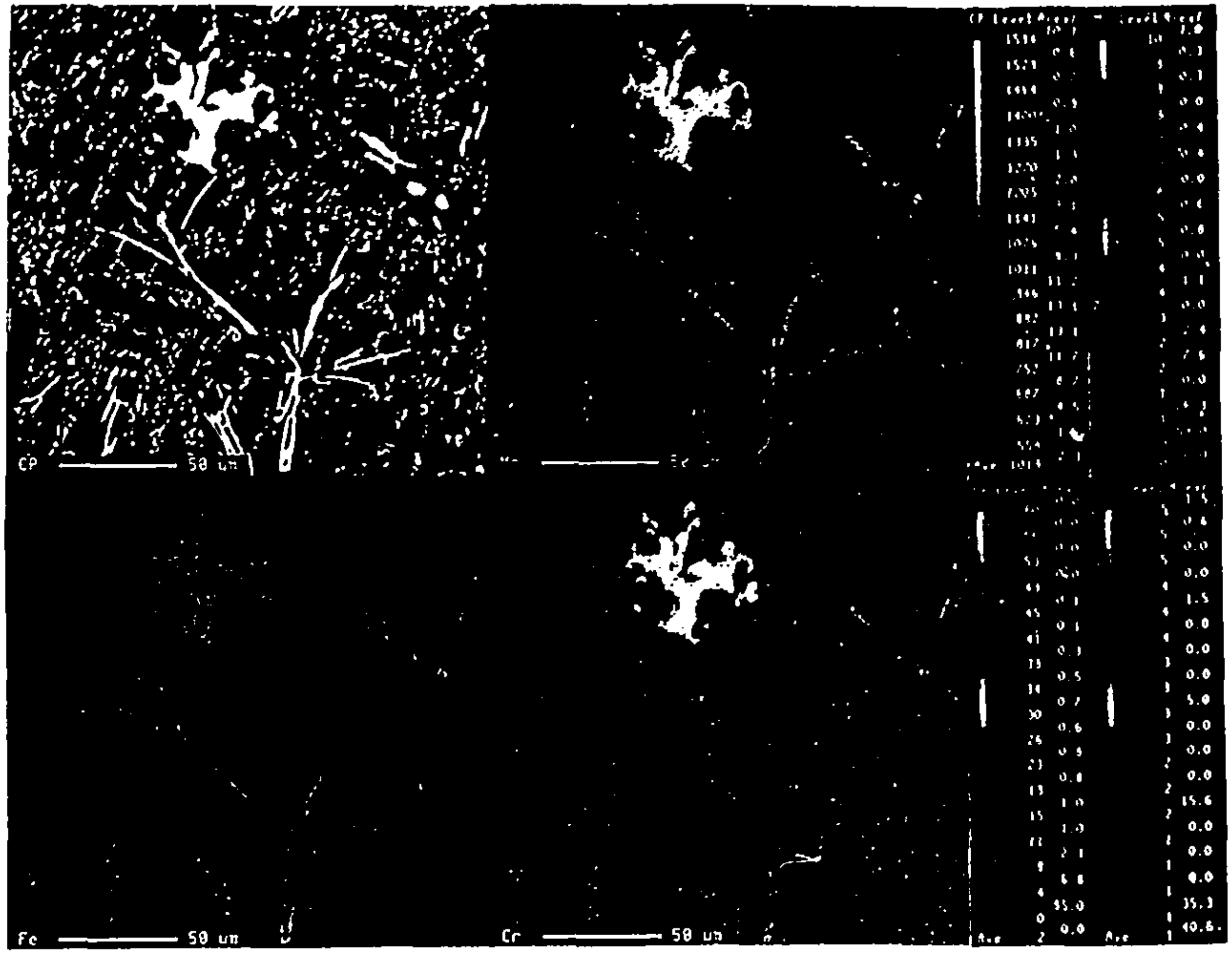

Figure 6.12 : X-Ray mapping of elements in the star-like and platelet phases

atoms are replaced by a maximum of 3 wt% manganese and chromium dissolved in the monoclinic crystal structure of the β-phase. The stoichiometry of the star-like and polyhedral phases is approximately the same and corresponds to the primary α-phase $Al_{12}(Fe,Mn,Cr)_3Si_2$.

Table 6.2: Chemical Composition of the Intermetallic Compounds (atomic %)

Phase	Al	Si	Fe	Mn	Cr
Platelet	66.87	18.02	13.88	1.19	0.05
Star-like	71.45	11.33	10.01	4.71	2.52
Polyhedral	71.75	11.35	9.81	4.61	2.49

6.4. Discussion

The experiments described here were designed to produce conditions of minimum convection. It should therefore be possible to compare the results to those predicted by Stokes' law for settling of particles in a stationary fluid.

6.4.1. Motion of Particles Settling in a Stationary Fluid

Motion of a particle in a viscous fluid is governed by Stokes' law. The Stokes' velocity or "terminal velocity" is the maximum velocity attained by a particle falling through a motionless fluid and corresponds to the point at which the relative weight of the particle just balances the viscous drag exerted by the fluid.

This velocity is given by Stokes' law as :

$$u_t=\frac{g.d^2.(\rho_p-\rho_f)}{18.\eta} \tag{1}$$

where, u_t is terminal velocity, d = particle diameter , ρ_p = density of particle , ρ_f = density of liquid, g = acceleration due to gravity, η = viscosity of the liquid.

Stokes' law is derived for spherical particles; non-spherical particles will attain a terminal velocity, but this velocity will be influenced by the shape of the particles. Nevertheless, this velocity can be used to characterize the particle. This value of " d " is referred to as the "Stokes' equivalent spherical diameter". It is also known as the "Stokes' diameter" or the "sedimentation diameter".[114] While the sludge particles are definitely not perfect spheres it is assumed that their predominately star-like shape can be approximated to a sphere for purposes of the Stokes' law calculation.

6.4.2. Comparison between Stokes' law and the experimental results

The terminal velocity (u_t) of the settling intermetallics has been calculated from both Stokes' law and the experimental data for settling times of 30, 90, and 180 minutes. Proper application of Stokes' law requires that the Reynolds number (Re) be less than 0.2.[93] It will be demonstrated later that this is true for the present experiments.

6.4.2.1. Calculation of settling speed based on the experimental results

The volume percent of intermetallic compounds settled at different locations in the mold in terms of time is shown in Figure 6.5. In order to find the settling velocity (u), we should first find the volumetric flow rate (Q) of intermetallics in the liquid in the mold from top to bottom. At a settling time of 30 minutes, the volume percent difference at L1 (18 mm) and L6 (188 mm) is 1.62%, and the volume of the melt in this part of the mold (L1-L6) is 154.08 cm^3. The volume of intermetallics settled is therefore,

$$V=154.08\times1.62\%=2.50 \quad cm^3$$

and the volumetric flow rate of intermetallics will be,

$$Q=\frac{V}{t}=\frac{2.50\times10^{-6}}{30\times60}=1.39\times10^{-9}\quad m^3/s$$

This volumetric flow rate is equal to the settling velocity multiplied by the effective area (A_{eff}).

$$Q=u.A_{eff} \tag{2}$$

The effective area (A_{eff}) is the cross-sectional area of the intermetallics on which the drag force operates. The average area percent of intermetallics (A_{Avg}) measured by image analysis from L1 to L6 is 3.7% (Table 6.3), and the effective area (A_{eff}) is calculated by multiplying the average area percent of intermetallics (A_{Avg}) by the cross-section of the liquid in the mold, i.e.

$$A_{eff}=3.7\%\ \times\ 3\times3\times10^{-4}\ =\ 3.31\times10^{-5}\quad m^2$$

Substituting in equation (2), the settling velocity is :

$$u=\frac{Q}{A_{eff}}\ =\ \frac{1.39\times10^{-9}}{3.31\times10^{-5}}\ =\ 4.19\times10^{-5}\quad \frac{m}{s}$$

Table 6.3: Area Percentage of Intermetallics in the Alloy at 630°C

height (mm)	30 minutes	90 minutes	180 minutes
18	3.00	1.29	0.20
53.5	3.17	2.24	0.90
89	3.27	3.61	2.60
125	3.85	4.34	3.95
160.5	4.21	5.28	5.87
188	4.62	6.18	7.22

6.4.2.2. Calculation of settling speed based on Stokes' law

The values of the constants used for the calculations are given in Table 6.4. The measured average diameter of the particles is $d = 10.05\ \mu m$; at a settling time of 30 minutes at 630°C. Substituting these values in the Stokes' equation (1), we obtain :

$$u_t = \frac{(10.05\times10^{-6})^2\times9.81\times(3460-2400)}{18\times1.20\times10^{-3}} = 4.86\times10^{-5}\ \frac{m}{s}$$

This terminal velocity is very close to the settling velocity obtained previously from the experimental results (4.19×10^{-5} m/s). The Reynolds number (Re) may now calculated from this terminal velocity to check if it is less than 0.2 as required for proper application of Stokes' law.

$$Re = \frac{\rho_l . u_t . d}{\eta} \tag{3}$$

and,

$$Re = \frac{2400\times(4.86\times10^{-5})\times(10.05\times10^{-6})}{1.20\times10^{-3}} = 9.77\times10^{-4} \ll 0.2$$

Stokes' law can therefore be applied with confidence to the present system.

Table 6.4: Values of Constants Used for Calculation of Settling Speed

constant	value	note
ρ_l	2400 $kg.m^{-3}$	ref. [115,116]
ρ_p	3460 $kg.m^{-3}$	ref. [30]
g	9.81 $m.s^{-2}$	ref. [93]
η	$1.20 . 10^{-3}$ $N.s.m^{-2}$	ref. [117,118]

Similar calculations have been performed for settling times of 90 and 180 minutes. The settling velocities obtained from the experiments are compared with those calculated from Stokes' law and summarized in Table 6.5 where it is seen that there is a good agreement between the experimental and calculated velocities. This agreement indicates that the assumptions of free settling of spherical particles is reasonable for the case of sludge in aluminum-silicon foundry alloys. Of course, the particles are not truly spherical, and the small differences between calculated and measured settling velocities may well be due to this fact. It is also evident that free particle, and not hindered, settling occurs. The maximum solid particle fraction measured was only 7% (Figure 6.2), and hindered settling is believed to be important at solid fractions of 15% or greater.[114,119,120]

A simple calculation based on the settling velocities presented in Table 6.5 predicts, for a mean particle size of 10 μm, that all particles should settle to the bottom of the column at times of 90 and 180 minutes. Clearly this is not the case (Figure 6.2) due to the fact that in reality a distribution of particle size exists. Fine particles with size much less than 10 μm will sink considerably more slowly. The behaviour of such fine intermetallics will be particularly affected by any limited convection in the experimental system.

Table 6.5: Settling Velocities Obtained by the Experiments and Calculated by Stokes' law (m/s)

	30 minutes	90 minutes	180 minutes
Stokes' law	$4.86 \,.\, 10^{-5}$	$4.38 \,.\, 10^{-5}$	$4.27 \,.\, 10^{-5}$
experimental	$4.19 \,.\, 10^{-5}$	$4.06 \,.\, 10^{-5}$	$3.28 \,.\, 10^{-5}$

Some investigators [121,122] have applied Stokes' law to model the settling of inclusions in casting or holding furnaces. They assumed that the bath of metal was stagnant and convection in the system was negligible. The models which they obtained were incapable of describing fully the settling phenomena since natural convection generated as a result of heat losses through the furnace side walls can play a major role in the molten bath, and the Stokes' velocity can then be influenced by the convection. In the present experiments, deliberate efforts were made to eliminate as much as possible all thermal gradients and to make the experiments isothermal.

It is important to determine when the settling speed of intermetallics reaches the terminal velocity and to what height in the mold the Stokes' velocity can be applied. For this the general equation for the motion of particles in the liquid has been used.[93]

$$u=\frac{a}{b}.[1-\exp(\frac{-b.t}{c})] \qquad (4)$$

where,

u is settling velocity, and :

$$a=\frac{\pi}{6}.d^3.g.(\rho_p-\rho_f)$$

$$b=3.\pi.d.\eta$$

$$c=\frac{\pi}{6}.d^3.\rho_p$$

The fastest settling speed will naturally occur for the largest particle. By substituting values from Table 6.4 and using the size of the largest particle measured (12.2 μm), we obtain :

$$u=6.88\times 10^{-5}\times[1-\exp(-43690.5\times t)] \qquad (5)$$

Based on this equation, the settling velocity of the particles versus time is plotted in

Figure 6.13 from which it is evident that the settling speed reaches the terminal velocity at very short times and very close to the top of the mold due to the small sizes of the intermetallics. Stokes' law is therefore applicable to virtually every point in the system used here.

Finally, the settling speeds for some inclusions of various densities have been compared with the settling speed of intermetallics in Figure 6.14. Different inclusion densities of 3.00 (arbitrary), 3.46 (intermetallic), 3.58 (MgO), 3.98 (Al_2O_3) g/cm^3 were used in Stokes' law, and the settling speeds were plotted in terms of particle diameter. The arbitrary density was chosen to illustrate the effect of small differences of densities from the molten alloy (2.40 g/cm^3). Figure 6.14 indicates that particles less than 20 μm have a very low settling velocity, and the settling speed increases with density. As most practical liquid melting or holding operations will experience natural or forced convection, appreciable settling of very fine particles (inclusions or sludge) is not to be expected.

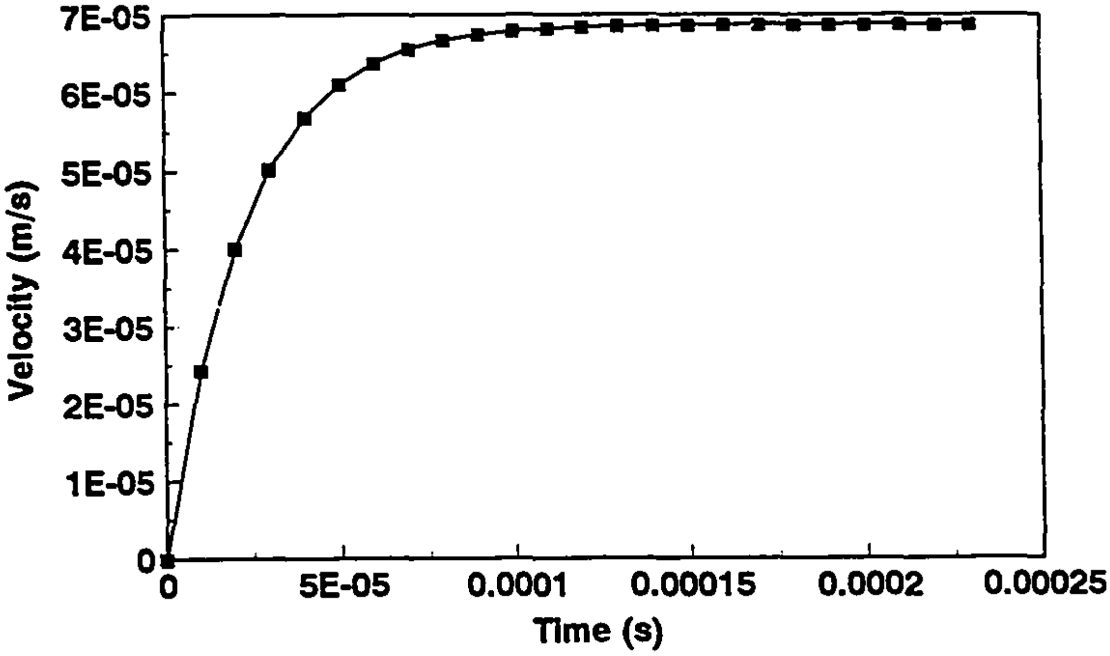

Figure 6.13: Settling velocity of intermetallics as a function of time

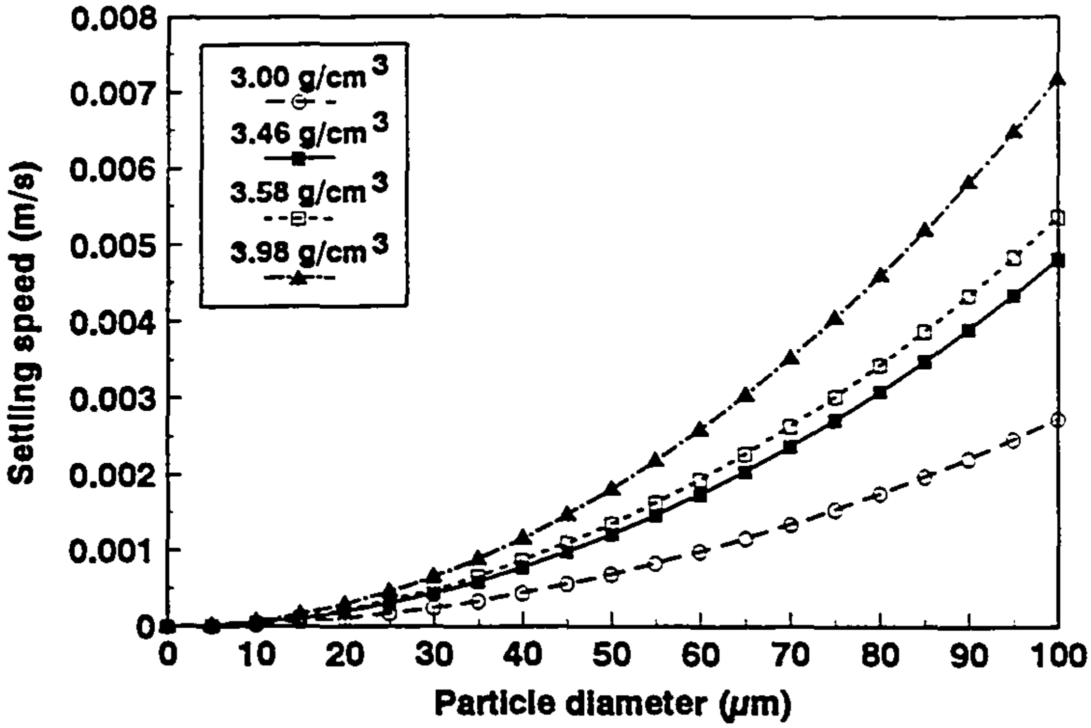

Figure 6.14: Settling speeds of some inclusions as a function of particle diameter

6.5. Summary

Primary crystals of intermetallics which are rich in iron, manganese, and chromium form at temperatures above the liquidus, and because their density is higher than that of liquid aluminum, they cause gravity segregation in the melt. The kinetics of settling of these intermetallic compounds in a melt of Al-12.5% Si having 1.2% Fe, 0.3% Mn, and 0.1% Cr has been studied. Sedimentation was investigated at 630°C for settling times of 30, 90, and 180 minutes in an electric resistance furnace. The effect of settling time and height of melt on the volume percent, number, and size of intermetallic compounds was studied by image analysis. The conclusions are summarized as follows:

(I) The volume percent of intermetallic compounds increases with distance from top of the mold due to settling. This occurs because the number of particles and their average size increases during sedimentation.

(II) The rate of settling varies with location in the mold due to depletion of intermetallics at the top and accumulation at the bottom.

(III) As the distance from the top of the mold increases, the content of iron, manganese, and chromium increases due to the gravity segregation of the intermetallic compounds, with greater concentrations at longer times.

(IV) The terminal velocity calculated by Stokes' law agrees well with the experimentally determined settling velocity due to minimum convection in the system and small size of intermetallics. As a result the terminal velocity is reached at very short times and very close to the liquid surface.

Chapter 7

Modification of Intermetallic Compounds

7.1. Introduction

The intermetallic compounds have different morphologies such as needle-like(platelet), Chinese script, star-like, and polyhedral. The morphology of the compounds plays an important role in determining the mechanical properties of the final product. Of all of these compounds, the needle-like(β-phase) intermetallic is the most harmful. Manganese is commonly used to neutralize the effect of iron and to change the morphology of β-phase(needle) to a less harmful form. This element is not always successful in this task for two reasons: 1) it reacts with other elements in the melt and forms primary phases or complex intermetallic compounds which are usually called "sludge". 2) the formation and growth of intermetallics are also affected by solidification conditions. A different approach to changing the morphology of intermetallics to less harmful forms may be to add surface active elements to the melt. Some limited work has been done on this subject.

Khudokormov[37] investigated an aluminum alloy with 12% Si, 2% Fe, 1.5% Mn. The complex iron-rich phase was modified with 0.05-0.5% of Na, K, Li, P, Sb, Bi, S, Se, and Te. The strongest effects on the form of the iron-rich phase were produced by S, Se, and Te. The particles became much finer and were reduced to a more equi-axed form. Sigworth[14,75] reported on the influence of molten metal processing on the mechanical properties of cast Al-Si-Mg alloys, and during his work, he noted that the formation of large brittle iron intermetallic phases can be suppressed in an exceedingly well modified alloy.

Haque and Kondic[128] indicated that strontium has some positive effect on the reduction of the amount of intermetallics during solidification of an aluminum-12.2% silicon alloy. The amount of iron-bearing phase as well as the primary silicon phase are reduced or become negligible and the tensile properties are improved by strontium treatment. Except for the two observations by Sigworth[75] and Kondic et.al.[128], there appears to be no comprehensive investigation of the effect of strontium on intermetallics in aluminum-silicon casting alloys.

There is, however, considerable evidence that strontium modifies and refines many of the detrimental intermetallic compounds in wrought alloys. In a 1975 Alcan patent[95], it is indicated that at 0.05% Sr all of the AlFeSi intermetallics in 6063 alloy are in the Chinese script form. It is also reported in a 1987 patent by ALCOA [96] that the addition of 0.01% to 0.10% strontium (nominally 0.05% Sr) to Al-Cu-Mg-Zn wrought alloys refines the intermetallic phases. A 1987 Japanese patent[97] also indicates that the addition of 0.005% to 0.10% strontium, in combination with similar quantities of zinc, reduces both the number and size of detrimental intermetallics. In recent work at McGill University, it has been reported that a Sr addition of 0.06% alters the needle-like β-phase to the Chinese script α-phase in synthetic 1XXX and 6061 alloys, and in DC cast commercial 6061 alloys.[98]

On the basis of the success achieved in wrought alloys, it was decided to do a comprehensive investigation of the effect of strontium on the modification of different morphologies of intermetallic compounds in sand cast and permanent mold cast aluminum-silicon alloys.

7.2. Experimental Procedure

7.2.1. Materials

The investigation focussed on two commercial die and permanent mold-casting alloys, A413, 413P, and one synthetic 413 alloy. Strontium was added to these alloys at different levels ranging from 0 to 0.08% Sr with microstructural investigation as the chief mode of study. 413P is a die-casting alloy which is used in piston manufacturing. The alloy used in this work was produced by Roth Brothers Smelting Company. A413 is a secondary alloy which is used in die-casting, and is produced by Aluminum Smelting and Refining Company. The synthetic 413 alloy was prepared by making appropriate additions to an Al-12.7% Si alloy manufactured from commercial purity aluminum and silicon in an induction furnace. Iron, manganese and chromium additions were made to this alloy by means of commercial master alloys of composition: Al-24.7% Fe, Al-25.7% Mn and Al-20.1% Cr. Strontium was introduced into the melt in the form of 10-90 (10% Sr balance Al) master alloy. All master alloys were provided by KB Alloys, Inc. Table 7.1 gives the chemical analysis of the master alloys as supplied by the company. The analyzed chemical composition of the alloys prepared for the present investigation is given in Table 7.2.

Table 7.1: Chemical Analysis of the Master Alloys, wt%

Master Alloy	Fe	Cr	Mn	Si	Zn	V	Ni	Sr
Al-24.7% Fe	24.7	<0.01	0.15	0.05	0.01	0.01	0.01	Nil
Al-20.1% Cr	0.14	20.1	0.01	0.15	0.01	0.02	<0.01	Nil
Al-25.2% Mn	0.14	<0.01	25.2	0.06	<0.01	0.01	<0.01	Nil
Al-10.2% Sr	0.13	<0.01	<0.01	0.05	0.02	0.01	<0.01	10.2

Table7.2: Chemical Composition of the Alloys (wt%)

Alloy	Si	Fe	Cu	Mn	Mg	Cr	Ni	Zn	Sr
413	12.46	1.21	<0.002	0.29	<0.01	0.10	<0.001	<0.008	<0.002
413P	12.37	0.60	0.96	0.28	1.07	0.004	1.18	0.27	<0.002
A413	12.29	0.96	0.23	0.31	0.05	0.06	0.02	0.20	<0.002

7.2.2. Melting and Casting

Melting was carried out in a small induction furnace. For each batch of melt, 220 g of 413 alloy was melted at 750°C. The alloy was held for 10 minutes at this temperature to obtain a homogenized melt. The melt was then cooled to 710°C and strontium was added at this temperature. Strontium was introduced into the melt by the Al-10% Sr master alloy to obtain levels of: 0, 0.02, 0.04, 0.06, 0.08% Sr. The melt was held for 15 minutes at 710°C to allow for complete dissolution of the strontium. Three samples were cast at this temperature for each alloy; two samples in a permanent mold (copper) and one sample in a small fire-clay crucible to simulate sand casting. It had previously been established that the cooling rates reached in the fire-clay crucible were similar to those found in sand casting.(1 °C/s) Thus the fire-clay crucible was chosen to alleviate the problem of manufacturing many sand molds. Although not strictly sand casting, this simulated version will be referred to as sand casting throughout the remainder of this chapter.

The dimensions of the copper molds were 20 mm in height and 40 mm in diameter. One of the samples from the permanent mold was used for microstructural investigation and image analysis while the other was used for chemical analysis by emission spectrometry. The same melting and casting procedure was used for alloys 413P and A413 except that the weight of the melt was about 330 g and 0.04% Sr was added in each experiment. Two samples of each alloy were cast into the permanent mold and one into the sand mold, both before and after adding strontium. In total, nine aluminum-silicon alloys were prepared for this study (Table 7.3) at two solidification conditions which were measured by thermal analysis and yielded slow to fast cooling rates ranging from 1°C/s to 10°C/s.

Table 7.3: Chemical Analysis of the Sr-treated Alloys, wt.%.

Alloy		Si	Fe	Cu	Mn	Mg	Cr	Ni	Zn	Sr
413	no Sr	12.21	1.18	0.004	0.32	<0.009	0.08	0.004	0.01	<0.002
	0.02% Sr	12.46	1.16	0.003	0.32	<0.009	0.08	0.004	0.01	0.018
	0.04% Sr	12.39	1.18	0.003	0.33	<0.009	0.08	0.004	0.01	0.037
	0.06% Sr	12.53	1.19	0.003	0.33	<0.009	0.09	0.004	0.01	0.058
	0.08% Sr	12.83	1.17	0.003	0.33	<0.009	0.08	0.004	0.01	0.077
A413	no Sr	12.29	0.96	0.23	0.31	0.05	0.06	0.02	0.20	<0.002
	0.04% Sr	12.12	0.98	0.28	0.32	0.06	0.07	0.02	0.22	0.039
413P	no Sr	12.35	0.60	0.96	0.28	1.07	0.004	1.18	0.27	<0.002
	0.04% Sr	12.38	0.61	0.96	0.29	1.09	0.006	1.19	0.27	0.037

7.2.3. Effect of Melt Superheat

The effect of superheat was investigated on alloy 413 both before and after strontium addition. The aim of this study was to investigate the effect of superheat, and the combined effects of superheat and strontium treatment on the morphology of the intermetallics. In this experiment, 280 g of alloy 413 was melted in an induction furnace. The melt was superheated to 850°C and held for 30 minutes at this temperature. It was then cooled to 710°C and held for 3 minutes to stabilize the melt temperature. Two samples were cast from this temperature; one into the permanent mold and the other into the sand mold. 0.04% Sr was then added to the alloy and the melt was held for 15 minutes at 710°C for complete dissolution of strontium. Again, two samples were cast into the permanent and sand molds. The operational cycle of this experiment is shown in Figure 7.1.

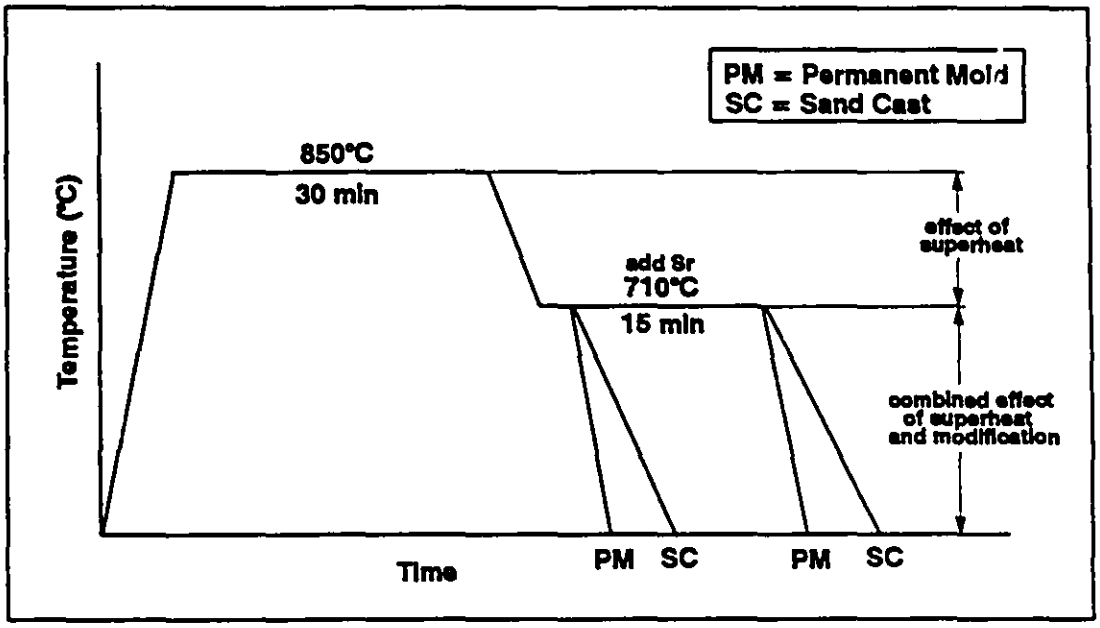

Figure 7.1: Operational cycle for the experiment on the effect of superheat

7.2.4. Effect of Casting Temperature

The aim of this experiment was to investigate the influence of casting temperature on the size and morphology of intermetallics in a strontium-treated alloy. For this purpose, 280 g of alloy 413 were melted at 750°C in an induction furnace. The melt was held for 10 minutes at this temperature for homogenization and was then cooled to 710°C. 0.08% Sr was added to the melt by means of an Al-10% Sr master alloy. The melt was held for a further 15 minutes at 710°C to allow for complete dissolution of the strontium. Two samples were cast into the sand and permanent molds to obtain a slow (1°C/s) to fast (10°C/s) cooling rate. The temperature of the melt was then lowered to 600°C and it was held for 5 minutes at this temperature. Again, two samples were cast with the same conditions as before. The operational cycle of this experiment is shown in Figure 7.2.

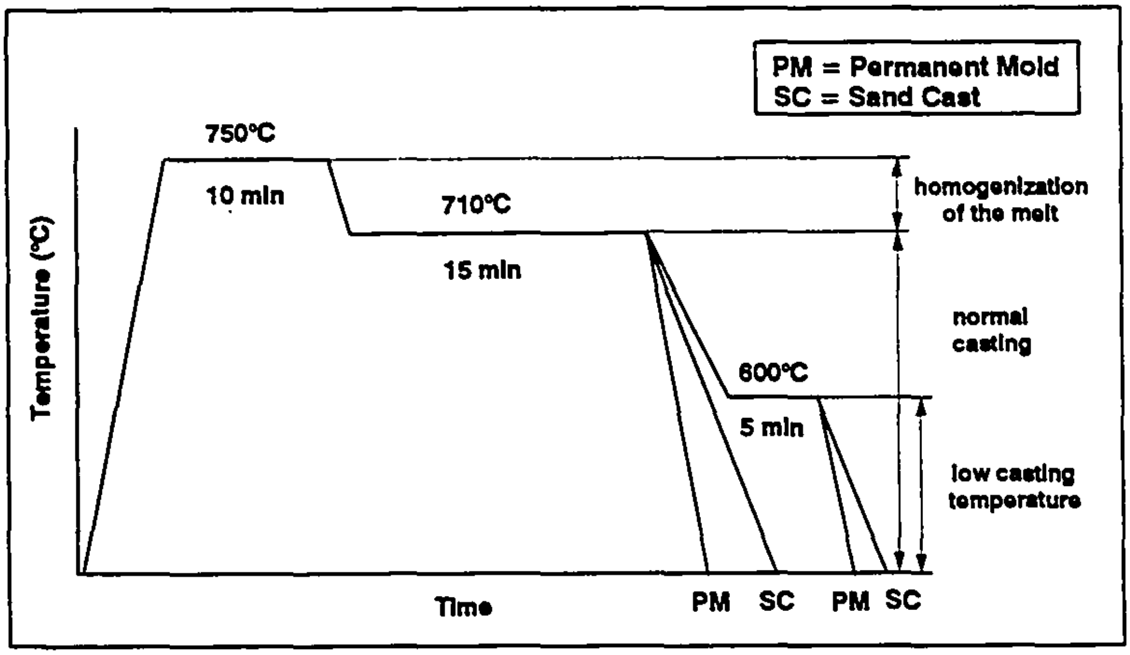

Figure 7.2: Operational cycle for the experiment on the effect of castingtemperature

7.2.5. Microstructural Study and Phase Analysis

Metallographic analysis was carried out on all alloys. The samples were polished up to 0.03 μm alumina powder then continued with colloidal silica and observed under the optical NEOPHOT 21 microscope. In order to develop a more consistent and less subjective evalution of the microstructure, quantitative metallography was employed using a LECO image analyzer interfaced with an optical microscope through the 2005 image analysis program. Various microstructural parameters were investigated and measured, such as the area percent of each phase, average size, number of intermetallics per unit area, roundness, length, width, and aspect ratio of the intermetallics.

A total of 20 fields at 300X magnification was evaluated on each sample. The data was processed automatically using statistical programs, and the mean values reported for each sample. In some cases, in order to differentiate the color contrast (grey level) between the intermetallics and other phases present in the structure, certain manual features such as BOOLEAN FUNCTIONS, COPY, EDIT, CLOSE, FILL available in the image analysis routine were used. Figure 7.3 shows a photograph of a typical sample with the phases highlighted by the image analyzer.

In order to study the effect of strontium on the morphology of the intermetallic compounds, some samples were observed under a scanning electron microscope (SEM), JEOL 840 linked to EDS. The stoichiometry of the phases was determined using an electron probe microanalyzer (EPMA) JEOL JXA-8900L WD/ED Combined microanalyzer and energy dispersive spectrometry (SEM-EDS). EPMA was used at a voltage level of 15KV for chemical analysis of the different phases, and the average of eight readings was calculated for each phase. For the element analysis, ZAF correction was made with reference to the standard pure element. Distribution of the elements was investigated in the intermetallics by using WDS Digital X-Ray Mapping with the JEOL 8900L. The entire experimental procedure is summarized in Figure 7.4.

Figure 7.3: Photograph of a typical sample using the special features in image analysis. Several phases are identified by different colors.(300X)

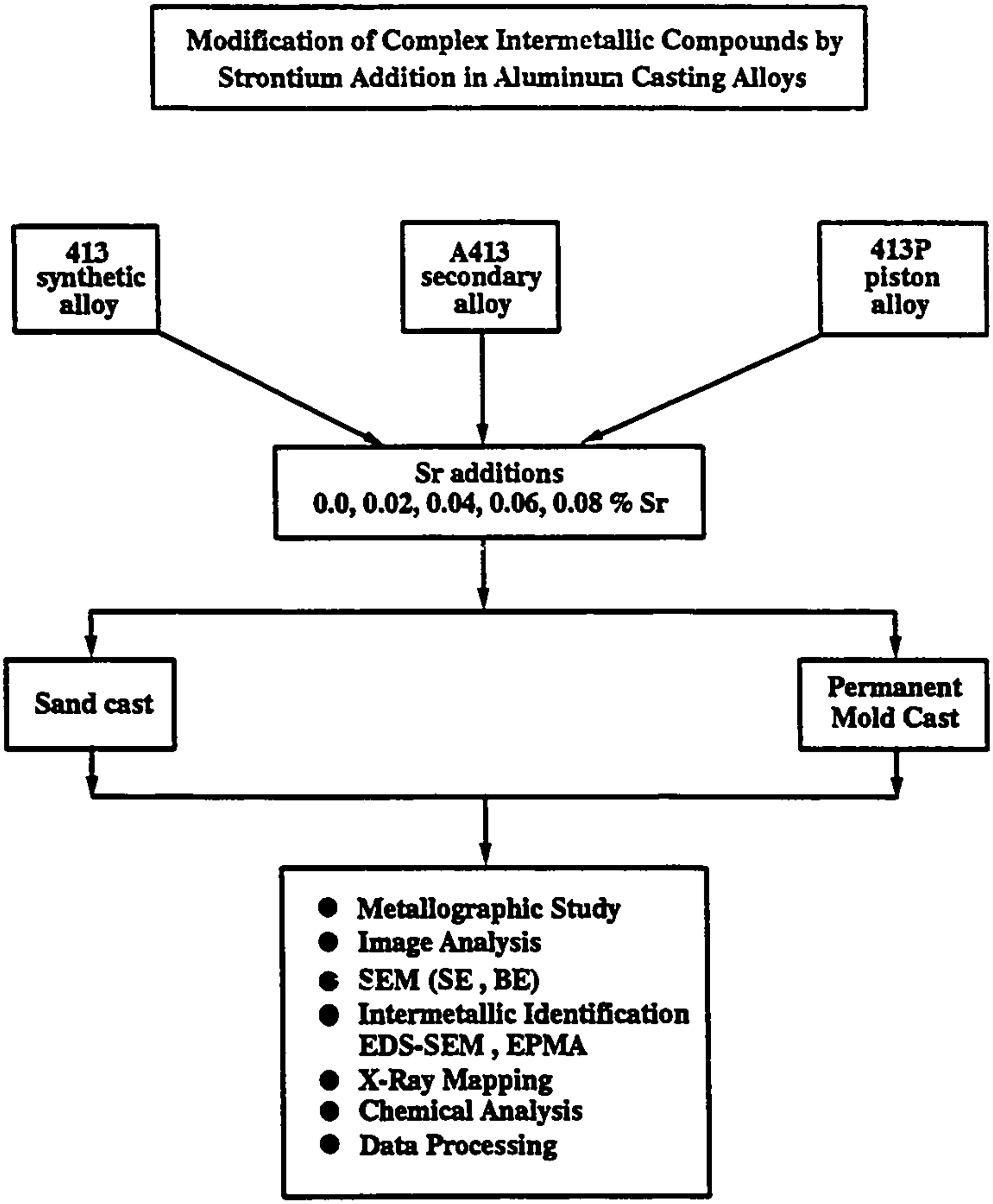

Figure 7.4: Experimental procedure used to study the effect of strontium on the modification of intermetallics

7.3. Results

7.3.1. Alloy 413

7.3.1.1. Permanent Mold

Metallographic observations on the 413 alloy containing 0 to 0.08% Sr (800 ppm), revealed that the microstructure of the alloy consisted of primary aluminum, very fine eutectic silicon, and intermetallic compounds. The compounds had star-like and indefinite shapes. The size of these intermetallics was decreased significantly by strontium additions to the alloy. The microstructures are shown in Figure 7.5(a-e).

a)

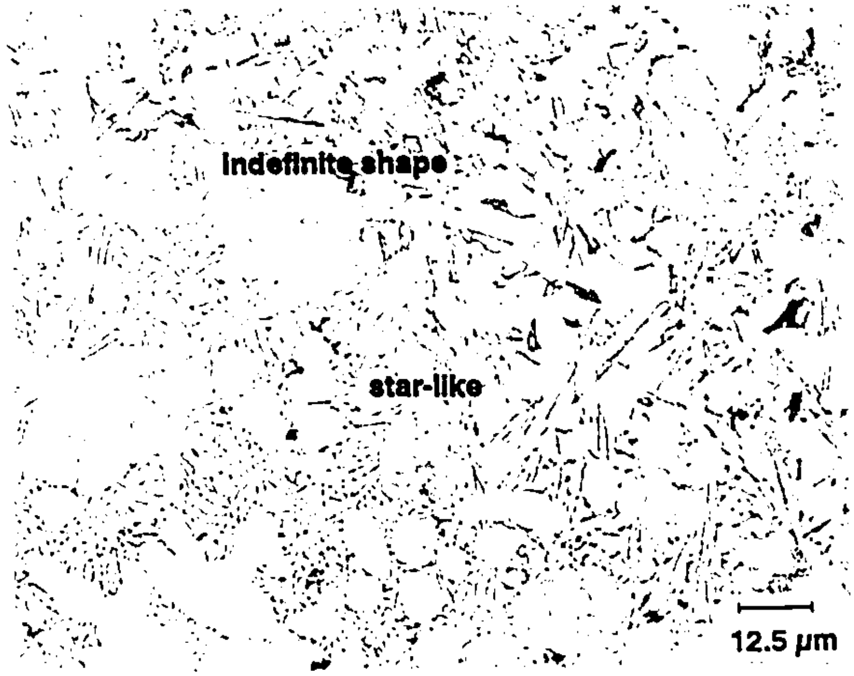

Figure 7.5: Effect of strontium on the shape of intermetallics in alloy 413 at permanent mold condition a) no Sr (400X)

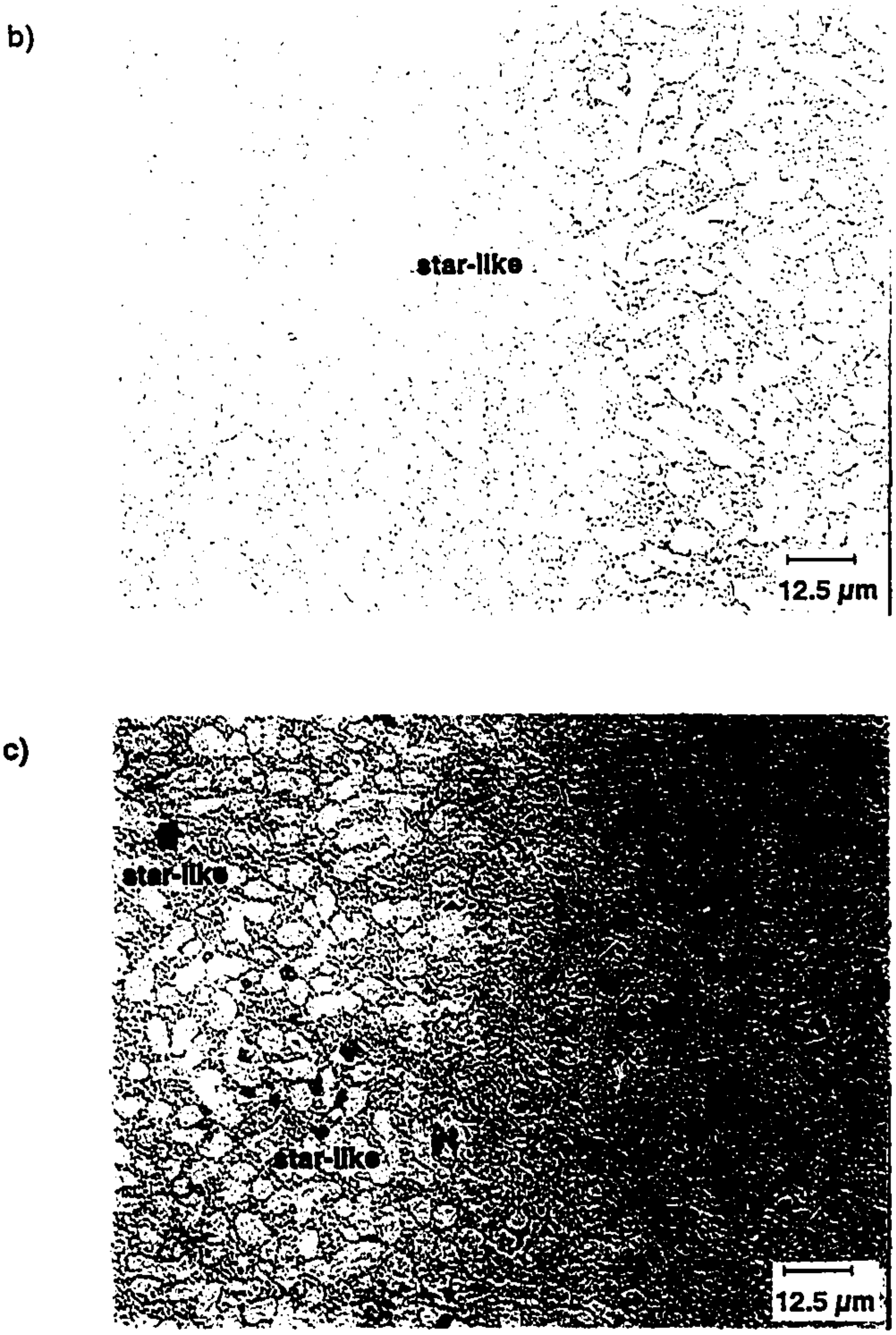

Figure 7.5 continued , b) 0.02% Sr , c) 0.04% Sr (400X)

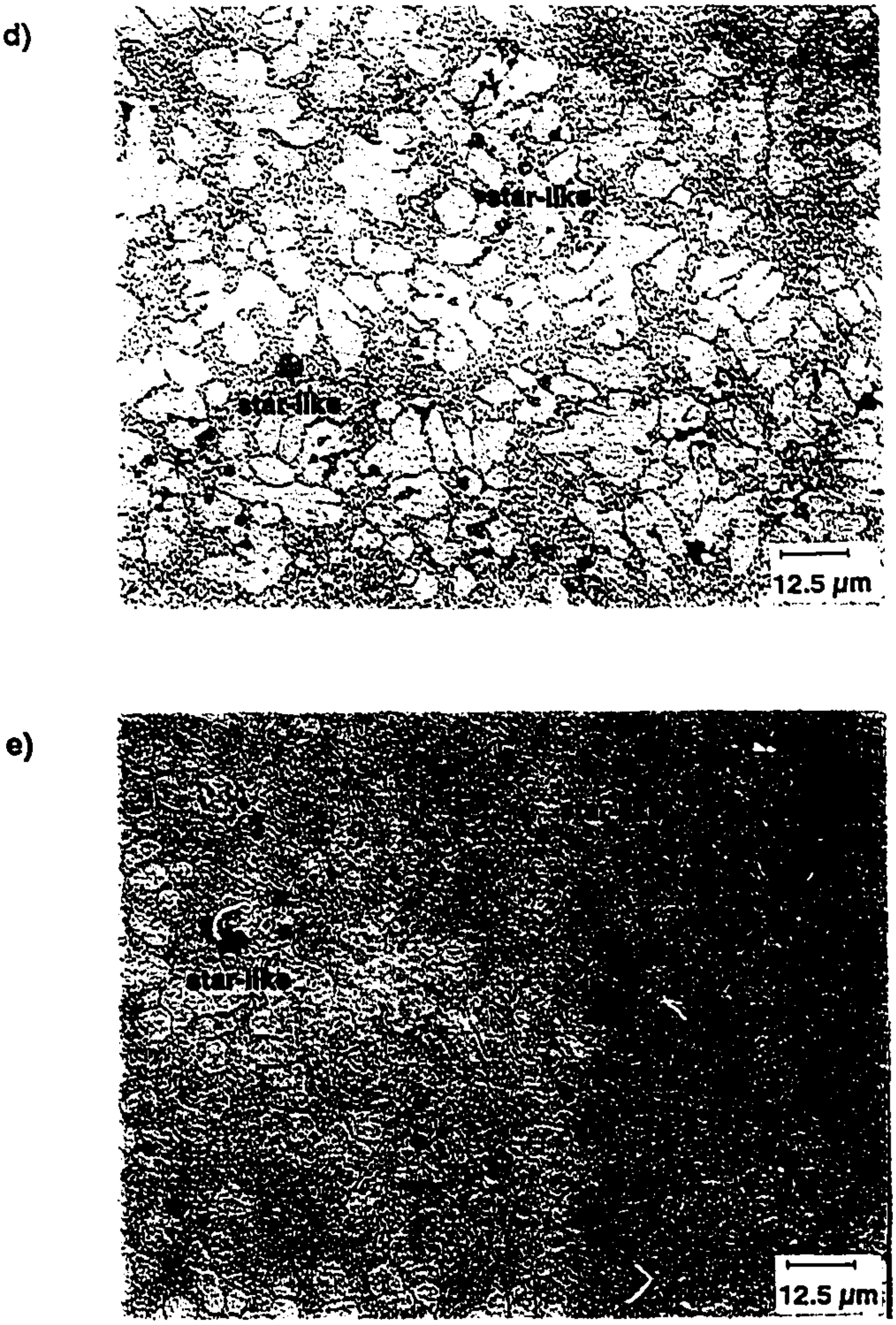

Figure 7.5 continued , d) 0.06% Sr , e) 0.08% Sr (400X)

The size and the number of intermetallics decreased in the alloy when 0.02% Sr was added as shown in Figure 7.5(b). The decrease was very significant when 0.04% Sr was added, (Figure 7.5(c)). In this figure, star-like phases were changed to the tiny and round intermetallics. This situation continued in the 0.06% Sr-treated alloy in which the intermetallics had a very small size and round shape.(Figure 7.5(d)) The size and the number of these intermetallic phases increased when more strontium was added e.g. 0.08% Sr.(Figure 7.5(e)) It was also observed that, in some sections of the microstructure, agglomeration of particles occurred. Image analysis results which show these trends quantitatively are given in Figures 7.6(a-c).

Figure 7.6(a) shows the effect of strontium on the average size and roundness of the intermetallics. Roundness is defined as: $4\pi A/P^2 \times 100\%$ (A = Area , P = Perimeter) For example, the roundness of a circle (sphere) is 100. From this figure, it is seen that the size of the intermetallics decreased from 6.70 μm to 3.67 μm and 3.68 μm at 0.04 and 0.06% Sr additions, respectively. There was a 45% decrease in the size of the intermetallic (sludge) particles at 0.04% Sr addition. The roundness of the particles always increased with the strontium additions, changing from 43% to 71% at 0.08% Sr. Strontium therefore has a major role in changing star-like and indefinite shapes to more round and spherical particles such as the tiny intermetallics shown in Figures 7.5(c) and (d).

The influence of strontium on the number of particles formed in a unit area (mm^2) is shown in Figure 7.6(b). The number of intermetallics decreased significantly by strontium addition. The results of image analysis indicate that the number of particles decreased from 957 in a strontium-free alloy to 201 particles per square millimetre in a 0.06% Sr-treated alloy. Thus, there was a reduction of 80% in the number of particles per unit area.

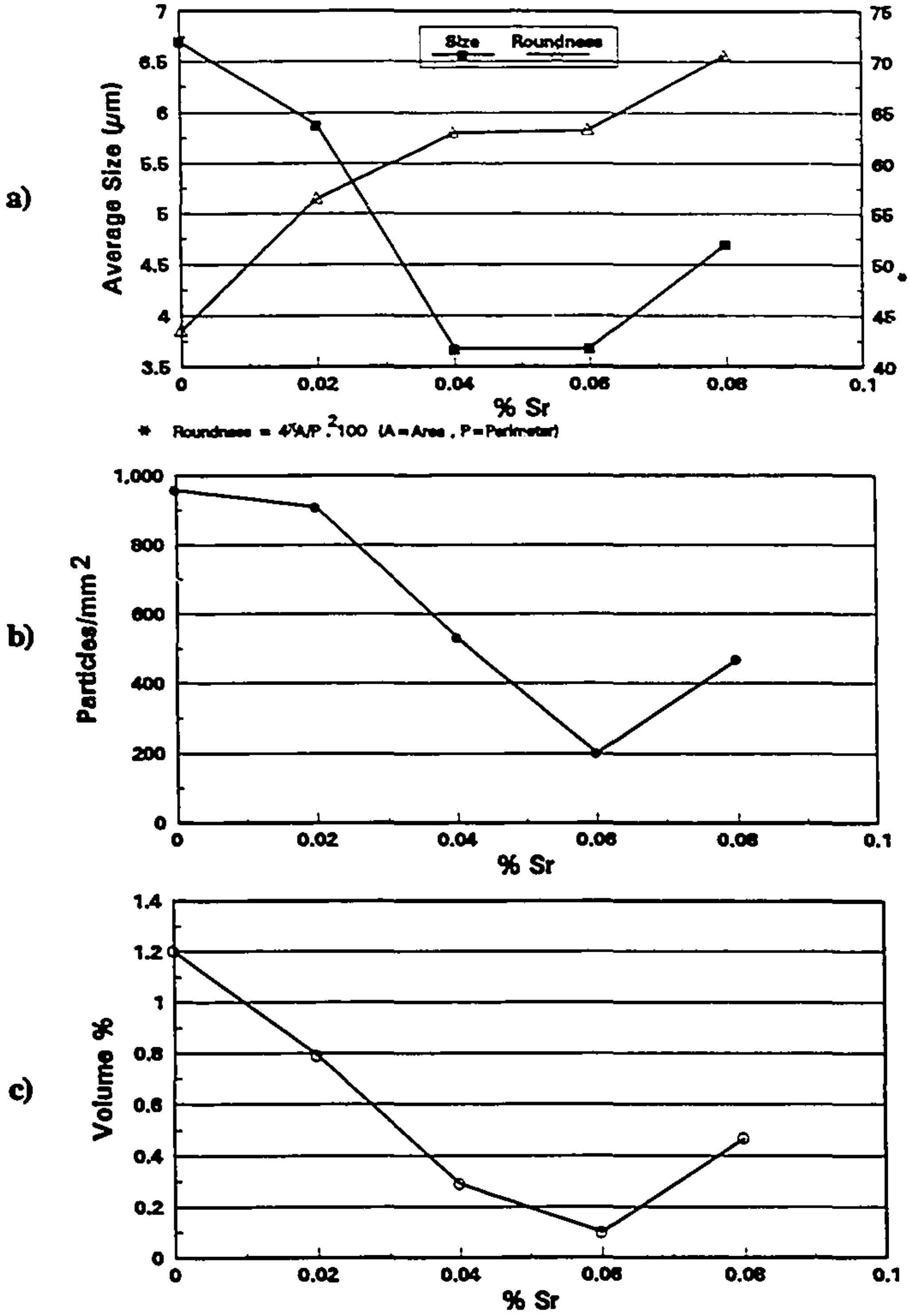

Figure 7.6: Effect of strontium on the intermetallic compounds in alloy 413 at permanent mold condition. a) Size and Roundness b) Particles/mm^2 c) Volume %

Figure 7.6(c) shows the effect of strontium on the volume percentage of star-like intermetallics in permanent mold cast samples. The volume percent of intermetallics was sharply decreased by strontium addition. Image analysis of the samples showed that the volume percent of star-like phase decreased from 1.20% in the strontium-free alloy to 0.29% in the 0.04% Sr-treated alloy. This volume reduction continued to 0.10% (almost zero) when 0.06% Sr was added to the alloy. Thus, there was a reduction of 92% in total volume percentage of the intermetallic compounds. Figure 7.6(a-c) also indicates an optimum level of 0.04 to 0.06% Sr for minimization of the intermetallics. The average size, the number, and the volume percentage of these phases increase when more strontium than this optimum level is added.

7.3.1.2. Sand Cast

Metallographic study of the sand cast 413 alloys revealed that the microstructures consisted of primary aluminum phase, very fine modified silicon, and intermetallic compounds. Compounds appeared in Chinese script (α-phase), indefinite, and needle-like (β-phase) morphologies as shown in Figures 7.7(a-e). As seen from figure 7.7(a) needles and Chinese script exist with coarse silicon in the strontium-free alloy. By adding 0.02% Sr to the alloy, needles fragment and their thickness decreases significantly in a very fine modified silicon microstructure as shown in Figure 7.7(b). Fragmentation of needles (β-phases) is evident in the 0.04% Sr-treated alloy shown in Figure 7.7(c). The needles are broken and thinner than in the 0.02% Sr-treated alloy. Figure 7.7(d) shows further fragmentation and thining of needles in the 0.06% Sr-treated alloy. This situation also exists in the 0.08% Sr-treated alloy, but the thickness and the width of needles have now increased. Figure 7.8(a,b) shows SEM micrographs of these broken needles at two different sections of the sample in a 0.04% Sr-treated alloy. Fragmentation is clearly evident in these micrographs.

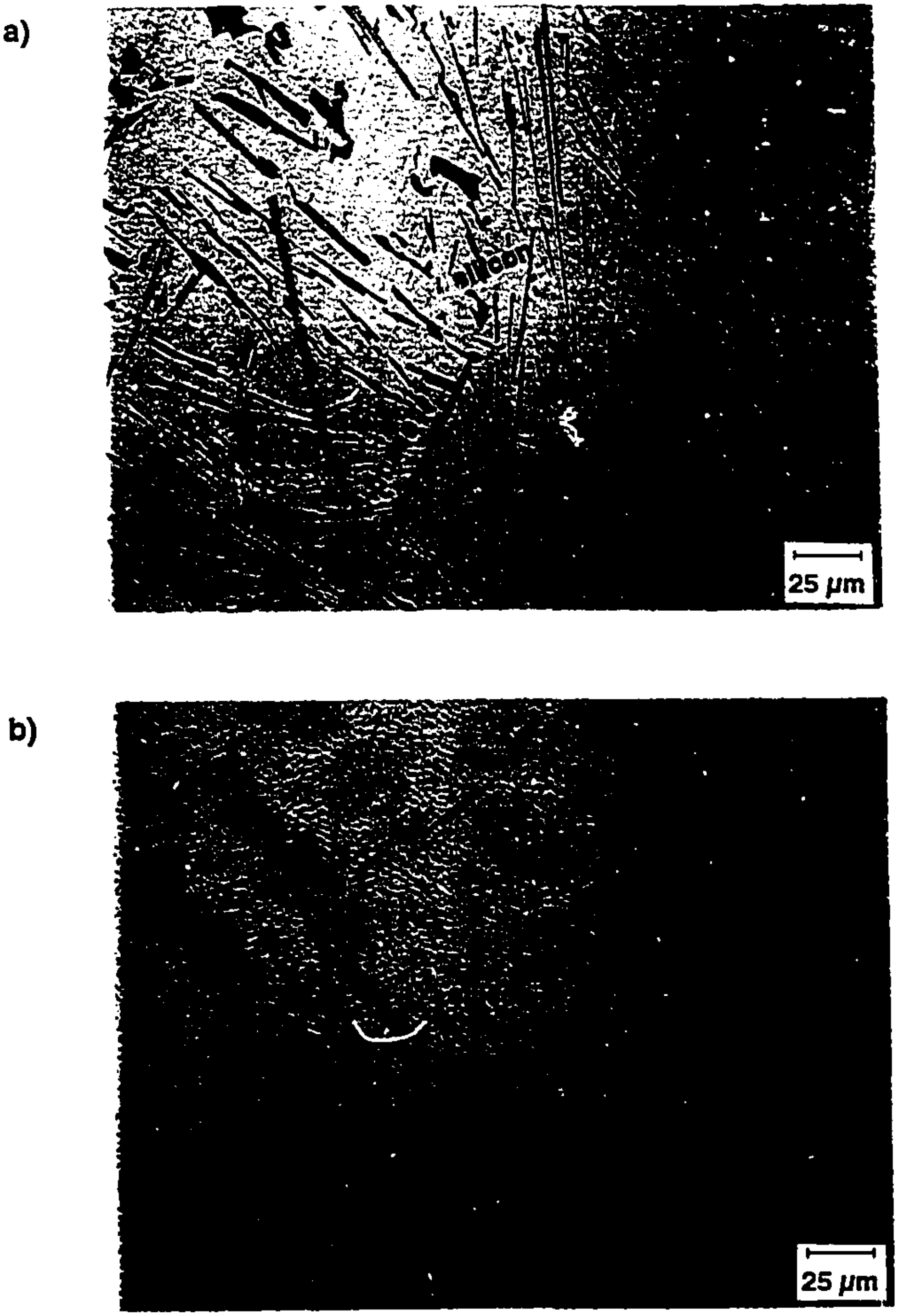

Figure 7.7: Effect of strontium on the shape of intermetallics in alloy 413 in the sand cast condition a) no Sr , b) 0.02% Sr (400X)

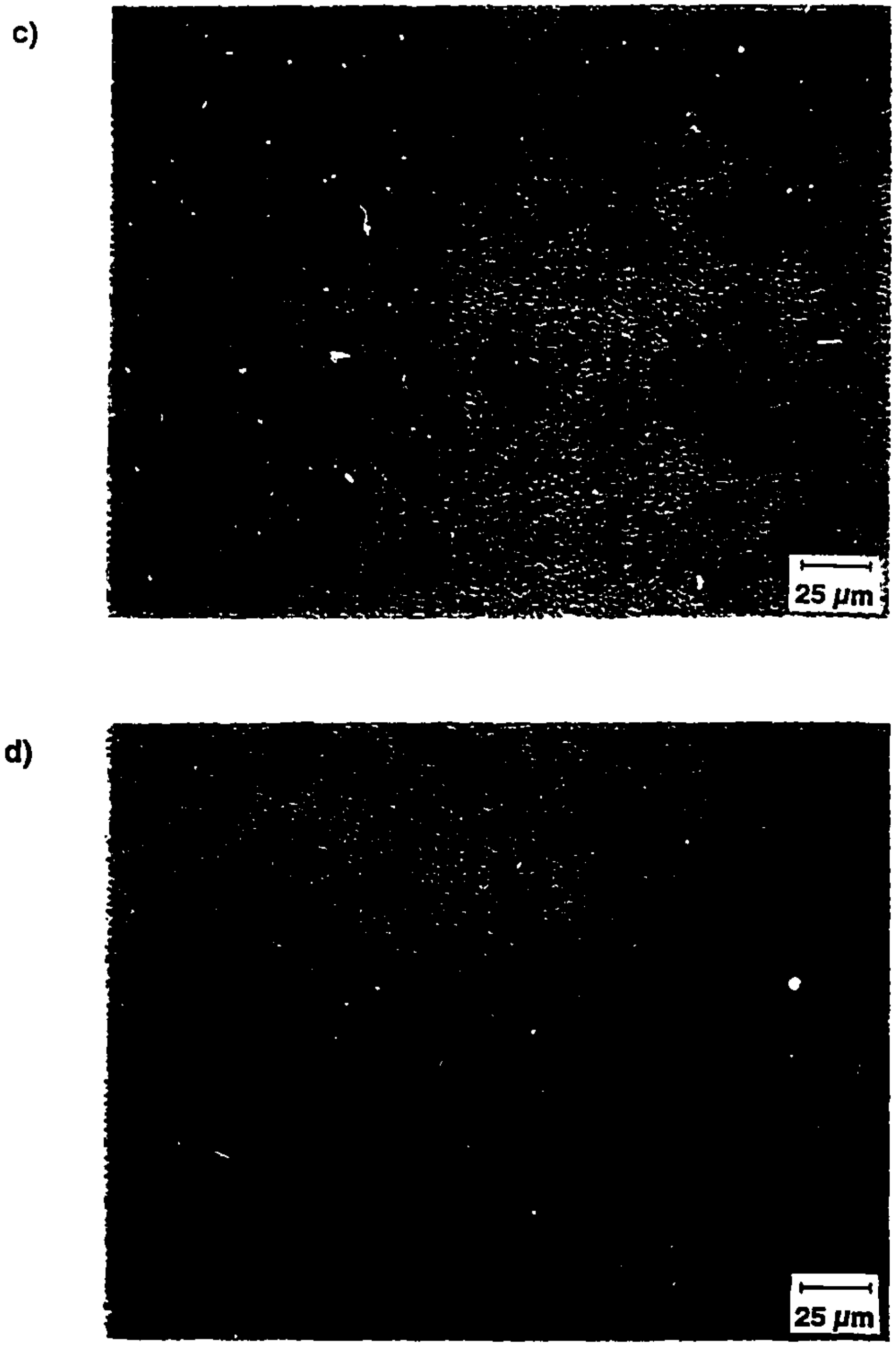

Figure 7.7 continued , c) 0.04% Sr , d) 0.06% Sr (400X)

e)

Figure 7.7 continued , e) 0.08% Sr (400X)

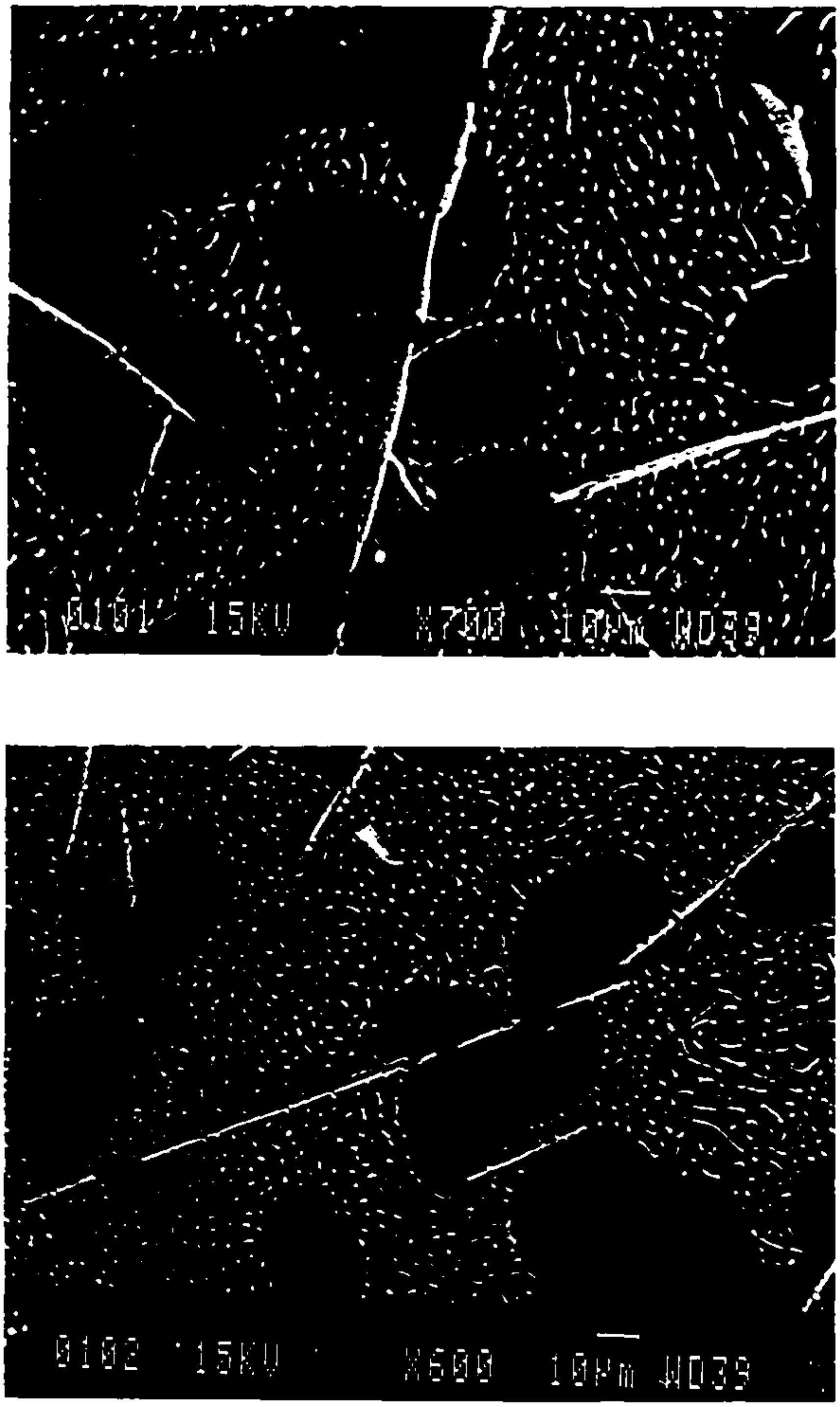

Figure 7.8: SEM micrographs of fragmentation of needles (β-phases) in 0.04% Sr-treated 413 alloy (etched with 0.5% HF)

All samples were also investigated through image analysis and the results are shown in Figures 7.9(a-c). The size of Chinese script and star-like intermetallics was measured by the FERET AVERAGE function available in the LECO 2005 image analyzer. By this function the average of thirty two straight line measurements made between tangents at various angles (0 to 157.5°) was calculated for each particle. The effect of strontium on the average size of the Chinese script (α-phase) morphology of the 413 alloy is shown in Figure 7.9(a). It is seen from this figure that strontium is very effective in reducing the size of Chinese script phases. The average size of the α-phase has decreased from 87.4 μm in a strontium-free alloy to 47.3 μm in the 0.06% Sr-treated alloy. This is a reduction of about 46%. Figure 7.9(b) shows the influence of strontium on the length and width of the needle (β-phase) morphology. The length of β-phase decreased only slightly with a 0.02% Sr addition but decreased sharply in the 0.04% Sr-treated alloy. This reduction also continued to 26.0 μm in the 0.06% Sr-treated alloy for a total reduction of 54% in length of needles.

The width of the β-phase also decreased by strontium addition, changing from 5.8 μm in the strontium-free alloy to 3.3 μm in the 0.06% Sr-treated alloy for a 43% reduction. These results clearly show that strontium is a very effective element in causing fragmentation and thinning of needle (β-phase) intermetallics.

The volume percent of β-phase was also reduced from 3.4% to 1.8% in the 0.06% Sr-treated alloy.(Figure 7.9(c)) The volume percent of α-phase increased from 0.78% in the strontium-free alloy to 1.05% in the 0.06% Sr-treated alloy and to 2.57% in the 0.08% Sr-treated alloy. The optimum level of strontium addition should be less than 0.06% Sr due to the fact that the size of the α-phase also increases when more than 0.06% Sr is added to the alloy.

The results given in Figure 7.9(a) and(c) indicate that the volume percentage of α-phase has increased by strontium addition even though the average size decreased.

Thus, it can be concluded that the number of α-phase particles has increased in the alloy. The results of image analysis also confirmed this conclusion as presented in the bar graphs of Figure 7.10(a). This figure also shows that even though the volume percent of β-phase decreases with strontium addition (Figure 7.9(c)), their number per unit area increases to the optimum level of strontium. The reason for this increase in the number of needles is due to their fragmentation which causes, at the same time, a reduction in length of these phases. (see Figure 7.9(b))

The influence of strontium on the relative volume percentage of intermetallics is presented as bar graphs in Figure 7.10(b). The relative volume percent is the volume percent of each phase compared to the total volume percentage of intermetallic compounds. This figure shows that the relative volume % of α-phase increases from 18.8% in the strontium-free alloy to 56.9% in the 0.08% Sr-treated alloy. At the same time the relative volume % of β-phase also decreased from 81.2% to 43.1% in the 0.08% Sr-treated alloy. Thus, strontium is an effective element in changing β-phase to α-phase.

The overall conclusion of this part of study is that strontium is a very effective element in reducing the average size of α-phase intermetallics and the size of needles (length and width) due to fragmentation. The volume percent of β-phase decreases by adding strontium, and the optimum level of strontium addition to alloy 413 under sand casting conditions is 0.04% to 0.06% Sr.

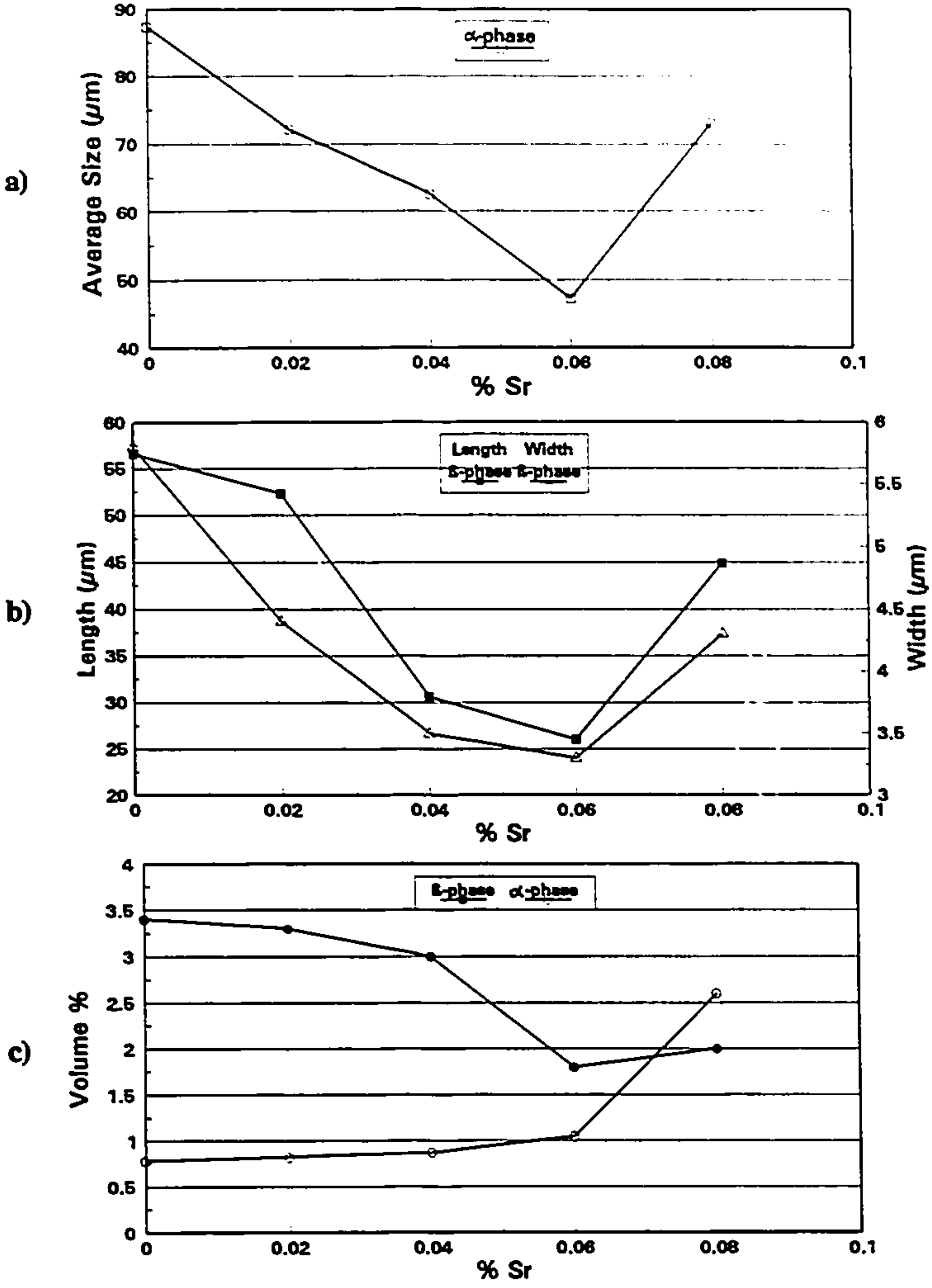

Figure 7.9: Effect of strontium on the intermetallic compounds in alloy 413 at sand cast condition. a) Size , b) Length and Width , c) Volume %

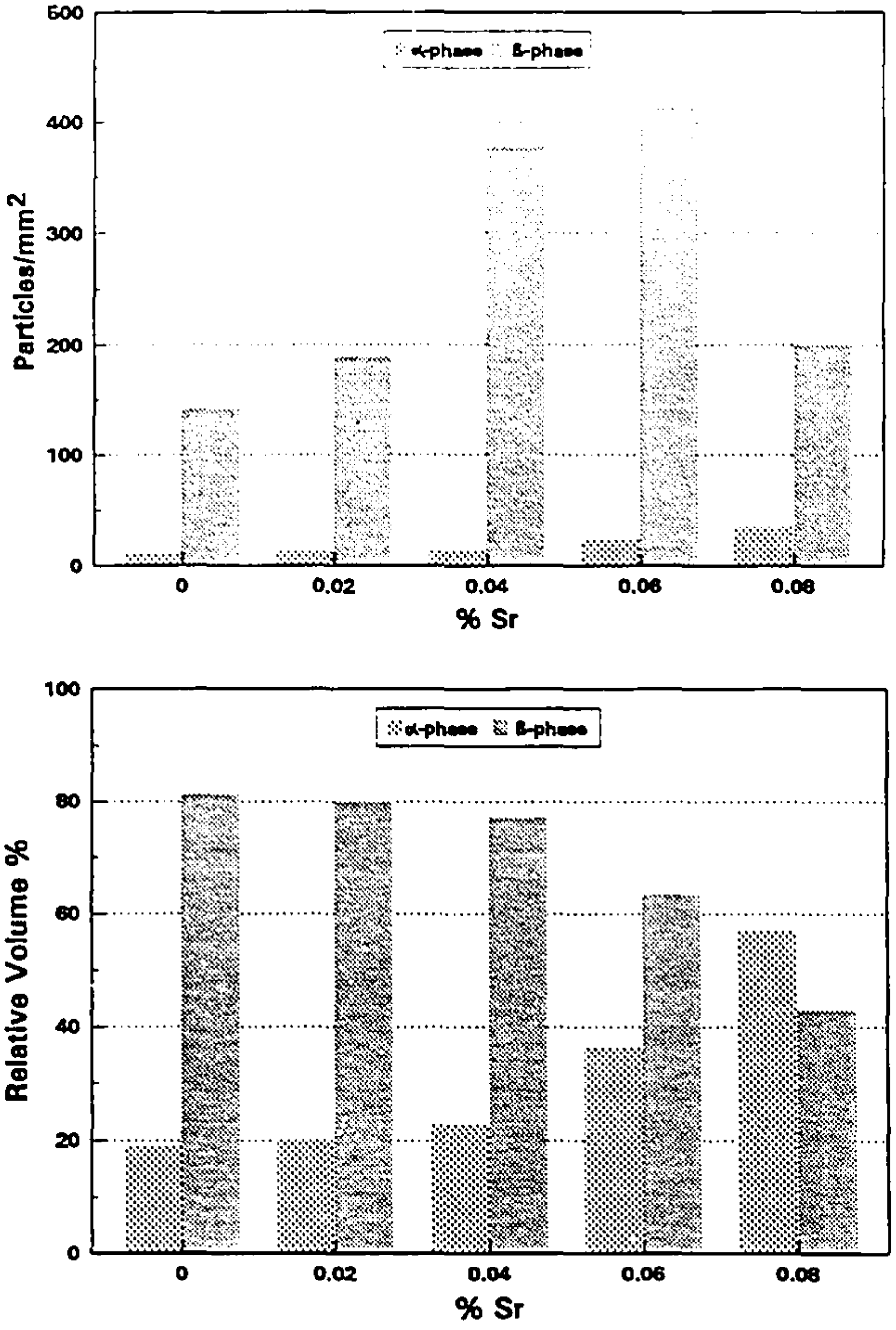

Figure 7.10: Influence of strontium on the intermetallic compounds of alloy 413 at sand cast condition. a) Particles/mm^2 b) Relative Volume %

7.3.2. Alloy A413

7.3.2.1. Permanent Mold

Metallographic observations on the permanent mold cast samples revealed that alloy A413 contains a fine eutectic microstructure and small star-like intermetallic compounds. This is shown in Figure 7.11(a). The amount of intermetallics decreased significantly, to almost zero, by adding 0.04% Sr to the alloy as shown in Figure 7.11(b). No needles nor sludge particles were observed in these samples.

The results of image analysis are presented in Table 7.4. The amount of intermetallics (sludge) was reduced from 0.45 vol% in strontium-free alloy to 0.08 vol% in the 0.04% Sr-treated alloy while their size decreased from 5.3 μm to 2.8 μm in the 0.04% Sr-treated alloy. The 0.04% strontium addition to this alloy has also decreased the number of intermetallics from 280 particles/mm^2 to 97 particles/mm^2. These particles are very small and appear as spots which are difficult to resolve by microscope even at 400X magnification. Thus, strontium is very effective in eliminating intermetallics in the microstructure and/or changing the star-like phases to very fine and round intermetallics.

Table 7.4: Image Analysis Measurement of Alloy A413 as Permanent Mold Cast

alloy	size (μm)	volume (%)	particles/ mm^2	roundness*
no Sr	5.3±2.4	0.45±0.12	280±112	48.5±25.3
0.04% Sr	2.8±1.1	0.08±0.05	97±58	54.9±20.2

* roundness = $4\pi A/P^2 \times 100$ (A=Area , P=Perimeter)

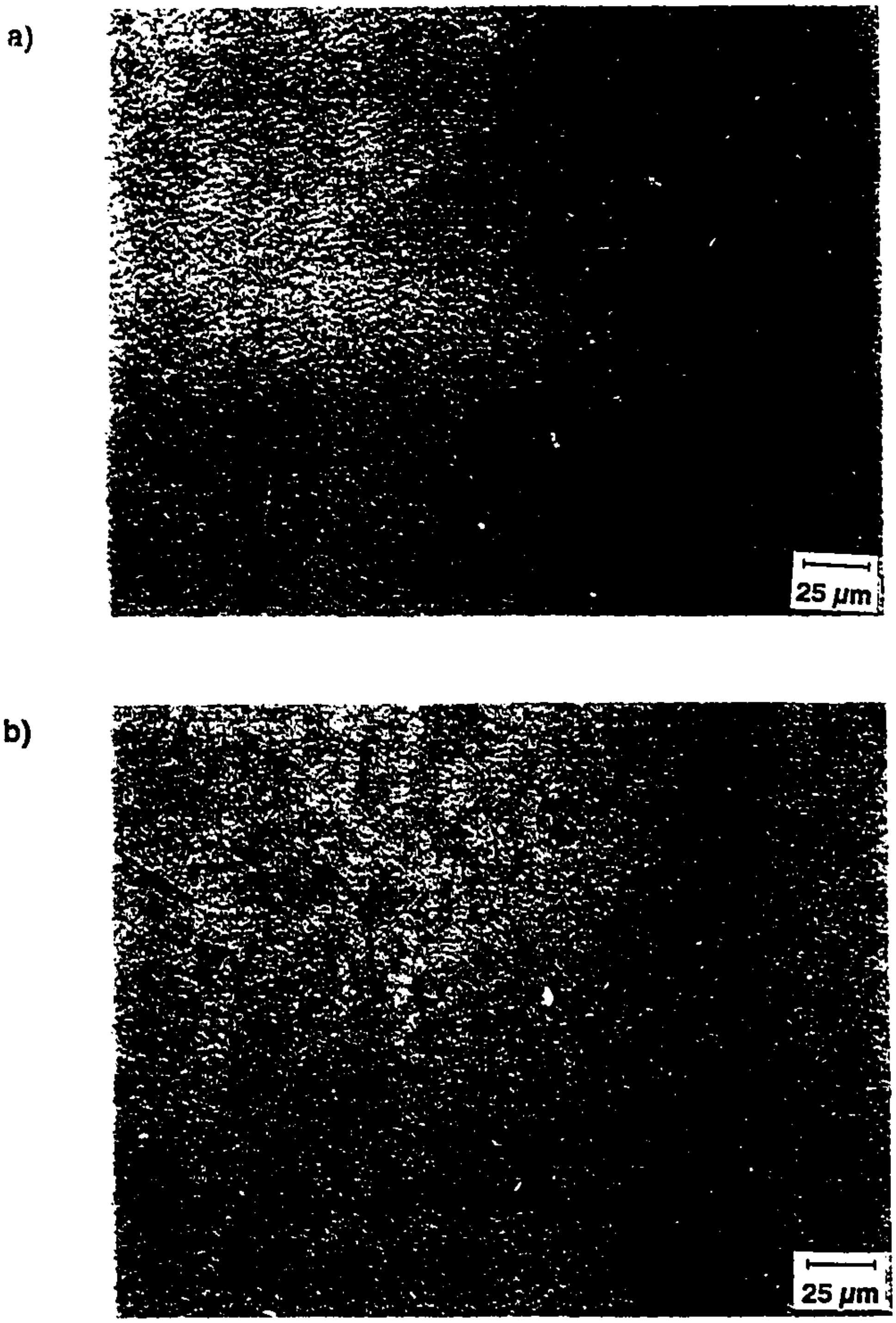

Figure 7.11: Elimination of intermetallics (sludge) in commercial alloy A413 as permanent mold cast a) no Sr b) 0.04% Sr

7.3.2.2. Sand Cast

The alloy to which no strontium was added contained coarse silicon, large Chinese script (α-phase), and large needles (β-phase) in the microstructure. By adding 0.04% Sr to the alloy, the amount of needles decreased significantly and they became very thin. Fragmentation of these phases was also observed in some sections of the sample, and the size of Chinese script was also reduced due to the strontium addition. Micrographs of the samples in the sand cast condition are shown in Figures 7.12(a) and (b).

The results of image analysis are presented in Table 7.5. From this table, it is seen that the volume percent of β-phase has been reduced from 1.9% to 0.2% in the 0.04% Sr-treated alloy. There has, therefore, been a reduction of 90% in the amount of needles by strontium addition. The length and the width of needles were also decreased about 62% and 60%, respectively by the 0.04% Sr addition. The number of needles decreased from 77 to 12 per mm^2 while the addition of 0.04% strontium to the alloy also reduced the size of the α-phases from 73.7 to 61.1 μm. The volume % of α-phase increased from 2.7% to 3.1% and the number of these particles rose from 30 to 47/mm^2 in 0.04% Sr-treated A413.

Table 7.5: Image Analysis Measurement of Alloy A413 as Sand Cast Condition

alloy		size (μm)	volume %	particles/ mm^2	relative volume %	length (μm)	width (μm)	aspect ratio
no Sr	β-phase	-	1.9±0.9	77±24.2	41.7	73.2±30.6	7.4±2.1	9.9
	α-phase	73.7±21.8	2.7±1.9	30±11.5	58.3	-	-	-
0.04% Sr	β-phase	-	0.2±0.1	12±4.2	6.4	28.2±8.4	2.9±0.9	9.7
	α-phase	61.1±18.8	3.1±0.8	47±18.4	93.6	-	-	-

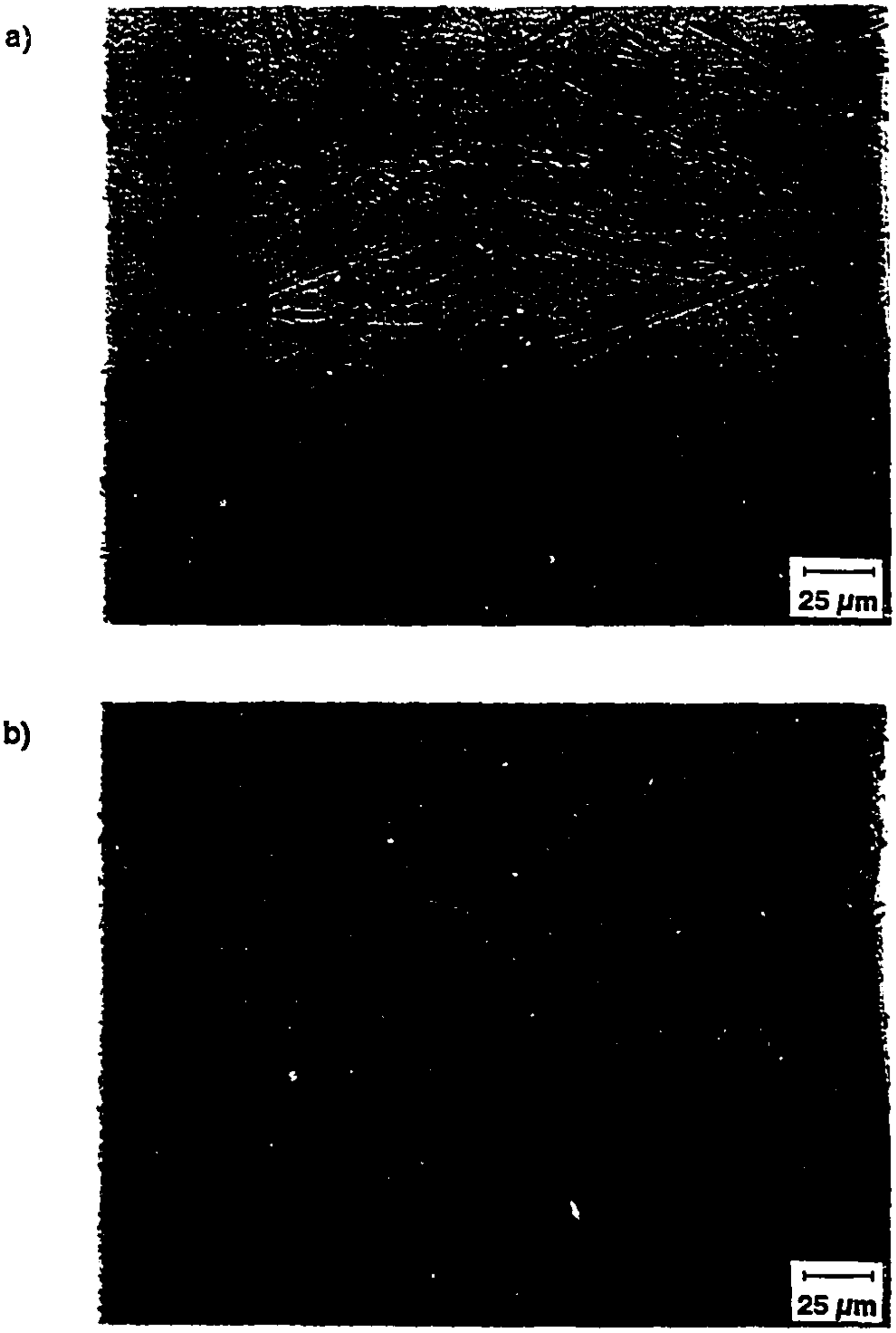

Figure 7.12: Reduction of needles (β-phases) in commercial alloy A413 as sand cast condition a) no Sr b) 0.04% Sr

The relative volume % of β-phase decreased from 41.7% to 6.4% and the α-phase increased from 58.3% to 93.6% by adding 0.04% Sr to the alloy. Strontium is very effective in changing the amount and the number of β-phase (needles) to the α-phase in commercial alloy A413.

7.3.3. Alloy 413P

7.3.3.1. Permanent Mold

The metallography of the samples revealed that the alloy 413P contains fine eutectic silicon, some primary silicon, and small indefinite intermetallics in the permanent mold cast condition. These intermetallics were completely eliminated by 0.04% Sr addition to the alloy. Figure 7.13(a,b) shows the micrographs of the samples before adding strontium and after adding 0.04% Sr to the alloy.

The results of image analysis of the samples are given in Table 7.6. The volume percent of intermetallics changed from 0.56% to zero in 0.04% Sr-treated alloy. These results confirmed the metallographic study that strontium is able to eliminate the intermetallic compounds in commercial 413P alloy.

Table 7.6: Image Analysis Measurement of Alloy 413P as Permanent Mold Cast

alloy	size (μm)	volume (%)	particles/mm^2	roundness*
no Sr	6.5±3.4	0.56±0.20	361±140	35.5±23.2
0.04% Sr	0	0	0	0

* roundness = $4\pi A/P^2 \times 100$ (A=Area , P=Perimeter)

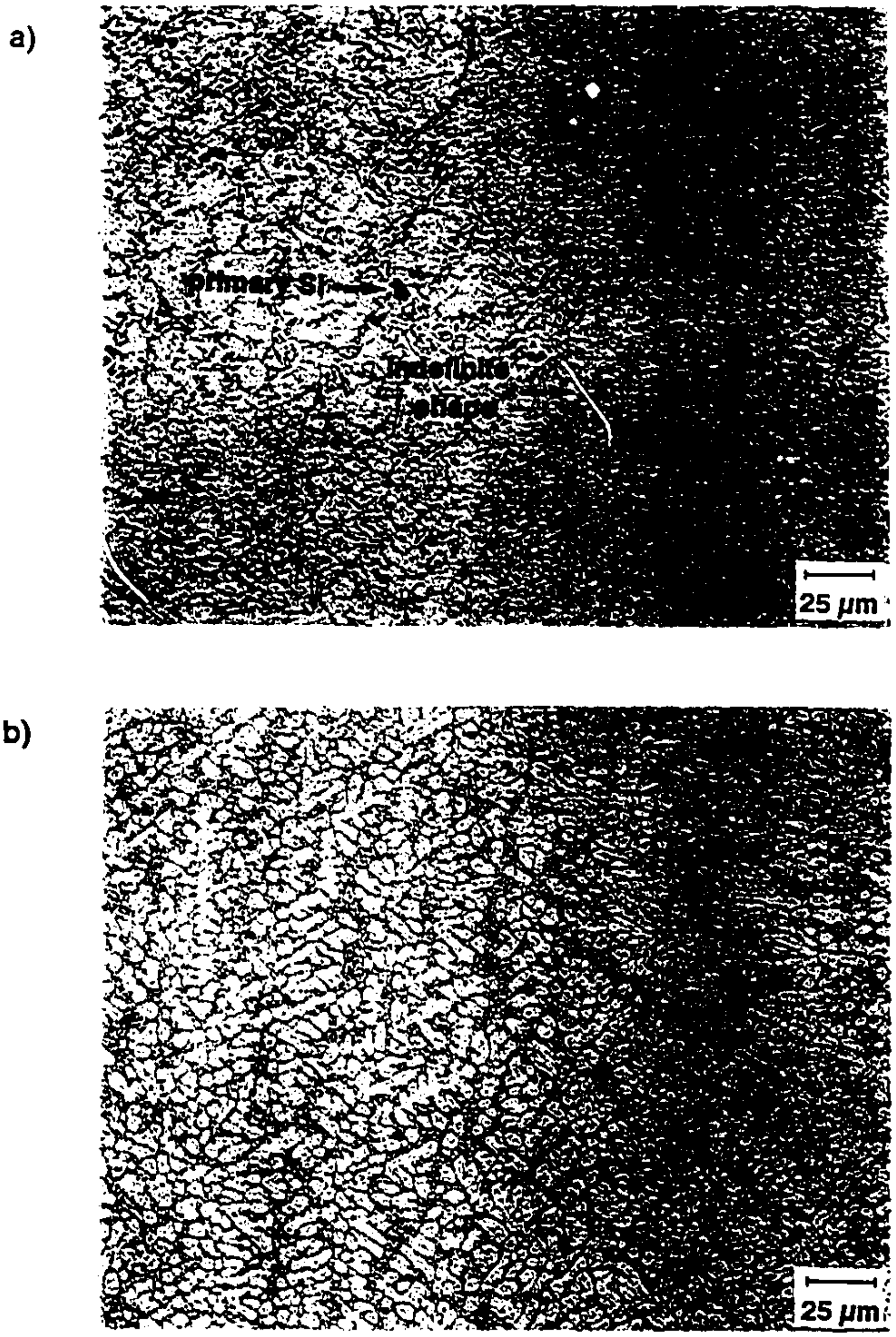

Figure 7.13: Complete elimination of intermetallics in commercial 413P alloy as permanent mold cast a) no Sr b) 0.04% Sr

7.3.3.2 Sand Cast

Alloy 413P is commonly used to make pistons. The microstructure of a typical sectioned piston is shown in Figure 7.14 which reveals primary silicon, coarse eutectic silicon, star-like (sludge), and Chinese script intermetallics in an aluminum matrix. This microstructure is very similar to the microstructure of alloy 413P in the sand cast condition as simulated in this study.(see Figure 7.15(a)) No needles were observed in this microstructure, and metallographic observations revealed that the size of Chinese script (α-phase) decreased in the 0.04% Sr-treated alloy as shown in Figure 7.15(b).

Figure 7.14: The micrograph of a piston manufactured from 413P alloy.

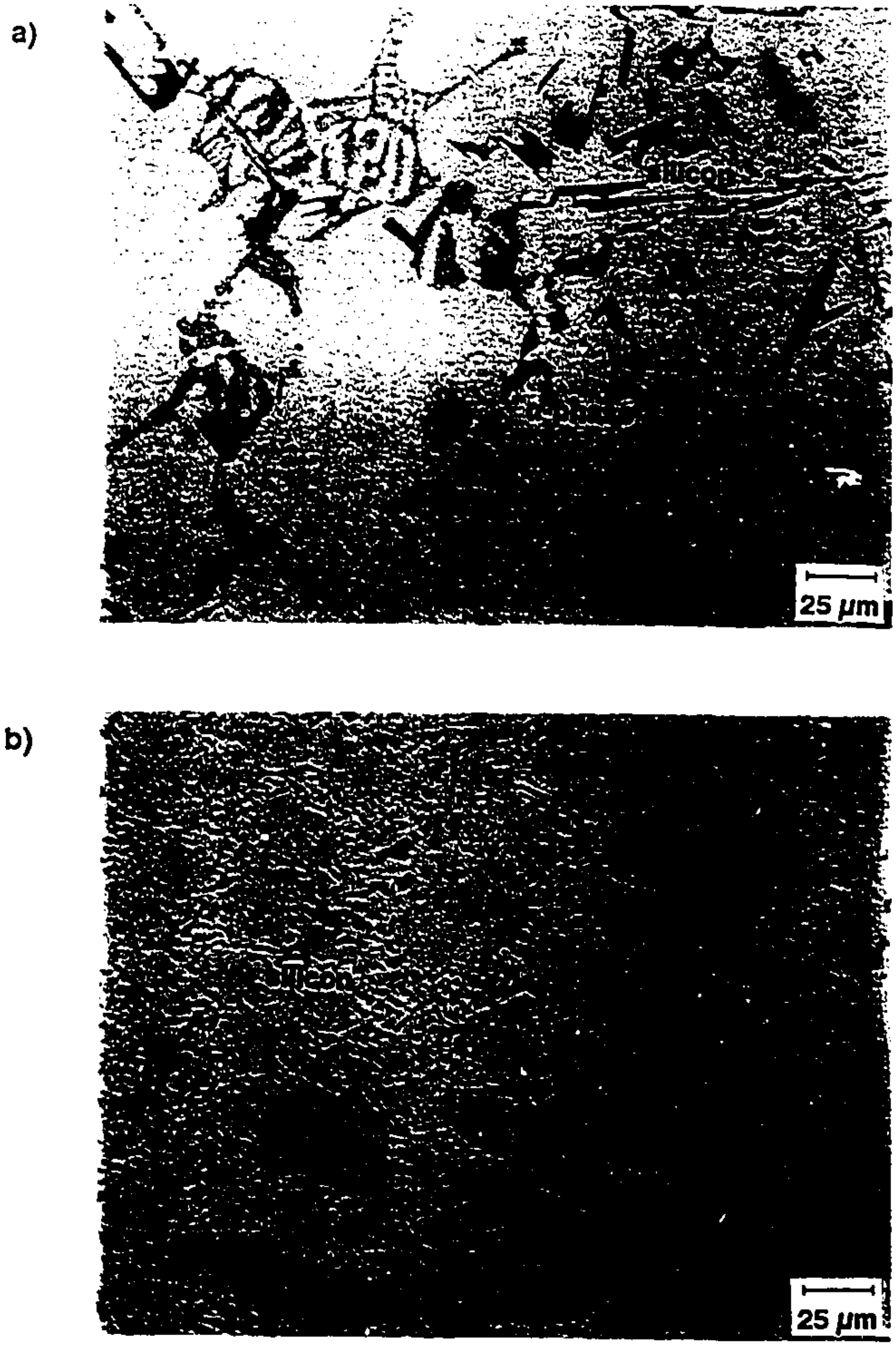

Figure 7.15: Reduction in the size and amount of α-phase in commercial alloy 413P as sand cast a) no Sr b) 0.04% Sr

The results of image analysis as presented in Table 7.7 show that the size of α-phase decreased from 58.3 μm to 47.8 μm as did the number of particles, from 83 to 64 per mm^2, in the 0.04% Sr-treated alloy. The volume percent of α-phase reduced from 5.5% in the strontium-free alloy to 4.1% in the 0.04% Sr-treated 413P alloy which is about 26% reduction in the amount of intermetallics. In general there is a trend for the size, volume %, and the number of particles to decrease with strontium addition.

Table 7.7: Image Analysis Measurement of Alloy 413P as Sand Cast Condition

alloy		size (μm)	volume (%)	particles/mm^2	relative volume %
no Sr	β-phase	0	0	0	0
	α-phase	58.3±22.8	5.5±2.4	83±32.7	100
0.04% Sr	β-phase	0	0	0	0
	α-phase	47.8±18.7	4.1±0.9	64±25.8	100

7.3.4. Phase Analysis

Several of the intermetallic compounds which were observed in this study were analyzed by SEM-EDS. The EDS spectra of elements in the intermetallic compounds are illustrated in Figures 7.16 and 7.17. This measurement is a qualitative analysis which shows the existence of different elements in the compounds. Figure 7.16(a) shows the EDS spectrum of star-like compounds in the 0.04% Sr-treated alloy 413 in the permanent mold cast condition. The EDS spectrum of needle-like intermetallics in the same alloy in the sand cast state is shown in Figure 7.16(b). The star-like compounds in the 0.04% Sr-treated alloy A413 were also analyzed by means of SEM-EDS and the results are presented in Figure 7.17. The existence of Al, Si, Fe, Mn, and Cr was evident in all intermetallics but strontium was not detectable in the compounds probably due to its low concentration.

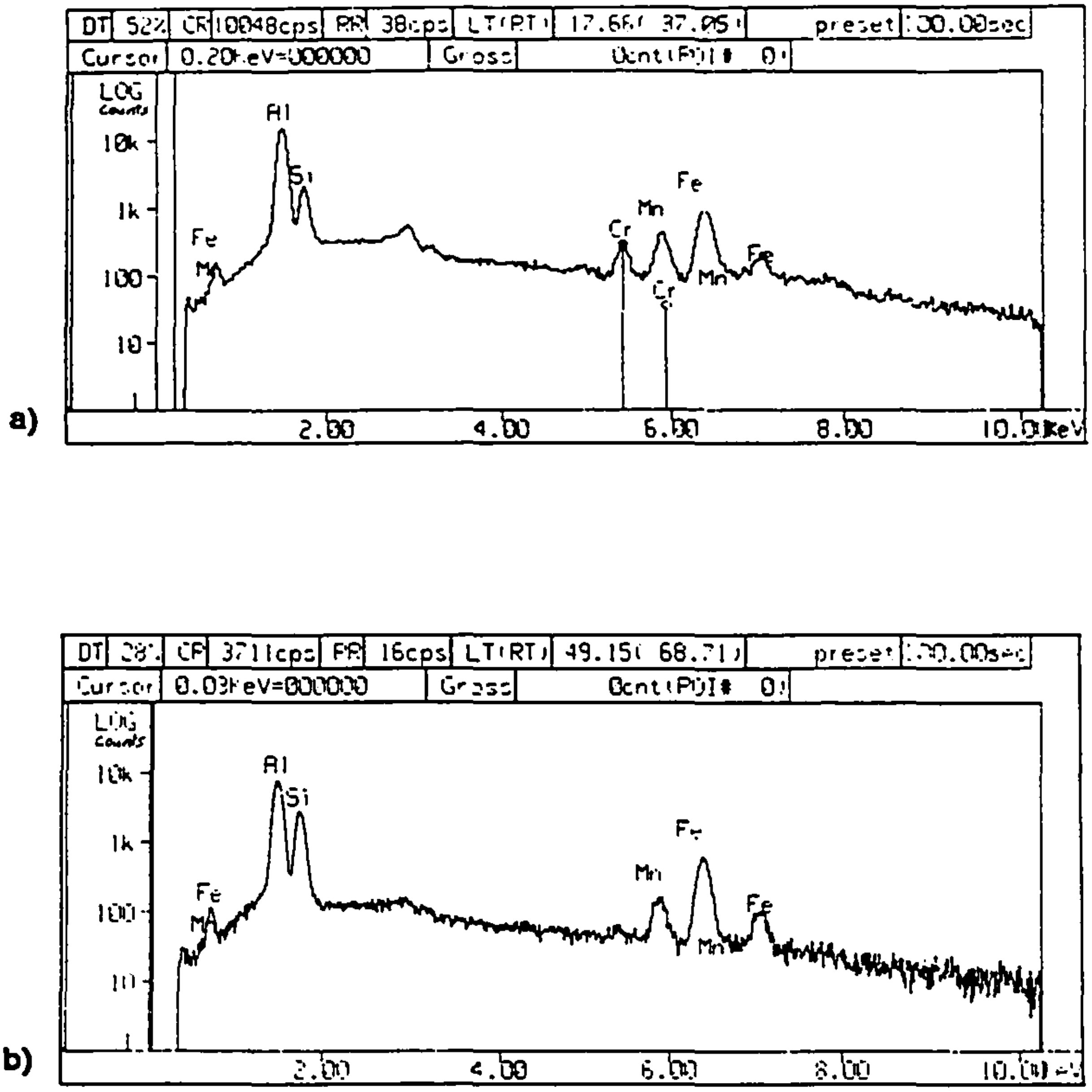

Figure 7.16: EDS spectra of intermetallics in the 0.04% Sr-treated alloy 413

a) star-like b) needle-like

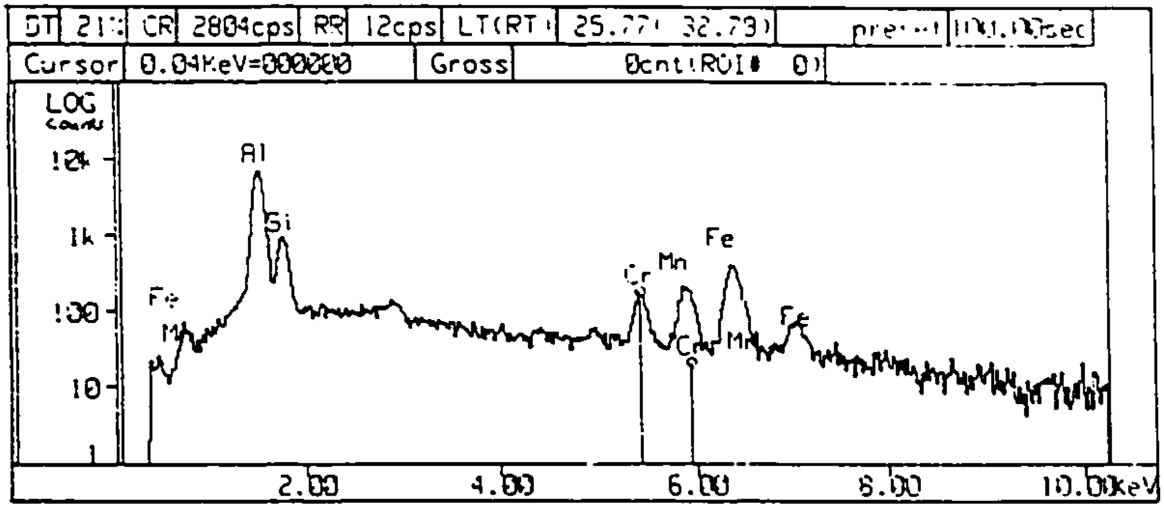

Figure 7.17: EDS spectrum of star-like in the 0.04% Sr-treated alloy A413.

The star-like intermetallic in the 0.04% Sr-treated alloy 413 shown in Figure 7.16(a) was analyzed by means of X-Ray mapping. The distribution of iron, manganese, chromium, and strontium in this phase is presented in Figure 7.18. This figure shows that the concentration of iron, manganese, and chromium is high in the star-like compounds. It can also be seen that the amount of strontium is very low and it is mostly concentrated on modified eutectic silicon and star-like compounds. This observation suggests that strontium probably affects the intermetallics in the same way that it affects modified silicon.

A quantitative analysis has been performed on the intermetallics by means of electron probe microanalyzer(EPMA). Table 7.8 gives the EPMA analysis of the complex intermetallic types studied in the present work. The chemical analysis given in this table is the average of at least eight measurements.

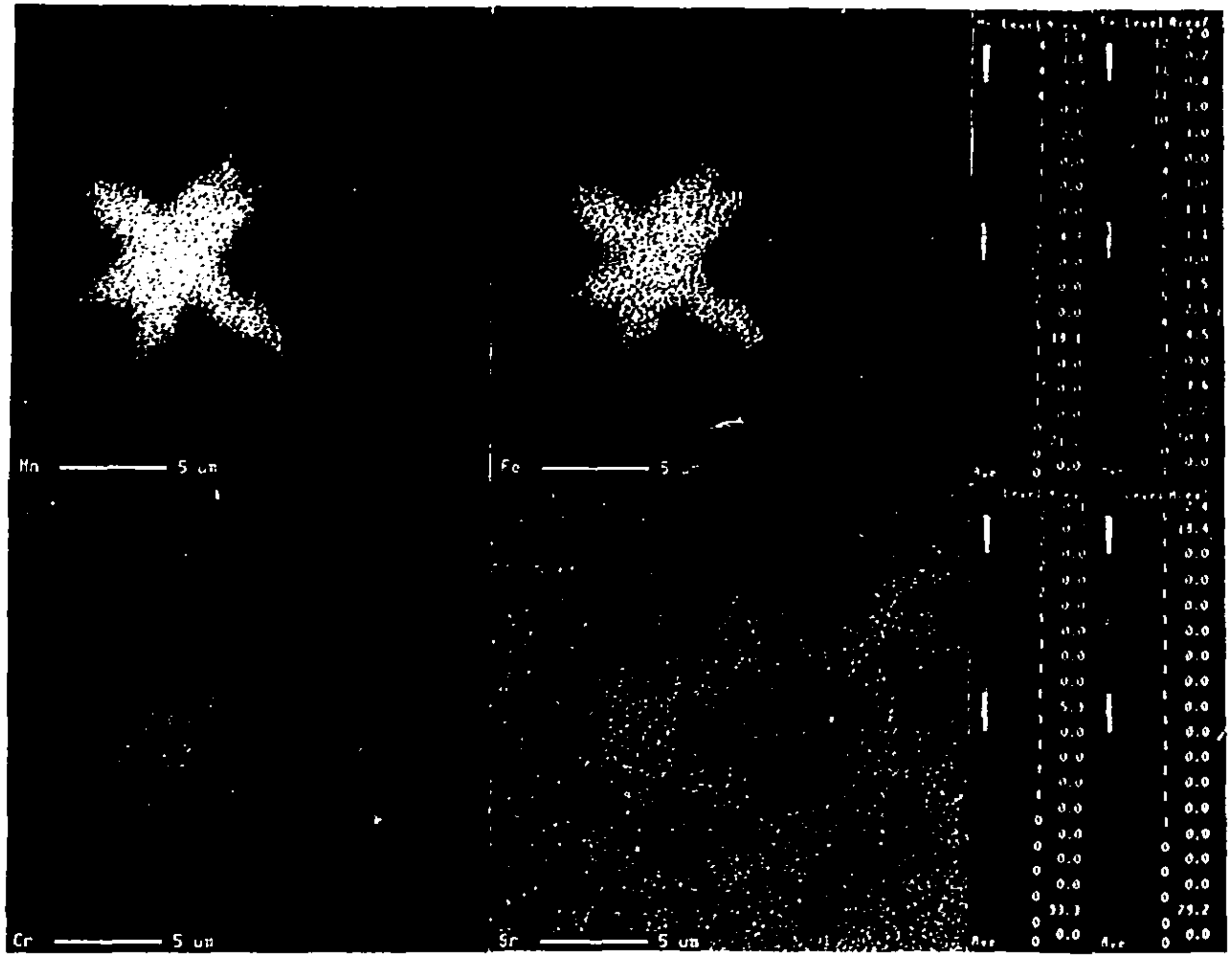

Figure 7.18 : X-Ray mapping of elements in the star-like phase in 0.04% Sr-treated alloy 413

The star-like and Chinese script (α-phase) had the same chemical composition in all alloys and their stoichiometry corresponds to $Al_{12}(Fe,Mn,Cr)_3Si_2$. The stoichiometry of the needle (β-phase) morphology also corresponds to $Al_5(Fe,Mn,Cr)Si$. The amount of strontium was too low to be analyzed precisely in the compounds and the compositions of the phases are the same as those reported in the previous chapters of this thesis.(Table 3.9)

Table 7.8: EPMA Analysis of Intermetallic Compounds (atomic %)

alloy	condition	phase	Al	Si	Fe	Mn	Cr
413 (no Sr)	PM*	star-like	72.2	11.2	11.0	3.8	1.7
413 (0.04% Sr)	PM	star-like	72.1	11.4	10.9	3.9	1.7
413 (0.04% Sr)	SC*	α-phase	70.9	12.0	9.6	4.4	2.9
	SC	β-phase	63.5	21.5	12.5	2.2	0.2
A413 (no Sr)	PM	star-like	71.3	11.7	9.9	4.3	2.6
A413 (0.04% Sr)	PM	star-like	71.8	11.4	10.0	4.2	2.3

* PM = Permanent Mold
SC = Sand Cast

7.3.5. Effect of Melt Superheat

a) Permanent Mold

Alloy 413 which was superheated to 850°C and cast at 710°C in a permanent mold was studied through metallography. The microstructure of the sample contained fine intermetallics as shown in Figure 7.19(a). 0.04% Sr was added to this previously superheated alloy at 710°C and the alloy was then cast into the permanent mold. The resultant microstructure shows very fine star-like intermetallics in modified eutectic silicon.(see Figure 7.19(b)) This is very similar to the microstructure of the 0.04% Sr-treated alloy 413 without superheating which has previously been shown in Figure 7.5(c). Thus, it seems that superheating of the melt before strontium addition does not influence the size or morphology of the intermetallics.

b) Sand Cast

The superheated alloy 413 was cast at 710°C into the sand mold. The microstructure contains large and long needles, large Chinese script, and intermetallics of indefinite shape along with coarse silicon. The needles (β-phases) are shown in Figure 7.20(a). The microstructure of the alloy treated with 0.04% Sr after superheating and casting into the sand mold is shown in Figure 7.20(b). This micrograph indicates that needles are broken, short and tiny. The size and the number of Chinese script and indefinite shape intermetallics are decreased. On comparison with the microstructure of the 0.04% Sr-treated alloy 413 in the sand cast condition without superheating,(Figure 7.7(c)), it can be concluded that there is little improvement in the *size* and the *number* of all kinds of intermetallics in the sand cast condition after superheating and strontium addition.

Based on the results of this study, superheating the melt before strontium addition is not recommended due to the fact that *firstly*, the improvement in the size, number, and morphology of the intermetallics is little, and *secondly*, superheating may cause oxidation of the melt and hydrogen pickup.

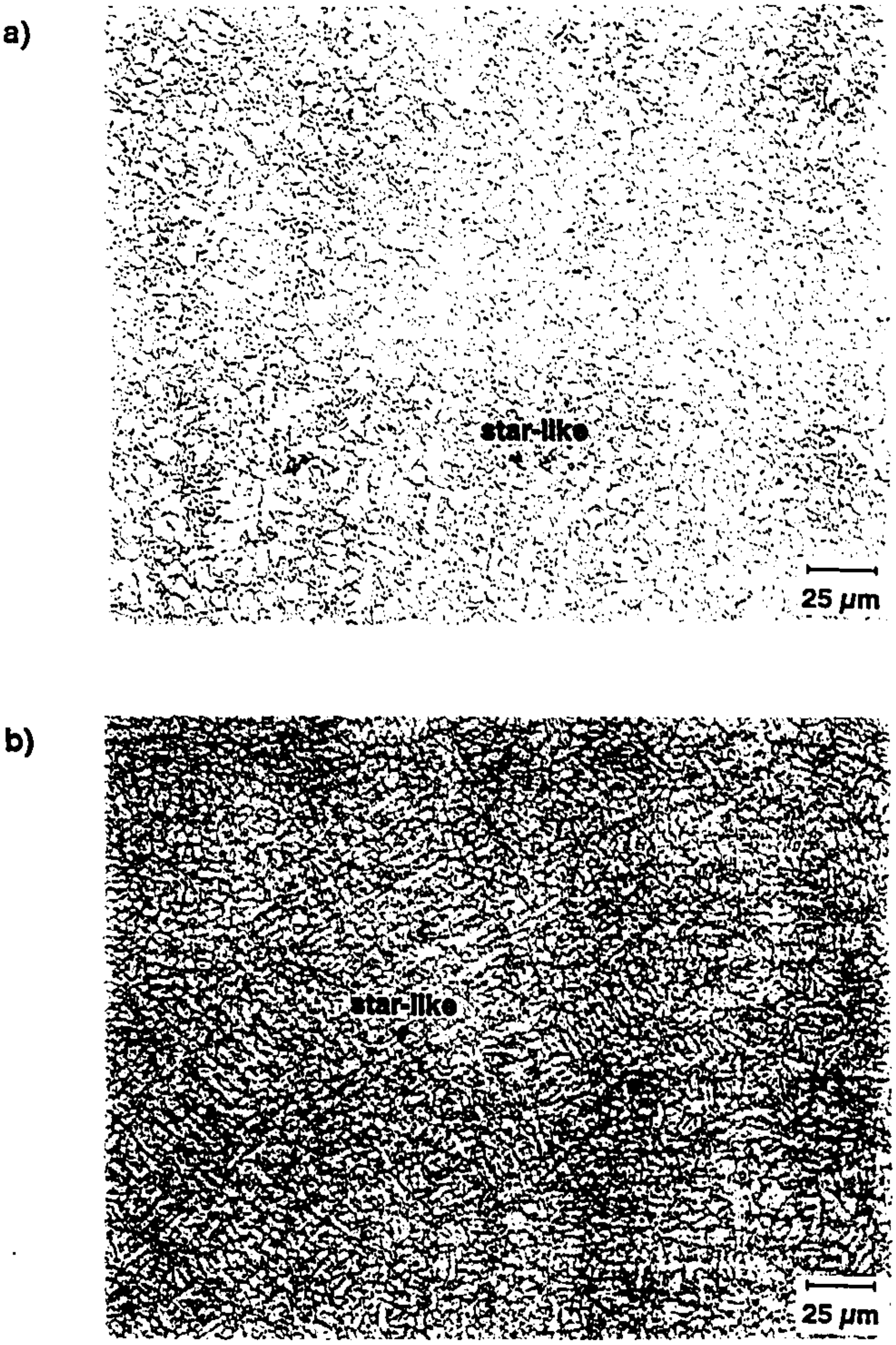

Figure 7.19: Effect of superheating on the intermetallics in alloy 413 in the permanent mold condition a) no Sr b) 0.04% Sr

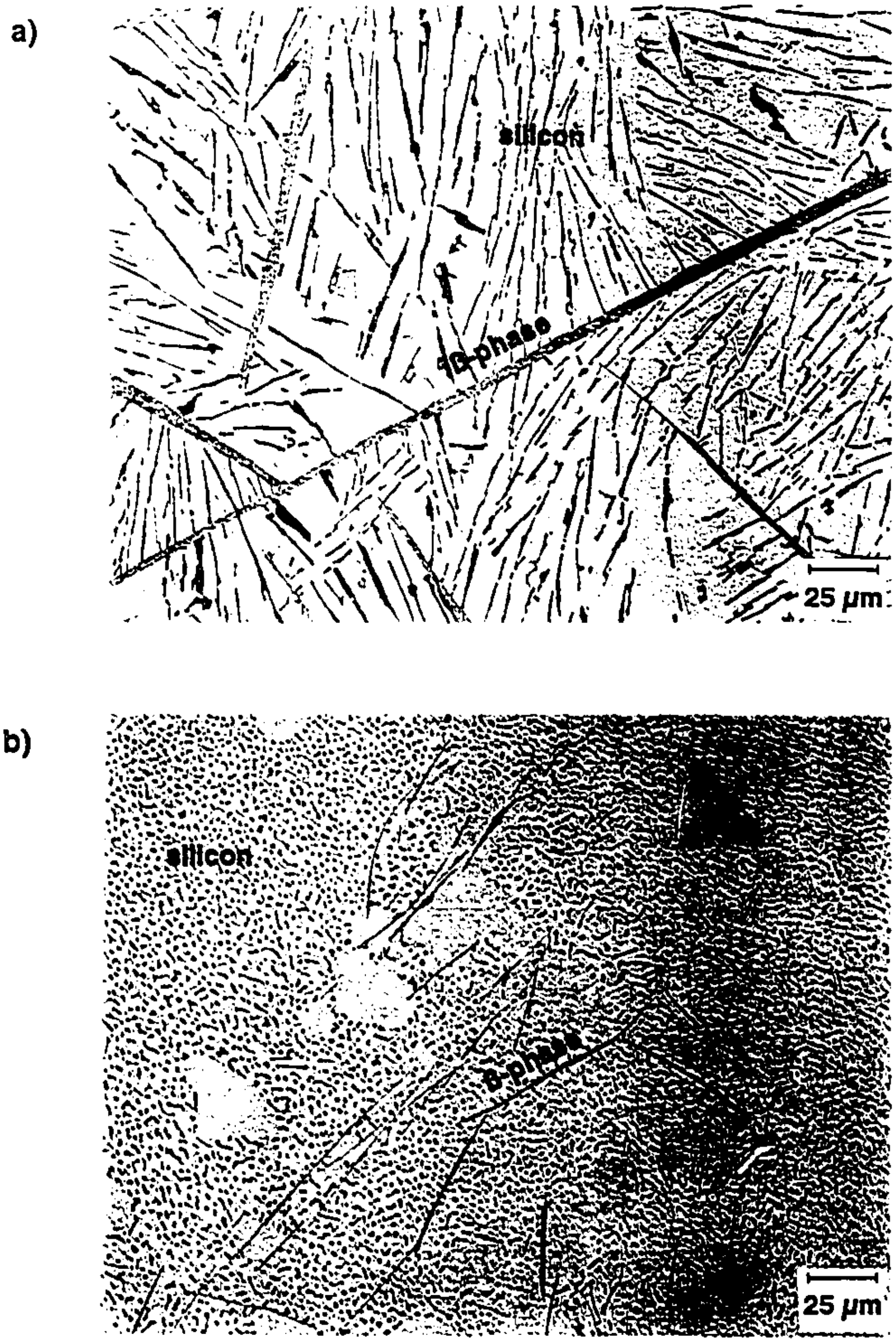

Figure 7.20: Effect of superheating on the intermetallics in alloy 413 as sand cast a) no Sr b) 0.04% Sr

7.3.6. Effect of Casting Temperature

The aim of this experiment was to investigate the influence of a low casting temperature (e.g. 600°C) on the size and morphology of intermetallics in the 0.08% Sr-treated alloy 413.

a) Permanent Mold

The microstructure of the strontium-treated alloy cast at 710°C into the permanent mold is similar to the microstructure shown in Figure 7.5(e). The micrograph contains small spot-like intermetallics in a modified silicon microstructure. When this alloy is cast at 600°C into the same mold, agglomeration and enlargement of the intermetallics are very evident. This phenomenon is shown in Figure 7.21(a).

b) Sand Cast

The microstructure of the 0.08% Sr-treated alloy 413 cast at 710°C into the sand mold is also similar to the microstructure indicated in Figure 7.7(e). It contains broken needles, star-like, and Chinese script compounds in a well modified silicon microstructure. Figure 7.21(b) shows the micrograph of the alloy cast at 600°C into the same mold. It is evident that large and long iron needles have been formed along with large sludge and polyhedral particles.

Thus a low casting temperature after strontium addition to the melt can cause enhancement of the size of intermetallics due to agglomeration in both permanent mold and sand cast conditions.

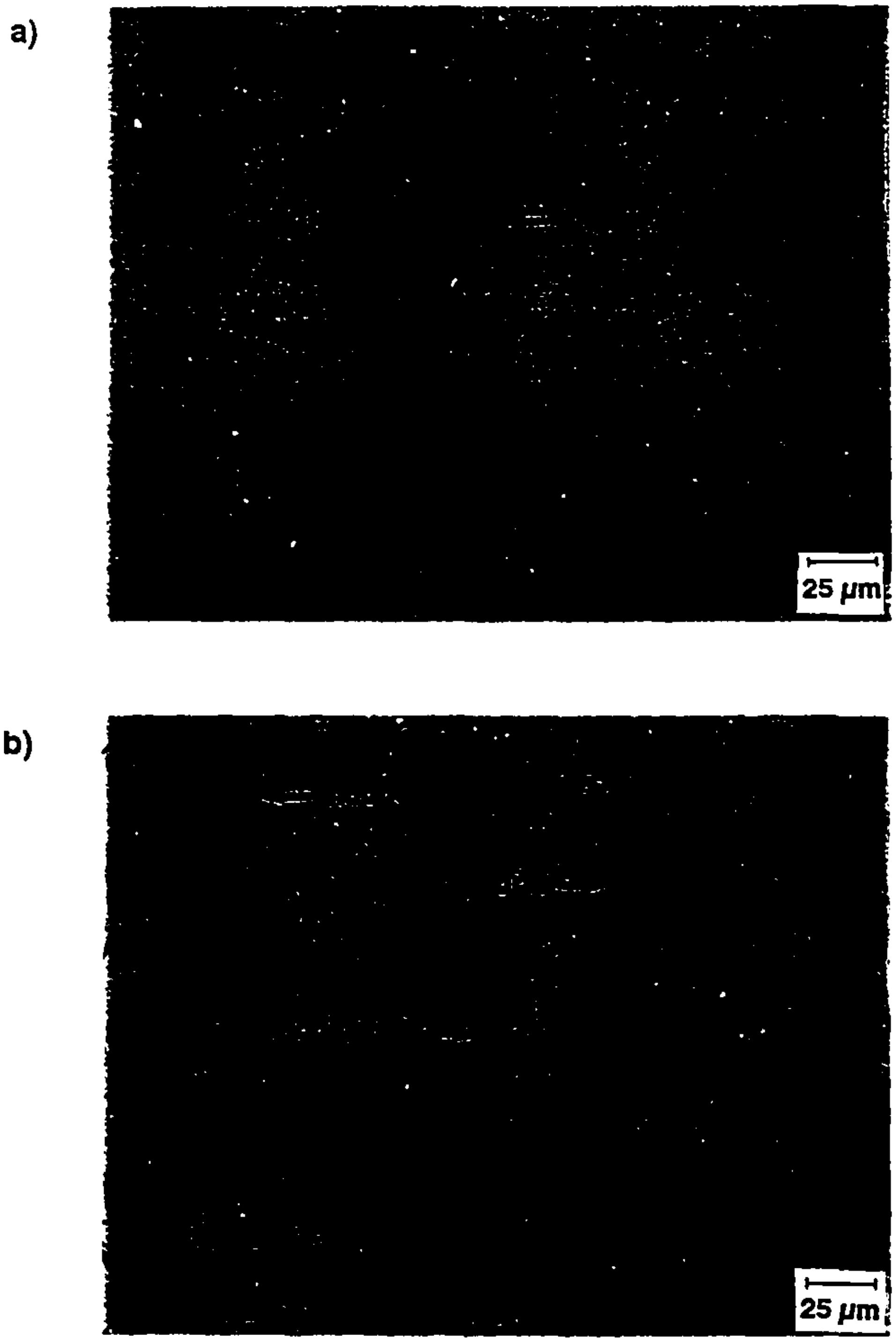

Figure 7.21: 0.08% Sr-treated alloy 413 cast at low temperature of 600°C into:
a) permanent mold b) sand cast

7.4. Discussion

This investigation has revealed that strontium is a very effective element to change or eliminate some morphologies of intermetallic compounds. The phenomenon has been observed in both commercial and synthetic aluminum-silicon alloys. The reduction in the size, number, volume percent, and transformation of all intermetallics to spot-like phases in the synthetic alloy 413; the elimination of all kinds of intermetallics in the commercial alloys A413 and 413P by strontium addition have been observed under a fast cooling rate solidification condition. Fragmentation of needles(β-phases), reduction in the length, width, volume percent of β-phase, and decrease in the size and the number of α-phase have been observed in both synthetic and commercial alloys under a slow cooling rate solidification condition typical of sand casting. In this solidification condition, strontium is very effective to reduce the amount, and size of the β-phase (needle) and to change the β-phase into the α-phase morphology.

The effect of strontium on changing the needle (β-phase) to the Chinese script (α-phase) morphology and also on the fragmentation of needles may be compared with the effect of strontium on the modification of silicon in aluminum-silicon alloys. It appears that there are many similarities in nucleation and growth between intermetallics and silicon. Crosley and Mondolfo[130] have found that in Al-Si alloys, the nucleation of silicon is controlled by aluminum phosphide (AlP). Since AlP has a crystal structure very close to that of silicon, the AlP acts as an effective nucleant. In commercial Al-Si alloys, the phosphorus content is sufficient to provide an abundance of AlP particles in the melt. This leads to the nucleation of the eutectic silicon at small undercoolings (<2°C) and the formation of coarse acicular silicon flakes. The modifier neutralizes the phosphorus, thus eliminating the nucleation by AlP.[130,131,132] By so doing, it increases the undercooling for nucleation of the silicon by aluminum. Yaneva et al.[46] state that Sr refines silicon particles, and to a certain degree the iron-intermetallics, probably due to the undercooling at the solidification front caused by strontium additions.[46]

Sigworth[75] has related the suppression of the formation of large brittle iron intermetallics (β-phases) in an exceedingly well modified alloy to the AlP crystals. He states that P present in the melt (probably as AlP) plays a role in nucleating the undesirable iron-bearing phases, and so Sr (or Na) modification may be important in controlling the iron phase.

Based on the results obtained in the present study, it has been found that the growth of the intermetallic compounds is highly sensitive to the amount of strontium. Modification of intermetallics is probably a result of impurity atoms "poisoning" the mechanism which provides for platelet growth. This poisoning is thought to be associated with the adsorption of strontium as a surface active element at the growth sites of the growing platelet. In addition, the cooling rate appears also to be a critical variable in determining growth behaviour. Thus, the poisoning effect of Sr on the formation of intermetallics combined with the fast solidification condition may also be the cause of elimination of intermetallic compounds in Al-Si alloys. A comprehensive TEM and Auger study is necessary to understand exactly the mechanism of Sr-modification of intermetallic phases.

7.5. Summary

The effect of strontium at various levels from 0 to 0.08% on the modification of intermetallic compounds has been investigated in two commercial die-casting alloys, A413, 413P, and one synthetic alloy 413. All alloys have been studied under two solidification conditions a) sand casting, b) permanent mold casting. The conclusions drawn from this study are summarized as follows:

(I) Strontium is a very effective element in modification of intermetallics in aluminum casting alloys. The optimum level of strontium additions in both sand casting and permanent mold casting in all alloys studied is 0.04-0.06% Sr.

(II) Strontium additions to alloy 413 in the permanent mold condition caused a reduction of 45% in the size of intermetallics (sludge), 80% in the number of intermetallics per unit area, and 92% in total volume percentage of intermetallic compounds.

(III) In the sand casting condition of alloy 413, strontium caused the fragmentation of needles (β-phases) and reductions of 54% in the length, 43% in the width, and 47% in the volume percent of β-phases. The size of the α-phase decreased about 46%, and its relative volume percent increased from 18.8% in Sr-free alloy to 56.9% in a 0.08% Sr-treated alloy. Thus, strontium is an effective element in changing the β-phase to the α-phase morphology.

(IV) In alloy A413, 0.04% Sr addition in the permanent mold condition reduced all intermetallics to almost zero (0.08 vol%). Fragmentation of β-phases was observed in the sand cast condition and there was a reduction of 90% in the amount, 62% in the length and width, and 84% in the number of β-phase particles. The relative volume percent of α-phase also increased from 58.3% to 93.6%.

(V) A 0.04% Sr addition to the alloy 413P in the permanent mold condition completely eliminated all intermetallic compounds. The size, number, and volume percent of α-phase was also decreased in the sand cast condition.

(VI) Superheating the melt before strontium addition is not effective in improvement of the size and morphology of the intermetallics under slow or fast solidification conditions.

(VII) A low casting temperature after strontium addition to the melt can cause enlargement of intermetallics due to agglomeration.

Chapter 8

Conclusions and Future Work

8.1. Overall Conclusions

Five areas concerning the formation of iron-bearing intermetallics in the 413 type of aluminum alloys have been thoroughly investigated. These include : a) the effect of melt chemistry, particularly iron and manganese concentration. b) the kinetics of formation considering the roles of holding temperature, holding time, and initial chemical composition of the alloy. c) the influence of solidification conditions on the morphology, size, and volume fraction of iron intermetallic phases. d) the effect of settling time and the rate of gravity segregation of intermetallic compounds in a stagnant liquid metal. e) modification of intermetallics by strontium in aluminum-silicon casting alloys. The main conclusions that can be drawn are :

- The volume percentage of intermetallic compounds increases as the iron or manganese content increases. This increase is a result of both size and number of star-like compounds. The combined effect of manganese and iron on the formation of intermetallics is represented by the equation: %Fe + 1.7 %Mn = 0.97. Intermetallics form if the iron and manganese concentrations are such that 0.97 is exceeded in this equation.

- Superheating the melt to high temperatures dissolves the intermetallics completely. When sludge is dissolved, it will not reform until a certain temperature is reached. Quenching experiments and thermal analysis revealed that sludge forms in a short period of time. In general, the temperature of sludge formation depends on the alloy composition and particularly, iron concentration. This temperature increases when the content of iron in the alloy is increased. A power equation describes the relation between sludge formation temperature and iron content.

- As the iron content increases, more intermetallics form at each holding temperature and holding time, and the volume percent of intermetallics increases. The average size of intermetallics does not change appreciably with holding time at each constant temperature but the number of intermetallics is strong function of holding time, because the nucleation kinetics are slow. Thus, a modified Avrami equation can describe the transformation kinetics of the intermetallics adequately.

- When the total volume percent of intermetallics increases with decreasing cooling rate, the number of particles of each phase per unit area decreases and the size of each morphology increases. The morphology and volume fraction of all types of intermetallic compounds are dependent on cooling rate. A fast cooling rate can transform the brittle iron platelet phases which are harmful to mechanical properties of the alloy into very small star-like compounds. An exponential equation can express the effect of cooling rate on the total volume percentage of intermetallic compounds.

- The rate of settling varies with location in the mold due to depletion of intermetallics at the top and accumulation at the bottom. As the distance from the top of the mold increases, the content of iron, manganese, and chromium increases due to the gravity segregation of the intermetallic compounds, with greater concentrations at longer times.

- The terminal velocity calculated by Stokes' law agrees well with the experimentally determined settling velocity due to minimum convection in the system and small size of intermetallics. As a result the terminal velocity is reached at very short times and very close to the liquid surface.

- Strontium is a very effective element in modification of intermetallics in aluminum casting alloys. It reduces significantly the size, number, and total volume percentage of intermetallics and may under certain conditions completely eliminate all intermetallic compounds in commercial alloys in the permanent mold cast condition.

- In the sand cast condition, strontium causes the fragmentation of needles (β-phases) and reduction in the length, width, number, and volume percent of β-phases. The relative volume percent of α-phase also increases in Sr-treated alloys. Thus, strontium is an effective element in changing the β-phase to the α-phase morphology.

8.2. Recommendations for future work :

The following areas for further work are suggested in order to extend the present studies.

1. Although the effect of strontium on the modification of intermetallic compounds was studied on 413 type of aluminum alloy, it is also necessary to extend the investigation to other important hypoeutectic die or permanent mold alloys: 380, 332, 319. Cooling rates typical of pressure die and permanent mold casting should be used to determine the optimum strontium level for removal, or minimization, of the iron bearing intermetallics.

2. A comprehensive TEM and Auger study is needed to understand exactly the mechanism of Sr-modification of intermetallic phases.

3. Study of the mechanism of β-phase to α-phase transformation by strontium additions. Quenching experiments combined with controlled thermal analysis are necessary to determine the sequences of the reactions in : $L \rightarrow \alpha(Al) + \alpha(AlFeSi)$, $L \rightarrow \alpha(Al) + \beta(AlFeSi)$, and the peritectic reaction of : $L + \alpha(AlFeSi) \rightarrow \beta(AlFeSi)$ to explain the effect of strontium in transformation of β-phase to α-phase.

4. Study of the effect of iron intermetallics on the porosity and fatigue behaviour of aluminum-silicon alloys.

5. Investigation on the intermetallic reactions based on thermodynamics to determine the stability of the phases in the Al-Fe-Si-Mn system.

6. Crystal structure determination of Al-Fe-Si-Mn phases by Convergent-Beam Electron Diffraction (CBED).

7. Investigation on the use of ceramic filters to eliminate or reduce sludge particles in aluminum-silicon alloys.

8.3. Statement of Originality

The specific original contributions made in this work can be summarized as follows :

1. The first systematic experimental study of the effect of iron and manganese on the formation of intermetallic compounds was conducted.

2. The temperature of sludge formation as a function of iron concentration was determined by using a designed system of rapid quenching of molten droplets and thermal analysis. A power equation was developed to describe the relation between sludge formation temperature and iron content.

3. For the first time, the kinetics of the formation of intermetallic compounds was investigated by considering the roles of holding temperature, holding time, and initial chemical composition of the alloy.

4. The effect of solidification conditions on the morphology, size, number, and volume fraction of iron intermetallic phases was quantitatively demonstrated by use of image analysis and metallography. It was shown that the morphology and volume fraction of all types of iron intermetallics were dependent on cooling rate.

5. The kinetics of the segregation of iron intermetallics in a stagnant liquid metal was quantitatively investigated for the first time. The effect of settling time and height of the melt on the volume percent, number, and size of iron intermetallics was demonstrated. The terminal velocity calculated by Stokes' law for the motion of solid particles in a viscous fluid was compared with the experimentally

determined settling velocity and the applicability of Stokes' law to this system was demonstrated.

6. For the first time, the effect of strontium on the modification of iron intermetallic phases was comprehensively studied in synthetic and commercial aluminum casting alloys by using image analysis and metallography. It was demonstrated that strontium is a very effective element in modification and/or elimination of intermetallics in both sand casting and permanent mold casting. The effect of melt superheating and casting temperature on intermetallic size and morphology in the presence of strontium was elucidated.

References :

1. Hatch, J.E., "Aluminum-Properties and Physical Metallurgy", *American Society for Metals (ASM)*, 1984, pp. 25-33

2. Altenpohl, D., "Aluminum Viewed From Within", *Aluminum-Verlag*. Dusseldorf, 1982

3. Eklund, J.E., "On the Effects of Impurities on the Solidification and Mechanical Behaviour of Primary and Secondary Commercial Purity Aluminum and Aluminum Alloys", Ph.D. Thesis, *Helsinki University of Technology*, June 1991

4. Groteke, D.E., "A Production Filtration Process for Aluminum Melts", *International Die Casting Congress and Exposition*, 1983, 7p.

5. Kaye, A., "Controlling Aluminum-Alloy Melts for Die-Casting", *Foundry Trade Journal*, Vol. 154, May 1983, pp. 661-670

6. Kaye, A., Street, A., "Die Casting Metallurgy", *Butterworth Scientific*, 1982, pp. 23-31, pp. 71-79

7. Groteke, D.E., "Eliminating Hard Spots from Aluminum Die Castings", *Die Casting Engineer*, No.9, Vol. 21, 1985, pp. 16-24

8. Murray, J.L. and McAlister, A.J., "The Aluminum-Silicon System", *Bulletin of Alloy Phase Diagrams*, Vol. 5, No.1, 1984, pp. 74-84

9. Gruzleski, J.E. and Closset, B.M., "The Treatment of Liquid Aluminum-Silicon Alloys", *The American Foundrymen's Society, Inc.*, 1990, 256p.

10. AFS, "Aluminum Casting Technology", 2nd edition, *The American Foundrymen's Society, Inc.*, 1993, pp. 45-110

11. ASM, "Properties and Selection : Nonferrous Alloys and Pure Metals", Metals Handbook Ninth Edition, Vol. 2, *American Society for Metals (ASM)*, 1979, pp. 172-174

12. Shivkumar, S., Wang, L., Apelian, D., "Molten Metal Processing of Advanced Cast Aluminum Alloys", *Journal of Metals*, Jan.1991, pp. 26-32

13. Gustafsson, G., Thorvaldsson, T., Dunlop, G.L., "The Influence of Fe and Cr

on the Microstructure of Cast Al-Si-Mg Alloys", *Metall. Trans. A*, Vol. 17A, Jan.1986, pp. 45-52

14. Sigworth, G.K., "Determining Grain Size and Eutectic Modification in Aluminum Alloys Castings", *Modern Casting*, July 1987, pp. 23-25

15. Smart, R.F., "Metallurgical Aspects of Aluminum-Silicon Eutectic Piston Alloys", *The British Foundryman*, Nov.1971, pp. 430-446

16. Westengen, H., "Formation of Intermetallic Compounds during DC Casting of a Commercial Purity Al-Fe-Si Alloy", *Z.Metallkunde*, Vol. 73, 1982, pp. 360-368

17. Bonsack Walter, "Iron-the Problematic Factor in Quality of Aluminum Alloy Die Castings", *AFS Trans.* Vol. 69, 1961, pp. 712-720

18. Bonsack, W., "Effects of Minor Alloying Elements on Aluminum Casting Alloys", Part II - Aluminum-Silicon Alloys, *ASTM Bulletin*, Oct.1943, pp. 41-51

19. Couture, A., "Iron in Aluminum Casting Alloys - A Literature Survey", *AFS International Cast Metals Journal*, No.4, Vol. 6, Dec.1981, pp. 9-17

20. Rooy, E.L., "Aluminum Scrap Recycling and its Impact on the Metal Castings Industry", *AFS Trans.* Vol. 93, 1985, pp. 935-938

21. Grand, L., "Influence of Some Impurities on the Quality of Aluminum Alloys", *Fonderie*, Vol. 217, March 1964, pp. 95-100

22. Colwell, D.L. and Kissling, R.J., "Die and Permanent Mold Casting Aluminum Alloy Minor Elements", *AFS Trans.* Vol. 69, 1961, pp. 610-616

23. Gowri, S., Samuel, F.H., "Effect of Alloying Elements on the Solidification Characteristics and Microstructure of Al-Si-Cu-Mg-Fe 380 Alloy", *Metall. Trans. A*, Vol. 25A, Feb.1994, pp. 437-448

24. Jorstad, J.L., "Understanding Sludge", *Die Casting Engineer*, Nov./Dec.1986

25. Ghomashchi, M.R., "Intermetallic Compounds in an Al-Si Alloy used in High Pressure Die-Casting", *Z.Metallkunde*, No.78, 1987, H.11, pp. 784-787

26. Simensen, C,J. and Vellasamy, R., "Determination of Phases Present in Cast Material of an Al-0.5 wt.% Fe-0.2 wt.% Si Alloy", *Z.Metallkunde*, Vol. 68, 1977, pp. 428-431

27. Dunn, R., "Aluminum Melting Problems and Their Influence on Furnace

Selection", *Die Casting Engineer*, Sept.1965, pp. 8-16

28. Osame, Y., Toyoda, K., and Tsumura, Y. "Sludge Deposition in Molten Aluminum Die Casting Alloys in the Holding Furnace", *Journal of Japan Institute of Light Metals*, No. 12, Vol. 36, 1986, pp. 813-818

29. Queener, C.A., Mitchell, W.L., "Effect of Iron Content and Sodium Modification on the Machinability of Aluminum Alloy Die-Castings", *AFS Trans.* Vol. 73, 1965, pp. 14-19

30. Mondolfo, L.F., "Aluminum Alloys : Structure and Properties", *Butterworths*, 1976, pp. 759-777, pp. 534-37, pp. 661-62

31. Liushuan, Y., "Effect of Iron on the Mechanical Properties of Piston Alloys", *Casting Technology*, Vol. 2, 1986

32. Liushuan, Y., "Effect and Elimination of Iron in Al-Si Piston Alloys", *Journal of Luo Yang Engineering Institute*, Vol. 3, 1987, pp. 49-55

33. Xiufang, B., Guohua, Z., Shengxu, Z., Jiaji, M., "The Spheroidisation of Needle-form Iron Compounds in an Al-Si Alloy", *Cast Metals*, No.1, Vol. 5, 1992, pp. 39-41

34. ASM, "Source Book on Selection and Fabrication of Aluminum Alloys", *ASM International*, 1978, pp. 153-157

35. Garat, M., "Evolution de L'A-S5U3", Research Report, *Aluminum Pechiney*, France, 1988, 15p.

36. Mondolfo, L.F., "Manganese in Aluminum Alloys", *The Manganese Centre*, 1978, Paris, pp. 1-35

37. Khudokormov, D.N., Galushko, A.M. and Lekakh, S.N., "Influence of Modification on the Form of Fe-rich Inclusions in Al Alloys", *Russian Casting Production*, May 1975, pp. 198-199

38. Zolotorevsky, V., Axenov, A. and Belov, N., "Neutralization of the Negative Influence of Iron and Silicon on the Mechanical Properties of Aluminum Casting Alloys", Key Engineering Materials, Vols. 44 & 45, *Trans Tech Publications, Switzerland*, 1990, pp. 347-364

39. Quadt, R.A., "Effect of Certain Elements on Mechanical Properties of 1% Cu, 5% Si and 0.5% Mg Aluminum Sand Casting Alloy", *AFS Trans.* Vol. 54, 1946, pp. 465-478

40. Colwell, D.L. and Tichy, O., "Machinability of Aluminum Die-Castings", *AFS Trans.* Vol. 64, 1956, pp. 236-241

41. Glaisher, W.H., "Segregation of Iron and Manganese in some Aluminum Casting Alloys", *Metallurgia*, Vol. 43, 1951, pp. 127-131

42. Pearson, W.B., "Handbook of Lattice Spacings and Structures of Metals and Alloys", Vol. 2, Oxford : *Pergamon Press*, 1967

43. Munson, D., "Clarification of the Phases Occurring in Aluminium-rich Aluminium-Iron-Silicon Alloys, with Particular Reference to Ternary Phase α-AlFeSi", *J. of the Institute of Metals*, Vol. 95, 1967, pp. 217-219

44. Gobrecht, J., "Segregations par Gravite du Fer, du Manganese et du Chrome dans les Alliages Aluminum-Silicium de Fonderie", *Fonderie*, No. 367, May 1977, p. 171-173

45. Barlock, J.G., Mondolfo, L.F., "Structure of some Aluminum-Iron-Magnesium-Manganese-Silicon Alloys", *Z.Metallkunde*, Vol. 66, 1975, pp. 605-611

46. Yaneva, S., Stoichev, N., Kamenova, Z., Budurov, S., "Quaternary Iron Containing Phases in Al-Si Cast Alloys", *Z.Metallkunde*, Vol. 75, 1984, pp. 395-398

47. Dons, A.L., "AlFeSi-Particles in Industrially Cast Aluminium Alloys", *Z.Metallkunde*, Vol. 76, 1985, pp. 609-612

48. Pratt, J.N. and Raynor, G.V., "The Intermetallic Compounds in the Alloys of Aluminium and Silicon with Cr, Mn, Fe, Co, Ni", *J.Institute of Metals*, Vol. 79, 1951, pp. 211-232

49. Phragmen, G., "On the Phases Occurring in Alloys of Aluminum with Copper, Magnesium, Manganese, Iron, and Silicon", *The journal of the Institute of Metals*, Vol. 77, 1950, pp. 489-553

50. Rosenhain, W., Achbutt, S.L., and Hanson, D., Eleventh Report to the Alloy Research Committee of the *Institution of Mechanical Engineers*, 1921, pp. 212-236

51. Stefaniay, V., Griger, A., Turmezey, T., "Intermetallic Phases in the Aluminum-Side Corner of the AlFeSi-Alloy System", *J. Materials Science*, Vol. 22, 1987, pp. 539-546

52. Gwyer, A.G. and Phillips, H.W., *Journal Institute of Metals*, Vol. 38, 1927, pp.

29-83

53. Phillips, H.W.L., Varley, P.C., "The Constitution of Alloys of Aluminum with Manganese, Silicon and Iron, III-The Ternary System : Al-Si-Fe, IV-The Quaternary System : Al-Mn-Si-Fe", *J.Institute of Metals*, Vol.LXIX, 1943, pp. 317-350

54. Armand, M., *Congrés International de L'Aluminium*, Paris, Vol. 1, (Revue de L'Aluminium, Paris), 1955, pp. 305

55. Liu, P., Thorvaldsson, T., Dunlop, G.L., "Formation of Intermetallic Compounds during Solidification of Dilute Al-Fe-Si Alloys", *Materials Science and Technology*, Vol. 2, Oct.1986, pp. 1009-1018

56. Awano, Y. and Shimizu,Y., "Non-Equilibrium Crystallization of AlFeSi Compound in Melt-Superheated Al-Si Alloy Castings", *AFS Trans.* Vol. 98, 1990, pp. 889-895

57. Gobrecht, J.B., "Schwereseigerungen von Eisen, Mangan und Chrom in Aluminium-Silicium-Gusslegierungen, Teil 2", *Giesserei*, Vol. 63, 1976, pp. 558-561

58. Simensen, C.J. and Spjlkavik, A.I., "Analysis of Oxides, Carbides, and Iron-rich Particles in Magnesium" , *Fresenius Z. Anal. Chem.*, No. 300, 1980, pp. 177-182

59. Simensen, C.J., Fartum, P., Andersen, A., " Analysis of Intermetallic Particles in Aluminum by Dissolutiom of the Sample in Butanol" , *Fresenius Z. Anal. Chem.*, No. 319, 1984, P.286-292

60. Lavelle, D.L., "Determining Abrasive Inclusions in Aluminum Alloy Castings", *Foundry*, Oct.1969, pp. 154-157

61. Ryvola, M. and Morris, L.R., "Examination of Insoluble Intermetallic Phases in Aluminum Alloys", *Aluminum Company of Canada, Ltd.*, 4p

62. Miki, I., Kosuge, H., and Nagahama, K., *Journal of Japan Institute of Light Metals*, Vol. 25, 1975, pp. 1-9

63. Young, R.M. and Clyne, T.W., *Scripta Met.*, Vol. 15, 1981, pp. 1211-1216

64. Hollingsworth, E.H., Frank, G.R., and Willett, R.E., *Trans. Met. Soc. AIME*, No. 224, 1962, pp. 188-189

65. Dons, A.L., "AlFeSi-Particles in Commercial Pure Aluminium", *Z.Metallkunde*,

Vol. 75, 1984, pp. 170-174

66. Dons, A.L., "Super structures in α-Al(Mn,Fe,Cr)Si", *Z.Metallkunde*, Vol. 76, 1985, pp. 151-153

67. Rivlin, V.G. and Raynor, G.V., "Critical Evalution of Constitution of Aluminium-Iron-Silicon System", *International Metals Reviews*, No. 3, 1981, pp. 133-152

68. Turmezey, T., Stefaniay, V. and Griger, A., "AlFeSi Phases in Aluminum", Key Engineering Materials, Vols. 44 & 45, *Trans Tech Publications, Switzerland*, 1990, pp. 57-68

69. Iglessis, J., Frantz, C., Gantois, M., "La Croissance par Propagation de Plans de Macle des Composes Eutectiques dans le Systeme Ternaire Al-Fe-Si", *Memoires Scientifiques Revue Metallurgie*, Feb. 1978, pp. 93-100

70. Hoier, R., Lohne, O., Mortvedt, S., "AlFeSi-Particles in an Al-Mg-Si-Fe Alloy", *Scandinavian Journal of Metallurgy*, No. 6, Vol. 1, 1977, pp. 36-37

71. Skjerpe, P., "Intermetallic Phases Formed during DC-Casting of an Al-0.25 wt.% Fe-0.13 wt.% Si Alloy", *Metall. Trans. A*, Vol. 18A, Feb.1987, pp. 189-200

72. Phillips, H.W., "Annotated Equilibrium Diagrams of Some Aluminum Alloy Systems", (Monograph No. 25), *Institute of Metal*, London, 1959, pp. 57-72

73. Griger, A., Stefaniay, V., Lendvai, A., and Turmezey, T., "Possible Modification of Cast Structure by Continuous Casting Technology in AlFeSi Alloys, Part III: Intermetallic Phases", Aluminium, No.10, Vol. 65, *Jahrgang* 1989, pp. 1049-1056

74. Tibballs, J.E., "Al-Si Substitution in Al(Fe,Mn)Si Phases", Key Engineering Materials, Vol. 44 & 45, *Trans Tech Publications, Switzerland*, 1990, pp. 233-246

75. Sigworth, G.K., Shivkumar, S., Apelian, D., "The Influence of Molten Metal Processing on Mechanical Properties of Cast Al-Si-Mg Alloys", *AFS Trans.*, Vol. 97, 1989, pp. 811-824

76. Vorren, O., Evensen, J.E., and Pedersen, T.B., "Microstructure and Mechanical Properties of AlSi(Mg) Casting Alloys", *AFS Trans.*, Vol. 92, 1984, pp. 459-466

77. Kovacs, E., Griger, A., Turmezey, T., and Suchanek, V., "Change of Structure and some Mechanical Properties during Processing of AlMn(Fe,Si) Alloys", Key

Engineering Materials, Vol. 44 & 45, *Trans Tech Publications, Switzerland,* 1990, pp. 271-284

78. Shewmon, P.G., "Transformation in Metals", *McGraw-Hill Book Company*, 1969

79. Iglessis, J., Frantz, C., Gantois, M., "Conditions de Formation des Phases au Fer dans les Alliages Aluminum-Silicium de Purete Commerciale", *Memoires Scientifiques Revue Metallurgie*, April 1977, pp. 237-342

80. Alker, K., "Einfluß Geringer Zusätze, Insbesondere von Mangan, auf GefÜge und Mechanische Eigenschaften Eisenarmer Aluminium-Silizium-Gußlegierungen", No. 49, *Aluminum*, 1973, pp. 417-421

81. Granger, D.A., "Investigation of a Star-Like Intermetallic Phase Occurring in Alloy 339", *AFS Trans.* Vol. 99, 1991, pp. 379-383

82. Backerud, L., Chai, G., Tamminen, J., "Solidification Characteristics of Aluminum Alloys", Vol. 2, Foundry Alloys, *AFS/Skanaluminium*, 1990

83. Tamminen, J., "Thermal Analysis for Investigation of Solidification Mechanisms in Metals and Alloys", Chemical Communications, No.2, *University of Stockholm*, 1988

84. Mascre, C., "Influence du Fer et du Manganese sur les Alliages du Type de l' A-S13 (Alpax)", *Fonderie*, Vol. 108, Jan.1955, pp. 4330-4336

85. Mondolfo, L.F. and Barlock, J.G., "Effect of Superheating on Structure of some Aluminum Alloys", *Metall. Trans. B*, Vol. 6B, Dec.1975, pp. 565-572

86. Gobrecht, B.J., "Schwereseigerungen von Eisen, Mangan und Chrom in Aluminium-Silicium-Gusslegierungen (Teil 1)", *Giesserei*, Vol. 62, 1975, pp. 263-266

87. Lavelle, D.L., "Aluminum Die Casting and Factors Affecting Pressure Tightness", *AFS Trans.*, Vol. 70, 1962, pp. 641-647

88. Miller, S.k., "Inclusion Control of Die Casting Alloys", *Die Casting Engineer*, Sept./Oct.1984, pp. 54-58

89. Kennerknecht, S., "Metallurgical Aspects of Quality Control in the Production of Premium Quality Aluminum Investment Castings for the Aerospace Industry", North Atlantic Treaty Organization, *Advisory Group for Aerospace Research and Development (AGARD) Conference Proceedings* No.325, 54th Meeting of the AGARD Structures and Materials Panel in Brussels, Belgium, 4-9 April 1982, pp.

1-52

90. Flores, A., Escobedo, J., Mendez, J., Mendez, M., "Kinetics of the Formation, Growth and Sedimentation of the $Al_{15}(Fe,Mn)_3Si_2$ Phase in Al-Si-Cu Alloys", Congress of Driving Die-Casting into the 21st Century, Detroit, *North American Die Casting Association (NADCA)*, 1991, pp. 293-297

91. Flores, A., Escobedo, J., Mendez, J., "Kinetic Mechanisms of Iron Segregation from Al-Si-Cu-Fe-Mn Melts", *Light Metals*, TMS-AIME, 1992, pp. 845-850

92. Flores, A., Escobedo, J., Mendez, J., Mendez, M., Mercado, H., "Application of the Segregation Process for the Iron Removal from Aluminum-Silicon Scrap", 3rd International Conference on Molten Aluminum Processing, Nov.9-10, Orlando, FL, *The American Foundrymen's Society, Inc.*, 1992, pp. 293-300

93. Coulson, J.M., Richardson, J.F., Backhurst, J.R., Harker, J.H., "Motion of Particles in a Fluid", chapter 3, Chemical Engineering, Vol. 2, *Pergamon Press*, 1991, pp. 95-131

94. Mondolfo, L.F., Barlock, J.G., Tomeo, A.P., "Control of Manganese Distribution in 3003 Aluminum Alloys", *Light Metals*, Vol. 2, 1976, pp. 365-386

95. Morris, L.R., Miners, F.B., *U.S. Patent* No. 3,926,690, 1975

96. Vernam, W.D., Lifka, B.W., *U.S. Patent* No. 4,711,762, 1987

97. Inaba, T., Shinano, N., *Japanese Patent* No. JP 62-207849, 1987

98. Mulazimoglu, M.H., Paray, F., Stephen, G., Kulunk, B., and Gruzleski, J.E., "Modification of Intermetallic Phases by Strontium in Aluminum Wrought Alloys", *Light Metals*, TMS, 1994, pp. 1047-1056

99. Dons, A.L., "Variations in the Composition of AlMnFeSi-Particles in Aluminum", *Scandinavia J. of Metallurgy*, Vol. 13, 1984, pp. 137-143

100. Yan, Y., Wang, R., Gui, J., "Stable and Metastable Phases in some Quarternary Al-Si-Mn-Fe Alloys", *J. Physics: condens. matter*, 2, 1990, pp. 7733-7741

101. Griger, A., Stefaniay, V., Turmezey, T., "Crystallographic Data and Chemical Compositions of Aluminum-rich Al-Fe Intermetallic Phases", *Z.Metallkunde*, Bd.77, 1986, H.1, pp. 30-35

102. Raynor, G.V., "Crystal Structure and Bond Mechanism of Intermetallic Phases", The physical Chemistry of Metallic Solutions and Intermetallic Compounds, Vol.1,

Chemical Publishing Co., Inc., New York, 1960, pp. 312-329

103. Jensen, C.L., Wyss, R.K., "Electron Diffraction Study of α- and α_T-AlFeSi", *Metall. Trans. A*, Vol. 19A, April 1988, pp. 893-898

104. Girgis, K., "Structure of Intermetallic Compounds", Chapter 5, "Physical Metallurgy" by Cahn, R.W. and Haasen, P., *Elsevier Science Publishers*, 1983, pp. 220-269

105. Flemings, M.C., "Solidification Processing", *McGraw-Hill*, Inc., 1974, 364P

106. Hawbolt, E.B., Chau, B., and Brimacombe, J.K., "Kinetics of Austenite-Ferrite and Austenite-Pearlite Transformation in a 1025 Carbon Steel", *Metall. Trans. A.*, Vol. 16A, April 1985, pp. 565-578

107. Brammer, W.N., "Melting Practice for Aluminum Castings Alloys", *AFS Trans.* Vol. 66, 1958, pp. 497-502

108. Miki, V.I. and Warlimount, H., "Morphology and Kinetics of Precipitation Processes in Aluminum-Rich Aluminium-Iron and Aluminium-Iron-Silicon Alloys", *Z.Metallkunde*, Bd.59, Apr.1968, pp. 254-264

109. Yeremenko, V., Natanzon, V., Dybkov, V., "The Effect of Dissolution on the Growth of the Fe_2Al_5 Interlayer in the Solid Iron-Liquid Aluminum System", *Journal of Materials Science*, Vol. 16, 1981, pp. 1748-1756

110. Denholm, W.T., Esdaile, J.D., Siviour, N.G., Wilson, B.W., "Crystallization Studies in the Aluminum-Iron-Manganese system", *Metall. Trans. A*, Vol. 15A, July 1984, pp. 1311-1317

111. Denholm, W.T., Esdaile, J.D., Siviour, N.G., Wilson, B.W., "The Nature of the $FeAl_3$ Liquid-$(FeMn)Al_6$ Reaction in the Al-Fe-Mn System", *Metall. Trans.A* Vol. 18A, March 1987, pp. 393-397

112. Gillett, B.A., Latimer, K.G., "Influence of some Alloying Elements on Tensile Properties of Pressure-Die Cast Aluminum Test-Bars", *Foundry Trade Journal*, Dec. 1970, pp. 955-959

113. Vander Voort, G.F., "Metallography, Principles and Practice", *McGraw-Hill Book Company*, 1984

114. Wills, B.A., "Mineral Processing Technology", Chapter 9, Fifth edition, *Pergamon Press*, 1992, pp. 365

115. Brahdes, E.A. and Brook, G.B., "Smithells Metals Reference Book", *Butterworth*, 1992, pp. 14-6 to 14-16

116. Harding, M.P., "Liquid Densities of Aluminum-Based Casting Alloys", *The Journal of Australian Institute of Metals*, Vol. 19, No. 2, June 1974, pp. 136-139

117. Sigworth, G.K. and Wang, C., "Mechanisms of Porosity Formation during Solidification : A Theoretical Analysis", *Metall. Trans. B.*, Vol. 24B, April 1993, pp. 349-364

118. Ganesan, S., Speiser, R., Poirer, D.R., "Viscosities of Aluminum-rich Al-Cu Liquid Alloys", *Metall. Trans. B.*, Vol. 18B, June 1987, pp. 421-424

119. Taggart, A.F., "Handbook of Mineral Dressing", Section 8, *Wiley*, New York, 1945, pp. 8-1 to 8-5

120. Burt, R.O., "Gravity Concentration Technology", *Elsevier Science Publishers*, 1984, pp. 124-126

121. Martin, J.P., Dubé, G., Frayce, D., Guthrie, R., "Settling Phenomena in Casting furnaces : A Fundamental and Experimental Investigation", *Light Metals*, 1988, pp. 445-455

122. Sztur, C., Balestrei, F., Meyer, JL., Hannart, B., "Settling of Inclusions in Holding Furnaces : Modeling and Experimental Results", *Light Metals*, 1990, pp. 709-716

123. Eckert, C.E., Miller, R.E., Apelian, D., Mutharasan, R., "Molten Aluminum Filtration : Fundamentals and Models", *Light Metals*, 1984, pp. 1281-1304 -78

124. White, F.M., "Fluid Mechanics", *McGraw-Hill Publishing Company*, 1986, pp. 412-419

125. Merchant, H.D., Morris, J.G., Hodgson, D.S., "Characterization of Intermetallics in Aluminum Alloy 3004", *Elsevier Science Publishing Co.*, 1990, pp. 339-373

126. Marsh, L.E., Reinemann, G., "Premium Quality Aluminum Castings Theory, Practice, and Assurances", *AFS Trans.*, Vol. 87, 1979, pp. 413-422

127. Mulazimoglu, M.H., Tenekedjiev, N., Closset, M., and Gruzleski, J.E., "Studies on the Minor Reactions and Phases in Strontium-Treated Aluminum-Silicon Casting Alloys", *Cast Metals*, No.1, Vol. 6, 1993, pp.16-28

128. Haque, M.M. and Kondic, V., "Influence of Strontium on Solidification of Aluminum-Silicon Alloys", Light Metals: Science and Technology, Proceedings of an International Symposium, *Trans Tech Publications*, Switzerland, 1985, pp. 159-170

129. Drouzy, M. and Richard, M., *Fonderie*, No. 285, 1969, pp. 500-511

130. Crosley, P.B. and Mondolfo, L.F., "The Modification of Al-Si Alloys", *Modern Casting*, Vol. 49, March 1966, pp. 89-100

131. Paray, F., "Heat Treatment and Mechanical Properties of Al-Si Modified Alloys", Ph.D. Thesis, *McGill University*, Dec. 1992

132. Granger, D.A. and Elliot, R., "Solidification of Eutectic Alloys: Aluminum-Silicon Alloys", Metals Handbook, 9th Edition, Vol. 15, *American Society for Metals (ASM)*, 1988, pp. 159-168